

Non-perturbative resummation in three dimensional Yang-Mills theory

Mark C. Abraao York

Doctor of Philosophy

Department of Physics

McGill University

Montreal, Quebec

April 2014

A thesis submitted to McGill University in partial fulfillment of the requirements of
the degree of Doctor of Philosophy

© Mark Abraao York, 2014

DEDICATION

For my grandparents...

ACKNOWLEDGEMENTS

Foremost, I am very grateful to my supervisor Guy Moore for the support and the many discussions that we have had throughout my time at McGill. I would like to acknowledge Marcus Tassler for his insight throughout the project described in Chapter 3, and Aleksi Kurkela for his collaboration on a separate publication unrelated to this work.

I would also like to acknowledge the faculty members and postdocs of the physics department at McGill, and in particular I would like to thank the instructors of the courses that I took as a graduate student at McGill. These courses were all well-taught and very interesting. Finally, I am grateful for the financial support which I received both from the physics department and the Natural Sciences and Engineering Research Council of Canada.

As a student at McGill I have had the chance to meet many interesting people, some of whom were my closest friends. My extracurricular involvement with the sailing and rowing communities here in Montreal was very rewarding, and I am indebted to both of these groups. I would like to especially thank my parents, and some of my closest friends Emerson Krock and Liam Kirwin. I would also like to thank Isabel Macquarrie for her enduring support.

STATEMENT OF ORIGINALITY

Chapters 1 and 2 and Appendices A and B consist primarily of introductory / review material and were composed by myself. Chapters 3, 4 and 5 as well as the remaining appendices present original work and are based almost entirely on

Mark C. Abraao York, Guy D. Moore and Marcus Tassler, *3-loop 3PI effective action for 3D $SU(3)$ QCD*, *JHEP* **1206** (2012) 077, [arXiv:1202.4756]

co-authored with Guy Moore and Marcus Tassler, as well as the soon to be submitted

Mark C. Abraao York and Guy D. Moore, *nPI Resummation in $SU(N)$ Higgs Theory*, *in preparation*.

Specifically, the application and resolution of n PI functional techniques in non-abelian gauge theory as described in these works and in this thesis constitute an original contribution to the field. Concerning my personal contributions, I played a primary role in carrying out the research described in this text and furthermore, I have performed all of the calculations described in Appendices C, D and F. I acknowledge that Guy Moore had originally suggested pursuing this topic, and that the three of us (myself, Guy and Marcus) collaborated together on addressing some of the numerical and conceptual challenges, particularly in the early phases of the project. I also acknowledge that Guy made some contributions to the text of Chapter 3 and

Appendix E (particularly to the introductory section including some edits throughout), as well as proposing the resolution of the phase space described in Appendix E. All of the computations described in this text leading to the presented results (for instance, any result that has been plotted on a graph, with the exception of the duly acknowledged replication of the Columbia Plot in Chapter 1 or any quoted lattice data) as well as the discussion of the solutions are elements of my contributions.

ABSTRACT

An n -particle-irreducible (n PI) effective action $\Gamma[\bar{\phi}, G, \dots]$ is a functional whose stationary points coincide with the exact Green's functions of a quantum theory (for $n = 2$ this is known as a Φ -derivable approximation). Any practical application would necessitate a truncation of Γ at some finite loop order; then, the stationary points of $\Gamma[\bar{\phi}, G, \dots]$ would correspond to a selective resummation to all orders in a perturbative expansion. This thesis explores the application of these functional techniques to non-abelian gauge theory in three spacetime dimensions.

3D gauge theories are physically relevant in that they provide an effective description of the non-perturbative sectors of high temperature 4D gauge theories. In this work we focus our attention on two particular 3D models, pure $SU(N)$ Yang-Mills and Yang-Mills coupled to a scalar field. In our study of pure Yang-Mills theory we address the technical and computational challenges associated with the resolution of the three-loop 3PI equations of motion; in the end obtaining solutions for the fully resummed two and three-point functions of the theory. Subsequently, the study of $SU(N)$ Higgs theory is physically motivated, in that this field theory provides a framework which can be used to compute gauge-invariant observables using the n PI method. In determining the phase diagram of $SU(N)$ Higgs theory (specifically in the three-loop 2PI formalism) we address the overall accuracy and applicability of these methods to the non-perturbative study of Yang-Mills theory.

ABRÉGÉ

Nous utilisons le formalisme n PI pour calculer les propagateurs et les fonctions de vertex de la théorie Yang-Mills en trois dimensions. Les solutions qui sont obtenus de cette méthode peuvent être considérés comme la somme sélective mais infini sur une certaine classe de topologies Feynman. Nous discutons d’une technique qui sert à régulariser les analogues n PI des équations Schwinger-Dyson, et nous permet de converger itérativement sur les solutions.

L’étude de Yang-Mills pur en 3D est réalisée dans une troncature du troisième ordre de l’action effective 3PI. Dans l’exécution de ce calcul, nous sommes en mesure de résoudre de nombreux défis techniques associés et en plus faire une comparaison entre nos résultats et les résultats obtenus des études de réseau en jauge-fixé. .

Par la suite, nous utilisons le formalisme 2PI dans le but de résoudre le diagramme des phases de la théorie $SU(N)$ Higgs en 3D. En faisant ceci nous utilisons la méthode pour mesurer directement des observables jauge-invariantes; nous permettant ainsi de faire des commentaires sur l’exactitude et l’efficacité globale de la méthode dans un contexte de théorie de jauge.

TABLE OF CONTENTS

DEDICATION	ii
ACKNOWLEDGEMENTS	iii
STATEMENT OF ORIGINALITY	iv
ABSTRACT	vi
ABRÉGÉ	vii
LIST OF TABLES	xi
LIST OF FIGURES	xii
1 Yang-Mills theory and QCD	1
1.1 Introduction	1
1.1.1 Organization of the thesis	8
1.2 Phase transitions and confinement	9
1.2.1 Phase transitions in non-abelian gauge theory with fermions	12
1.2.2 Phase transitions in non-abelian gauge theory with scalars .	16
1.3 Gauge-invariance and gauge-fixing	19
1.3.1 Covariant gauges	23
1.3.2 Generalized R_ξ gauge	28
1.4 Thermal Yang-Mills	31
1.4.1 3D effective models	35
1.4.2 Resummation	41
2 Φ -derivable approximations and the n PI formalism	45
2.1 Attempt at an exact solution in the Φ -derivable approximation . .	45
2.2 1PI generating functions	54
2.2.1 Saddle point evaluation of $\Gamma[\bar{\phi}]$	57
2.2.2 1PI effective action and symmetry breaking	59

2.3	The 2PI effective action	64
2.3.1	Loop expansion	66
2.3.2	Recovery of the Φ -derivable approximation	70
2.3.3	Generalization to 3PI and higher n	71
3	Three-loop 3PI effective action in 3D Yang-Mills theory	73
3.1	Resummation in a hot gauge theory	73
3.2	The 3PI effective action	79
3.3	Divergences and regularization	85
3.3.1	Divergences in self-energies	86
3.3.2	Divergences upon p -integration	95
3.4	Variational <i>Ansätze</i>	98
3.4.1	Numerical implementation	105
3.5	Results	113
3.6	Discussion	116
3.6.1	Comparison with other approaches	116
3.6.2	Slavnov-Taylor identities	123
3.7	Concluding remarks for Chapter 3	125
4	2PI resummation in $SU(N)$ Higgs theory	128
4.1	Introduction: the phase diagram of $SU(N)$ Higgs theory	128
4.2	$SU(N)$ Yang-Mills + Higgs theory in the n PI formalism	133
4.2.1	General remarks and notation	133
4.2.2	The three-loop 2PI effective action	134
4.2.3	Remarks on gauge-fixing	142
4.2.4	The use of covariant gauge	146
4.3	Extremization of the effective action	149
4.3.1	Variational <i>Ansätze</i>	149
4.3.2	Initial conditions and root finding	152
4.4	Analysis and results	153
4.5	Discussion	164
4.5.1	Location of the critical end point	164
4.5.2	Properties of the solutions	166
4.5.3	Comparison with the lattice	171
4.5.4	Comparison with perturbation theory	175
4.5.5	Effectiveness of the 2PI formalism in the Higgs phase	178
4.5.6	Comparison between Landau and Feynman gauges	181

4.6	Concluding remarks for Chapter 4	183
5	Conclusions	185
Appendix A		
	Group theory for $SU(N)$	188
Appendix B		
	Euclidean space Feynman rules for Yang-Mills and $SU(N)$ Higgs theory . .	191
Appendix C		
	Self-energies computed in dimensional regularization	193
Appendix D		
	Three-gluon and ghost-gluon vertices	203
Appendix E		
	Phase space integrations	209
Appendix F		
	Remarks on the regularization of $\Gamma[D_+] - \Gamma[D_-]$	216
	References	223

LIST OF TABLES

<u>Table</u>		<u>page</u>
3-1	Feynman rules for the Yang-Mills 3PI effective action.	81
3-2	Landau gauge variational coefficients.	119
4-1	Colour factors for the two and three-loop Higgs topologies.	139
4-2	Conversion of x and y to physical 4D quantities.	173

LIST OF FIGURES

<u>Figure</u>	<u>page</u>
1–1 The Columbia Plot: mass dependence of the phase transition in QCD at $\mu = 0$	14
1–2 Feynman diagrams in the daisy sum.	43
2–1 Daisy and super daisy Feynman diagrams.	50
2–2 One-loop effective potential for scalar theory in 3D.	60
2–3 Two-loop topologies in the 1PI effective action.	61
3–1 NLO heavy quark diffusion.	75
3–2 Inclusion of additional HTLs.	75
3–3 Transverse gluon self-energy as a function of the number of integration points.	109
3–4 Evolution of the transverse gluon and ghost self-energies under gradient descent.	111
3–5 Convergence of the $H(p_1, p_2, p_3)$ vertex function.	114
3–6 Convergence of the ghost-gluon vertex functions.	114
3–7 Transverse, longitudinal and ghost self-energies.	115
3–8 Comparison between the 2PI and 3PI solutions.	116
3–9 Vertex functions in Landau gauge.	117
3–10 Vertex functions in Feynman gauge.	118
3–11 Comparison between a lattice determined transverse gluon propagator and the 3PI result in Landau gauge.	123

3–12	Propagator WST identity.	124
3–13	Vertex WST identity.	124
4–1	Phase diagram for $SU(N)$ Higgs theory.	130
4–2	Evolution of the 2PI equations of motion under gradient descent. . . .	154
4–3	Evolution of the symmetric phase Higgs two-point function with increasing y , and coexistence of symmetric and Higgs phases. . . .	156
4–4	Transverse gluon and ghost two-point functions.	157
4–5	Dependence of the scalar condensate on y	160
4–6	Evolution of stable solutions with x	161
4–7	Convergence of the scalar condensate over \mathcal{N} iterations of the algorithm.	163
4–8	Convergence of initial conditions.	167
4–9	Stability of symmetric and Higgs phase solutions.	168
4–10	Evolution of D_+ and D_- in Feynman gauge.	182

CHAPTER 1

Yang-Mills theory and QCD

1.1 Introduction

Following the early stages of a heavy ion collision, hadronic matter briefly exists in a deconfined state known as quark-gluon plasma (QGP), a state which was also present in the early universe. This existence and properties of QGP is a field of active research in experiments at RHIC and CERN [1, 2, 3, 4, 5, 6], as well as theoretically on the lattice [7, 8, 9, 10, 11, 12]. What is known theoretically is that this phase actually shares many features with an electromagnetic plasma [13], such as Debye screening, Landau damping, plasma oscillations and so forth. However, one major distinction between the two is the non-perturbative screening of static magnetic fields, which remain unscreened to all orders in QED. Infrared divergences lead to a failure of the perturbative expansion of static quantities; for the pressure of hot QCD this break-down occurs at four-loops, or $\mathcal{O}(g^6)$. This is the well-known Linde problem [14], and it illustrates that a perturbative description of the underlying physics is not possible at the energy scales of interest; for instance, those within the vicinity of the conjectured QCD critical end point.

In QCD, the QGP phase appears in the vicinity of $T_c \sim \Lambda_{\text{QCD}}$ and it coincides with the approximate restoration of chiral symmetry (for reviews see [15, 16]). At present, the details of this phase transition are poorly understood. In fact, referring to it as a phase transition is a misnomer, since in nature it is believed that the transition

to the QGP at vanishing chemical potential is in fact a cross-over. Studying the QCD phase diagram is difficult due to the lack of first-principles analytic methods which are effective at strong coupling. Furthermore a theoretical description based on the lattice suffers from other challenges associated with the fermion sign problem of QCD at finite chemical potential [17]. For example, the relationship between chiral symmetry breaking and deconfinement is not fully understood [18].

Many groups are involved in the determination of the location of the QCD critical end point both experimentally and theoretically [19, 20, 21, 22, 23, 24], the existence of which is motivated by effective low temperature, high baryon density models [25]. However, even the very existence of a critical end point is debated, as it has also been shown that the nature of the phase transition arising from these models is sensitive to the model parameters [26]. In addition, other phases which are believed to occur at very high density have also been postulated [27], though no experimental signatures of these phases have been observed.

QCD is defined by the Lagrangian

$$\mathcal{L}_{\text{QCD}} = -\frac{1}{2}\text{Tr } F^{\mu\nu} F_{\mu\nu} + \sum_{i=1}^{N_f} \bar{\psi}_i (i\not{D} - m_i) \psi_i \quad (1.1)$$

with i summing over the six flavours that exist in nature: up, down, strange, charm, bottom and top. The Yang-Mills field strength and gauge-covariant derivative are¹

$$F_{\mu\nu} = \partial_\mu A_\nu - \partial_\nu A_\mu - ig[A_\mu, A_\nu] \quad (1.2)$$

$$D_\mu = \partial_\mu - igA_\mu. \quad (1.3)$$

In QCD the gauge group is $SU(3)$, and the fermions transform in the fundamental representation. One of the defining features of QCD and Yang-Mills theory in general is asymptotic freedom [28], which results in the coupling $\alpha_s = g^2/4\pi$ becoming weaker at higher energies. In 4 dimensions Eq. (1.2) describes a renormalizable field theory, which naturally leads to a logarithmic scale dependence of α_s . The scale dependence is given perturbatively by the β -function

$$\beta(\alpha_s) = \frac{d\alpha_s}{d\log\mu} = -\frac{33 - 2N_f}{6\pi}\alpha_s^2 - \frac{153 - 19N_f}{12\pi^2}\alpha_s^3 - \mathcal{O}(\alpha_s^4), \quad (1.4)$$

an expression which is known up to four-loops [29]. Furthermore, the value of α_s at the scale of the Z boson mass has been measured experimentally (see [30] and references therein), its value is

$$\alpha_s(\mu = M_Z) = 0.1185 \pm 0.0006. \quad (1.5)$$

¹ The metric convention $g^{\mu\nu} = \text{diag}(-, +, +, +)$ is assumed in 4D.

The growth of the coupling strength in the IR leads to the definition of the QCD scale Λ_{QCD} , as the energy at which α_s diverges. For $N_f = 5$

$$\Lambda_{\text{QCD}}^{\overline{\text{MS}}} = 214 \pm 7 \text{ MeV}. \quad (1.6)$$

The stated value is computed in the $\overline{\text{MS}}$ renormalization scheme, since the β -function is scheme dependent at three and four-loops. It is not really a physical quantity, since the divergence of the coupling is actually a byproduct of perturbation theory. In nature α_s grows to an $\mathcal{O}(1)$ value at which point the perturbative expansion breaks down [31]. However, the significance of Λ_{QCD} is that it gives a rough idea of the scale at which the physics of the strong-force is non-perturbative. With massless fermions we can identify it with the length scale on which colour confinement occurs. In physical units, $1/\Lambda_{\text{QCD}} \sim \mathcal{O}(1 \text{ fm})$, which is comparable to the size of a proton. In other words, at length scales $r \gg 1/\Lambda_{\text{QCD}}$ only colour singlet bound states (like mesons and baryons) are observed [32].

QCD is difficult to study analytically due to the non-linearity of the gauge field self-interactions. However, to gain some insight into the dynamics of the strong force in nature, in many situations it is favourable to study variants and generalizations of QCD. This could potentially involve:

- altering the fermion content
- excluding fermions all together
- setting quark masses to zero
- modifying the gauge group
- changing the dimension or topology of spacetime

- including scalars and other Standard Model fields;

this list is not exhaustive.

The underlying motivation to adopt any of these particular generalizations depends on the physics one is interested in. To give a few examples, in studying the chiral phase transition / cross-over, which occurs at $T_c \sim \Lambda_{\text{QCD}}$ the up and down (any perhaps also the strange) quark masses may be set to zero while excluding the relatively heavy species since their masses are large compared to the relevant scales of the problem, $m_c, m_b, m_t \gg T_c$. The nature of the chiral phase transition (whether it is first order, second order or a cross-over) is sensitive to the quark masses [33]. Thus varying the “light” quark masses leads to a determination of their effect on the phase diagram. Alternatively, as a more specific example, if one is interested in studying the gluon fusion $gg \rightarrow H$ process in the Standard Model, the amplitude at one-loop will be dominated by the contributions from the heavy quarks which couple strongly with the Higgs [34]. In this case light quarks can be neglected (in fact, even including the bottom quark represents a minor correction to this particular amplitude).

Concerning the dimensionality and topology of spacetime, there is some interest in the study of QCD with multiple compact dimensions (e.g. [35]). In particular, 4D QCD with a single compact Euclidean time direction is essentially QCD at finite temperature. An effect of the topology is that without matter fields present, varying the radius of the compact dimension (i.e. changing the temperature) results in a confinement / deconfinement phase transition. In the finite temperature context, 3D Euclidean formulations of QCD are of interest since they offer an effective description

of a hot 4D theory [36, 37]. Non-perturbative infrared physics can be studied on the lattice with 3D Yang-Mills coupled to an adjoint scalar; this is known as electric QCD (eQCD). Furthermore, the purely non-perturbative magnetic sector is described by pure 3D Yang-Mills; this is magnetic QCD (mQCD). 3D Euclidean Yang-Mills happens to be the primary focus of this work.

Pure Yang-Mills theory [38] is of particular relevance to the study of the mathematical aspects of confinement; the finite temperature confinement / deconfinement phase transition is related to Z_N centre symmetry breaking [39] via a non-zero expectation value for the Polyakov-Loop.² This feature has motivated the study of Yang-Mills with, for instance, a G_2 gauge group, due to it simultaneously being non-abelian and having a trivial centre [40]. Confinement is manifested in QCD (i.e. in nature) by an observable physical spectrum consisting entirely of colour singlet states, for instance, protons, neutrons, pions etc. Furthermore, confinement is an inherently non-perturbative phenomenon and it is a generic feature of Yang-Mills theory in 4D due to the non-abelian character of the gauge-group (where gauge fields self-interact). Throughout this work, it should be assumed that the discussion is specifically centred around $SU(N)$ gauge-groups.

To better understand QCD, it is helpful to consider what makes it so different from QED. As a first example, the QED field strength $F_{\mu\nu}$ is gauge-invariant. Its components are observable and are identified with electric and magnetic fields.

² Phase transitions can still in general occur with fundamental quarks present, but then, the Z_N symmetry is at best approximate; see Section 1.2.1.

Furthermore, the current density operator $J^\mu = e\bar{\psi}\gamma^\mu\psi$ is gauge-invariant. Electric charge, which is specified by the J^0 component, is also observable in effect. In QCD, neither of these statements are true. For instance, the would-be colour charge operator $J^{a0} = g\bar{\psi}T^a\gamma^0\psi$ transforms non-trivially under a gauge-transformation $\psi \rightarrow \Lambda\psi$ with $\Lambda \in \text{SU}(N)$ since $[\Lambda, T^a] \neq 0$. The gauge-invariance of the current and field strength in QED is entirely due to it being an abelian theory.

What are generally regarded as signatures of confinement in pure Yang-Mills theory are area-law behaviour of Wilson Loops [41] and the existence of a mass gap [42]. However, this statement is not precisely rigorous; in fact, at the time of writing the Yang-Mills existence and mass gap Millennium Problem remains unsolved [43]. That being said, these two properties of confinement are generally accepted by the physics community. The standard interpretation of area-law is that if two heavy fundamental representation charges (i.e. test quarks) are introduced into the medium, the energy required to pull them apart would grow linearly with separation. Hypothetically, if this were attempted in nature, the energy in the “string” between the quarks would grow until a point where a quark / anti-quark pair would form out of the vacuum and bind to the 2 initially free charges. This is known as string-breaking [44], and as a result, in a physical theory like QCD, the static potential eventually levels off. As a direct consequence, with dynamical quarks present, area-law for large Wilson loops is not observed. To complicate matters further, the order parameter which defines the confinement / deconfinement phase transition in pure Yang-Mills is not applicable in a strict sense to QCD due to the presence of fermions. We will return to this point in Section 1.2.1, but before doing so it is best to start

the next section with an overview of the situation in pure Yang-Mills, which has a *well defined* phase transition. However, we will now comment briefly on the contents of the remainder of this chapter.

1.1.1 Organization of the thesis

This thesis specifically explores the topic of resummation in non-abelian gauge theory via the n -particle-irreducible (n PI) formalism (closely related to what are known as Φ -derivable approximations). Technical details concerning the n PI formalism and a presentation and discussion of the results are contained throughout Chapters 2, 3 and 4 and the appendices, whereas Chapter 1 serves as an introduction. There will be several recurring themes throughout this work, namely phase transitions, gauge-fixing / gauge-invariance and the study of 3 dimensional effective models. Essentially, we will be applying the n PI formalism to pure Yang-Mills and $SU(N)$ Higgs theory in 3D, which requires working in a fixed gauge. Our main goal is to use the method to resolve the non-perturbative phase diagram of $SU(N)$ Higgs theory.

Therefore, the remainder of Chapter 1 is devoted to a review of each of these topics, with a focus on certain key points that are relevant to the discussion later in this work. Section 1.2 begins with a presentation of phase transitions in pure Yang-Mills theory as well as Yang-Mills coupled to matter (particularly scalar) fields. Section 1.3 introduces the necessity to fix a gauge perturbatively. The focus is initially on covariant gauge; however, we eventually switch over to a discussion of Vacuum Expectation Values (VEVs), R_ξ gauge and spontaneous symmetry breaking. Finally, in Section 1.4 we will go over the construction of an effective 3D description

of thermal Yang-Mills that is valid in the infrared, which motivates our study of 3D field theories. Chapter 1 ends with a simple example of a resummation.

In Chapter 2 we then present the n PI formalism as a resummation scheme via its definition as the Legendre transform of the generating function of connected Green's functions. Furthermore, we discuss what are known as Φ -derivable approximations, which form a subset of the n PI formalism. In Chapter 3 we express the 3PI effective action for pure Yang-Mills theory (magnetic QCD) in covariant gauge; subsequently we explicitly compute the resummed two and three-point Green's functions. Finally, in Chapter 4 we use the formalism to explore the phase diagram of $SU(N)$ Higgs theory which is related to the electroweak phase diagram. Since this final task involves the computation of gauge-invariant observables, it serves as a definitive test of the accuracy and overall usefulness of the method in general.

1.2 Phase transitions and confinement

At zero temperature, confinement in pure Yang-Mills theory occurs on a characteristic length scale r_C , known as the confinement radius. On dimensional grounds, $r_C \sim 1/\Lambda_{SU(N)}$. The quantity $\Lambda_{SU(N)}$ is defined in an similar fashion to Λ_{QCD} , except that in a pure-gauge theory, $\Lambda_{SU(N)}$ is the only scale present. The spectrum at zero temperature consists of colour singlet bound states of gluons [45], or *glueballs*, with masses proportional to $\Lambda_{SU(N)}$, again on dimensional grounds [46]. At a heuristic level, one could ask what would happen at high temperatures where the electric screening length $r_D \sim 1/gT$ becomes small so that $r_D < r_C$? The answer is that eventually colour charges becomes deconfined, and in a sense they are *liberated*. In fact, at very high temperatures, Yang-Mills theory resembles an ideal gas [47].

A more precise statement can be made by considering the behaviour of the static potential $V_{q\bar{q}}(r)$ between two heavy fundamental sources [39]. At zero temperature, consistent with the area-law signature of confinement, it diverges linearly at large separation

$$V_{q\bar{q}}(r) \sim \sigma r + \text{constant}, \quad (1.7)$$

where the proportionality constant σ is known as the string tension and it has been measured on the lattice [48]. At high temperature, $V_{q\bar{q}}(r)$ changes over to the form of a screened Coulomb potential³

$$V_{q\bar{q}}(r) \sim \frac{g^2 e^{-m_D r}}{r} + \text{constant}. \quad (1.8)$$

The gauge-invariant order parameter for this transition is the expectation value of the Polyakov-loop

$$L(x) = \frac{1}{N} \text{Tr} \mathcal{P} e^{ig \int_0^\beta d\tau A_0(\tau, x)} \quad (1.9)$$

in the fundamental representation. This quantity is directly related to the low and high temperature forms of the static $q\bar{q}$ potentials (Eq. (1.7) and Eq. (1.8)) via the thermal average of its two-point correlation function [50, 51, 52]

$$\langle L(r) L^\dagger(0) \rangle = \frac{N^2 - 1}{N} e^{-\beta V_{q\bar{q}}^{\mathbf{8}}(r)} + \frac{1}{N} e^{-\beta V_{q\bar{q}}^{\mathbf{1}}(r)}. \quad (1.10)$$

A few remarks: the expressions Eq. (1.7) and Eq. (1.8) included constants which arise due to the renormalization of the free energy; following renormalization we can make

³ This should not be taken as implying a perimeter law for large spatial Wilson-loops. Rather, spatial Wilson-loops always exhibit area-law [49].

a firm connection with Eq. (1.10). Thus, $V_{q\bar{q}}^{\mathbf{1}} / V_{q\bar{q}}^{\mathbf{8}}$ can be physically understood as the free energy associated with introducing a $q\bar{q}$ pair into the system. On a technical note, the superscripts $\mathbf{1}$ and $\mathbf{8}$ account for pairing in either the colour singlet or octet states, viz.

$$\mathbf{3} \otimes \bar{\mathbf{3}} = \mathbf{1} \oplus \mathbf{8}. \quad (1.11)$$

Hence, the labelling $\mathbf{8}$ is proprietary to $\text{SU}(3)$; however, $\mathbf{8}$ should really be understood as $\mathbf{N}^2 - \mathbf{1}$ for $\text{SU}(N)$.

Due to the cluster decomposition property, at large separation

$$\langle L(r)L^\dagger(0) \rangle \rightarrow \langle L(r) \rangle \langle L^\dagger(0) \rangle. \quad (1.12)$$

Therefore, whether or not the one-point function $\langle L(r) \rangle$ vanishes distinguishes between the high temperature and low temperature forms of $V_{q\bar{q}}(r)$. When $\langle L(r) \rangle = 0$, the free energy associated with introducing a $q\bar{q}$ pair into the system and separating it to infinity is divergent.

The deconfining phase transition via a non-zero expectation value of $L(r)$ in a pure Yang-Mills theory is related to the breaking of centre⁴ symmetry of the gauge-group [39, 53]. Consider the action for pure $\text{SU}(N)$ Yang-Mills at finite temperature

$$S_{\text{YM}} = \int_0^\beta d\tau \int d^3x \frac{1}{2} \text{Tr} F^{\mu\nu} F_{\mu\nu}. \quad (1.13)$$

⁴ The centre of a group is defined as the set of elements which commute with all of the elements of the group.

In addition to the usual periodic local gauge transformation

$$F^{\mu\nu}(\tau, x) \rightarrow \Lambda^\dagger(\tau, x) F^{\mu\nu}(\tau, x) \Lambda(\tau, x) \quad (1.14)$$

with $\Lambda(\tau + \beta, x) = \Lambda(\tau, x)$ the action is also invariant under transformations where $\Lambda(\tau + \beta, x) = c^n \Lambda(\tau, x)$. For $SU(N)$, $c = e^{\frac{i2\pi}{N}}$ is an element of the group centre, which is isomorphic to the cyclic group Z_N . The Polyakov-loop (in the fundamental representation), on the other hand, is not invariant under these centre transformations, since we have $L(x) \rightarrow cL(x)$. Its non-zero expectation value serves as a true order parameter for the deconfinement phase transition. For $SU(3)$ this phase transition is first order [54], while for $SU(2)$ it is second order with Z_2 universality [55, 56]. There have been claims that for $N \geq 4$ the phase transition may revert to being second order [57]. However, numerical evidence reveals the contrary [58, 59, 60], in fact favouring a first order phase transition which strengthens with increasing N .

1.2.1 Phase transitions in non-abelian gauge theory with fermions

Consider what happens to adjoint Polyakov-loops, $L^{\text{adj.}}$ in the pure gauge theory. Under a centre symmetry transformation, $L^{\text{adj.}} \rightarrow cc^\dagger L^{\text{adj.}}$, so it is always invariant (this can be understood from Eq. (1.11)). In effect, $\langle L^{\text{adj.}}(r) \rangle \neq 0$, which at low temperature has the interpretation that if adjoint charges are sufficiently separated, gluons will appear out of the vacuum and form colour singlet glueballs. This is possible in $SU(3)$ because adjoint matter is in the **8** representation and the product

$$\mathbf{8} \otimes \mathbf{8} = \mathbf{1} \oplus \mathbf{8} \oplus \mathbf{8} \oplus \overline{\mathbf{10}} \oplus \mathbf{10} \oplus \mathbf{27} \quad (1.15)$$

contains a singlet. For general N , the product of two adjoint representations always contains the singlet.

Consequentially, in QCD where dynamical quarks in the fundamental representation are present, $\langle L \rangle$ cannot be an exact order parameter for the confinement / deconfinement phase transition. In fact, the presence of fermions in the QCD Lagrangian explicitly breaks the Z_N symmetry. The potential between two quarks rises linearly, up to the point where there is sufficient energy to form a $q\bar{q}$ pair out of the vacuum.

This does not necessarily mean that the deconfinement phase transition does not occur with *heavy* quarks present. For $N = 3$ (where the deconfinement transition is first order), sufficiently heavy quarks $m_q \gg \Lambda_{\text{QCD}}$ enter as a perturbation which weakens the strength of the phase transition [61]. In this case, the Polyakov-loop is an approximate order parameter, which still exhibits a discontinuity at the phase boundary [62]. However, the deconfinement phase transition for $N = 2$ as it is second order can only persist in the limit $m_q \rightarrow \infty$, where the Z_N symmetry is exact. Moreover, in nature where there are *light* quarks (relative to the scale Λ_{QCD}) this heavy quark limit is not physically realized [63, 64].

In spite of the explicit breaking of centre symmetry, on the other end of the spectrum with *light* quarks present it is possible to have a phase transition resulting from the high temperature approximate restoration of chiral symmetry [15, 16]. Then, the order parameter (in the massless limit) is not the Polyakov-loop, but

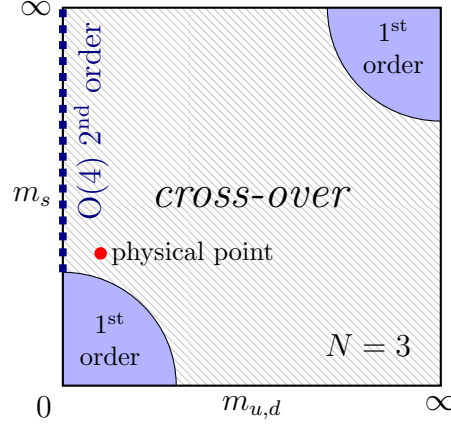


Figure 1–1: Schematic depiction of the Columbia Plot [65], which illustrates the quark mass dependence of the QCD phase transition at vanishing chemical potential with $N_f = 3$ and $m_u = m_d$. The generic features depicted are the first order phase transitions in the chiral (bottom left) and pure $N = 3$ Yang-Mills (top right) limits, with a cross-over region in between. Additionally, the $O(4)$ second order phase transition with massless up / down quarks and a heavy strange quark is indicated along the left-most axis. The plot is not to scale, but the physical point in the cross-over region is depicted as being “close” to the chiral first order region, since the possibility of a first order phase transition in nature has been considered.

rather the chiral condensate $\langle \bar{\psi}(1 + \gamma_5)\psi \rangle$. Chiral symmetry breaking is well beyond the scope of this work, so the remainder of this section is devoted to commenting on the contrast between the situation in pure Yang-Mills with that in

QCD. Though Z_3 symmetry is not present, the QCD Lagrangian with N_f massless quarks possesses and $SU(N_f) \otimes SU(N_f)$ flavour symmetry⁵ (vector and axial-vector rotations on the massless flavours). Chiral symmetry breaking is expressed as $SU(N_f) \otimes SU(N_f) \rightarrow SU(N_f)$, yielding a multiplet of massless Goldstone bosons.

For models with an initial $SU(2) \otimes SU(2)$ symmetry, the chiral phase transition is second order with $O(4)$ universality. However, when that symmetry is $SU(3) \otimes SU(3)$ the transition is first order [33]. The question is, does nature with three light quarks (defined as $m_q \ll \Lambda_{\text{QCD}}$) approximately resemble either of these cases? The $O(4)$ second order phase transition could not be realized in nature with any finite quark masses. However, since the $N_f = 3$ phase transition is first order, it will continue to be first order even if it is perturbed by small non-zero quark masses. So, it would be seemingly possible to have a first order phase transition in nature, except that it is not clear that the assumption $m_s \ll \Lambda_{\text{QCD}}$ holds for the physical value $m_s \sim 100$ MeV, see Figure 1–1. Therefore, in this simplified model there are two possible scenarios for the QCD phase transition at zero chemical potential (corresponding to the location of the “physical point” in Fig. 1–1)

- the strange quark is indeed “light” (automatically so are the up and down quarks). Then the $N_f = 3$ massless case is approximately realized and the first order phase transition survives in nature.

⁵ There are additional vector and axial $U(1)$ factors which we have not written; the axial $U(1)$ is anomalous and the vector $U(1)$ is associated with baryon number conservation.

- The strange quark is “heavy,” meaning that the $N_f = 3$ massless case is not a good approximation. Since a second order $O(4)$ phase transition is not possible with any finite up / down masses, there is a cross-over.

From a theoretical standpoint, the lattice has confirmed that at vanishing chemical potential a cross-over occurs [7]. Hence there is not a true phase transition, and nature more closely resembles the second of these two idealized scenarios above. Recently published values of the cross-over temperature tend to lie in the approximate range $T_c \sim 150 - 175$ GeV [11, 12]. Variation in the theoretical estimates is primarily due to different observables yielding different values of T_c (e.g. Polyakov-loop susceptibility vs. chiral susceptibility).

1.2.2 Phase transitions in non-abelian gauge theory with scalars

Electroweak theory is similar to QCD in that it is a non-abelian gauge theory coupled to fermions (except with an $SU(2)$ gauge group instead of $SU(3)$ and chiral couplings). It can also undergo a phase transition, characterized by the symmetry breaking [66]

$$SU(2)_L \otimes U(1)_Y \rightarrow U(1)_{EM}. \quad (1.16)$$

However, unlike in QCD, this phase transition (or cross-over) is mediated by a scalar field, namely the Higgs boson [67, 68, 69]. This is often explained as an $SU(2)_L \otimes U(1)_Y$ gauge symmetry that is “spontaneously broken” down to the electromagnetic $U(1)_{EM}$ that is observed in nature at low energies [70]. Some may object to this statement, on the grounds that the notion of spontaneous breaking of gauge-symmetry is inherently gauge-dependent, and hence unphysical [71]. However, for a non-abelian gauge theory coupled to a scalar field, over a certain range of the

model parameters there *is* a first order phase boundary between a high temperature symmetric phase with charge screening (analogous to QGP) and a low temperature Higgs phase [72, 73, 74]. In this regime, we can distinguish between the two phases via the discontinuities in thermodynamic variables at the phase boundary.

Therefore, a more precise statement is that electroweak theory possesses a phase diagram on the temperature - Higgs mass⁶ plane. And in fact, a broader statement is that $SU(N)$ gauge theories coupled to scalars in representation R will possess non-trivial phase diagrams (see [76]), which continues to be the case in three dimensions. Lattice based studies of 3D effective models of electroweak theory have demonstrated that high and low temperature phases are separated by a first order phase transition which terminates at a critical end point [77]. These studies have further shown that at physical values of the Higgs mass the electroweak “phase-transition” is in fact a cross-over.

The characteristic scale of electroweak interactions is $G_F^{-1/2} \sim 293$ GeV (several orders of magnitude greater than Λ_{QCD}). Since electroweak theory is non-abelian, there is an additional scale denoted as $\Lambda_{\text{SU}(2)}$ which is associated with confinement in the pure $SU(2)$ gauge theory. What makes the QCD phase transition (or cross-over) different from the electroweak phase transition (or cross-over) is that $T_{\text{EW}}^c \sim \mathcal{O}(G_F^{-1/2}) \gg \Lambda_{\text{SU}(2)}$ while in QCD, $T_{\text{QCD}}^c \sim \Lambda_{\text{QCD}}$. At T_{EW}^c the electroweak coupling

⁶ The electroweak phase diagram is also parametrized by the Weinberg angle; however, in the construction of certain effective models it is a reasonable approximation to set it to zero, in effect decoupling the $U(1)$ group [75].

is still “weak,” $g_{\text{EW}} \sim 2/3$; that is, the transition cuts off the growth of the coupling into the IR.⁷

The Higgs phase in electroweak theory is interesting in that it is analytically connected with a low-energy confining phase [72, 79] which would be realized if $T_{\text{EW}}^c \sim \Lambda_{\text{SU}(2)}$ (as in QCD). In this phase, the physical spectrum is described by gauge-invariant SU(2) singlet operators e.g. $W_0 = \text{Tr } \Phi^\dagger \Phi$ and $W_\mu = \text{Tr } \Phi^\dagger D_\mu \Phi \tau^i$ (with the complex scalar field Φ expressed as a 2×2 matrix).

Even though a gauge-invariant order parameter cannot be defined for the electroweak phase transition, high and low temperature phases can still be distinguished non-perturbatively by gauge-invariant condensates and their associated susceptibilities [80]. Furthermore, these condensates would also resolve the cross-over over the range of model parameters where it occurs, i.e. at physical values of the Higgs mass. That being said, a lot can still be learned by applying a perturbative treatment of the Higgs phase, which requires working in a fixed gauge. Then, perturbatively one argues that the Higgs phase coincides with the scalar field taking on a non-zero vacuum expectation value (VEV). The topic of gauge-fixing happens to be the focus of the next section; since the definition of a VEV is dependent upon the gauge-fixing procedure, we will come back to the perturbative treatment of the Higgs phase in Section 1.3.2.

⁷ This should not be interpreted as an implication that perturbation theory can be applied in the vicinity of the phase transition. The critical end point, in fact, must be resolved non-perturbatively; this has motivated a lattice determination of its location (as in [77]; see also [78]).

1.3 Gauge-invariance and gauge-fixing

Now that we have started to discuss the potential significance of gauge dependent quantities (i.e. the vacuum expectation value of a scalar field coupled to gauge fields), this is good place to introduce gauge-fixing, both in pure Yang-Mills and Yang-Mills with scalars. An overview of the concepts of gauge-freedom and gauge-fixing can be found in virtually every introductory quantum field theory textbook (see for instance [81, 82]). As a consequence, the discussion that follows will be for the most part review. However, since covariant gauge-fixing plays an essential role in the calculations performed in Chapters 3 and 4, this section is included for completeness. Additionally, since Chapter 4 involves the non-perturbative study of a gauge theory in a symmetry broken, or “Higgs” phase, this is also appropriate place to give an overview of spontaneous breaking of gauge-symmetry at the perturbative level.

The starting point is the path-integral (where to be consistent with the calculations later in this work, a Euclidean convention is being adopted)

$$Z = \int D[\Phi] e^{-S}. \quad (1.17)$$

For a non-abelian gauge theory coupled to matter fields, the action in D dimensions can be written as

$$S = \int d^D x (\mathcal{L}_{\text{YM}} + \mathcal{L}_{\text{M}}) \quad (1.18)$$

where \mathcal{L}_{YM} and \mathcal{L}_{M} represent the pure Yang-Mills and matter field (fermion and/or scalar) contributions. The path integral measure $D[\Phi]$ uses the generic label Φ to indicate integration over all of the fields present in S . Let us now suppose that

we have an $SU(N)$ gauge theory coupled to a complex scalar ϕ in the fundamental representation. The Lagrangian is

$$\mathcal{L}_{\text{YM}} = \frac{1}{2} \text{Tr } F^{\mu\nu} F_{\mu\nu} \quad (1.19)$$

$$\mathcal{L}_{\text{M}} = (D^\mu \phi)^\dagger (D_\mu \phi) + m^2 \phi^\dagger \phi + \frac{\lambda}{2} (\phi^\dagger \phi)^2. \quad (1.20)$$

The Yang-Mills field strength and gauge fields can be expressed as elements of the Lie algebra of $SU(N)$, $F_{\mu\nu} = F_{\mu\nu}^a T^a$ and $A_\mu = A_\mu^a T^a$, where T^a are $N \times N$ traceless Hermitian generators that are defined to satisfy the normalization $\text{Tr } T^a T^b = \delta^{ab}/2$. A local gauge transformation on the gauge and scalar fields takes the form

$$A_\mu(x) \rightarrow \Lambda(x) \left(A_\mu(x) + \frac{i}{g} \partial_\mu \right) \Lambda^\dagger(x) \quad (1.21)$$

$$\phi(x) \rightarrow \Lambda(x) \phi(x) \quad (1.22)$$

where $\Lambda(x)$ is an arbitrary matrix in $SU(N)$

$$\Lambda(x) = e^{-ig\theta^a(x)T^a}. \quad (1.23)$$

A gauge transformation acts on the Yang-Mills field strength and covariant derivatives like a rotation,

$$F_{\mu\nu}(x) \rightarrow \Lambda(x) F_{\mu\nu}(x) \Lambda^\dagger(x) \quad (1.24)$$

$$D_\mu(x) \rightarrow \Lambda(x) D_\mu(x) \Lambda^\dagger(x); \quad (1.25)$$

from these expressions it is apparent that S is gauge-invariant. In other words, the theory possesses a non-abelian gauge freedom. A well known consequence is that a mass term of the form $\text{Tr } A_\mu A^\mu$ would not be allowed in S .

Physical observables cannot be affected by gauge-transformations of the type Eq. (1.21). Since the operators from which S is constructed are individually gauge-dependent, they do not have a one to one correspondence with the physical spectrum.⁸ Rather, observables must correspond with gauge-invariant operators; for instance the correlators

$$\langle \text{Tr } F^{\mu\nu}(x) F_{\mu\nu}(x) \rangle \quad (1.26)$$

$$\langle \text{Tr} \{ F^{\mu\nu} F_{\mu\nu}(x) \} \text{Tr} \{ F^{\alpha\beta} F_{\alpha\beta}(y) \} \rangle \quad (1.27)$$

are indeed physical. Eq. (1.26) is the gluon condensate, and the long-range exponential fall-off of Eq. (1.27) tells us about the mass of the lightest P-even C-even spin 0 bound state. Recall from Section 1.1 that in QED, due to the abelian nature of gauge-transformations, the field strength tensor is gauge-invariant; QED is special in this regard. Its components are identified with physical electric and magnetic fields. By contrast, in a more general non-abelian theory the would-be correlator of colour-electric or colour-magnetic fields

$$\langle \text{Tr } F_{\alpha\beta}(x) F_{\delta\gamma}(y) \rangle \quad (1.28)$$

⁸ In the sense that the mapping of gauge-dependent fields to the physical degrees of freedom is not injective.

is unphysical, as it transforms non-trivially under Eq. (1.21). A “physical” version of Eq. (1.28) can be constructed with the inclusion of Wilson lines,

$$U(x, y) = \mathcal{P} e^{ig \int_{\mathcal{C}} dx^\mu A_\mu(x)} \quad (1.29)$$

where the path \mathcal{C} connects the points x and y . Then,

$$\langle \text{Tr } F_{\alpha\beta}(x) U(x, y) F_{\delta\gamma}(y) U^\dagger(x, y) \rangle \quad (1.30)$$

is gauge-invariant. Field-strength correlators of the form Eq. (1.30) are important in the study of QCD in that they reveal information about the non-perturbative structure of the vacuum and confinement [83].

In performing the path integral, gauge-equivalent configurations are summed over by the measure $D[\Phi]$. Accordingly, gauge-freedom manifests itself in the path-integral as a divergent over-counting with respect to the physical degrees of freedom. However, the resulting divergence in Z is not in and of itself a problem. If we were interested in the expectation value of a gauge-invariant operator \mathcal{O} , its expression as a path integral would formally read

$$\langle \mathcal{O}_{ij\dots}(x_i, x_j, \dots) \rangle = \frac{\int D[\Phi] \mathcal{O}_{ij\dots}(x_i, x_j, \dots) e^{-S}}{\int D[\Phi] e^{-S}}. \quad (1.31)$$

The over-counting occurs both in the numerator and the denominator, hence in simply writing down Eq. (1.31), gauge-fixing is not required. To actually compute a correlation function viz. Eq. (1.31) we would need to adopt some form of regularization. One option is the lattice. The lattice formulation of Z and Eq. (1.31) involves a functional integration over a finite number of link variables. This does not stop

the lattice from sampling over gauge-equivalent configurations indiscriminately, but due to the discretized spacetime, the overall normalization is finite. Hence the lattice is naturally equipped to deal with the associated redundancy, due to the inherent absence of a divergence in Z .

1.3.1 Covariant gauges

Summing over the gauge-freedom becomes a problem when we try to perform perturbation theory, which is where we first encounter a necessity to fix a gauge. Looking back at the action Eq. (1.18), the kinetic term for the A -field in momentum-space reads

$$S \sim \int \frac{d^D p}{(2\pi)^D} \frac{1}{2} A_\mu^a(-p) (p^2 g^{\mu\nu} - p^\mu p^\nu) A_\nu^a(p). \quad (1.32)$$

If we were to naively identify $G_{\mu\nu}^{-1}(p) = p^2 g^{\mu\nu} - p^\mu p^\nu$, we would immediately run into a problem since $G_{\mu\nu}^{-1}$ is strictly transverse, and hence, not invertible. Consequentially, the path integral sum over purely longitudinal configurations is undamped, leading to the aforementioned divergence in Z . We can remedy the situation by working in what is known as covariant gauge, which is actually a family of gauge-choices parametrized by a number ξ . This leads to the well known tree-level expression for the *invertible* gauge field propagator

$$G_{\mu\nu}^{-1}(p) = p^2 g^{\mu\nu} - p^\mu p^\nu + \frac{1}{\xi} p^\mu p^\nu \longrightarrow G_{\mu\nu}(p) = \frac{1}{p^2} \left(g^{\mu\nu} - (1 - \xi) \frac{p^\mu p^\nu}{p^2} \right), \quad (1.33)$$

where $G_{\mu\nu}$ is assumed to be diagonal in colour indices. To show how this expression comes about we will now go over the steps that are taken in fixing a gauge.

Going back to the path integral, the first thing that we want to accomplish is factoring out the redundant integration over gauge-orbits so that the path integral

to takes on the general form

$$\int D[\Phi] \longrightarrow \int D\theta \int D[\Phi_\theta]. \quad (1.34)$$

Since we initially parametrized the gauge-transformation matrix Λ by the functions $\theta^a(x)$, the integral over the gauge-freedom is denoted by $\int D\theta$. This should really be understood as an integral over the group measure of $SU(N)$. Then $\int D[\Phi_\theta]$ indicates the remaining path integral restricted to physical configurations, i.e. those which by definition intersect each gauge-orbit only once. If we reconsider the generic gauge-invariant correlation function that we had written down previously, we now have

$$\langle \mathcal{O}_{ij\dots}(x_i, x_j, \dots) \rangle = \frac{\int D[\Phi_\theta] \mathcal{O}_{ij\dots}(x_i, x_j, \dots) e^{-S}}{\int D[\Phi_\theta] e^{-S}}. \quad (1.35)$$

In the gauge-fixed setting its value is unaffected since both \mathcal{O} and S are constant on each orbit. However, if in fact the operator $\mathcal{O}_{ij\dots}(x_i, x_j, \dots)$ transformed non-trivially (i.e. was θ -dependent), then the integral over the gauge-orbit would not factor out entirely. Rather, we would be integrating an object that transforms in the non-singlet representation of $SU(N)$ over the group manifold; this is an integral that must vanish. This reiterates the utility of gauge-fixing as a computational tool.

The factorization in Eq. (1.34) can be achieved by specifying a function $\mathcal{G}[A]$ so that the condition $\mathcal{G}[A] = 0$ occurs in principle once per gauge-orbit. This is known as an ideal or complete gauge-fixing. For covariant gauges, the defining function is

$$\mathcal{G}[A] = \partial^\mu A_\mu(x) - g(x) \quad (1.36)$$

where we will assume for now that $g(x) = g^a(x)T^a$ is arbitrary. The specific case $g(x) = 0$ would result in an implementation of Landau gauge. It has been pointed out that Eq. (1.36) does not in fact result in a complete gauge-fixing, in that this condition does not have a unique intersection with each orbit [84]. These redundant configurations are known as Gribov copies, and they occur at non-perturbatively large values of A . Since perturbation theory relies on an expansion about the tree level minimum $A = 0$, it is safe to proceed in covariant gauge as though it was in fact complete [85].

The gauge-fixing is implemented via the Faddeev-Popov trick [86], which amounts to picking out a particular configuration on each gauge-orbit by inserting a δ -functional in the path integral. For a continuous function of one variable $f(x)$ with one zero at $x = x_0$, we have

$$1 = \int dx \delta(x - x_0) = \int dx |f'(x_0)| \delta(f(x)). \quad (1.37)$$

The generalization to the infinite variable case involves a functional determinant

$$\int D[\Phi] \longrightarrow \int D\theta \int D[\Phi] \det \left| \frac{\delta \mathcal{G}}{\delta \theta} \right|_{\mathcal{G}=0} \prod_a \delta(\mathcal{G}^a[A]), \quad (1.38)$$

with the derivative evaluated at the specific point on the gauge-orbit A_θ which satisfies the gauge condition, i.e. $\mathcal{G}[A_\theta] = 0$. The result is

$$\frac{\delta \mathcal{G}}{\delta \theta} = -\partial^\mu (\partial_\mu - ig A_{\theta\mu}^a F^a), \quad (1.39)$$

which should be understood as a $d_A \times d_A$ matrix (for $\text{SU}(N)$, $d_A = N^2 - 1$); $F_{bc}^a = -if^{abc}$ are the generators of the adjoint representation. Upon inserting Eq. (1.39)

back into the path integral we can drop the explicit dependence on θ since the desired representative from each gauge-orbit is guaranteed to be picked out by the δ -functional. Said differently, with the δ -functional present, the measure $D[\Phi]$ can continue to sum over fields indiscriminately.

The determinant can be re-expressed as a path-integral over adjoint Grassmann fields,

$$\det \left| \frac{\delta \mathcal{G}}{\delta \theta} \right| = \int Dc D\bar{c} e^{-\int d^D x \bar{c}(x) [\delta \mathcal{G} / \delta \theta](x) c(x)}, \quad (1.40)$$

with an appropriate overall normalization implied. The δ -functional is eliminated by introducing an additional normalized path-integral

$$1 = \int Dg e^{-\int d^D x \frac{1}{2\xi} g^a(x) g^a(x)} \quad (1.41)$$

so that our final expression for Z reads

$$Z = \left[\int D\theta \right] \int Dc D\bar{c} D[\Phi] e^{-S_g}. \quad (1.42)$$

As a result of the gauge-fixing procedure, S_g contains the original invariant action of the theory as well as additional “gauge-fixing” and “ghost” terms

$$S_g = S + \int d^D x \frac{1}{2\xi} (\partial^\mu A_\mu^a)^2 + \partial^\mu \bar{c} D_\mu^{\text{adj}} c. \quad (1.43)$$

In Eq. (1.42) it should be understood that the redundant integration over the gauge-orbits has now been completely factored out.

The Gaussian term which was included in the final step of the derivation effectively performs a weighted average over gauge configurations, with a weight given by ξ . This term directly leads to a damping of longitudinal modes, and thus, by taking

the limit $\xi \rightarrow 0$ (Landau gauge) we strictly enforce the gauge condition $\partial^\mu A_\mu = 0$. However, for non-zero values of ξ the Gaussian damping term appears alongside the gauge field kinetic term

$$\int d^D x \frac{1}{2\xi} g^a(x) g^a(x) \sim \int \frac{d^D p}{(2\pi)^D} \frac{1}{2\xi} A_\mu^a(-p) p^\mu p^\nu A_\nu^a(p). \quad (1.44)$$

This precisely generates the longitudinal term in the tree-level propagator that was introduced earlier. The gluon propagator has been rendered invertible.

The Feynman rules for perturbation theory in covariant gauge must be read from the action S_g with a value of ξ chosen arbitrarily. In vacuum perturbation theory, a common choice is Feynman gauge $\xi = 1$, a choice which drastically simplifies higher loop calculation due to the resulting simple form of $G_{\mu\nu}$. Interactions between ghosts and gluons must be properly accounted for at all values of ξ , and since the ghost fields \bar{c} and c obey Grassman statistics, their loops enter with relative minus signs. The appearance of ghost fields is a generic feature of gauge-fixing, as they arise from the determinant that appeared alongside the δ -functional.

To recap, gauge-fixing was introduced to facilitate perturbative calculations (it is not required on the lattice), so that one should opt to work in a gauge which leads to tractable expressions for scattering amplitudes. In the study non-abelian gauge theory in vacuum, covariant gauges have many desirable properties in this regard. However, gauge-freedom implies that this choice is arbitrary.

1.3.2 Generalized R_ξ gauge

Switching over to a model of a non-abelian gauge theory coupled to a scalar field, the matter contribution to the action is

$$S_M = (D^\mu \phi)^\dagger (D_\mu \phi) + m^2 \phi^\dagger \phi + \frac{\lambda}{2} (\phi^\dagger \phi)^2. \quad (1.45)$$

Supposing that we were in a situation where λ is positive, but the tree-level squared mass is negative. The potential would still be bounded from below due to the quartic term, but it would no longer reach its minimum at $\phi = 0$. Rather, the perturbative ground-state would occur when the vector ϕ has a non-zero magnitude $|\phi| = \bar{\phi}$. Choosing a direction for ϕ results in spontaneous symmetry breaking and the quantity $\bar{\phi}$ is the magnitude of the scalar field VEV.

If gauge fields were absent, Eq. (1.45) would be the Lagrangian of an $O(2N)$ symmetric model. In this case, a scalar field VEV would be a physical quantity, as it would be an order parameter. However, with gauge fields present, we have run into a contradiction; the statement $|\phi| = \bar{\phi} > 0$ suggests a non-zero one-point function $\langle \phi \rangle$. But then, the operator ϕ transforms non-trivially under gauge-transformations $\phi \rightarrow \Lambda \phi$; we argued earlier that its expectation value necessarily vanishes. Rather, in a gauge theory a constant scalar VEV should be understood as a gauge-choice [87]. It is not a physical quantity, as it cannot be defined in a gauge-invariant manner.

To do perturbation theory one must define a VEV, because perturbation theory requires expanding fields around their classical minima. For example, the computation of perturbative corrections to scattering amplitudes in the Standard Model assumes a VEV for the Higgs field. In this situation, however, it turns out that the

covariant gauges introduced previously are not the best option. This leads to the definition of “generalized” covariant, or R_ξ gauges [88].

In an $SU(N)$ gauge theory, a scalar field in representation R can be written as a complex d_R -component column vector. To specify a VEV, we can shift the scalar field by a constant

$$\phi(x) \rightarrow \chi(x) + v \quad (1.46)$$

so that the gauge-fixed one-point functions are $\langle \phi(x) \rangle = v$ and $\langle \chi(x) \rangle = 0$. The gauge fields interact with ϕ via the covariant derivative (with T_R^a now denoting a generator of representation R), resulting in

$$D_\mu \phi(x) \rightarrow D_\mu \chi(x) - ig A_\mu^a(x) T_R^a v. \quad (1.47)$$

We will now adopt the notation $\mathcal{F}^a = g T_R^a v$; this is a quantity that is closely related to the gauge-boson masses. If $\mathcal{F}^a \neq 0$, the corresponding generator is said to be broken. For example, with a fundamental scalar in $SU(2)$, the defining representation is

$$T^1 = \frac{1}{2} \begin{pmatrix} 0 & 1 \\ 1 & 0 \end{pmatrix} \quad T^2 = \frac{1}{2} \begin{pmatrix} 0 & -i \\ i & 0 \end{pmatrix} \quad T^3 = \frac{1}{2} \begin{pmatrix} 1 & 0 \\ 0 & -1 \end{pmatrix}. \quad (1.48)$$

All three generators are guaranteed to be broken for any orientation of v . However, in $SU(3)$, if we perform a global rotation on the fields resulting in the alignment $v^\dagger = (0, 0, \bar{\phi})$, then the generators

$$T^1 = \frac{1}{2} \begin{pmatrix} 0 & 1 & 0 \\ 1 & 0 & 0 \\ 0 & 0 & 0 \end{pmatrix} \quad T^2 = \frac{1}{2} \begin{pmatrix} 0 & -i & 0 \\ i & 0 & 0 \\ 0 & 0 & 0 \end{pmatrix} \quad T^3 = \frac{1}{2} \begin{pmatrix} 1 & 0 & 0 \\ 0 & -1 & 0 \\ 0 & 0 & 0 \end{pmatrix} \quad (1.49)$$

survive, so that we are left with an SU(2) invariant subgroup. In this example, the three corresponding gauge-bosons remain massless. In terms of \mathcal{F}^a the gauge field mass-matrix is given by

$$\mathcal{M}_{ab}^2 = (\mathcal{F}^{\dagger b} \mathcal{F}^a + \mathcal{F}^{\dagger a} \mathcal{F}^b) = v^\dagger \{T_R^a, T_R^b\} v, \quad (1.50)$$

which arises out of the expansion of the original kinetic term

$$(D^\mu \phi)^\dagger (D_\mu \phi) \rightarrow (D^\mu \chi)^\dagger (D_\mu \chi) - A_\mu^a \partial^\mu i(\chi^\dagger \mathcal{F}^a - \mathcal{F}^{\dagger a} \chi) + \frac{1}{2} \mathcal{M}_{ab}^2 A^{a\mu} A_\mu^b. \quad (1.51)$$

In Eq. (1.51) there is now a potentially troublesome gauge field scalar cross term. To see how it is eliminated, recall that we had already assumed gauge-fixing. As a result, our full Lagrangian is of the form

$$\mathcal{L}_g = \mathcal{L}_{\text{YM}} + \mathcal{L}_{\text{M}} + \frac{1}{2\xi} g^a g^a + \bar{c} \frac{\delta \mathcal{G}}{\delta \theta} c. \quad (1.52)$$

The covariant gauges that we had presented earlier resulted from the simple choice $\mathcal{G}^a[A] = \partial^\mu A_\mu^a - g^a$. However, with scalars present, the cross-term can be eliminated with the choice

$$\mathcal{G}^a = \partial^\mu A_\mu^a - \xi i(\chi^\dagger \mathcal{F}^a - \mathcal{F}^{\dagger a} \chi) - g^a. \quad (1.53)$$

As a result, an explicitly gauge-dependent mass term and ghost-scalar interactions will appear in the ghost Lagrangian,

$$\mathcal{L}_{\text{ghost}} = \bar{c} \frac{\delta \mathcal{G}}{\delta \theta} c = \bar{c} \partial_\mu D_\mu^{\text{adj}} c + g\xi \mathcal{M}_{ab}^2 \bar{c}^a c^b + g\xi (\chi^\dagger T_R^b \mathcal{F}^a + \mathcal{F}^{\dagger a} T_R^b \chi) \bar{c}^a c^b. \quad (1.54)$$

The gauge field and ghost mass matrices are identical up to an overall factor of ξ . Thus, the same change of basis which diagonalizes the gauge fields also diagonalizes the ghosts.

At this point without having specified N or the representation of the scalar field the perturbative spectrum is difficult to read directly from the Lagrangian. This is mainly due to the fact that the Lie algebra of $SU(N)$ is not closed under anti-commutation of the generators (see Appendix A); a generic expression for \mathcal{M}_{ab}^2 is not very helpful in this regard. However, as a general remark, the Feynman rules will consist of gauge-scalar, gauge-ghost and ghost-scalar vertices.

The limit $\xi \rightarrow 0$, which in R_ξ is equivalent to covariant Landau gauge with a VEV, offers drastic simplification in that the ghosts remain massless and the ghost-scalar interactions vanish. Then, in R_ξ “Landau gauge” the perturbative spectrum is given by a combination of massless and massive scalar and gauge fields (the number of each depending on which linearly independent generators are broken) as well as massless ghosts. The opposite limit $\xi \rightarrow \infty$ (unitary gauge) yields a different spectrum in which fields with masses proportional to ξ decouple from the gauge fields. According to Eq. (1.53), this includes the scalar Goldstone modes associated with the symmetry breaking. The point is that the perturbative spectrum is gauge-dependent. As in the symmetric phase, the operators in S_g do not directly correspond to the observed particles and resonances in nature.

1.4 Thermal Yang-Mills

The study of phase transitions in a quantum field theory necessitates a set of computational tools which can be applied at finite temperature [89]. One of these

tools is dimensional reduction [36, 37], which provides a systematic procedure of mapping a hot 4D field theory to a 3D Euclidean field theory in vacuum. For the most part, computations at finite temperature are not directly performed in this work as we are primarily interested in the 3D effective models. The purpose of this section rather is to provide a conceptual overview of finite temperature Yang-Mills theory leading to the construction of its effective description at high temperatures.

We know from statistical mechanics that static quantities such as the pressure and entropy density of a system that is in thermal equilibrium can be derived from the partition function

$$Z = \text{Tr}\{\rho(\beta)\} \quad (1.55)$$

where $\rho(\beta) = e^{-\beta(\hat{H} - \mu_i \hat{N}_i)}$ is the thermal density operator and $\beta = 1/T$ is the inverse temperature. An important associated quantity is the free energy, $F = -T \log Z$, which carries all of the information about the system's state. The density matrix $\rho(\beta)/Z$ also appears explicitly in the expression for the thermal average of an operator $\langle \cdot \rangle_\beta$,

$$\langle \mathcal{O} \rangle_\beta = \frac{1}{Z} \text{Tr}\{\mathcal{O} \rho(\beta)\}. \quad (1.56)$$

As written, $\rho(\beta)$ takes the form of an evolution operator in imaginary time $t = -i\beta$. This observation forms the basis of the imaginary time formalism (ITF), in which static thermal correlation functions are obtained from a Euclidean path integral

$$Z = \int D[\Phi] e^{-\int_0^\beta d\tau \int d^{D-1}x \mathcal{L}(\tau, x)}, \quad (1.57)$$

that is, the path integral representation of the partition function. The fields in \mathcal{L} are evaluated on a compact dimension and must satisfy the following periodicity conditions,

$$\begin{aligned} \text{Bosons:} \quad \phi(0, x) &= \phi(\beta, x) \\ \text{Fermions:} \quad \psi(0, x) &= -\psi(\beta, x). \end{aligned} \tag{1.58}$$

One final remark is that the free energy, as it is proportional to the logarithm of Z , is the finite temperature analogue of the generating function of connected correlators in vacuum.

As a consequence of the compactness of the Euclidean time dimension, the fields in \mathcal{L} have discrete expansions in Matsubara modes indexed by an integer n

$$\phi(\tau, x) = \sum_{\omega_n} \phi_n(x) e^{i\omega_n \tau} \quad \omega_n = 2\pi n T \tag{1.59}$$

$$\psi(\tau, x) = \sum_{\nu_n} \psi_n(x) e^{i\nu_n \tau} \quad \nu_n = 2\pi \left(n + \frac{1}{2}\right) T. \tag{1.60}$$

As in vacuum, these Matsubara frequencies appear in the bosonic and fermionic propagators alongside the tree-level masses

$$G_\phi(\omega, \mathbf{p}) = \frac{1}{k^2 + \omega_n^2 + m_\phi^2} \tag{1.61}$$

$$G_\psi(\omega, \mathbf{p}) = \frac{m_\psi - \mathbf{p} \cdot \boldsymbol{\gamma} - \gamma_E^0 \nu_n}{p^2 + \nu_n^2 + m_\psi^2}, \tag{1.62}$$

where $p^2 = \mathbf{p} \cdot \mathbf{p}$. From the mode expansions Eq. (1.59) and Eq. (1.60), we can now visualize a 4D thermal field theory in the IFT as a 3D Euclidean vacuum field theory with an infinite number of fields. These fields have masses of the form $\omega_n^2 + m_\phi^2$ (bosons) / $\nu_n^2 + m_\psi^2$ (fermions).

Potentially massless bosonic $n = 0$ modes may lead to IR divergences in a perturbative expansion; this prompts us to adopt a nomenclature where bosonic 0-modes are “light,” while non-zero bosonic and all fermionic modes are “heavy.” In certain circumstances, there is an effective decoupling between heavy and light modes; when this is the case it is possible to integrate out the heavy modes all together.⁹ The result would then be a 3D *effective* field theory with a *finite* number of fields and non-renormalizable interactions. This is the essence of dimensional reduction.

Despite the potential for IR divergences, thermal non-abelian gauge theory still admits a weak-coupling expansion. At finite temperature, one is able to compute the leading order correction to the Debye mass [90, 91]

$$m_D = \sqrt{\frac{N}{3} + \frac{N_f}{6}} gT, \quad (1.63)$$

for an $SU(N)$ gauge theory with N_f fermions. IR problems only arise if we try to apply the perturbative treatment at NLO; for m_D , the best that can be done perturbatively is a determination of the coefficient at $\mathcal{O}(g^2 T \log(1/g))$ [92, 93].

The same calculation also reveals that at leading order static magnetic fields are unscreened. In QED, this statement would remain accurate to all orders in perturbation theory [94]. However, in QCD, the infrared divergences which appear at NLO indicate a failure of the perturbative expansion. A transverse screening

⁹ However, see Section 1.4.1; this statement is intuitive but not entirely accurate.

mass¹⁰ is an entirely non-perturbative effect, and it is conjectured to occur at [14]

$$m_T = \mathcal{O}(g^2 T). \quad (1.64)$$

For this reason, computing the full $\mathcal{O}(g^2 T)$ correction to m_D also happens to be beyond perturbation theory. The scale $g^2 T$ associated with magnetic screening is known as the supersoft scale, and at length scales $1/g^2 T \gg 1/gT$, non-perturbative physics become dominant. The infrared divergences present in 4D continue to be present in the 3D effective model obtained via dimensional reduction. Therefore, 3D effective theories of this sort provide a suitable framework to essentially isolate and study the non-perturbative physics. The lattice is well-equipped to investigate IR phenomena, and the construction of an effective description offers the advantage that 3D Euclidean effective field theories are generically easier to implement on the lattice over their 4D counterparts [80]. The lattice, for instance, can be used to determine the $\mathcal{O}(g^2 T)$ correction to m_D [95].

1.4.1 3D effective models

As previously remarked, the construction of a three dimensional effective description of Yang-Mills theory begins with the observation that non-zero Matsubara modes (fermionic and vector) are massive compared to the soft scales of the theory. To illustrate the concept, let us suppose that we are interested in studying correlations functions at some length scale l , or alternatively momentum $p \sim 1/l$.

¹⁰ A transverse screening mass should be understood in the sense that long range correlations in the magnetic sector do not occur [51].

Contributions arising from the summation over non-zero modes can be formally expressed in a power series of the dimensionless ratio p^2/T^2 ; in a Green's function these naturally appear alongside other terms involving other mass scales present in the theory. In an effective theory, p^2/T^2 contributions manifest themselves as higher derivative operators. If the scale of interest is $p \sim T$, then these terms are $\mathcal{O}(1)$, at which point it does not make sense to speak in terms of a “low energy” effective model.

At weak coupling, which for simplicity¹¹ we define as $g^2 \ll 1$, the electric field screening scale is $m_D \sim gT \ll T$. At length scales $l_D \sim 1/gT \gg 1/T$, the correlations of the heavy modes are suppressed by their mass, so that relatively dominant contributions arise from the 0-modes. Therefore, at weak coupling, an effective description is sensible at length scales $l > 1/gT$. This leads to the interpretation of the effective model as a 3D theory of the light 0-modes of the original 4D theory [96]. If scalars are present in the 4D theory, the associated 0-modes will appear in 3D, provided that their tree-level masses are small compared to the hard thermal scale T ; in other words, they must also be “light.” Furthermore, fermionic fields would never appear in the 3D description, as the lightest fermionic thermal mass is $\sim \pi T$.

Dimensional reduction, when applied to non-abelian gauge theories, occurs on two levels as a result of the scale hierarchy $g^2 T \ll gT \ll T$. These are respectively the supersoft, soft and hard scales of the theory. The exact form of the expansion

¹¹ In practice, the relevant expansion parameter would involve an additional overall constant, i.e. $g^2/16\pi^2$.

parameters (for instance, whether the hard scale is T vs. $2\pi T$, or whether the expansion parameter is g vs. $g/4\pi$) does not affect the overall construction. However, in practice we must take this into account. The key property is the occurrence of a separations of scales, which for Yang-Mills theory coincides with our previous definition of weak-coupling. Then, the first step of dimensional reduction produces a theory valid at soft scales (distances $l \gtrsim 1/gT$), while the second step results in an 3D model that is accurate at the supersoft scale (distances $l \gtrsim 1/g^2T$).

Though it is intuitive to understand this procedure as “integrating out the heavy degrees of freedom,” this statement is not entirely correct beyond one-loop. Non-local terms generally appear in higher-loop corrections to Green’s functions, and when they are present, an expansion in p^2/T^2 would not be possible (see for instance [97]). Rather, as advocated in [98], dimensional reduction should be really be understood as a “matching procedure” between the parameters of a 3D and a 4D theory.

The matching procedure begins with writing down the most general 3D Lagrangian constructed out of operators consistent with the original symmetries of the theory [99],

$$\begin{aligned} \mathcal{L}_{3D} = & \frac{1}{2} \text{Tr } F_{ij} F_{ij} + \text{Tr } (D_i^{\text{adj}} A_0)^2 + m_A^2 \text{Tr } A_0^2 + \frac{\lambda_A}{2} (\text{Tr } A_0^2)^2 + \frac{\bar{\lambda}_A}{2} \text{Tr } A_0^4 \\ & + (D_i \phi)^\dagger D_i \phi + m_\phi^2 \phi^\dagger \phi + \frac{\lambda_\phi}{2} (\phi^\dagger \phi)^2 + \lambda_{A\phi} (\text{Tr } A_0^2) \phi^\dagger \phi + \delta \mathcal{L}. \end{aligned} \quad (1.65)$$

For now we have neglected higher dimension operators on the assumption that they are relatively suppressed. In Eq. (1.65), the adjoint scalar A_0 is expressed as an element of the Lie Algebra $A_0 = A_0^a T^a$, so that $D_i^{\text{adj}} A_0 = \partial_i A_0 - ig_{3D} [A_i, A_0]$ (a slightly different convention from Section 1.3.1). The fields appearing in \mathcal{L}_{3D} have

canonical dimension $[\text{mass}]^{\frac{1}{2}}$ as does the 3D gauge coupling; it is related to the 4D coupling via

$$g_{3\text{D}}^2 = g^2(\mu_{4\text{D}})T + \mathcal{O}(g^4), \quad (1.66)$$

where the leading order term is its tree-level expression. It may appear as though $g_{3\text{D}}^2$ exhibits an uncontrolled dependence on the 4D renormalization scale $\mu_{4\text{D}}$; by including the $\mathcal{O}(g^4)$ term, that dependence is shifted up to $\mathcal{O}(g^6)$. Upon including the one-loop correction, it is consistent to say that $g_{3\text{D}}$ is independent of $\mu_{4\text{D}}$ at that loop-order. The full series for $g_{3\text{D}}$ is an RG invariant, and in general, the coupling constants appearing in $\mathcal{L}_{3\text{D}}$ do not renormalize. As a technical subtlety, there are UV divergent two-loop self-energy graphs in the 3D model which lead to a scale dependence in the mass parameters [100].

The accuracy of the effective description depends on the extent of the perturbative matching of the two and four-point functions of the 3D theory to those in 4D. Essentially, one carries out a perturbative calculation both in 3 and 4 dimensions, and one insists that they match up to a desired accuracy in g . For instance, the adjoint scalar mass has a series expansion

$$m_A^2 = T^2(c_1 g^2 + c_2 g^4 + \dots). \quad (1.67)$$

To determine the coefficients c_1, c_2 etc., we can compare the two-point function of the 3D adjoint scalar to that of the 4D A_0 0-mode (with $\Pi_L(0, p)$ in 4D evaluated at $\omega = 0$)

$$\frac{1}{p^2 + \Pi_L(0, p)} \quad \longleftrightarrow \quad \frac{1}{p^2 + m_A^2 + \Pi_A(p)}. \quad (1.68)$$

and insist that they agree (up to a specified order in g), which may additionally require field redefinitions. Infrared divergences present in the perturbative expansion do not interfere with the matching provided that IR regulators are employed in a consistent manner. Then, IR divergences in 4D coincide with IR divergences in 3D.

Truncating this series at g^2 and setting the coefficient c_1 in Eq. (1.67) to the one-loop expression for the Debye mass (suitably generalized to include scalar fields) would result in a one-loop matching for the adjoint scalar mass. To achieve a two-loop matching, we would need to keep terms up to $\mathcal{O}(g^4)$. If we recall that the matching procedure generally involves redefinitions of the 3D field, it is apparent that at higher orders dimensional reduction becomes a non-trivial task. Precise details of the matching of electroweak theory to 3D $SU(N)$ Higgs theory beyond the conceptual level can be found in [80, 98, 100].

Since the matching procedure will invariably involve a truncation, Green's functions computed in the 3D effective model will deviate from their 4D analogs with relative errors expressed as powers of the coupling constant. As a concrete example, it has been shown that with the 3D Lagrangian Eq. (1.65) and perturbative matching at the two-loop level,¹² an accuracy of $\mathcal{O}(g^2/16\pi^2)$ relative to 4D $SU(N)$ Higgs theory is attained [98].

Simply increasing the loop-order of the matching procedure with the objective of improving the precision of the effective model does not work in practice, as there is an inherent limitation arising from the exclusion of higher dimension operators in the

¹² Specifically, a two-loop matching for masses and one-loop for coupling constants.

3D Lagrangian. The contributions made by these operators are indeed suppressed, but not necessarily by inverse powers of T . For instance, an operator of the form $h^{(6)}g^6(\text{Tr } A_0^2)^3$ would yield a correction $\sim h^{(6)}m_A^2g^6 \sim h^{(6)}g^8T^2$ to the adjoint scalar mass. This is leading order in T , but $\mathcal{O}(g^4)$ relative to the two-loop matching. The inclusion of higher dimension operators in Eq. (1.65) becomes necessary when constructing an effective model whose accuracy is better than $\mathcal{O}(g^4)$.

As a final remark, suppose now that we were only interested in studying the non-perturbative sector of the theory at length scales $1/g^2T$. Then, the adjoint scalar is a “heavy” degree of freedom, and can be integrated out. This is the second level of dimensional reduction which results in an effective Lagrangian that is absent of the adjoint scalar,

$$\mathcal{L}_{\text{3D}} = \frac{1}{2}F_{ij}F_{ij} + (D_i\phi)^\dagger D_i\phi + m_\phi^2\phi^\dagger\phi + \frac{\lambda_\phi}{2}(\phi^\dagger\phi)^2 + \delta\mathcal{L}. \quad (1.69)$$

The matching procedure occurs in exactly the same manner as earlier, except that odd powers of the coupling appear in expansions of the form Eq. (1.67) due to contributions $\sim g^2\sqrt{m_A^2}$ from A_0 loops.

To summarize, Yang-Mills theory at length scales $\sim 1/g^2T$ is non-perturbative. As a result, the weak coupling expansion exhibits poor convergence except at very high temperatures. We have shown that the inherently non-perturbative physics can be described by 3D effective models but that these 3D theories do not facilitate a fully perturbative description as they are also afflicted with infrared divergences. However, working in 3D streamlines the weak coupling expansion (since the effective theories occur in vacuum without compact dimensions) up to the point where it

breaks down. Then, beyond that, non-perturbative corrections to static quantities can be computed on the lattice, where the availability of a 3D description offers many advantages over a direct study in 4D [101].

1.4.2 Resummation

Beyond the scope of thermal field theory, models like Eq. (1.69) are interesting in their own right, as they are non-perturbative at low energies, and furthermore, they exhibit confinement. This thesis is specifically intended to explore the topic of non-perturbative resummation in Yang-Mills theory, which is indeed relevant in the finite temperature context. But even though it is helpful to visualize these 3D theories via their relationships to 4D, our primary motivation in studying 3D Yang-Mills is that it cannot be described perturbatively. In addition to Eq. (1.69), we will also be interested in the comparatively simpler model

$$\mathcal{L}_{\text{mQCD}} = \frac{1}{2} \text{Tr } F_{ij} F_{ij}, \quad (1.70)$$

that is, magnetic QCD.

One-loop self-energy corrections in 3D $\text{SU}(N)$ Higgs theory and mQCD *can* be computed using perturbation theory; furthermore, these corrections are finite in dimensional regularization. At large momenta, one-loop self-energies are parametrically $\sim g_{3\text{D}}^2 p$, where p is the momentum. However, this is just about as far as you can go. If you naively try to compute the two-loop $\mathcal{O}(g_{3\text{D}}^4)$ correction, which on dimensional grounds generates a mass, you encounter an IR divergence.

IR divergences indicate a limitation of the strict loop-expansion, and therefore it may be possible to make progress with some form of a weak coupling expansion if

we reorganize the perturbation series. This is often what resummation schemes set out to achieve, of which there are many (for good reviews see [102, 103, 104]). In fact, resummations are relevant to theories even with massive fields at tree-level, see for instance [105].

In this thesis the specific focus is on the n PI approach, which will be presented at a formal level in Chapter 2. For now we will end Chapter 1 with a heuristic introduction to the overall concept. The specific goal here is to clarify why resummation is a potentially viable solution to the infrared divergences of perturbation theory.

To illustrate what we mean by “reorganizing a perturbation series” we can consider a very simple model where resummation plays a non-trivial role in the generation of the weak coupling expansion [106]. Namely, this is scalar ϕ^4 at finite temperature,

$$\mathcal{L} = \frac{1}{2} \partial^\mu \phi \partial_\mu \phi + \frac{1}{24} \phi^4. \quad (1.71)$$

We write the full propagator as

$$G(p) = \frac{1}{p^2 - \Pi(p)} \quad (1.72)$$

and then the lowest order correction to the self-energy is simply a tadpole diagram,

$$\Pi^{(1, \text{tp})} \equiv \Pi^{(1)} = -\frac{\lambda}{2} T \sum_n \frac{1}{\bar{\mu}^{2\epsilon}} \int \frac{d^D q}{(2\pi)^D} \frac{1}{q^2 + (2\pi n T)^2} = -\frac{1}{24} \lambda T^2. \quad (1.73)$$

The integral is computed using dimensional regularization with $D = 3 + 2\epsilon$. When we write down the two-loop expression for the tadpole (labelled tp since there is also a sunset graph which we are not considering), we encounter a formally IR divergent

contribution from the 0-mode (as well as a UV divergence)

$$\Pi^{(2,\text{tp})} = -\frac{\lambda T}{2\bar{\mu}^{2\epsilon}} \left[\int \frac{d^D q}{(2\pi)^D} \frac{\Pi^{(1)}}{q^4} + \sum_{n \neq 0} \int \frac{d^D q}{(2\pi)^D} \frac{\Pi^{(1)}}{(q^2 + (2\pi n T)^2)^2} \right]. \quad (1.74)$$

This prompts us to also consider the m loop version of this diagram,

$$\Pi^{(m,\text{tp})} = -\frac{\lambda T}{2\bar{\mu}^{2\epsilon}} \left[\int \frac{d^D q}{(2\pi)^D} \frac{(\Pi^{(1)})^{m-1}}{q^{2m}} + \sum_{n \neq 0} \int \frac{d^D q}{(2\pi)^D} \frac{(\Pi^{(1)})^{m-1}}{(q^2 + (2\pi n T)^2)^{2m}} \right]. \quad (1.75)$$

These diagrams could naively be computed individually in dimensional regularization, each of which making a contribution to the self energy proportional to λ^m . As a consequence of doing the integrals in D dimensions, the formally IR divergent 0-mode contributions vanish at each order in the expansion. In this treatment, the tadpole contributions to Π resemble a standard perturbation series; however, this is in fact not the correct approach.

Rather, a much more interesting result is obtained by not discarding the IR divergent 0-mode contribution, but instead resumming them

$$\sum_{m=1}^{\infty} \Pi^{(m,\text{tp})} = -\frac{\lambda T}{2\bar{\mu}^{2\epsilon}} \int \frac{d^D q}{(2\pi)^D} \frac{1}{q^2 - \Pi^{(1)}} + \Pi^{(1)} + \mathcal{O}(\lambda^2), \quad (1.76)$$

depicted diagrammatically in Fig. 1–2. This resummation is commonly known as

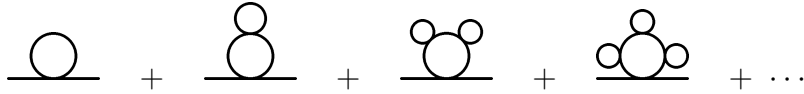


Figure 1–2: Diagrammatic representation of the daisy sum, Eq. (1.76).

a *ring-improvement* or *daisy sum* [107, 108, 109]. An explicit computation reveals that the higher order terms involving a summation over $n \neq 0$ modes generate a

series containing only integer powers of λ , so we will set them aside. The 0-mode resummation yields a contribution proportional to $\lambda^{\frac{3}{2}}$,

$$\sum_{m=1}^{\infty} \Pi^{(m, \text{tp})} = -\frac{1}{24} \lambda T^2 + \frac{1}{16\pi\sqrt{6}} \lambda^{\frac{3}{2}} T^2 + \mathcal{O}(\lambda^2). \quad (1.77)$$

Thus, by summing over an infinite series of diagrams, we have obtained a result which would not have appeared in a standard perturbative expansion. Namely, the NLO term is non-analytic in the coupling constant. The strict loop-expansion did not yield the correct result since it assumed a massless form for the scalar propagator, as it appears at tree-level. In other words, we could have arrived at the same result by including the screening mass directly in the one-loop computation from the onset,

$$\Pi = -\frac{\lambda T}{2} \sum_n \frac{1}{\bar{\mu}^{2\epsilon}} \int \frac{d^D q}{(2\pi)^D} \frac{1}{q^2 - \Pi^{(1)}} + \text{higher order}. \quad (1.78)$$

In the scalar theory, the one-loop mass acts as a regulator for the previously encountered IR divergences, but in a non-abelian gauge theory, the situation is significantly more complex. Indeed we will continue to operate on the assumption that the would-be IR divergences encountered in perturbation theory are regulated by a screening mass $\sim g_{3D}^2$. However, unlike in the scalar theory, the leading order correction to the magnetic screening cannot be computed directly from the loop-expansion. As a result, self-consistently accounting for magnetic screening in an attempt to construct a weak-coupling expansion in Yang-Mills theory is a highly non-trivial task. In the following chapters, we will proceed to address several of the technical challenges associated with the application of resummations to gauge theories.

CHAPTER 2

Φ -derivable approximations and the n PI formalism

2.1 Attempt at an exact solution in the Φ -derivable approximation

The previous chapter ended on the notion that massless fields can give rise to infrared divergences in a perturbative expansion, but that these divergences may be cured by implementing some form of resummation (see for instance [89, 110]). This was illustrated with the very well known example of ring-improvement [108] which involves the resummation of tadpole diagrams in massless 4D scalar field theory at finite temperature via an application of the geometric series formula

$$\frac{1}{1 + \Pi} = 1 - \Pi + \Pi^2 - \Pi^3 + \dots \quad (2.1)$$

This is indeed a very basic example, but it nevertheless serves to illustrate the concept. Resumming Feynman diagrams in a gauge theory will require a more sophisticated approach and as a result we will turn to the n PI formalism [111, 112, 113, 114].

The n PI approach is centred around a mathematical object referred to as an n PI *effective action* which respects the symmetries of the original quantum field theory, to be generically denoted as $\Gamma[\bar{\phi}, G, \dots]$ throughout. By locating its stationary points, an n PI effective action forms the basis of a resummation scheme by yielding integral equations which encode a *selective* resummation in a quantum field theory (in terms of diagrams summed over, we will see that n PI resummations are much more intricate than the tadpole sum previously encountered). This approach allows us to abandon

the perturbative notion of an expansion about a free theory, but rather solve for correlation functions while self-consistently accounting for fluctuations in the field. This way, the n PI approach is inherently *non-perturbative*. At the same time, in the context of a gauge theory any selective resummation is guaranteed to violate abelian or non-abelian Ward identities at some loop order; thus the application of the n PI formalism to gauge theories brings about certain potential ambiguities concerning gauge-invariance [115, 116, 117]. As a consequence, gauge-invariance is a topic that has motivated and will be discussed throughout this work.

This chapter will begin with an introduction to the n PI formalism via a second attempt at a resummation in scalar theory. Moreover, in this chapter we will also start to adopt a diagrammatic notation and continue to steer the focus towards the study of three dimensional field theories.

The n PI formalism is more commonly known in the literature as the Φ -derivable approach [118, 119, 120, 121, 122, 123], especially in the context of thermal field theory (see e.g. the reviews [102, 103, 104]). In fact, as we will see in Section 2.3.2, a Φ -derivable approximation is *equivalent* to an n PI effective action for $n = 2$. The integral equations resulting from n PI effective actions are analytically intractable in many cases of interest [124], as they share many similarities with Schwinger-Dyson (SD) equations [125, 126, 127].¹ Exact solutions can only be obtained in essentially the simplest possible models e.g. the two-loop approximation applied to

¹ A derivation of Schwinger-Dyson equations can be found in many QFT texts, for instance [128].

$O(N)$ scalar ϕ^4 theory in the large N limit [107]. Relaxing the assumption of large N and subsequently attempting to solve the three-loop Φ -derivable approximation leads to a drastic increase in complexity. Some progress towards a solution can then be made by considering series expansions [129, 130, 131] and certain other approximation schemes [132, 133].

Let us suppose once again that we are interested in scalar ϕ^4 theory, except now at zero temperature²

$$S = \int d^D x \frac{1}{2} \partial^\mu \phi \partial_\mu \phi + \frac{1}{2} (m^2 + \delta m^2) \phi^2 + \frac{\lambda}{24} \phi^4 \quad (2.2)$$

(which is assumed to be in the symmetric phase, and since the spacetime is Euclidean, there is no significance to the raising and lowering of indices). For $D = 3 + 2\epsilon$,³ the coupling constant and the field strength do not renormalize, but a mass counter-term is required. In this set-up, the scalar field propagator is a function of a single invariant, labelled as p^2 , and as usual, corrections to the two-point function beyond

² Note that by “zero temperature” we are referring to a spacetime with no compact dimensions. For a 3D theory, this does not preclude a possible connection to a finite temperature 4D theory via dimensional reduction.

³ As an aside, the dimension of spacetime is labelled by D indicating that divergences will be regularized within the framework of dimensional regularization [134, 135]. As a convention throughout this work, integrals in D dimensions are understood to be divergent when $1/\epsilon$ poles appear in taking the limit $D \rightarrow D_0$ with $D = D_0 + 2\epsilon$ and $D_0 \in \mathbb{N}$. However, when we occasionally refer to power-law divergences, these should be understood as those that would arise with a momentum cutoff. Accordingly, loop integrals in $D = 3 + 2\epsilon$ dimensions should appear with a factor of the $\overline{\text{MS}}$ scale $\bar{\mu}^{2\epsilon}$, $\int \frac{d^3 p}{(2\pi)^3} \rightarrow \frac{1}{\bar{\mu}^{2\epsilon}} \int \frac{d^D p}{(2\pi)^D}$ with $\bar{\mu}^2 = \mu^2 e^\gamma / 4\pi$.

tree-level will be contained in a self-energy $\Pi(p)$

$$G(p) = \frac{1}{p^2 + m^2 - \Pi(p)}. \quad (2.3)$$

It is now convenient to adopt the diagrammatic notation

$$G = \text{---} \quad -\lambda = \text{X} \quad -\delta m^2 = \text{---}\star\text{---}; \quad (2.4)$$

in expressing G as single line throughout this chapter we mean the *dressed* propagator (but the vertex is taken to be at tree-level for now).

An n -loop Φ -derivable approximation is by definition the extremum of a potential that takes on the general form [118]

$$\Gamma[\Pi] = -\frac{1}{2\bar{\mu}^{2\epsilon}} \int \frac{d^D p}{(2\pi)^D} \left[\log G^{-1}(p) + G(p)\Pi(p) \right] + \frac{1}{2}\Phi[\Pi] \quad (2.5)$$

where the functional $\Phi[\Pi]$ is non-linear “interaction” functional of the self-energy. Since in practice Φ is expressed diagrammatically via a loop expansion (which determines the loop-order of the approximation), it is at times alternatively understood as a functional acting directly on G . The assumption of a stationarity condition on $\Gamma[\Pi]$ yields an equation of motion for $\Pi(p)$ and equivalently $G(p)$,

$$\frac{\delta\Gamma[\Phi]}{\delta G(p)} = \frac{\delta\Gamma[\Phi]}{\delta\Pi(p)} = 0 \quad \longrightarrow \quad \Pi(p) = \frac{\delta\Phi[\Pi]}{\delta G(p)}. \quad (2.6)$$

This expression lies at the core of the Φ -derivable approach and the n PI formalism in general, as it provides a self-consistent equation for the self-energy.

Without even having written an expression for $\Phi[\Pi]$, we can already start to appreciate where two main challenges in solving an equation such as Eq. (2.6) will

lie. First, in the context of our Euclidean study, $\Gamma[\Pi]$ is a functional that acts on an infinite dimensional vector space $\Pi(p) \in \mathcal{D}$, namely, continuous functions $\Pi(p)$ whose domain is a real variable $p \in (0, \infty)$.⁴ Second, Eq. (2.5) is power-law divergent, and needs to be regularized.

The simplest possible expression for Φ is trivially $\Phi[\Pi] = 0$ so that the equation of motion Eq. (2.6) yields $\Pi(p) = 0$. In other words, this is solved when G is equal to its tree-level expression. The lowest non-trivial order is two-loops, where the Φ -derivable approximation for scalar ϕ^4 theory is given by

$$\Phi[\Pi] = -\frac{\lambda}{4\bar{\mu}^{4\epsilon}} \int \frac{d^D p}{(2\pi)^D} \frac{d^D q}{(2\pi)^D} \frac{1}{p^2 + m^2 - \Pi(p)} \frac{1}{q^2 + m^2 - \Pi(q)} = \frac{1}{4} \text{ (diagram of two circles connected by a vertical line) } . \quad (2.7)$$

This is commonly known as a “super daisy” approximation [137]. The resulting equation of motion for $\Pi(p)$

$$\Pi(p) = -\frac{\lambda}{2\bar{\mu}^{2\epsilon}} \int \frac{d^D q}{(2\pi)^D} \frac{1}{q^2 + m^2 - \Pi(q)} = \frac{1}{2} \text{ (diagram of a circle) } \quad (2.8)$$

fully resums the one-loop tadpole graph to all orders, and when drawn, the diagrams have a fractal-like resemblance to daisy petals (see Fig. 2–1). The super daisy sum can immediately be recognized as an extended version of the regular “daisy”

⁴ This statement is not applicable in general as a self-energy is often defined at complex frequencies [136]; we are not specifically interested in an analytic continuation to $2 + 1$ dimensions, so the analyticity assumptions that we make about $\Pi(p)$ reflect the range of 3D Euclidean momenta that we study. The solutions we seek do not have any poles at positive p^2 .

sum encountered in Chapter 1, Section 1.4.2, in that the diagrams summed over previously only form a subset of those encoded in Eq. (2.8).

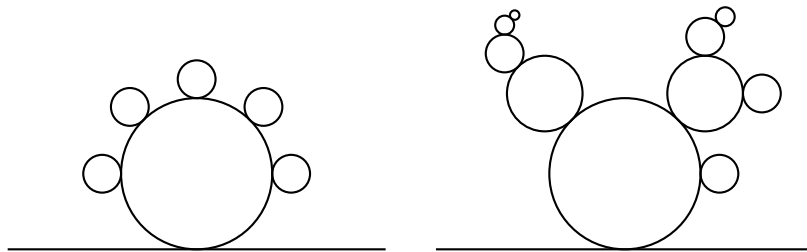


Figure 2-1: Typical daisy (left) and super daisy (right) Feynman diagrams.

Eq. (2.8) is relatively straightforward to solve, since the tadpole does not depend on the external momentum thus implying $\Pi(p) = \text{constant}$, which will be denoted simply as Π . In 4D this expression would have been quadratically divergent. However, in 3D we can perform the integral in dimensional regularization, where the would-be linear divergence is not realized. For Π we obtain the gap equation

$$\Pi = \frac{\lambda}{8\pi} \sqrt{m^2 - \Pi}. \quad (2.9)$$

Had we been studying an $O(N)$ scalar theory, the tadpole would have entered with a prefactor of $\lambda(N+2)$. At large N , one observes that the diagrams in the super daisy sum make the only leading order contributions in λN [107], so that the perturbation series *is equivalent* to the super daisy sum, barring $1/N$ corrections. In this limit, Eq. (2.9) is exact.

At finite N , the super daisy approximation is just that: an approximation. Naturally, $\Gamma[\Pi]$ could be improved by including the next higher-loop contribution to

$\Phi[\Pi]$. At three-loops, we have

$$\Phi[\Pi] = \frac{1}{4} \text{ (figure-eight)} + \frac{1}{24} \text{ (sunset)} + \text{ (triangle with cross)} , \quad (2.10)$$

yielding the following integral equation for $\Pi(p)$

$$\begin{aligned} \Pi(p) &= \frac{1}{2} \text{ (loop)} + \frac{1}{6} \text{ (circle)} + \text{ (triangle with cross)} \\ &= -\frac{\lambda}{2\bar{\mu}^{2\epsilon}} \int \frac{d^D q}{(2\pi)^D} G(q) \end{aligned} \quad (2.11)$$

$$+ \frac{\lambda^2}{6\bar{\mu}^{4\epsilon}} \int \frac{d^D q}{(2\pi)^D} \frac{d^D k}{(2\pi)^D} G(q) G(k-q) G(k-p) - \delta m^2 . \quad (2.12)$$

Since the two-loop sunset graph is logarithmically divergent in three dimensions, invoking a counter-term prescription at this stage became unavoidable. To solve this equation, a good place to start would be with applying what we already know about $\Pi(p)$; that is, it has a weak-coupling expansion. At large momentum, the ratio λ^2/p^2 is small so in this limit $\Pi(p)$ must converge to its perturbation series⁵

$$\Pi(p) = \frac{\lambda m}{8\pi} - \frac{\lambda^2}{192\pi^2} \left(\frac{6m}{p} \arctan \frac{p}{3m} + \log \frac{p^2 + 3m^2}{\mu^2} - \frac{3}{2} \right) + \mathcal{O}(\lambda^3), \quad (2.13)$$

Performing this expansion also serves to exactly fix the value of the additive counter-term, as there are no higher-loop UV divergences.

⁵ In three dimensions (and odd dimensional spacetimes in general), due to the availability of a representation in terms of half-integer Bessel functions, the massive sunset graph with equal masses is relatively easy to compute analytically, see [138].

This may prompt an attempt at solving Eq. (2.12) via a series expansion of $\Pi(p)$, but this essentially leads us right back to doing perturbation theory (in this particular example). Furthermore, treating λ/p as a small parameter would not even be accurate in the IR. We had originally sought out a resummation scheme due to the inherent limitations associated with applying perturbation theory to massless fields in 3D; therefore, we will avoid this route, since we soon intend to apply the formalism to a massless gauge theory.

What Eq. (2.13) does serve to illustrate though is that at the two-loop *perturbative* level, $\Pi(p)$ is already a transcendental function of p that needs to be renormalized. Even if we simply inserted the perturbative expression for $\Pi(p)$ back into Eq. (2.12), it would not be possible to perform the integral analytically (notwithstanding the challenges associated with obtaining its value in D dimensions). In terms of obtaining an exact solution to Eq. (2.12), it is not apparent how to make further progress analytically.

Therefore, at this point we will abandon our attempt at determining the exact solution to the three-loop Φ -derivable approximation for scalar theory. However, as an alternative approach it may be possible to obtain an approximate solution by reformulating the equation of motion as a variational problem, along the lines of [129, 130]. We can start by assuming a tractable form for $\Pi(p)$, the simplest choice being $\Pi(p) = \text{constant}$, and then reattempt to solve for the extremum of Γ . In this approximation scheme, $\Gamma[\Pi]$ becomes a *function* of a single variable Π , and the

stationarity condition is reformulated as a variational equation

$$\frac{\delta\Gamma[\Pi]}{\delta\Pi(p)} = 0 \quad \longrightarrow \quad \frac{d\Gamma(\Pi)}{d\Pi} = 0. \quad (2.14)$$

The extremal point on the right of Eq. (2.14) (that is, the root of the derivative with respect to the variable Π) will not in general coincide with the extremal point on the left. Therefore, the constant Π obtained from the recasted variational equation is not the *exact solution*, but at best an approximation. The quality of this result will depend on the amount by which Γ differs between its true extremum on \mathcal{D} , and that which lies on the subset of \mathcal{D} containing only constant functions.

As a way of improving and controlling this approximation, we can consider an extension in which we assume a momentum dependent *Ansatz* for $\Pi(p) = \Pi^*(p)$, parametrized in terms of a *finite* set of m coefficients $\{c_1, \dots, c_m\}$. These functions $\Pi^*(p) \in \mathcal{D}^*$ span a subset of the original space $\mathcal{D}^* \subset \mathcal{D}$, naturally being larger than the set of constant functions. The variational equation now takes the form

$$\frac{\delta\Gamma[\Pi]}{\delta\Pi(p)} = 0 \quad \longrightarrow \quad \nabla\Gamma(c_1, c_2, \dots) = 0 \quad (2.15)$$

effectively replacing the functional derivative with a gradient $\nabla = (\frac{\partial}{\partial c_1}, \frac{\partial}{\partial c_2}, \dots)$. This variational equation determines $\Gamma(c_1, \dots, c_m)$'s extremum on the restricted space \mathcal{D}^* . The quality of such an approximation can now be controlled by redetermining the variational extremum with increasing numbers of variational coefficients, in effect converging iteratively to the true extremum. This is the approach that we will be adopting in Chapters 3 and 4, so further technical details will be deferred until then.

From a computational perspective, pure scalar theories are easy to work with since their Feynman rules contain no tensor structures. For QED and QCD, the potential $\Gamma[\Pi_{\mu\nu}]$ has been worked out long ago [139]. Contrasted against a scalar theory, QED is significantly more complex with fermionic field content, transverse and longitudinal projectors in the gauge two-point functions as well as gauge field to fermion interactions. Even this is mild compared to what one encounters in Yang-Mills theory, where gauge fields self-interact, resulting in the appearance of rank-three tensors in the Feynman rules. However, before discussing the situation in a gauge theory, we will devote the remainder this chapter to presenting the Legendre transforms from which the n PI formalism is derived.

2.2 1PI generating functions

To arrive at the expressions for the 2PI and 3PI effective actions, the best place to start is by considering the well known 1PI formalism. The derivation of the loop expansion of the 1PI effective action is available throughout the literature (see for instance [81, 128, 140]), and to give meaning to the formalism we will go over some of the key conceptual details in this section. The starting point is the generating function of connected diagrams with a real single particle source

$$W[J] = -\log \int \mathcal{D}\phi \, e^{-S[\phi] - J\phi} \, , \quad (2.16)$$

keeping a sign convention that is consistent with a Euclidean spacetime. We will assume that the systems of interest are spacetime translation invariant. As our focus is specifically on the details of the Legendre transform, in the interest of being concise a schematic notation will be used (taking the form of a real source J coupled to a

real field ϕ). In general, the arguments of functions and integrations are suppressed and should be inferred from context, for instance⁶

$$J\phi \equiv \int d^D x \ J(x)\phi(x) \quad S[\phi] \equiv \int d^D x \ \mathcal{L}(\phi(x)), \quad (2.18)$$

also bearing in mind throughout that functional differentiation is defined via

$$\frac{\delta J(x)}{\delta J(y)} = \delta^D(x - y). \quad (2.19)$$

By differentiation with respect to J , we formally obtain the connected one and two-point functions of the theory in the presence of a source

$$\bar{\phi} = \frac{\delta}{\delta J} W[J] \quad (2.20)$$

$$G = -\frac{\delta^2}{\delta J^2} W[J], \quad (2.21)$$

and so forth for the higher n -point functions. In the language of the n PI formalism, $W[J]$ is a 1PI generating functional; by definition, the 1PI effective action $\Gamma[\bar{\phi}]$ is

⁶ In general we may encounter couplings of the form $J^\dagger \phi + \phi^\dagger J$ for complex scalar fields, $J^{a\mu} A_\mu^a$ for gauge fields etc. For an extension to more elaborate field content, we can understand the shorthand as

$$J\phi \equiv \int d^D x \ \sum_i J_i(x)\phi_i(x). \quad (2.17)$$

with i representing Lorentz, colour, species etc. indices. These indices would then need to be accounted for throughout the derivation, for instance $\delta/\delta J \rightarrow \delta/J_i(x)$, $\delta J_i(x)/\delta J_j(y) = \delta_{ij}\delta^D(x - y)$.

obtained from the Legendre transform

$$\Gamma[\bar{\phi}] = J\bar{\phi} - W[J]. \quad (2.22)$$

We have denoted $\bar{\phi}$ as the conjugate variable to J . As we are interested in expressing J in terms of $\bar{\phi}$, we must now invert the relationship

$$\bar{\phi} - \frac{\delta W}{\delta J} = 0. \quad (2.23)$$

The effective action $\Gamma[\bar{\phi}]$ has a similar diagrammatic interpretation to $W[J]$: just as $W[J]$ is the sum of connected diagrams with an arbitrary number of single particle source insertions, $\Gamma[\bar{\phi}]$ is the expansion of one-particle-irreducible vertex functions with field insertions. Taking derivatives of Γ with respect to $\bar{\phi}$ yields the 1PI vertex functions of the theory,

$$\frac{\delta^n}{\delta J^n} W[J] \Big|_{J=0} \implies n\text{-point connected Green's function} \quad (2.24)$$

$$\frac{\delta^n}{\delta \bar{\phi}^n} \Gamma[\bar{\phi}] \Big|_{\bar{\phi}=\bar{\phi}_0} \implies n\text{-point 1PI vertex function.} \quad (2.25)$$

Furthermore, in recovering the physical limit $J = 0$, $\Gamma[\bar{\phi}]$ specifies the ground state of the system $\bar{\phi}_0$,

$$\frac{\delta \Gamma[\bar{\phi}]}{\delta \bar{\phi}} \Big|_{\bar{\phi}=\bar{\phi}_0} = 0, \quad (2.26)$$

which can be used to infer the properties and existence of phase transitions. For clarity, in this section we will explicitly define the effective potential as $V(\bar{\phi}) = -\mathcal{V}^{-1}\Gamma[\bar{\phi}]$ so that $V(\bar{\phi})$ opens upwards (\mathcal{V} being the volume of spacetime).⁷

2.2.1 Saddle point evaluation of $\Gamma[\bar{\phi}]$

To directly compute the loop expansion of Γ , we will proceed with a saddle point evaluation of the path integral. As is common in the literature, we will make the assumption that $\bar{\phi}$ satisfies the classical equations of motion for the action S with a source J . As we will see momentarily, this can be understood as invoking a “counter-term” prescription for J . Using the notation

$$S'_{\bar{\phi}} \equiv \left. \frac{\delta S[\phi]}{\delta \phi} \right|_{\phi=\bar{\phi}}, \quad (2.27)$$

a Taylor expansion of the action about $\bar{\phi}$ takes the following form

$$S[\phi] + J\phi = S[\bar{\phi}] + J\bar{\phi} + (\phi - \bar{\phi})(S'_{\bar{\phi}} + J) + \frac{1}{2}(\phi - \bar{\phi})^2 S''_{\bar{\phi}} + S^{\text{int}}_{\bar{\phi}}[\phi - \bar{\phi}]. \quad (2.28)$$

Now, by virtue of $\bar{\phi}$ satisfying the classical equations of motion (with a source J , the classical source being its tree-level component), the linear term in this series is required to vanish at tree-level. So, we will define $Y = S'_{\bar{\phi}} + J$ and treat it as a counter-term to appear alongside the other interactions in the Lagrangian (any

⁷ Elsewhere throughout this work we interchangeably use the term effective action as a direct reference to the volume rescaled object. As we have assumed spacetime translation invariance, the volume is simply an overall multiplicative factor, and, we are not interested in directly evaluating Γ but rather locating its extrema. Moreover, the overall sign is simply a matter of convention.

other counter-terms present in $S''_{\bar{\phi}}$ are also shuffled into $S^{\text{int}}_{\bar{\phi}}$). Since the path-integral measure is invariant under the shift $\phi \rightarrow \phi - \bar{\phi}$, we can insert Eq. (2.28) directly into Eq. (2.16) and obtain

$$W[J] = S[\bar{\phi}] + J\bar{\phi} - \log \int \mathcal{D}\phi \, e^{-\frac{1}{2}\phi S''_{\bar{\phi}}\phi - Y\phi - S^{\text{int}}_{\bar{\phi}}[\phi]}. \quad (2.29)$$

Performing the Legendre transform is now simply a matter of subtracting the $J\bar{\phi}$ term.⁸ What we are left with is very similar to the original Eq. (2.16), except with a modified tree-level propagator $S''_{\bar{\phi}}$ and vertices generated by the Taylor series. A loop expansion of $\Gamma[\bar{\phi}]$ follows naturally,

$$\Gamma[\bar{\phi}] = \Gamma^{(0)}[\bar{\phi}] + \Gamma^{(1)}[\bar{\phi}] + \Gamma^{(2)}[\bar{\phi}] + \dots \quad (2.30)$$

or, explicitly matching these terms order by order

$$\Gamma[\bar{\phi}] = \underbrace{-S[\bar{\phi}]}_{\Gamma^{(0)}} + \underbrace{\log \int \mathcal{D}\phi \, e^{-\frac{1}{2}\phi S''_{\bar{\phi}}\phi}}_{\Gamma^{(1)}} + \underbrace{\log \int \mathcal{D}\phi \, \left(e^{-S^{\text{int}}_{\bar{\phi}}[\phi] - Y\phi} - 1 \right) e^{-\frac{1}{2}\phi S''_{\bar{\phi}}\phi}}_{\Gamma^{(2)}+\dots}. \quad (2.31)$$

The familiar one-loop expression is recovered by integrating the middle term

$$\Gamma[\bar{\phi}] = -S[\bar{\phi}] - \frac{1}{2}\text{Tr} \log S''_{\bar{\phi}} + \Gamma^{(2)}[\bar{\phi}] + \dots \quad (2.32)$$

⁸ Though hidden, one may observe that J still explicitly appears in Y . As a result, it may appear as though we have not actually eliminated the J dependence in Γ . In terms of $\bar{\phi}$, J is fixed by the requirement that tadpoles vanish in the expansion of Γ ; therefore, $\Gamma[\bar{\phi}]$ is in fact not explicitly dependent on J . See Section 2.2.2.

and in general, higher-loop terms originate from the diagrammatic expansion of $\Gamma^{(2)} + \dots$. This path integral can still generate tadpole topologies, but these are subtracted by a suitable choice of Y . Then, all that remains is a series of one-particle-irreducible graphs with tree-level propagator $S''_{\bar{\phi}}$, and interaction vertices obtained from $S^{\text{int}}_{\bar{\phi}}[\phi]$.

2.2.2 1PI effective action and symmetry breaking

As a concrete example, consider for simplicity the action $S[\phi]$ of a real scalar field near three dimensions with $m^2 > 0$ and tree-level propagator $G^{(0)}(p) = 1/(p^2 + m^2)$,

$$S[\phi] = \frac{1}{2}\phi G^{(0)-1}\phi + \delta m^2 \phi^2 + \frac{\lambda}{24}\phi^4. \quad (2.33)$$

Then

$$S''_{\bar{\phi}} = G^{(0)-1} + \frac{\lambda}{2}\bar{\phi}^2 \quad (2.34)$$

$$Y\phi + S^{\text{int}}_{\bar{\phi}}[\phi] = Y\phi + \frac{1}{2}\delta m^2 \phi^2 + \frac{\lambda\bar{\phi}}{3!}\phi^3 + \frac{\lambda}{4!}\phi^4. \quad (2.35)$$

To recover the perturbative expansion of one-loop vertex functions, we *could* expand the logarithm in powers of λ ,

$$-\frac{1}{2}\text{Tr} \log S''_{\bar{\phi}} = \frac{1}{2}\text{Tr} \log G^{(0)} + \frac{1}{2}\text{Tr} \sum_{n=1} \frac{1}{n} \left(\frac{-\lambda\bar{\phi}^2}{2} G \right)^n. \quad (2.36)$$

Alternatively, we may as well just sum the whole series by directly evaluating the $\text{Tr} \log$ in dimensional regularization

$$-\frac{1}{2\mathcal{V}}\text{Tr} \log S''_{\bar{\phi}} = \frac{1}{6\pi} \left(m^2 + \frac{\lambda\bar{\phi}^2}{2} \right)^{3/2}, \quad (2.37)$$

thus yielding the one-loop effective potential [107, 141, 142, 109]

$$V(\bar{\phi}) = \frac{1}{2}m^2\bar{\phi}^2 + \frac{\lambda}{24}\bar{\phi}^4 - \frac{1}{6\pi}\left(m^2 + \frac{\lambda\bar{\phi}^2}{2}\right)^{3/2} + \text{two-loops}. \quad (2.38)$$

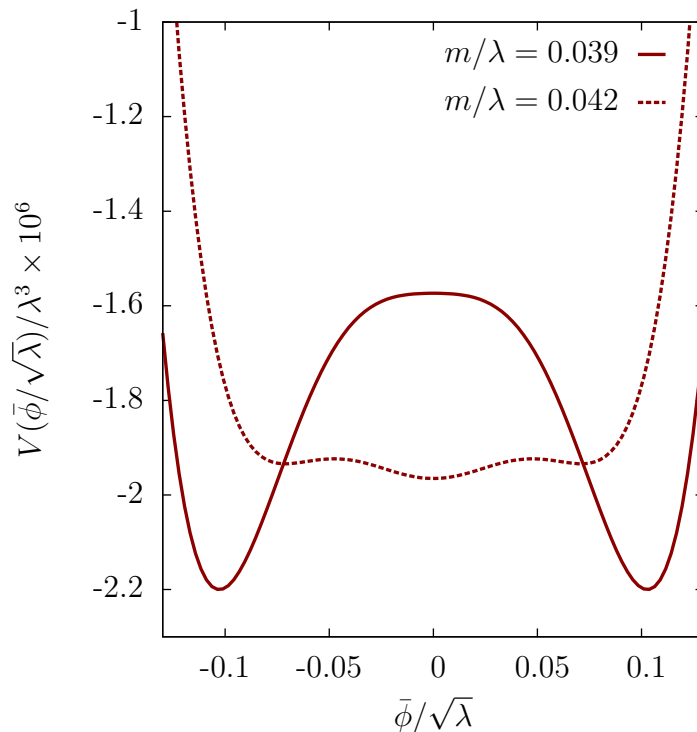


Figure 2-2: One-loop effective potential for scalar theory in 3D. The $m/\lambda = 0.039$ curve indicates that the system is in the broken phase, with a phase transition expected to occur between $m/\lambda = 0.039$ and $m/\lambda = 0.042$. As m is further increased, the broken phase becomes completely unstable.

The significance of this expression is that even though at tree-level the ground state (that is, the global minimum of $V(\bar{\phi})$) occurs at $\bar{\phi} = 0$, this may cease to be the case upon the inclusion of the one-loop term. In fact this is precisely what we observe; see Fig. 2-2. By including the one-loop correction, we infer that the configuration $\bar{\phi} = 0$ becomes unstable as m/λ crosses $1/8\pi \approx 0.0397$. The curve depicted in Fig.

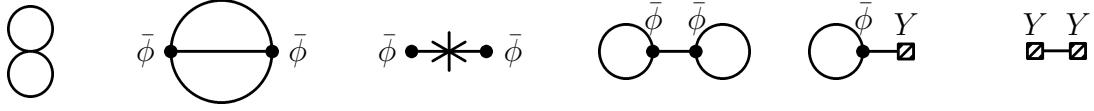


Figure 2-3: Two-loop topologies corresponding to Eq. (2.40), where $\bar{\phi}$ and Y vertex insertions are labelled explicitly (note that in this section a single line is a tree-level propagator, which is implicitly dependent on $\bar{\phi}$). The diagrams on the left are 1PI, whereas the diagrams on the right vanish with a suitable choice of Y , which in turn specifies J at one-loop.

2-2 is characteristic of a first order phase transition, as $\bar{\phi}$ is expected to make a discontinuous jump from the broken phase minimum at $\bar{\phi} \neq 0$ to the symmetric phase $\bar{\phi} = 0$ as m is increased.

As shown, the one-loop effective potential predicts a first order phase transition in a situation where it is known to be second order [143]. Thus, the one-loop effective potential has failed to accurately describe the phase transition, which we can attribute to certain non-perturbative effects associated with large contributions from higher-order diagrams in vicinity of the phase transition [109]. As we will see in Chapter 4, this is similar to the situation in 3D $SU(N)$ Higgs theory where the one-loop effective potential (which is gauge-dependent in this case [144]) predicts a first order phase transition over a range of the phase diagram where a cross-over is known to occur. We will return to this topic in Chapter 4.

For now, we will comment that in presenting the one-loop result we have skipped over a few potentially significant considerations:

- Foremost, we have neglected any effects due to renormalization. In this particular example, the scalar mass renormalizes at two-loops which would necessitate

the replacement of m^2 with $m^2(\mu)$ in Eq. (2.38). This may appear to introduce an arbitrary dependence on the scale μ ; however, certain cancellations occur in the full two-loop calculation which cause the μ dependence to actually be shifted up to three-loops [100]. Nevertheless, in general $V(\bar{\phi})$ is scale dependent, and hence is only defined up to a constant.

- Second, the function that we have plotted is *non-convex*, despite being defined via a Legendre transform. This should be understood as a property of the truncation rather than indicating a real problem; indeed the full expression for $V(\bar{\phi})$ is convex (see for instance [145]).
- Finally, a solution $\bar{\phi}_0 \neq 0$ naively contradicts the assumption that $\bar{\phi}_0$ satisfies the classical equations of motion with $J = 0$ on which the saddle point evaluation of $W[J]$ was reliant. In fact, as we will see momentarily, it does not.

Up to this point, we have argued that locating the extrema of $V(\bar{\phi})$ determines the ground state. Alternatively, we may proceed by directly evaluating J , for which we will assume a loop expansion of the form

$$J = J^{(0)} + J^{(1)} + \dots \quad (2.39)$$

$J^{(0)}$ should immediately be recognized as the term which enters the classical equation of motion. Now let us consider the two-loop correction to $\Gamma[\bar{\phi}]$

$$\Gamma^{(2)}[\bar{\phi}] = \log \int \mathcal{D}\phi \left(\frac{Y^2}{2} \phi^2 + \frac{Y\lambda\bar{\phi}}{3!} \phi^4 + \frac{\lambda^2\bar{\phi}^2}{2(3!)^2} \phi^6 - \frac{\lambda}{4!} \phi^4 \right) e^{-\frac{1}{2}\phi(G^{(0)-1} + \lambda\bar{\phi}^2/2)\phi}, \quad (2.40)$$

noting that there is also a mass counter-term from $S[\bar{\phi}]$ floating about (the corresponding topologies are shown in Fig. 2–3). As depicted, tadpole topologies are

being generated, but a quick calculation shows that at this loop-order they can be made to vanish by setting

$$Y = \frac{\lambda\bar{\phi}}{8\pi} \sqrt{m^2 + \frac{\lambda\bar{\phi}^2}{2}}. \quad (2.41)$$

This precisely determines $J^{(1)}$ (as a function of $\bar{\phi}$), hence, this is what was meant earlier by “invoking a counter-term prescription” for J . The connection to the ground state of the system is as follows: at non-zero values of J , we have $\delta\Gamma[\bar{\phi}]/\delta\bar{\phi} = J$ (which can be obtained directly from the Legendre transform). Therefore, the ground state *is* obtained by setting $J = 0$, which is not necessarily equivalent to $J^{(0)} = 0$.

Indeed, the classical equation of motion is satisfied provided that $J^{(0)} = -S'_{\bar{\phi}}$. Supplementing this with the one-loop expression

$$J = -m^2\bar{\phi} - \frac{\lambda}{6}\bar{\phi}^3 + \frac{\lambda\bar{\phi}}{8\pi} \sqrt{m^2 + \frac{\lambda\bar{\phi}^2}{2}} + \text{two-loops}, \quad (2.42)$$


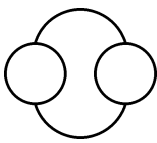
it is easy to verify that the values of $\bar{\phi}$ which cause $J^{(0)} + J^{(1)}$ to vanish coincide exactly with the extremal point(s) of Eq. (2.38). Clearly the symmetric phase $\bar{\phi} = 0$ solves $J = 0$, corresponding to the *classical* solution that requires $J^{(0)} = 0$. Upon including the one-loop correction, $\bar{\phi} = 0$ does not necessarily continue to be the stable ground state. As observed in Fig. 2–2, values of $\bar{\phi}$ for which $J = 0$ can yield stable, unstable and metastable extrema in general, depending on the curvature and value $V(\bar{\phi})$ at that location. The ground state is said to occur at the infimum of $V(\bar{\phi})$.

In the context of gauge theories, in spite of the effective potential being a gauge-dependent quantity [144] (after all, a VEV is gauge-dependent), there remains a physical significance to the solutions of $J = 0$. The value of the effective potential

at its infimum, as it is related to $W[0]$ via a Legendre transform, *is* necessarily gauge-invariant [87, 146].

2.3 The 2PI effective action

The defining characteristic of a 1PI diagram is that if any internal line is cut, the resulting graph remains connected. Two-particle-irreducible (2PI) graphs satisfy a similar criterion, except involving the cutting of two lines.⁹ Imposing the 1PI condition on vacuum graphs results in tadpole topologies being discarded; likewise, the 2PI condition yields diagrams that do not contain an internal self-energy insertions (these are also known as *skeleton* diagrams [124]). When a graph is not 2PI, it is said to be two-particle-reducible or 2PR.



(2.43)

2PI
2PR

The 2PI formalism was presented by Cornwall, Jackiw and Tomboulis in Ref. [147] (closely related to the previous work in [118, 119, 148]), in which they derive the 2PI effective action. In this section we will go over the formalism from a more diagrammatic perspective, in the process illustrating the key result that the 2PI effective action is indeed an expansion in 2PI diagrams. The starting point is yet again the generating function of connected diagrams Eq. (2.16), except now we will include

⁹ It should be noted that the definition of n -particle-irreducibility via the cutting of n lines does not immediately generalize to $n > 2$.

a two particle source, $K(x, y)$ (adopting a schematic notation that is compatible with the previous section)

$$W[J, K] = -\log \int \mathcal{D}\phi \, e^{-S[\phi] - J\phi - \frac{1}{2}\phi K\phi}. \quad (2.44)$$

The one and two-point functions $\bar{\phi}$ and G in the presence of both sources are still obtained by differentiation with respect to J ,

$$\bar{\phi} = \frac{\delta}{\delta J} W[J, K] \quad (2.45)$$

$$G = -\frac{\delta^2}{\delta J^2} W[J, K]. \quad (2.46)$$

and additionally, we have

$$\frac{\delta}{\delta K} W[J, K] = \frac{1}{2}(G + \bar{\phi}^2). \quad (2.47)$$

We will assume once again that the systems of interest are spacetime translation invariant (and as a consequence, G is diagonal in momentum space). The 2PI effective action is by definition the *double* Legendre transform of Eq. (2.44),

$$\Gamma[\bar{\phi}, G] = J \frac{\delta W}{\delta J} + K \frac{\delta W}{\delta K} - W[J, K], \quad (2.48)$$

and as earlier, the conjugate variable to J is $\bar{\phi}$. Now we also have G as a conjugate variable to K .

The Legendre transform can be performed sequentially; to eliminate the explicit dependence on J we proceed with a saddle point evaluation as in the 1PI case. The

two-particle source adds an additional term to the “classical” equation of motion,

$$S'_{\bar{\phi}} + K\bar{\phi} + J = Y, \quad (2.49)$$

where it can again be assumed that Y vanishes at tree-level. The resulting counter-term prescription for tadpole graphs is reminiscent of the 1PI case, in observing that the additional $K\bar{\phi}$ term in Eq. (2.49) coincides with the 2PI extended variation $\delta\Gamma/\delta\bar{\phi}$, specifically

$$\frac{\delta\Gamma[\bar{\phi}, G]}{\delta\bar{\phi}} = J + K\bar{\phi}. \quad (2.50)$$

For simplicity, we will omit future reference to Y under the assumption that tadpole graphs are made to vanish. From Eq. (2.48) we have

$$\Gamma[\bar{\phi}, G] = -S[\bar{\phi}] + \frac{1}{2}KG + \log \int \mathcal{D}\phi \, e^{-\frac{1}{2}\phi(S''_{\bar{\phi}}+K)\phi - S^{\text{int}}_{\bar{\phi}}[\phi]}, \quad (2.51)$$

where the full dependence on G is still implicit in K .

2.3.1 Loop expansion

To derive a working expression for the 2PI effective action, we have to eliminate the dependence on K in favour of G . What we will remark at this point is that we have still have a 1PI generating function in Eq. (2.51) (with inverse propagator $S''_{\bar{\phi}} + K$). However, we are claiming that the 2PI effective action is an expansion in 2PI vacuum diagrams. So, to see why this must be the case, we can express K in terms of G via a loop expansion. As a starting point, Eq. (2.48) requires that

$$\frac{\delta\Gamma[\bar{\phi}, G]}{\delta G} = \frac{K}{2}, \quad (2.52)$$

and, as in the previous section, our intention will be to recover the physical limit by eventually setting $K = 0$. To keep track of the order, we will use the loop counting parameter \hbar ,¹⁰ so that

$$\Gamma[\bar{\phi}, G] = \frac{1}{\hbar} \Gamma^{(0)}[\bar{\phi}] + \Gamma^{(1)}[\bar{\phi}, G] + \hbar \Gamma^{(2)}[\bar{\phi}, G] + \dots \quad (2.53)$$

$$K[\bar{\phi}, G] = K^{(1)}[\bar{\phi}, G] + \hbar K^{(2)}[\bar{\phi}, G] + \dots \quad (2.54)$$

In terms of Eq. (2.53) and Eq. (2.54), Eq. (2.52) must be satisfied order by order in \hbar . $\Gamma^{(0)}[\bar{\phi}]$ is the tree-level action, and therefore independent of G , resulting in an expansion for K that automatically starts at $\mathcal{O}(\hbar^0)$. To arrive at the expression for K , we can explicitly perform the variation of Eq. (2.51) with respect to G ,

$$\frac{\delta}{\delta G} \Gamma[\bar{\phi}, G] = \frac{K}{2} + \frac{1}{2} \frac{\delta K}{\delta G} \left(G - \frac{1}{\hbar} \frac{\int \mathcal{D}\phi \, \phi \phi \, e^{-\frac{1}{2\hbar} \phi(S''_{\phi} + K)\phi - \frac{1}{\hbar} S_{\phi}^{\text{int}}[\phi]}}{\int \mathcal{D}\phi \, e^{-\frac{1}{2\hbar} \phi(S''_{\phi} + K)\phi - \frac{1}{\hbar} S_{\phi}^{\text{int}}[\phi]}} \right), \quad (2.55)$$

so that Eq. (2.52) will dictate that the term in brackets must vanish. Defining

$$\langle \phi \phi \rangle_K = \frac{1}{\hbar} \frac{\int \mathcal{D}\phi \, \phi \phi \, e^{-\frac{1}{2\hbar} \phi(G^{-1} + K)\phi - \frac{g}{3! \hbar} \phi^3 - \frac{\lambda}{4! \hbar} \phi^4}}{\int \mathcal{D}\phi \, e^{-\frac{1}{2\hbar} \phi(G^{-1} + K)\phi - \frac{g}{3! \hbar} \phi^3 - \frac{\lambda}{4! \hbar} \phi^4}}, \quad (2.56)$$

we have

$$\langle \phi \phi \rangle_K - G = 0. \quad (2.57)$$

Expanding this path integral is a straightforward task as $\langle \phi \phi \rangle_K$ is precisely a two-point function, but this will require us to make some assumptions about the form of the classical action. For simplicity, we will consider a real scalar field in

¹⁰ Not to be confused with a loop counting parameter that determines the order of a perturbation series.

three dimensions with cubic and quartic interactions, as this will generate the set of topologies which would, for instance, appear in a non-abelian gauge theory. Since we are primarily interested in the variation of Γ with respect to G and not $\bar{\phi}$ we will adopt the following generic labelling for vertices

$$S_{\bar{\phi}}^{\text{int}}[\phi] = \frac{1}{2}\delta m^2\phi^2 + \frac{g}{3!}\phi^3 + \frac{\lambda}{4!}\phi^4 \quad (2.58)$$

$$S_{\bar{\phi}}'' = G^{(0)-1}. \quad (2.59)$$

omitting explicit reference to a dependence on $\bar{\phi}$. If we were specifically interested in the scalar ϕ^4 theory from the previous section, then the dependence on $\bar{\phi}$ would enter via the coupling $g = \lambda\bar{\phi}$ and tree-level propagator $G^{(0)-1}(p) = p^2 + m^2 + \lambda\bar{\phi}^2/2$.

Given the interactions, we can essentially read off the resulting diagrams. At lowest order in \hbar ,

$$\langle\phi\phi\rangle_K = \frac{1}{G^{(0)-1} + K^{(1)}} + \mathcal{O}(\hbar), \quad (2.60)$$

so that $K^{(1)} = G^{-1} - G^{(0)-1}$. Substituting $K^{(1)}$ back into $\langle\phi\phi\rangle_K$, up to $\mathcal{O}(\hbar)$

$$\langle\phi\phi\rangle_K = \frac{1}{G^{-1} + \hbar K^{(2)}} + \hbar G^2 \left[\frac{g^2}{2} \int_{\text{D}} G^2 - \frac{\lambda}{2} \int_{\text{D}} G \right] + \mathcal{O}(\hbar^2), \quad (2.61)$$

where \int_{D} is used to indicate an integration over internal loop momenta. It is more intuitive to switch over to a diagrammatic notation, so we define

$$\begin{aligned} G &= \text{---} & -g &= \text{---} \text{---} \text{---} \\ -\lambda &= \text{---} \times \text{---} & -\delta m^2 &= \text{---} \text{---} \text{---} \\ K^{(2)} &= \text{---} \text{---} \text{---} \text{---} \text{---} & K^{(3)} &= \text{---} \text{---} \text{---} \text{---} \text{---} \end{aligned} \quad (2.62)$$

additionally, dots will be used to indicate the ends of non-amputated diagrams. Our expression for the two-point function now reads

$$\frac{1}{G^{(0)-1} + K} = \text{---}\bullet\text{---}\bullet\text{---} - \hbar \text{---}\bullet\text{---}\textcircled{2}\text{---}\bullet\text{---} + \hbar^2 \left[\text{---}\textcircled{2}\text{---}\textcircled{2}\text{---}\bullet\text{---} - \text{---}\bullet\text{---}\textcircled{3}\text{---}\bullet\text{---} \right] + \mathcal{O}(\hbar^3). \quad (2.63)$$

The $\mathcal{O}(\hbar)$ expression for K is entirely determined by Eq. (2.61),

$$K^{(1)} = \frac{1}{2} \text{---}\bigcirc\text{---} + \frac{1}{2} \text{---}\bigcirc\text{---}. \quad (2.64)$$

To obtain the full picture at $\mathcal{O}(\hbar^2)$ we have to start by accounting for all of the $\mathcal{O}(\hbar)$ corrections to the propagators in the one-loop term

$$\frac{\hbar}{(G^{-1} + \hbar K^{(2)})^2} \left(\frac{g^2}{2} \int_{\text{D}} \frac{1}{(G^{-1} + \hbar K^{(2)})^2} - \frac{\lambda}{2} \int_{\text{D}} \frac{1}{(G^{-1} + \hbar K^{(2)})} \right) =$$

$$\hbar \text{---}\textcircled{2}\text{---}\bullet\text{---} - \hbar^2 \left[2 \text{---}\textcircled{2}\text{---}\textcircled{2}\text{---}\bullet\text{---} + \text{---}\bullet\text{---}\textcircled{2}\text{---}\bullet\text{---} + \frac{1}{2} \text{---}\bullet\text{---}\textcircled{2}\text{---}\bullet\text{---} \right] + \mathcal{O}(\hbar^3). \quad (2.65)$$

From this expression as well as Eq. (2.63) it is apparent that $\langle \phi \phi \rangle_K$ contains 2PI as well as 2PR diagrams. However, if we account for the remaining $\mathcal{O}(\hbar^2)$ terms arising from the expansion of the path-integral as well as those from Eq. (2.63), it is straightforward to verify that cancellations occur between Eq. (2.63), Eq. (2.65) and the remaining terms in $\langle \phi \phi \rangle_K$ in such a way that

$$K^{(3)} = \frac{1}{2} \text{---}\bigcirc\text{---} + \text{---}\bigcirc\text{---} + \frac{1}{6} \text{---}\bigcirc\text{---} + \frac{1}{4} \text{---}\bigcirc\text{---} + \text{---}\bigcirc\text{---} + \text{---}\bigcirc\text{---}.$$

These diagrams are all 2PI.

2.3.2 Recovery of the Φ -derivable approximation

Going back to Section 2.1, the Φ -derivable approximation presented earlier is obtained by initially truncating K at a finite loop-order and then subsequently setting $K = 0$ (to coincide with the stationary point $\delta\Gamma/\delta G = 0$), the end result being a self-consistent approximation for the two-point function G . As earlier, we will define the self-energy as $\Pi = G^{(0)-1} - G^{-1}$, so that setting $K = 0$ yields

$$\Pi = \hbar K^{(2)} + \hbar^2 K^{(3)} + \dots \quad (2.66)$$

A one-loop truncation is solved by $K^{(1)} = -\Pi = 0$, recovering the tree-level propagator $G^{(0)-1} = G^{-1}$; this is equivalent to the “trivial” Φ -derivable approximation. Keeping the two-loop¹¹ term $K^{(2)}$

$$\Pi = \frac{1}{2} \text{---}\bigcirc\text{---} + \frac{1}{2} \text{---}\bigcirc\text{---} ; \quad (2.67)$$

this is precisely the equation of motion from the two-loop Φ -derivable approximation of Section 2.1 (suitably extended to include cubic interactions).

In general, an n -loop truncation of a 2PI effective action yields the corresponding n -loop Φ -derivable approximation for the self-energy. For the action itself we can write (reverting back to $\hbar = 1$)

$$\Gamma[\bar{\phi}, G] = -S[\bar{\phi}] + \frac{1}{2} \text{Tr} \log G + \frac{1}{2} \text{Tr} G(G^{-1} - G^{(0)-1}) + \frac{1}{2} \Phi[\bar{\phi}, \Pi] \quad (2.68)$$

¹¹ Two-loops refers to the fact that the expression for Γ contains two-loop diagrams in this truncation.

where the content of Φ reflects the loop-order of the truncation. At three-loops we would have

$$\Phi[\bar{\phi}, \Pi] = \frac{1}{6} \text{circle with horizontal line} + \frac{1}{4} \text{figure-eight} + \frac{1}{12} \text{circle with three radial lines} + \frac{1}{24} \text{circle with two horizontal lines} + \frac{1}{4} \text{circle with three arcs from center} + \text{circle with star} . \quad (2.69)$$

This expansion in terms of 2PI diagrams can be directly verified by inserting the two-loop expression we had obtained earlier for K back into Eq. (2.48) and then carefully collecting terms at each order in \hbar . In a practical computation we are able to neglect divergent constants such as $\text{Tr } GG^{-1} = \text{Tr } \mathbf{1}$ in the expression for Γ as we restrict ourselves to determining its variations.

2.3.3 Generalization to 3PI and higher n

Following the presentation of the 1PI and 2PI effective actions, the generalization to higher n will now seem very natural. At higher n , an n PI effective action takes the form $\Gamma^{n\text{PI}}[\bar{\phi}, G, V_3, \dots, V_n]$, where V_n denotes the n -point vertex functions of the theory [149]. In analogy to the 1PI and 2PI cases, $\Gamma^{n\text{PI}}$ is defined via a Legendre transform (with respect to higher point sources) and likewise, it obeys a similar set of stationarity conditions

$$\frac{\delta \Gamma^{n\text{PI}}}{\delta \bar{\phi}} = \frac{\delta \Gamma^{n\text{PI}}}{\delta G} = \dots = \frac{\delta \Gamma^{n\text{PI}}}{\delta V_n} = 0. \quad (2.70)$$

As in the 2PI case, expressions for n -point functions at the extremum (which we will often refer to as *solutions*) are fully resummed. Further analogously, a truncation at m -loops necessarily dictates which topologies enter the resummation. Therefore, an m -loop n PI effective action is said to describe a *selective* resummation of a perturbation series.

n PI effective actions also exhibit a hierarchy [113] (see also [149]). Recall that we observed that the one-loop truncation of $\Gamma^{2\text{PI}}$ was trivially solved with G being equal to its tree-level expression $G^{(0)}$; in other words, $\Gamma^{2\text{PI}}$ at one-loop is equivalent to $\Gamma^{1\text{PI}}$ at one-loop. The general statement is that an n PI effective action truncated at m -loops only contains non-trivial information about vertex functions V_n for $n \leq m$. Thus, a 3PI effective action requires at least a three-loop treatment.

In this work we opt to apply a three-loop truncation (of both the 2PI and 3PI effective actions), so we will not proceed any further with derivations involving the loop expansion, bringing Chapter 2 to a close. The presentation involving scalar fields though illustrative may seem overly simplistic; however, we will see in the next chapter that $\Gamma[\bar{\phi}, G, \dots]$ actually generalizes in a very straightforward manner to more elaborate field content. In Chapter 3 we will present the specific details of the extension to a gauge theory and formalize the definition of the 3PI effective action. Following this we will switch the focus to the technical details concerning a practical application (regularization, numerical challenges, *Ansätze*, etc.) eventually leading to a resolution of the variational equations.

CHAPTER 3

Three-loop 3PI effective action in 3D Yang-Mills theory

3.1 Resummation in a hot gauge theory

Many of the most interesting questions in the context of electroweak theory or QCD have to do with dynamics or unequal time correlations. For instance, real-time correlations and non-equilibrium currents are important in understanding whether electroweak baryogenesis can occur at a first order electroweak phase transition [150, 151]. In the heavy ion context there are many dynamical quantities we would like to know, such as the viscosity [152, 153, 154, 155], heavy quark diffusion rate [156, 157, 158], photon production rate [159, 160, 161], and so forth. Dynamical properties of QCD are also important at much higher temperatures such as the electroweak temperature, where they could play a role in baryogenesis and in various phase transitions.

The problem is that we have no first-principles, intrinsically non-perturbative technique for theoretically predicting such real-time properties, even in equilibrium or linear response. We have models and phenomenological fitting (for instance, of the viscosity using elliptic flow in heavy ion collisions [155]), but the only tool we have which is close to first principles is perturbation theory. However, many of the properties of QCD and Yang-Mills plasmas in general (for instance, the strength of the electroweak phase transition, or the thermodynamics of QCD near the scale Λ_{QCD}) *cannot* be described perturbatively. This motivates their study via the lattice,

both in the context of electroweak theory [162, 163] and QCD [164, 165]. The lattice *is* limited in its applicability to real-time dynamics [166] or QCD at finite chemical potential [167, 168], thus motivating the development of alternative non-perturbative approaches.

Perturbation theory is notoriously poorly convergent when applied to hot gauge theories. For instance, the expansion for the pressure of QCD as a series in α_s is known to order $\alpha_s^3 \ln \alpha_s$, but the series only appears to be useful at temperatures many times the scale Λ_{QCD} [47]. For real-time quantities, certain (Hard Thermal Loop or HTL) resummations [169, 170] are necessary even to find leading order results for transport coefficients [171, 172]. Even so, the perturbative expansion for real-time quantities appears to be even worse behaved than it is for the pressure and other thermodynamic quantities, at least if we restrict attention to transport coefficients, which involve either zero frequency and momentum or lightlike momentum limits of external 4-momenta. Only two such quantities are known beyond leading order; the diffusion coefficient for a heavy quark [173] and the transverse momentum diffusion for a fast charge [174]. In each case the first corrections enter at order g , not order g^2 as would be normal in a vacuum perturbative expansion, and the corrections represent of order 100% shifts in the transport coefficients for $\alpha_s \sim 0.05$, a value obtained only at temperatures well above 1 TeV! Though it is a little dangerous to extrapolate from two examples, it appears that even at the electroweak scale, the QCD sector of the Standard Model is probably not well described by perturbation theory, as far as dynamics are concerned.

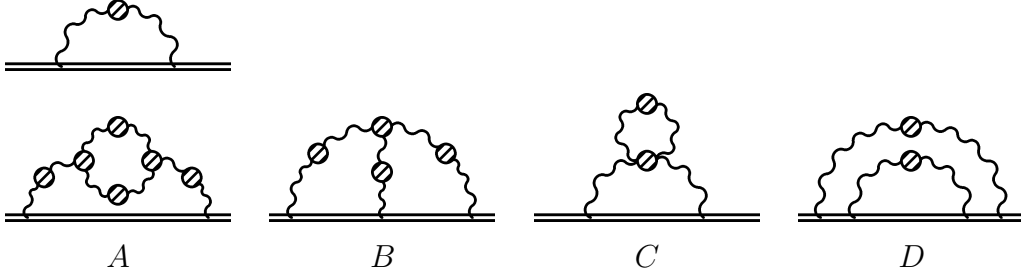


Figure 3-1: NLO heavy quark diffusion.

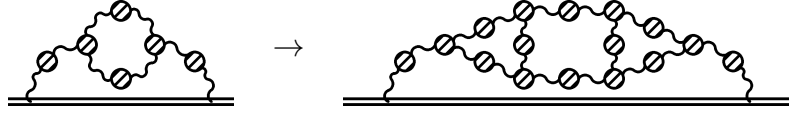


Figure 3-2: Inclusion of additional HTLs.

Let us analyze the problem in a little more detail, for the case of heavy quark diffusion [173]. The leading order diagram and the four next-to-leading order diagrams are shown in Fig. 3-1. Here the double line is the Wilson line heavy quark trajectory, and hatched blobs represent Hard Thermal Loop (HTL) resummation. In particular, the leading order diagram is already one-loop self-energy resummed. The contribution from diagram *A* is 5 to 10 times as large as that of the other diagrams (in Coulomb gauge, the choice used in [173]). Therefore the physics which is problematic for the perturbative expansion is presumably the physics represented by this diagram. This diagram resembles the leading order diagram, except that in the leading diagram the momentum in the self-energy loop is assumed to be large compared to the propagator momentum, while in diagram *A* it is allowed to be of the same order. When the momentum is soft, it is also necessary to include HTLs

on the propagators and vertices of the self-energy in diagram A . The large size of diagram A indicates that the soft loop momentum region in the self-energy is almost as important as the region where the loop momentum is hard. This is a problem because in this soft region, the HTL corrections must also be included on the propagators and vertices in diagram A . But why shouldn't these loops also receive large corrections from their soft-momentum regions? Then we also need to include the region where we replace the HTLs in diagram A with soft momenta, as suggested in Fig. 3-2. But when these momenta are soft, there are new vertices and propagators requiring HTL corrections. These may also have large soft corrections, bringing in more diagrams – and we are “off to the races.”

The problem is that the low-momentum (gT) region is not really a small part of phase space, and it is not really weakly coupled. But the good news is that the dominance of diagram A above suggests that it is really only the soft corrections to the HTLs present in the previous order which are important. This leads to an infinite number of diagrams contributing, but only a restricted (infinite) set of diagrams being “most important” – those suggested in Fig. 3-2. If these diagrams could be resummed somehow, then we would likely capture all the most important corrections, and the range of validity of perturbation theory might be significantly expanded.

There *is* a procedure for performing an iterative resummation of all one-loop self-energy and three-point vertex corrections, as suggested in Fig. 3-2. It is the three-loop, three-particle irreducible (3PI) resummation scheme [113]. The above discussion suggests that a 3PI resummation may capture the most important higher-order physics and greatly improve the convergence of the perturbative expansion –

even capturing some non-perturbative information. But this is by no means guaranteed, since the 3PI approach performs an incomplete resummation of higher-order effects, which furthermore is not gauge-invariant [115, 116]. That is, a selective resummation would violate non-abelian Ward-Slavnov-Taylor identities at loop orders beyond the specific order of the truncation.

As of writing, this work is the only known direct application of the 3PI technique to a non-abelian gauge theory. In addition to performing the resummation, we would also like to *test* whether or not the resummation technique is reliable in a somewhat more controlled setting; this will be the focus of the study of $SU(N)$ Higgs theory in Chapter 4. For now we will consider a slightly simpler problem as a warm-up exercise, and as a testing ground for whether or not the 3PI technique is potentially effective in non-abelian gauge theory. Our focus now is primarily on developing the tools necessary for resolving the 3PI (and hence also 2PI) equations of motion and to do so, we will investigate the three-loop, 3PI resummation of 3D Yang-Mills theory.

Working in 3 Euclidean dimensions simplifies the problem in two ways. First, the UV behaviour of 3D Yang-Mills theory is much milder than in 4D, since the theory is super-renormalizable. The second simplification is that the vacuum Euclidean theory has fewer Lorentz invariants than the finite temperature, Minkowski theory (or the Euclidean theory with periodic time direction). For instance, in (vacuum) Euclidean space the propagator $G^{\mu\nu}$ is built from two tensorial structures and is a function of one invariant; $G^{\mu\nu}(p) = \mathbf{T}^{\mu\nu}G_T(p^2) + \mathbf{L}^{\mu\nu}G_L(p^2)$. In real time at finite temperature, or in imaginary time with periodic boundary conditions, it has more tensorial structures and is a function of *two* variables, p^2 and the energy P^0 .

Note however that 3D Yang-Mills theory is far from trivial. The flip side of super-renormalizability is that, since the gauge coupling is dimensionful, it establishes a scale (momentum scale $p \sim g^2$ or length scale $l \sim 1/g^2$) where we expect strongly coupled, non-perturbative behaviour. Therefore 3D Yang-Mills theory displays both weak or strong coupling, depending on the energy scale. 3D Yang-Mills theory is also physically interesting. Recall also from Chapter 1, Section 1.4.1 that at the thermodynamic level, the infrared behaviour of thermal 4D Yang-Mills theory (with any fermionic matter content) is 3D Yang-Mills with an adjoint scalar [36, 37, 99, 175]. The non-perturbative scale $g^2 \equiv g_{3D}^2$ corresponds to the scale $g_{4D}^2 T$ of the full theory (at leading perturbative order). It is believed that the poor convergence of perturbation theory at intermediate couplings in QCD is due to the non-perturbative physics of the 3D theory. Therefore in a sense studying the 3D gauge theory by non-perturbative means is treating most of the physics which makes thermal QCD poorly behaved (at intermediate couplings).

The goal at this point is to produce a complete solution to the three-loop truncation of the 3PI effective action for 3D QCD. As outlined above, this should be viewed as a warm-up problem to what we would really like to do, which is use the method to directly compute gauge-invariant observables. Then, based on the outcome, it may be interesting to consider an application in 3+1 dimensions in a thermal (or even non-equilibrium) context, though this is presently beyond the scope of this thesis. For now, this first step is well motivated. As already emphasized, the 3D theory is a subset of the 3+1D theory (the theory we would really want to solve). And the 3D theory can be studied non-perturbatively on a lattice, which means we will be able

to test to a limited extent the 3PI resummation procedure in a non-perturbative context by seeing whether its predictions are successful.¹ Such a test is necessary because the 3PI resummation captures only an incomplete and gauge-noninvariant subset of diagrams, so there is no hard guarantee that it will successfully reproduce the non-perturbative IR physics (though it is indeed possible that gauge-dependence is small [117]). To emphasize again, this chapter will concentrate on the resummation; we will focus more on the comparison with non-perturbative lattice studies in Chapter 4.

3.2 The 3PI effective action

The 3PI effective action is obtained by a Legendre transform of the generating functional of connected diagrams

$$W[J, K, L] = -\log \int \mathcal{D}\phi \, e^{-\left(S[\phi] + J\phi + \frac{1}{2}K\phi^2 + \frac{1}{6}L\phi^3\right)} \quad (3.1)$$

with one, two and three-particle sources, J , K and L (the notation is schematic, as in Chapter 2). Conjugate to J , K and L are the variables $\bar{\phi}$, G and G_3 , which are labelled as such since they are equal to the connected one, two and three-point functions at the stationary point of the effective action. The functional derivatives

¹ To the extent that the study of pure Yang-Mills in this chapter is limited to the computation of gauge-fixed quantities.

of W are given by

$$\frac{\delta W}{\delta J} = \bar{\phi} \quad (3.2)$$

$$\frac{\delta W}{\delta K} = \frac{1}{2}(G + \bar{\phi}^2) \quad (3.3)$$

$$\frac{\delta W}{\delta L} = \frac{1}{6}(G_3 + 3G\bar{\phi} + \bar{\phi}^3), \quad (3.4)$$

and the 3PI effective action follows,

$$\Gamma[\bar{\phi}, G, G_3] = J \frac{\delta W}{\delta J} + K \frac{\delta W}{\delta K} + L \frac{\delta W}{\delta L} - W[J, K, L].$$

In terms of Γ the equations of motion for $\bar{\phi}$, G and G_3 read

$$\frac{\delta \Gamma}{\delta \bar{\phi}} = \frac{\delta \Gamma}{\delta G} = \frac{\delta \Gamma}{\delta G_3} = 0. \quad (3.5)$$

We will now specialize this procedure to the case of mQCD. Since we consider pure Yang-Mills there is no Higgs mechanism and we expect the one-point functions to vanish at the extremum;² hence we can set the VEVs of A^μ , \bar{c} and c to zero and work only with the two and three-point functions. To write down the exact form of Γ relevant to the Yang-Mills field content, it is useful to define Feynman Rules for the propagators and vertex functions;³ see Table 3–1. The one-particle-irreducible

² When Grassman fields such as ghosts are present, the extremum is generally a saddle-point rather than a maximum, as the associated $\text{Tr} \log$ enters with an overall minus sign relative to bosonic fields.

³ We will generally suppress colour indices as well as Lorentz indices when they can be inferred from context. For instance, $G = G_{\mu\nu} = G_{\mu\nu}^{ab}$, $V_{\mu\nu\rho} = V_{\mu\nu\rho}^{abc}$ etc.

	Resummed	Bare
Gluon Propagator	$G_{\mu\nu}^{ab} = \text{wavy line with dots}$	$G_{\mu\nu}^{(0)ab} = \text{wavy line}$
Ghost Propagator	$\Delta^{ab} = \text{dotted line with triangle}$	$\Delta^{(0)ab} = \text{dotted line}$

Table 3–1: Feynman rules for the Yang-Mills propagators in the 3PI effective action. Vertices are denoted by a large black dot whenever they are “resummed,” otherwise they are bare. See also Appendix B.

three-vertex V is related to the three-point function via $G_3 = (G)^3 V$; extremizing with respect to G and G_3 is equivalent to extremizing with respect to G and V , which we find to be more convenient variables. The 3PI effective action is given in terms of G , Δ , V and \mathbb{V} by

$$\begin{aligned}
\Gamma = & \frac{1}{2} \text{Tr} \log G - \frac{1}{2} \text{Tr} [G^{(0)}]^{-1} G - \text{Tr} \log \Delta + \text{Tr} [\Delta^{(0)}]^{-1} \Delta \\
& + \frac{1}{6} \text{diagram} - \frac{1}{12} \text{diagram} + \frac{1}{8} \text{diagram} \\
& - \text{diagram} + \frac{1}{2} \text{diagram} \\
& + \frac{1}{48} \text{diagram} + \frac{1}{24} \text{diagram} + \frac{1}{8} \text{diagram} \\
& - \frac{1}{3} \text{diagram} - \frac{1}{4} \text{diagram},
\end{aligned} \tag{3.6}$$

(where we have explicitly written symmetry factors associated with diagrams and signs associated with ghost loops for clarity, as we will throughout), from which we have the following four equations of motion

$$\frac{\delta\Gamma}{\delta G} = \frac{\delta\Gamma}{\delta\Delta} = \frac{\delta\Gamma}{\delta V} = \frac{\delta\Gamma}{\delta\mathbb{V}} = 0. \quad (3.7)$$

To illustrate the physics of Eq. (3.7), consider $\delta\Gamma/\delta G(p)$. Performing the variation using the expression in Eq. (3.6), we find

$$G^{-1}(p) = G^{(0)-1}(p) - \Pi(p), \quad (3.8)$$

$$\begin{aligned} \Pi^{(1)}(p) = & \text{[diagram: wavy line with a star loop]} - \frac{1}{2} \text{[diagram: wavy line with a star loop and a dot]} + \frac{1}{2} \text{[diagram: wavy line with a star loop]} \\ & - 2 \text{[diagram: wavy line with a circle loop]} + \text{[diagram: wavy line with a circle loop and a dot]} \end{aligned} \quad (3.9)$$

which we recognize as the resummed one-loop self-energy (with the superscript denoting the loop order, i.e. $\Pi = \Pi^{(1)} + \Pi^{(2)}$; we have not shown the similar graphical representation of $\Pi^{(2)}$). It is worth noting that a three-loop truncation only resums planar graphs; a resummation involving a non-planar diagram would require a four-loop treatment.

Similarly, variation with respect to V gives the vertex 3PI equation of motion

$$\text{[diagram: wavy line with a vertex]} = \text{[diagram: wavy line with a vertex]} + \text{[diagram: wavy line with a vertex and a loop]} + \frac{3}{2} \text{[diagram: wavy line with a star loop]} - 2 \text{[diagram: wavy line with a vertex and a loop]} \quad (3.10)$$

closely resembling a Schwinger-Dyson (SD) equation.⁴ The propagators appearing in all diagrams in Eq. (3.8) and Eq. (3.10), as well as all vertices (except certain vertices in the one-loop self-energies), are the full objects. Therefore these equations must be solved *self-consistently*. The self-consistent solution of these equations represents our main challenge. We face two chief difficulties:

- Decomposing the propagator into its transverse and longitudinal parts,

$$\begin{aligned} G^{\mu\nu}(p) &= G_T^{\mu\nu}(p) \mathbf{T}^{\mu\nu} + G_L^{\mu\nu}(p) \mathbf{L}^{\mu\nu}, \\ \mathbf{L}^{\mu\nu} &\equiv \frac{p^\mu p^\nu}{p^2}, \quad \mathbf{T}^{\mu\nu} \equiv g^{\mu\nu} - \mathbf{L}^{\mu\nu}, \end{aligned} \quad (3.11)$$

the propagators are determined in terms of three *arbitrary* functions of one continuous variable, $G_T(p), G_L(p)$ and $\Delta(p)$ with $p = \sqrt{p^2}$. Similarly, the vertex $V_{\mu_1\mu_2\mu_3}(p_1, p_2, p_3)$ (with $p_{3\mu} = -p_{1\mu} - p_{2\mu}$) can be expressed in terms of *six* independent tensorial structures (see below), each multiplying an undetermined function of the *three* invariants p_1^2, p_2^2 , and $p_1 \cdot p_2$ (or equivalently p_1^2, p_2^2 , and p_3^2). The challenge is that we are not merely solving for a few numbers, but self-consistently solving for unknown functions of one to three continuous variables.

⁴ The exact Schwinger-Dyson equations are derived in terms of the 1PI effective action from the relations $\delta\Gamma/\delta\bar{\phi} = J$ and $0 = \int D\phi (\frac{\delta S}{\delta\phi} + J)e^{-S[\phi]-J\phi}$. The exact SD equations for the n -point function of a given theory are *qualitatively* similar to the n PI equations of motion, except that they are not closed. For further background material on SD equations, see e.g. [128, 176], and for a direct comparison to the n PI formalism, see [113].

- The one-loop gluon self-energy diagrams are linearly divergent, and the two-loop gluon self-energy diagrams are individually logarithmically divergent. Divergences of this sort must be regulated in a manner which respects gauge-invariance,⁵ such as dimensional regularization. However since the propagators and vertices appearing in the diagrams are general functions of momentum which are presumably only known numerically and only in $D = 3$ dimensions, we will have to perform these integrations numerically.

The issue of divergences in self-energies is a technical issue which can be handled rather easily in 3 dimensions. The key fact is that at large momenta G, Δ, V and \mathbb{V} approach their free values up to power suppressed corrections. We therefore know the exact form of the UV divergences. If we can find an expression with the same UV divergent behaviour which is simple enough to integrate using dimensional regularization, we can add and subtract it. The subtraction renders the numerical integration of the full self-energy expressions finite, while the added version is integrated using dimensional regularization. We will explain this procedure in more detail in the next section.

In order to fit arbitrary functions of one or a few real variables, we will write down a sufficiently flexible *Ansatz* for each function, with some set of variational

⁵ One might argue that, since the 3PI technique truncated to three-loops is not gauge-invariant, the use of a gauge-invariant regulator is unnecessary. But we believe that it is necessary; first, our approach at least retains gauge-invariance to low loop order, which would be lost without a gauge-invariant regularization. And second, a gauge non-invariant regularization at one-loop order would allow divergent masses, which fundamentally damage the physics.

parameters. That is, we take $G_T(p) = G_T(c_i, p)$ where c_i are coefficients – in practice, we take $G_T(p)$ to be a rational function of p , and the c_i are coefficients of this rational function. Extremization of Γ with respect to $G(p)$ is then replaced by its extremization with respect to the coefficients c_i of each propagator and vertex function. Under this procedure, some set of integral moments of the 3PI equations of motion will be satisfied, rather than the equations being satisfied at every momentum value. We can determine the quality and limitations of this approach by seeing how the determined correlation functions change as the sizes of the variational *Ansätze* are changed; and we can directly test how well the 3PI equations of motion are obeyed by computing directly the self-energies and vertex corrections at various momenta and comparing to the *Ansatz*, or measuring an integrated mean squared failure of the equations of motion.

3.3 Divergences and regularization

As discussed above, variation of Γ with respect to a propagator gives rise to a self-consistent equation involving self-energies written in terms of G and V . These will be, in general, complicated functions. Yet the self-energies may be UV divergent and so they must be regulated. Even after taming these self-energy divergences, the variation with respect to a propagator or vertex *Ansatz* coefficient $\delta\Gamma/\delta c_i$ may lead to a divergent integral over the propagator momentum p . We must also ensure that such divergences do not occur. We will handle these two problems in turn. Throughout we denote the momentum entering a self-energy as p , and use k and q for internal loop momenta.

3.3.1 Divergences in self-energies

In 3 dimensions the only divergent subdiagrams are gluon self-energies. To handle these divergences we must work in a regularization scheme which renders the self-energy diagrams finite *and* preserves gauge invariance. Therefore we will perform all integrals in dimensional regularization (DR), so $\int d^3q \rightarrow \frac{1}{\bar{\mu}^{2\epsilon}} \int d^Dq$ with $D = 3 + 2\epsilon$, $\bar{\mu}^2 = \mu^2 e^\gamma / 4\pi$. Unfortunately the self-energies contain the functions G and V , which are complicated and are only known in 3 dimensions. However, for any integral which is finite and well behaved in 3 dimensions, the $\epsilon \rightarrow 0$ limit of the DR value is the same as the value directly computed in 3 dimensions. Therefore we will start with identifying the UV divergent behaviour of the full integrals containing G and V so that we can subtract and add simple integrals with the same divergences. We can then perform the (finite) subtracted versions numerically in 3 dimensions, and finish off by adding back the simple integrals using DR.

Dressed vertices and propagators are well behaved in the IR, hence the only divergences that we expect to see arise from the region of momentum space where q is large. Therefore we need to determine the asymptotic behaviours of G and V . Our theory is super-renormalizable, meaning that the coupling g^2 carries dimension, $[g^2] = [q]$. For large q , g^2 is small compared to the relevant scale q , so the large q region is weakly coupled and has a perturbative expansion. Further, powers of g^2 in the expansion must be balanced against powers of q on dimensional grounds. Therefore the leading and first subleading behaviour of the propagator in 3 dimensions is

$$G_{\mu\nu}(q) = \frac{1}{q^2} (\mathbf{T}_{\mu\nu}(q) + \xi \mathbf{L}_{\mu\nu}(q)) + \frac{g^2 \pi_{\text{YM}}^{(1,0)}}{q^3} \mathbf{T}_{\mu\nu}(q) + \mathcal{O}(q^{-4}). \quad (3.12)$$

Similarly, the vertex goes as

$$V \sim q + g^2 q^0 + \mathcal{O}(q^{-1}) \quad (3.13)$$

with q generically denoting a single power of external momentum. The specific form of the g^2 correction to V is known, see Appendix D; but as we see in a moment we do not need it here. The one-loop correction to the gluon self-energy is also known. It is purely transverse and equals [36] (see also Appendix C)

$$\Pi_{\text{YM};\mu\nu}^{\text{B}(1,0)}(q) = \frac{g^2 N}{64} p(\xi^2 + 2\xi + 11) \mathbf{T}_{\mu\nu}(q), \quad (3.14)$$

hence $\pi_{\text{YM}}^{(1,0)}$ introduced in Eq. (3.12) is⁶

$$\pi_{\text{YM}}^{(1,0)} = \frac{N}{64} (\xi^2 + 2\xi + 11). \quad (3.15)$$

Now, consider the diagram

$$\text{Diagram} = \frac{1}{\bar{\mu}^{2\epsilon}} \int \frac{d^D q}{(2\pi)^D} V_{\mu\alpha\delta} V_{\nu\beta\kappa} G^{\alpha\beta}(p+q) G^{\delta\kappa}(q), \quad (3.16)$$

⁶ The notation used for the one-loop self-energy warrants a bit of explanation, as it may seem overly cumbersome. In general, we write self-energy corrections as $\Pi_{\text{YM};\mu\nu}^{\text{B}(m,\epsilon)}(p)$; “B” indicates that we mean an object constructed out of bare (and not resummed) tree-level propagators and vertices (to be distinguished from the labels SD and NP to be used later in this chapter), “YM” indicates that all internal lines are either gauge fields or ghosts (i.e. no scalars), m is used to count the loop order, and ϵ refers to the analytic continuation to $D = 3 + 2\epsilon$ dimensions. With this notation there is an exact correspondence with the symbols in Appendix C.

where traces over internal colour indices are implied (and hence the overall diagram is proportional to the colour identity). Expanding the integrand in powers of $1/q$, for $D = 3$ the large q region of the integral behaves as

$$\begin{aligned}
\text{Diagram} &\sim g^2 \int d^3q \left[(q)^2 \frac{1}{(q^2)^2} \right. \\
&\quad + \underbrace{2g^2(q)^2 \frac{\pi_{\text{YM}}^{(1,0)}}{q^3} \frac{1}{q^2}}_{\text{NLO propagator}} + \underbrace{2g^2(q) \frac{1}{(q^2)^2}}_{\text{NLO vertex}} + \underbrace{\mathcal{O}(g^4 q^{-4})}_{\text{NLO}^2 + \text{NNLO}} + \dots \Big]. \quad (3.17)
\end{aligned}$$

The first term arises from the leading order (bare) terms in the vertices and propagators, and the next two terms originate from the one-loop corrections (as marked). These first three integrals diverge, so we will have to add and subtract something to cancel their divergent behaviour.

Actually, the NLO vertex corrections above will cancel when we sum over the one-loop self-energy corrections. To see this, consider the two diagrams, with one and with two full vertices:

$$\left[\text{Diagram 1} - \frac{1}{2} \text{Diagram 2} \right]_{q \gg g^2} \sim \frac{1}{2} \text{Diagram 3} \Big|_{q \gg g^2} \quad (3.18)$$

The diagram with one full vertex enters with -2 times the weight of the diagram with two full vertices. Therefore the NLO vertex contributions from these two diagrams cancel, and the UV behaviour is the same at NLO as the behaviour of a loop with no vertex corrections. Provided that we perform the two diagrams by adding their integrands inside the integration, this cancellation takes place at the level of the

integrand and does not lead to a log divergence in the integral in 3 dimensions. (This cancellation does not mean that the NLO vertex correction disappears; instead this correction will be accounted for explicitly when we include two-loop self-energy corrections.)

Next consider the bare part of Eq. (3.17), which is linearly divergent in 3 dimensions. We will add and subtract a diagram made out of the bare vertex and propagator functions,

$$\text{Diagram} = g^2 \frac{1}{\bar{\mu}^{2\epsilon}} \int \frac{d^D q}{(2\pi)^D} V_{\mu\alpha\delta}^{(0)} V_{\nu\beta\kappa}^{(0)} G^{(0)\alpha\beta}(p+q) G^{(0)\delta\kappa}(q) \quad (3.19)$$

with $G^{(0)}$'s are $V^{(0)}$'s denoting bare propagators and vertices. The difference

$$\frac{1}{2} \text{Diagram} - \frac{1}{2} \text{Diagram} \quad (3.20)$$

is only logarithmically divergent in 3 dimensions. Moreover, Eq. (3.19) is finite when computed in DR and its $D \rightarrow 3$ limit is

$$\left. \frac{1}{2} \text{Diagram} \right|_{\text{DR}} = \frac{g^2 N}{64} p \left((\xi^2 + 2\xi + 11) \mathbf{T}_{\mu\nu}(p) - g_{\mu\nu} - \frac{p_\mu p_\nu}{p^2} \right). \quad (3.21)$$

This diagram, plus the bare ghost diagram which cancels the non-transverse piece above, gives rise to $\Pi_{\text{YM};\mu\nu}^{\text{B}(1,0)}$ stated earlier.

Lastly, we must subtract something with the same NLO “propagator” behaviour remaining in Eq. (3.17). Naively, we could do this by defining the one-loop corrected

propagator⁷

$$G_{\mu\nu}^{\text{B}(1,\epsilon)}(p) = G_{\mu\alpha}^{(0)}(p) \Pi_{\text{YM}}^{\text{B}(1,\epsilon)\alpha\beta}(p) G_{\beta\nu}^{(0)}(p) = \frac{\pi_{\text{YM}}^{(1,\epsilon)}}{\mu^{2\epsilon}} \frac{1}{p^{3-2\epsilon}} \mathbf{T}_{\mu\nu}(p) \quad (3.22)$$

with $\Pi_{\text{YM};\alpha\beta}^{\text{B}(1,\epsilon)}(p)$ and $\pi_{\text{YM}}^{(1,\epsilon)}$ defined by Appendix C, Eq. (30) and Eq. (33), and then “adding and subtracting” the following diagram:

$$\begin{aligned} \text{Diagram} &= g^2 \frac{1}{\bar{\mu}^{2\epsilon}} \int \frac{d^D q}{(2\pi)^D} V_{\mu\alpha\delta}^{(0)} V_{\nu\beta\kappa}^{(0)} G^{(0)\alpha\beta}(p+q) G^{\text{B}(1,\epsilon)\delta\kappa}(q) \\ &= \frac{\mathcal{A}}{\epsilon} g_{\mu\nu} - \frac{\mathcal{B}}{\epsilon} \left(g_{\mu\nu} - \frac{p_\mu p_\nu}{p^2} \right) + \text{finite}. \end{aligned} \quad (3.23)$$

The problem is that, as the above equation shows, the diagram is not only UV divergent (as expected, with coefficient \mathcal{A} which we give below), but also IR divergent (with coefficient \mathcal{B} , whose exact value will not be relevant). If we add and subtract this diagram, we will cause an IR divergence where none should appear. Instead, we will add and subtract an appropriately regulated self-energy corrected propagator,

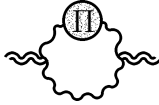
$$G_{\mu\nu}^{\text{B}(\text{IR}1,\epsilon)}(p) = \frac{\pi_{\text{YM}}^{(1,\epsilon)}}{\mu^{2\epsilon}} \frac{1}{(p^2 + \omega_0^2)^{\frac{3}{2}-\epsilon}} \left(g_{\mu\nu} - \frac{p_\mu p_\nu}{p^2 + \omega_0^2} \right) \quad (3.24)$$

so that the integration in

$$\text{Diagram} = g^2 \frac{1}{\bar{\mu}^{2\epsilon}} \int \frac{d^D q}{(2\pi)^D} V_{\mu\alpha\delta}^{(0)} V_{\nu\beta\kappa}^{(0)} G^{(0)\alpha\beta}(p+q) G^{\text{B}(\text{IR}1,\epsilon)\delta\kappa}(q) \quad (3.25)$$

⁷ Note that since we anticipate a $1/\epsilon$ divergence at two-loops, we now have to be careful with the treatment of terms $\mathcal{O}(\epsilon)$.

can still be performed analytically in DR. Upon integration, this diagram has the following form:

$$\left. \text{Diagram} \right|_{\text{DR}} = \frac{\mathcal{A}}{\epsilon} g_{\mu\nu} + \text{finite}. \quad (3.26)$$


The coefficient that multiplies the UV $1/\epsilon$,

$$\mathcal{A} = -\frac{g^4 N^2}{768 \pi^2} \frac{p^{4\epsilon}}{\mu^{4\epsilon}} (\xi + 4)(\xi^2 + 2\xi + 11), \quad (3.27)$$

is identical to that of Eq. (3.23) due to the simple fact that

$$\lim_{q \rightarrow \infty} G_{\mu\nu}^{\text{B(IR1}, \epsilon)}(q) = \lim_{q \rightarrow \infty} G_{\mu\nu}^{\text{B(1}, \epsilon)}(q). \quad (3.28)$$

Naturally, the finite parts of Eq. (3.23) and Eq. (3.25) will differ.

It may worry some readers that we have introduced an IR mass regulator. But we emphasize that we are *not* adding such a regulator to the full propagator $G^{\mu\nu}(p)$. We are only adding an IR mass regulator to a term which we add and subtract, for reasons of computational convenience. Hence, the value of the regulator – in fact, the effect of the whole term which we are adding and subtracting – exactly cancels when we combine the (analytic) result of Eq. (3.25) and the (numerical) result of the full but subtracted diagram in Eq. (3.30). We have naturally checked that the value of the regulator in Eq. (3.24) has no effect on our results for the full self-energy and therefore for the determined value of the full propagator.

Returning to Eq. (3.17), we now have

$$\begin{aligned}
& \left[\text{Diagram 1} - \frac{1}{2} \text{Diagram 2} - \frac{1}{2} \text{Diagram 3} - \text{Diagram 4} \right] \\
& + \left[\frac{1}{2} \text{Diagram 5} + \text{Diagram 6} \right] \sim \frac{\mathcal{A}}{\epsilon} g_{\mu\nu} + \text{finite} .
\end{aligned} \tag{3.29}$$

The first line is the only part which contains full propagators; but it is finite at $D = 3$. Therefore its value in DR in the $D \rightarrow 3$ limit simply equals its finite value in 3 dimensions, which we can find by numerical integration. The second line is divergent in 3D but can be carried out relatively easily in DR. It gives rise to the $\mathcal{A}g_{\mu\nu}/\epsilon$ contribution, and to some of the finite terms presented in Appendix C, Eq. (58).⁸

The procedure for handling the two-loop graphs is similar. While the graphs are more complicated, the procedure is simpler, since in every case the only UV divergences arise when all components of the graph take their bare values. Further, no two-loop graph we need, when built out of bare quantities, is IR divergent. Therefore we may simply subtract from each two-loop graph, built using G and V , the same graph built using $G^{(0)}$ and $V^{(0)}$. The bare two-loop graphs can be performed in

⁸ Appendix C, Eq. (58) is the sum of Eq. (3.25), a similarly IR regulated tadpole diagram as well as a few topologically similar graphs involving scalars. Pure Yang-Mills contributions (that is, diagrams which do not contain scalar loops) can be recovered by setting $T_R = C_R = 0$ in Appendix C.

DR and will also give rise to a $g_{\mu\nu}/\epsilon$ divergence plus a finite part; the sum of these diagrams is given by Appendix C, Eq. (57). In the end, we find that all of the $1/\epsilon$'s cancel between two-loop diagrams: the $\mathcal{O}(g^4)$ IR regulated gluon self-energy is UV finite in DR (the complete expression for which is given by Appendix C, Eq. (54)).

With this procedure in place, the self-consistent equation, Eq. (3.8), becomes

$$G^{-1}(p) = G^{(0)-1}(p) - \Pi^{(1)}(p) - \Pi^{(2)}(p), \quad (3.30)$$

$$\Pi_{\mu\nu}^{(1)} + \Pi_{\mu\nu}^{(2)} =$$

$$\begin{aligned} & \text{Diagram 1} - \frac{1}{2} \text{Diagram 2} + \frac{1}{2} \text{Diagram 3} - 2 \text{Diagram 4} \\ & + \text{Diagram 5} - \frac{1}{2} \text{Diagram 6} - \text{Diagram 7} - \frac{1}{2} \text{Diagram 8} \\ & - \frac{1}{2} \text{Diagram 9} + \text{Diagram 10} + 2 \text{Diagram 11} \\ & + \frac{1}{6} \text{Diagram 12} + \frac{1}{2} \text{Diagram 13} + \text{Diagram 14} + \frac{1}{4} \text{Diagram 15} \\ & - \text{Diagram 16} - 2 \text{Diagram 17} \\ & - \frac{1}{6} \text{Diagram 18} - \frac{1}{2} \text{Diagram 19} - \text{Diagram 20} - \frac{1}{4} \text{Diagram 21} \\ & + \text{Diagram 22} + 2 \text{Diagram 23} \\ & + \lim_{\epsilon \rightarrow 0} \left(\Pi_{\text{YM};\mu\nu}^{\text{B}(1,\epsilon)}(p) + \Pi_{\text{YM};\mu\nu}^{\text{B}(2,\epsilon)}(p) \right). \end{aligned}$$

where the $\Pi^{B(a,b)}$'s represent the sum all bare diagrams computed analytically in dimensional regularization (their values can be read from Appendix C).⁹ In writing this equation we have suppressed the Lorentz indices, as written one should take $\frac{1}{2}\mathbf{T}_{\mu\nu}\Pi^{\mu\nu}$ to get the transverse part of the self-energy needed to resum G_T and $\mathbf{L}_{\mu\nu}\Pi^{\mu\nu}$ to get the self-energy needed to resum G_L .

All ghost self-energies are finite after angular averaging, and the vertex loops are power-counting finite, so no similar subtractions are needed in these cases. Nevertheless, we will still encounter divergences when it comes time to integrate the ghost equations of motion over propagator or vertex momenta.

3.3.2 Divergences upon p -integration

Our plan is to find an approximate extremum of Γ by writing variational *Ansätze* for the propagators and vertices and to vary with respect to the *Ansatz* parameters. For instance, one could assume that the transverse propagator $G_T(p)$ is the sum of a set of test functions with unknown coefficients, $G_T(p) = \sum_i c_i \phi_i(p)$. More generally, we choose $G_T(p)$ to have some functional form with a set of variational parameters c_i ; we will give our specific choice in Section 3.4. Then variation of Γ with respect

⁹ As shown in [177] it is generally possible to alternatively express a self-energy equation of this sort as a genuine Schwinger-Dyson equation by including the vertex equation of motion. However, for our approach this representation offers the advantage that regularization occurs on a diagram by diagram basis.

to c_j would yield

$$\frac{\delta\Gamma}{\delta c_j} = \int d^3p \frac{\delta G_T(p)}{\delta c_j} \frac{\delta\Gamma}{\delta G_T(p)} = \int d^3p \frac{\delta G_T(p)}{\delta c_j} \left(G_T^{-1}(p) - G_T^{(0)-1}(p) + \Pi_T(p) \right), \quad (3.31)$$

and similarly for G_L and Δ . In the last section we ensured that the integrals involved in all self-energies Π are finite. But this does not guarantee that the p integral above will be finite. For instance, if we chose the *Ansatz*

$$G_T[p, c_i, \text{example}] = \frac{c_1}{p^2 + m^2} + \frac{c_2}{(p^2 + m^2)^{\frac{3}{2}}} + \frac{c_3}{(p^2 + m^2)^2} \quad (3.32)$$

then $\delta G_T(p)/\delta c_1 = \frac{1}{p^2 + m^2}$. And if $c_1 \neq 1$, then for large p , $G_T^{-1}(p) - G_T^{(0)-1}(p) + \Pi_T(p) \sim p^2$. In this case Eq. (3.31) would be cubically divergent. Physically this means that if we allow $G(p)$ to vary from its correct value in a way which does not die away fast in the UV, then Γ will be divergently far from its extremum.

Continuing with the same example, if we fix $c_1 = 1$, forcing the propagator to have the correct free-theory limit in the UV, then the most severe UV divergence arises from c_2 . For large p we have $\delta G_T(p)/\delta c_2 \sim p^{-3}$ and $G_T^{-1}(p) - G_T^{(0)-1}(p) + \Pi_T(p) \sim p$ (by virtue of the cancellation of the p^2 terms in G_T^{-1} and $G_T^{(0)-1}$). In this case the integral is $\sim \int d^3p (1/p^3)(p)$ which is linearly divergent. This is better but still unacceptable. To ensure a finite answer we must choose an *Ansatz* which automatically enforces the right $\mathcal{O}(p^2)$ and $\mathcal{O}(p)$ behaviour in $G_T^{-1}(p)$, namely,

$$G_T(p) = \frac{1}{p^2} + \frac{g^2 \pi_{\text{YM}}^{(1,0)}}{p^3} + (\text{Ansatz starting at } \mathcal{O}(p^{-4})). \quad (3.33)$$

In this case, $\delta G(p)/\delta c_i \lesssim \mathcal{O}(p^{-4})$ automatically, and $G_T^{-1}(p) - G_T^{(0)-1}(p) + \Pi_T(p) \sim \mathcal{O}(p^0)$. This is sufficient to ensure that the integral in Eq. (3.31) will be UV finite.

The same argument applies to G_L and Δ ; in each case we must build in the correct $1/p^2$ and $1/p^3$ behaviour of the propagator (or $\mathcal{O}(p^2)$ and $\mathcal{O}(p)$ behaviour in the inverse propagator) into our *Ansatz*; but having done so, the variations $\delta\Gamma/\delta c_i$ will all automatically be finite (unless there are IR problems).

Applying the same reasoning to the vertices, the variation of Γ with respect to a generic coefficient d_i determining V gives rise to a correction of order (the phase space is explained in Appendix E)

$$\frac{\delta\Gamma}{\delta d_i} \sim \int p dp q dq k dk \frac{\delta V}{\delta d_i} G(p)G(q)G(k) \left(V - V_{\text{bare}} - \delta V \right). \quad (3.34)$$

If we allow our *Ansatz* to change V on the scale of its leading behaviour $\sim p, k, q$ then this expression is quadratically divergent. Therefore our *Ansatz* must be restricted such that V takes on its correct (free) asymptotic limiting behaviour. Even so, in this case $\delta V/\delta d_i$ and $V - V_{\text{bare}}$ will be $\mathcal{O}(p^0)$, giving rise to a log divergence. Therefore we must compute and implement the first subleading behaviour of V and only allow our *Ansatz* to change V at NNLO, $\mathcal{O}(p^{-1}, k^{-1}, q^{-1})$. This will ensure finite variations of Γ with respect to the parameters d_i (again assuming there are no infrared issues).

It is not necessary to determine the NNLO behaviour of either self-energy or vertex corrections in order to avoid potential divergences. This is a good thing, because the $\mathcal{O}(p^{-4})$ propagator correction (or $\mathcal{O}(p^0)$ self-energy correction) is where non-perturbative physics first arises. To see this, consider the one-loop self-energy diagram in Eq. (3.16). Let us estimate the contribution when the external momentum p is large but one of the internal propagators is at a small momentum $q \sim g^2$. There is a factor of $g^2 p^2$ from the vertices, $1/p^2$ from the hard propagator, and

$\int d^3q/q^2 \sim q \sim g^2$ from the momentum integration and soft propagator in the soft region. So the contribution when one propagator is soft is of order $\Pi_{\text{soft}} \sim g^4$. This contribution is non-perturbative because the behaviour of the propagator at small momentum is. Therefore we actually *cannot* determine the NNLO behaviour of the propagator at large momenta; the perturbative expansion we alluded to earlier actually fails at this order. Fortunately, determining this order turns out to be unnecessary to eliminate divergences and render our extremization problem well posed.

Note that the elimination of divergences, both in subdiagrams and in the final variation of Γ with respect to variational *Ansatz* parameters, is much easier in $D = 3$ spacetime dimensions than it would be in $D = 4$. In that case, self-energies would be quadratically divergent at all loop orders and $\delta\Gamma/\delta c_i$ would generically be quartically divergent. It is therefore not completely clear as to how this procedure could be extended to four dimensions without some changes or restrictions. However, the focus here is on a 3D study, so we will not address this issue further.

3.4 Variational *Ansätze*

We will now start to actually solve, rather than discuss, the problem by writing out the variational *Ansätze* used for all propagators and vertices. The only dimensionful constant in 3D Yang-Mills theory is g . Moreover, a three-loop truncation of Γ only contains planar diagrams, and the only subleading in N correction which enters when evaluating them is an overall factor of (N^2-1) ; that is, the coupling and group theory factor for an m -loop bubble diagram is $(N^2-1)(g^2N)^{m-1}$. Therefore, to the loop order we work, the coupling expansion is strictly an expansion in the 't

Hooft coupling $g^2 N$. In $D = 3$ dimensions the 't Hooft coupling has dimensions of energy, and it therefore sets the natural energy scale in the problem. Therefore we will factor out the overall $(N^2 - 1)$ and will scale all dimensionful quantities by the appropriate power of $g^2 N$, i.e., quantities with dimension $[\text{mass}]^\alpha$, are expressed in units of $(g^2 N)^\alpha$. For the most part, this eliminates any explicit reference to g^2 or N in the remainder of this chapter.

Variational coefficients will be generically denoted by c_i . This is a slight abuse of notation, and one should recall throughout that the c_i are independent for each function. For instance, it should not be interpreted from expressions like $G_T(c_i; p)$ and $G_L(c_i; p)$ that G_T and G_L are defined by the same set of parameters. In practice we will use rational functions (Padé approximants) for our variational *Ansätze*; we distinguish coefficients in numerators from those in denominators by labelling the former by a_i and the latter by b_i , so that $\{c_i\} = \{a_i, b_i\}$ (or $\{c_i\} = \{a_{ijk}, b_{ijk}\}$ for vertex function coefficients). Finally, it is now always implied that when we refer to a correlation function, we are specifically referring to its *Ansatz*. We will drop the c_i from the arguments of these functions, so $G(p)$ implies $G(c_i; p)$.

Continuing on, G is first decomposed into transverse and longitudinal components as per Eq. (3.11). From the arguments of the previous section, we know that whatever we write down for $G_T(p)$ has to converge to Eq. (3.33) at large p (and likewise for $G_L(p)$ and $\Delta(p)$). Hence,

$$\begin{aligned}
G_T(p) &= \frac{1}{p^2 - \Pi_T(p)} & \Pi_T(p) &= \mathcal{C}_T p + (\text{Ansatz starting at } \mathcal{O}(p^0)) \\
G_L(p) &= \frac{\xi}{p^2 - \xi \Pi_L(p)} & \Pi_L(p) &= \mathcal{C}_L p + (\text{Ansatz starting at } \mathcal{O}(p^0)) \\
\Delta(p) &= \frac{1}{p^2 (1 - \frac{\Sigma(p)}{p^2})} & \Sigma(p)/p^2 &= \frac{\mathcal{C}_\Delta}{p + \omega_0} + (\text{Ansatz starting at } \mathcal{O}(p^{-2}))
\end{aligned} \tag{3.35}$$

with

$$\mathcal{C}_T = \frac{\xi^2 + \xi + 11}{64}, \quad \mathcal{C}_L = 0, \quad \mathcal{C}_\Delta = \frac{1}{16}. \quad (3.36)$$

We see that $\mathcal{C}_{T/L/\Delta}$ must be measured in units of g^2N since $[\mathcal{C}_{T/L/\Delta}] = [\text{mass}]$, while $[G_T] = [\text{mass}]^{-2}$.

The *Ansatz* for Δ differs from G_T and G_L ; namely, we assume that $\Sigma(p) \propto p^2$, and therefore $\Delta \propto p^{-2}$, at small p . This is a condition which arises due to the structure of ghost vertices, which we will discuss in a little more detail when we present the ghost vertices. The parameter ω_0 is not treated as a variational parameter; instead its value is fixed to $\omega_0 = 1$ (really $\omega_0 = g^2N$). This choice should not be important, provided the variational *Ansatz* is flexible enough.

We will use Padé approximants for the propagator *Ansätze*. The “order” of these *Ansätze* will be denoted by $N_{\text{max}}^{\text{P}}$, which refers to the highest power of momentum appearing in the numerator and denominators. With this choice, the expressions in Eq. (3.35) read

$$\Pi_T(p) = \mathcal{C}_T p + \Pi_T^{\text{NP}}(p) = \mathcal{C}_T p + \frac{\sum_{i=0}^{N_{\text{max}}^{\text{P}}} a_i^{\{G_T\}} p^i}{\sum_{i=1}^{N_{\text{max}}^{\text{P}}} b_i^{\{G_T\}} p^i + 1} \quad (3.37)$$

$$\Pi_L(p) = \mathcal{C}_L p + \Pi_L^{\text{NP}}(p) = \frac{\sum_{i=0}^{N_{\text{max}}^{\text{P}}} a_i^{\{G_L\}} p^i}{\sum_{i=1}^{N_{\text{max}}^{\text{P}}} b_i^{\{G_L\}} p^i + 1} \quad (3.38)$$

$$\Sigma(p) = \mathcal{C}_\Delta p + \Sigma^{\text{NP}}(p) = \frac{\mathcal{C}_\Delta p^2}{p + \omega_0} + \frac{\sum_{i=2}^{N_{\text{max}}^{\text{P}}} a_i^{\{\Delta\}} p^i}{\sum_{i=1}^{N_{\text{max}}^{\text{P}}} b_i^{\{\Delta\}} p^i + 1}. \quad (3.39)$$

In each case we define Π^{NP} as the self-energy minus its one-loop perturbative (linear in momentum) part. In the case of Σ this is *not* the same as the part determined by the variational *Ansatz*.

In constructing the most general gluon three-vertex V (where it is assumed that momentum flows out of a vertex), six independent tensor structures require consideration. We will adopt the basis used in [178, 179], which is

$$\begin{aligned}
\mathbf{A}_{\mu_1\mu_2\mu_3} &= g_{\mu_1\mu_2}(p_1 - p_2)_{\mu_3} \\
\mathbf{B}_{\mu_1\mu_2\mu_3} &= g_{\mu_1\mu_2}(p_1 + p_2)_{\mu_3} \\
\mathbf{C}_{\mu_1\mu_2\mu_3} &= [p_1 \cdot p_2 g_{\mu_1\mu_2} - p_{1\mu_2} p_{2\mu_1}](p_1 - p_2)_{\mu_3} \\
\mathbf{F}_{\mu_1\mu_2\mu_3} &= [p_1 \cdot p_2 g_{\mu_1\mu_2} - p_{1\mu_2} p_{2\mu_1}][(p_2 \cdot p_3)p_{1\mu_3} - (p_1 \cdot p_3)p_{2\mu_3}] \\
\mathbf{H}_{\mu_1\mu_2\mu_3} &= g_{\mu_1\mu_2}[(p_1 \cdot p_3)p_{2\mu_3} - (p_2 \cdot p_3)p_{1\mu_3}] + \frac{1}{3}(p_{1\mu_3}p_{2\mu_1}p_{3\mu_2} - p_{1\mu_2}p_{2\mu_3}p_{3\mu_1}) \\
\mathbf{S}_{\mu_1\mu_2\mu_3} &= p_{1\mu_3}p_{2\mu_1}p_{3\mu_2} + p_{1\mu_2}p_{2\mu_3}p_{3\mu_1}.
\end{aligned} \tag{3.40}$$

Colour dependence can be factored out of the vertex function,

$$V_{\mu_1\mu_2\mu_3}^{a_1a_2a_3}(p_1, p_2, p_3) = F^{a_1a_2a_3} V_{\mu_1\mu_2\mu_3}(p_1, p_2, p_3) \tag{3.41}$$

where $F^{abc} = -if_{abc}$ is the adjoint representation matrix, satisfying $F^{iab}F^{jba} = C_A\delta^{ij}$, $C_A = N$ for $SU(N)$. In a similar fashion to the propagators, our *Ansatz* for V is designed so that it can be easily made to converge to its perturbative form at large momenta. We will separate the various contributions to V much like we did with the propagators,

$$gV_{\mu_1\mu_2\mu_3} = g(V_{\mu_1\mu_2\mu_3}^{(0)} + V_{\mu_1\mu_2\mu_3}^{\text{B}(1)} + V_{\mu_1\mu_2\mu_3}^{\text{NP}}). \tag{3.42}$$

The tree-level and one-loop corrections are denoted by $V^{(0)}$ and $V^{\text{B}(1)}$, while V^{NP} denotes the non-perturbative correction to the vertex that has to be solved for self-consistently by finding the stationary point of Γ . The bare term, $V^{(0)}$ is simply

$$V_{\mu_1\mu_2\mu_3}^{(0)} = (p_2 - p_3)_{\mu_1} g_{\mu_2\mu_3} + (p_3 - p_1)_{\mu_2} g_{\mu_1\mu_3} + (p_1 - p_2)_{\mu_3} g_{\mu_1\mu_2} \quad (3.43)$$

which is expressed entirely in terms of cyclic permutations of the \mathbf{A} tensor, i.e.

$$V_{\mu_1\mu_2\mu_3}^{(0)} = A^{(0)} \mathbf{A}_{\mu_1\mu_2\mu_3} + \text{cyclic perms.} \quad (3.44)$$

with $A^{(0)} = 1$. The one-loop correction to the vertex $V^{\text{B}(1)}$ has a much more intricate tensor structure

$$\begin{aligned} V_{\mu_1\mu_2\mu_3}^{\text{B}(1)}(p_1, p_2, p_3) &= A^{\text{B}(1)}(p_1, p_2; p_3) \mathbf{A}_{\mu_1\mu_2\mu_3} + B^{\text{B}(1)}(p_1, p_2; p_3) \mathbf{B}_{\mu_1\mu_2\mu_3} \\ &+ C^{\text{B}(1)}(p_1, p_2; p_3) \mathbf{C}_{\mu_1\mu_2\mu_3} + F^{\text{B}(1)}(p_1, p_2; p_3) \mathbf{F}_{\mu_1\mu_2\mu_3} \\ &+ H^{\text{B}(1)}(p_1, p_2, p_3) \mathbf{H}_{\mu_1\mu_2\mu_3} + S^{\text{B}(1)}(p_1, p_2, p_3) \mathbf{S}_{\mu_1\mu_2\mu_3} \\ &+ \text{cyclic perms.} \end{aligned} \quad (3.45)$$

and likewise for V^{NP} . As we discussed above, we need the explicit forms of the one-loop vertex corrections in order to eliminate logarithmic UV divergences in the variational problem. We present explicit results for the one-loop vertices in Appendix D and we use those results in the following.¹⁰ Note in particular that $S^{\text{B}(1)} = 0$. However it remains to write variational *Ansätze* for V^{NP} . Here we make no assumptions

¹⁰ Setting $\omega_V = 1/4$; this parameter serves an analogous purpose to ω_0 as it appears in the ghost propagator, see Appendix D, Eq. (85).

about the vanishing of the coefficients for any of the tensorial structures. The functions A , C and F are symmetric in their first two arguments, B is antisymmetric in its first two arguments, H is fully symmetric and S is fully antisymmetric. We respect these symmetry properties by choosing the following *Ansätze*:

$$A^{\text{NP}}(p_1, p_2; p_3) = \frac{1}{p_1^2 + p_2^2 + p_3^2 + \omega_0^2} \frac{\sum_{i \geq j} a_{ijk}^{\{A\}} (p_1^i p_2^j + p_1^j p_2^i) p_3^k}{\sum_{i \geq j} b_{ijk}^{\{A\}} (p_1^i p_2^j + p_1^j p_2^i) p_3^k} \quad (3.46)$$

$$B^{\text{NP}}(p_1, p_2; p_3) = \frac{1}{p_1^2 + p_2^2 + p_3^2 + \omega_0^2} \frac{\sum_{i > j} a_{ijk}^{\{B\}} (p_1^i p_2^j - p_1^j p_2^i) p_3^k}{\sum_{i \geq j} b_{ijk}^{\{B\}} (p_1^i p_2^j + p_1^j p_2^i) p_3^k} \quad (3.47)$$

$$C^{\text{NP}}(p_1, p_2; p_3) = \frac{1}{p_1^4 + p_2^4 + p_3^4 + \omega_0^4} \frac{\sum_{i \geq j} a_{ijk}^{\{C\}} (p_1^i p_2^j + p_1^j p_2^i) p_3^k}{\sum_{i \geq j} b_{ijk}^{\{C\}} (p_1^i p_2^j + p_1^j p_2^i) p_3^k} \quad (3.48)$$

$$F^{\text{NP}}(p_1, p_2; p_3) = \frac{1}{p_1^6 + p_2^6 + p_3^6 + \omega_0^6} \frac{\sum_{i \geq j} a_{ijk}^{\{F\}} (p_1^i p_2^j + p_1^j p_2^i) p_3^k}{\sum_{i \geq j} b_{ijk}^{\{F\}} (p_1^i p_2^j + p_1^j p_2^i) p_3^k} \quad (3.49)$$

$$H^{\text{NP}}(p_1, p_2, p_3) = \frac{1}{p_1^4 + p_2^4 + p_3^4 + \omega_0^4} \frac{\sum_{i \geq j \geq k} a_{ijk}^{\{H\}} (p_1^i p_2^j p_3^k + \text{perms.})}{\sum_{i \geq j \geq k} b_{ijk}^{\{H\}} (p_1^i p_2^j p_3^k + \text{perms.})} \quad (3.50)$$

$$S^{\text{NP}}(p_1, p_2, p_3) = \frac{1}{p_1^4 + p_2^4 + p_3^4 + \omega_0^4} \frac{\sum_{i > j > k} a_{ijk}^{\{S\}} (\epsilon_{xyz} p_x^i p_y^j p_z^k)}{\sum_{i \geq j \geq k} b_{ijk}^{\{S\}} (p_1^i p_2^j p_3^k + \text{perms.})} \quad (3.51)$$

which automatically have these symmetries built into them (ϵ_{xyz} is the permutation symbol). Each sum is truncated so that $(i+j+k) \leq N_{\text{max}}^V$.

Notice that not all six tensors are of the same dimension; \mathbf{A} and \mathbf{B} have dimensions of [mass], \mathbf{C} , \mathbf{H} and \mathbf{S} are [mass]³ and \mathbf{F} is [mass]⁵. In every case the UV behaviour of the vertex function must satisfy $V^{\text{B}(1)} \propto 1$ and $V^{\text{NP}} \propto p^{-1}$. We enforce the correct momentum scaling for the vertex functions by hand, so that the Padé approximants are all $\mathcal{O}(1)$; this way, despite the individual dimensionalities of the vertex functions, all of the *Ansätze* are the same “size.”

The ghost-gluon vertex \mathbb{V} is somewhat simpler. Factoring out explicit colour dependence,

$$g\mathbb{V}_{\mu_3}^{a_1 a_2 a_3}(p_1, p_2, p_3) = gF^{a_1 a_2 a_3}\mathbb{V}_{\mu_3}(p_1, p_2, p_3) \quad (3.52)$$

with the outgoing ghost and gluon indexed by (a_1, p_1) and (a_3, μ_3, p_3) respectively (p_1 flows outwards), we have

$$\mathbb{V}_{\mu_3}(p_1, p_2, p_3) = \mathbb{A}(p_1, p_2, p_3)p_{1\mu_3} + \mathbb{B}(p_1, p_2, p_3)p_{2\mu_3}, \quad (3.53)$$

where

$$\mathbb{A}(p_1, p_2, p_3) = \mathbb{A}^{(0)} + \mathbb{A}^{\text{B}(1)} + \mathbb{A}^{\text{NP}} \quad (3.54)$$

$$\mathbb{B}(p_1, p_2, p_3) = \mathbb{B}^{\text{B}(1)} + \mathbb{B}^{\text{NP}}, \quad (3.55)$$

and

$$\mathbb{A}^{\text{NP}} = \frac{1}{p_1^2 + p_2^2 + p_3^2 + \omega_0^2} \frac{\sum a_{ijk}^{\{\mathbb{A}\}} p_1^i p_2^j p_3^k}{\sum b_{ijk}^{\{\mathbb{A}\}} p_1^i p_2^j p_3^k} \quad (3.56)$$

$$\mathbb{B}^{\text{NP}} = \frac{1}{p_1^2 + p_2^2 + p_3^2 + \omega_0^2} \frac{p_1 \sum a_{ijk}^{\{\mathbb{B}\}} p_1^i p_2^j p_3^k + (p_2 - p_3) \sum a_{ij}^{\{\mathbb{B}\}} p_2^j p_3^k}{\sum b_{ijk}^{\{\mathbb{B}\}} p_1^i p_2^j p_3^k} \quad (3.57)$$

In this case $\mathbb{A}^{(0)} = 1$, and as above, $\mathbb{A}^{\text{B}(1)}$ and $\mathbb{B}^{\text{B}(1)}$ are one-loop corrections (read directly from Appendix D, Eqs. (86) and (87), modulo $g^2 N$).

The *Ansatz* for \mathbb{B} is chosen so as to guarantee that $\lim_{p_1 \rightarrow 0} \mathbb{B} = 0$, linearly in p_1 . Let us briefly discuss this assumption, and our similar assumption that the ghost self-energy $\Sigma(p) \propto p^2$ at small p . Both properties arise because the tree-level ghost vertex $\mathbb{V}_\mu^{(0)}(p_1, p_2, p_3) \propto p_{1\mu}$ the outgoing ghost momentum. In any loop diagram modifying \mathbb{V} , with arbitrarily many loops, the outgoing ghost line, with momentum

p_1 , always encounters a bare \mathbb{V} , leading to a proportionality of the full diagram to p_1 . This proportionality is automatic in the \mathbb{A} term; we are also enforcing it in the \mathbb{B} term. One could argue that this argument assumes a strict diagrammatic expansion and might be violated somehow when we fully resum. However, it is at least self-consistent that $\mathbb{B} \propto p_1$ (note that $\lim_{p_1 \rightarrow 0} (p_2 - p_3) = 0$ linearly in p_1). And if it is, this is enough to ensure that any vertex correction, with resummed as well as bare vertices, is still always proportional to p_1 . Since the vertices are always proportional to p_1 , the self-energy must also vanish at least linearly in p ; but assuming that $\Sigma(p)$ is smooth at small p (which is true provided that there are no IR divergences in ghost self-energy corrections), $\Sigma(p)$ must in fact vanish quadratically in p . Building these properties into our *Ansätze* improves the stability of the numerical extremization; however we have also tried to solve the variational problem without these assumptions (using *Ansätze* which allow $\mathbb{B} \propto p_1^0$ and $\Sigma(p) \propto p^0$), with results which are consistent with the assumed $\propto p_1$ and $\propto p^2$ behaviours.

3.4.1 Numerical implementation

Obtaining the solution in terms of the variational coefficients involves performing three non-trivial tasks, which together can be referred to as the numerical implementation. These tasks are

- Tensor contraction and diagram generation
- Numerical integration over a 9D phase-space (three-loops)
- Using an extremization algorithm to locate the extremum of Γ .

Concerning diagram generation, the purely gluonic *Mercedes-Benz* is by far the most complicated diagram. Each propagator has 2 tensorial structures, each vertex

has 14 (the permutations of the 6 structures described in the last subsection). An inefficient tensor contraction would therefore contain $2^6 14^4 = 2458624$ terms. Therefore it is important to perform the tensorial contractions carefully, building intermediate structures with the minimum number of terms. For instance, the *Mercedes-Benz* can be regarded as

The diagram shows a 'Mercedes-Benz' diagram (a hexagon with three internal lines meeting at a central point) on the left, followed by an equals sign, then a 'vertex' diagram (a central point with three external lines) multiplied by a 'triangle' diagram (a triangle with three internal lines meeting at a central point), and finally a comma and the equation number (3.58).

which we will write as *vertex* contracted with *triangle*. The *triangle* can be represented in terms of a basis of 36 tensors (all three-index objects that can be constructed out of three momenta [two external and one loop] and the metric), and likewise, the resummed vertex contains 14 distinct tensors (all three-index objects that can be constructed out two momenta and the metric, due to momentum conservation). Specifically, the vertex *after* contracting the tensors associated with the propagators is of the form

$$\begin{aligned}
V_{\mu_1 \mu_2 \mu_3} = & Z_{001} g_{\mu_1 \mu_2} p_{1 \mu_3} + Z_{010} g_{\mu_1 \mu_3} p_{1 \mu_2} + Z_{100} g_{\mu_2 \mu_3} p_{1 \mu_1} \\
& + Z_{002} g_{\mu_1 \mu_2} p_{2 \mu_3} + Z_{020} g_{\mu_1 \mu_3} p_{2 \mu_2} + Z_{200} g_{\mu_2 \mu_3} p_{2 \mu_1} \\
& + Z_{112} p_{1 \mu_1} p_{1 \mu_2} p_{2 \mu_3} + Z_{121} p_{1 \mu_1} p_{2 \mu_2} p_{1 \mu_3} + Z_{211} p_{2 \mu_1} p_{1 \mu_2} p_{1 \mu_3} + Z_{111} p_{1 \mu_1} p_{1 \mu_2} p_{1 \mu_3} \\
& + Z_{221} p_{2 \mu_1} p_{2 \mu_2} p_{1 \mu_3} + Z_{212} p_{2 \mu_1} p_{1 \mu_2} p_{2 \mu_3} + Z_{122} p_{1 \mu_1} p_{2 \mu_2} p_{2 \mu_3} + Z_{222} p_{2 \mu_1} p_{2 \mu_2} p_{2 \mu_3}. \quad (3.59)
\end{aligned}$$

With the *vertex* and *triangle* factored as such, standard algebraic packages can perform all of the remaining tensor contractions and simplifications.

In addition to drastically simplifying diagram construction, the use of these bases allows for an economical use of floating point operations. The *triangle* is contained in all gluonic derivatives of Γ ; furthermore; the 36 *triangle* Z -coefficients are by far the

largest polynomials contained within the problem. With the triangle expressed as such, each of these 36 functions need only to be computed a single time at each point in a 6D space of integration variables. This is important because high-dimensional numerical integration will require of order 10^5 evaluations of each diagram *per step* in the extremization procedure for Γ .

With the Lorentz algebra in hand, we turn to the problem of multidimensional numerical integration. The first step is to choose a convenient basis for integration. Our choice is described in Appendix E. Performing the global (Eulerian) angular integrations, two-loop diagrams require a 3D integration and three-loop integrals require a 6D integration. These happen to be the same as the number of propagators in the bubble diagrams built with three-point vertices. And it is possible, and convenient, to choose integration variables which are precisely the magnitudes of the momenta on each propagator (this is a special feature of phase space integration in 3 dimensions, discussed in Appendix E). The most numerically challenging integration is again the *Mercedes-Benz* topology. In the notation of Appendix E, the three finite-range (angular) integrations, over k' , q' , and l , as well as the p integration, were performed using Gaussian quadratures, while the (infinite) k and q momentum axes were rescaled into the unit interval and sampled using an array of

points constructed with a quasi-random hopping Halton series [180].¹¹ Our quadratures procedure is symmetric over intervals, which ensures that certain cancellations on angular integration are preserved, and it avoids edgepoint evaluations. Also, since neither algorithm uses random or pseudorandom numbers or dynamic mesh refinement, each integration evaluation is over exactly the same distribution of phase-space points. This ensures that the effective action Γ is not “noisy” in the sense that it does not fluctuate between evaluations with the same or almost the same choices of propagator and vertex functions, a feature which is essential for conjugate-gradient and other differential extremum seeking algorithms.

To test the stability of our algorithm against changes in the number of integration points, we computed the two-loop self-energy for particular values of full propagators and vertices with varying numbers of integration points. As illustrated in Fig. 3-3, the results converge when sufficiently many integration points are used. Finally, as an additional check, our numerical procedure for performing three-loop integrals was tested against the known result for the bare massive three-loop *Mercedes-Benz* in 3D [181], with which we find agreement.

Now that we have explained how numerical integrations can be performed, we turn to the problem of extremizing the effective action Γ . One challenge is that, because of gauge fixing and ghosts, the extremum is actually a saddle, rather than a

¹¹ More specifically, we first write $k = px/(1-x)$ with $x \in [0, 1)$. Then we write $x = 3y^2 - 2y^3$ with $y \in [0, 1)$ chosen with uniform weight. The former transformation ensures that k, q, p are of comparable magnitude; the latter transformation increases the sampling at the top and bottom relative to the middle of the range.

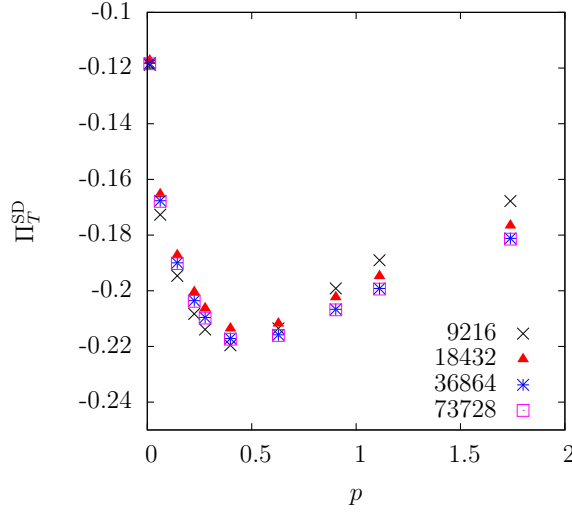


Figure 3–3: Non-perturbative correction to Π_T . viz. Eq. (3.60), as a function of the total number of integration points along the k , q , k' , q' and l integration axes (labelled in the bottom right corner).

maximum or minimum. This can be easily seen from the first line of Eq. (3.6), where the gluon propagator G and the ghost propagator Δ enter with opposite sign. With the sign conventions chosen there, the extremum of the one-loop action with respect to G is a maximum; with respect to Δ it is a minimum. This rules out any straightforward application of the conjugate gradient algorithm. The Newton-Raphson algorithm can find general extrema, but it is inefficient and tends to converge well only in rather small basins of attraction. So some hybrid approach is needed.

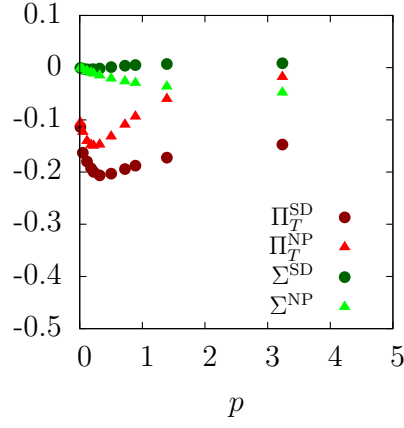
Fortunately, despite it being not at all *a priori* obvious, one observes for the most part that each individual function that makes up the extremization problem has relatively little effect on the others. This opens up the possibility of iteratively extremizing each constituent function (G , Δ , V and \mathbb{V}). Our procedure was to

start with vertices set to their one-loop values and propagators set to some naive initial guess. Then we perform a conjugate gradient extremization with respect to G , then a conjugate gradient extremization with respect to Δ (with opposite sign on the gradient).¹² Iteratively extremizing G and Δ solves the three-loop 2PI problem. Then we use gradient descent to extremize Γ with respect to the three-gluon vertex functions. Finally, the ghost vertex corrections are improved using the Newton-Raphson method. Then the procedure is iterated (propagators and gluon vertices, then ghost vertices) until convergence is achieved.

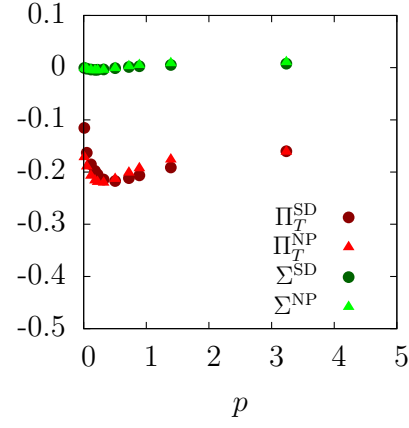
The convergence of the algorithm, when applied to the three-loop 2PI problem in Landau gauge, is depicted in Fig. 3–4. The figure compares the *Ansatz* value for the self-energies, Π_T^{NP} and Σ^{NP} as defined in Eq. (3.37), Eq. (3.39), to the values directly evaluated by summing the self-energy diagrams, Π_T^{SD} and Σ^{SD} ; in each case we have removed the one-loop linear-in- p contribution. That is,

$$\Pi_T^{\text{SD}} \equiv \mathbf{T}^{\mu\nu}(\Pi_{\mu\nu}^{(1)} + \Pi_{\mu\nu}^{(2)})/(\text{D} - 1) - \mathcal{C}_T p, \quad (3.60)$$

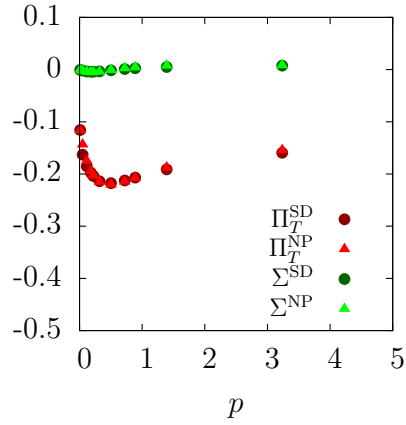
¹² In practice we also accelerate this procedure as follows. We evaluate the self-energy diagrams $\Pi(p)$ at a sample of p values holding G fixed. Then we conjugate-gradient extremize G in Eq. (3.31) but treating the self-energy Π as fixed. We insert the new value of G into the evaluation of the self-energy and iterate. This minimizes the number of evaluations of $\Pi(p)$, the most numerically expensive part of the procedure, needed to converge to the extremum. But the extremum obtained by this procedure is the one which satisfies Eq. (3.31), as desired.



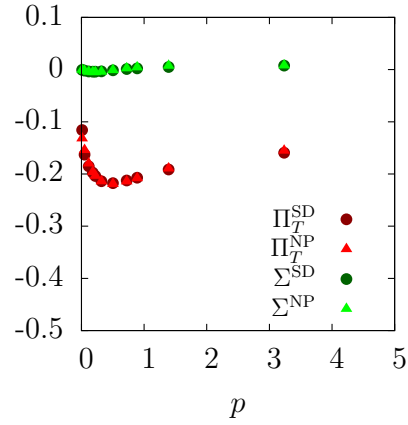
(a) Initially...



(b) 5 Iterations



(c) 100 Iterations



(d) 200 Iterations

Figure 3–4: Evolution of the self-energy under the gradient descent algorithm. Here Π^{NP} is the non-perturbative self-energy according to the *Ansatz*, while Π^{SD} is the value as determined by evaluating the self-energy diagrams. As the algorithm is iterated, the *Ansatz* approaches a correct reproduction of the self-energy.

and similarly for Σ^{SD} (the notation SD is intended as a reminder that these quantities are computed directly from the diagrams in the integral equations). The extremization procedure for the effective action with respect to one of the variational coefficients in G_T , Eq. (3.31), then corresponds to

$$\frac{\delta\Gamma}{\delta c_j} = \frac{(D-1)(N^2-1)}{2} \int \frac{d^3p}{(2\pi)^3} \frac{\delta G_T(p)}{\delta c_j} (-\Pi_T^{\text{NP}}(p) + \Pi_T^{\text{SD}}(p)). \quad (3.61)$$

Fig. 3–4 shows two things. First, even though the initial guess for the self-energy falls quite far off the actual value, after relatively few iterations the fitted and true values of the self-energy become similar, and the eventual convergence is excellent. Second, the value of the self-energy Π_T^{SD} actually depends quite weakly on the precise form of $\Pi_T^{\text{NP}}(p)$. That is why our procedure of varying Γ with respect to individual functions (rather than trying to do everything at once) works so effectively. The presence of vertices definitely makes matters more complicated; however, it is also observed that $\Pi_T^{\text{SD}}(p)$ is fairly insensitive to their inclusion.

Eq. (3.61) should be interpreted as an Euler-Lagrange type of equation for Π , and a vertex analogue can be defined as follows. For instance when c_i belongs to the gluon H -function, the variation of Γ takes on the following form

$$\frac{\delta\Gamma}{\delta c_j} = \int \frac{d^3p}{(2\pi)^3} \frac{d^3k}{(2\pi)^3} \frac{\delta H^{\text{NP}}(p, k, x)}{\delta c_j} (-\mathbf{H} \cdot V^{\text{NP}}(p, k, x) + \mathbf{H} \cdot V^{\text{SD}}(p, k, x)), \quad (3.62)$$

with

$$\begin{aligned} \mathbf{H} \cdot V^{\text{NP}}(p, k, x) \equiv \\ -(N^2-1) \mathbf{H}_{\mu_1\mu_2\mu_3} G^{\mu_1\nu_1}(p) G^{\mu_2\nu_2}(k) G^{\mu_3\nu_3}(x) \left(\frac{1}{6} V_{\nu_1\nu_2\nu_3} - \frac{1}{6} V_{\nu_1\nu_2\nu_3}^{(0)} \right) \end{aligned} \quad (3.63)$$

where the overall minus sign comes from the ordering of colour indices. $\mathbf{H} \cdot V^{\text{SD}}(p, k, x)$ is defined in a similar manner, except that the term in brackets in Eq. (3.63) contains all of the higher-loop terms in the vertex equation of motion, Eq. (3.10). The values of $\mathbf{H} \cdot V^{\text{SD}}(p, k, x)$ and $\mathbf{H} \cdot V^{\text{NP}}(p, k, x)$ along the curve defined by $k = p/4$ and $\cos \theta_{pk} = 1/4$ are plotted in Fig. 3–5. Fig. 3–6 contains plots of a similarly defined set of quantities related to the ghost vertex.

The *Ansätze* in Figs. 3–4 - 3–6 correspond to $N_{\text{max}}^{\text{P}} = 3$ and $N_{\text{max}}^{\text{V}} = 3$, from which we observe that the solution is well described by third order Padés. However, the size of the *Ansätze* can have a major effect on the outcome of this technique. With too few coefficients, the numerics are much simpler, but one is not able to obtain the correct final answer. However, as the number of coefficients increases, the problem becomes very numerically difficult (considering the relative ease with which poles may form in the denominators of the Padé approximants). Furthermore, the data will eventually be over-fitted as additional coefficients behave in a decreasingly linearly-independent manner and the associated gradients become small. We find that at $N_{\text{max}}^{\text{P}} = 3$ and $N_{\text{max}}^{\text{V}} = 3$ the problem is still not overly difficult to solve, despite there being a total of 174 coefficients in Landau gauge (with an additional 33 in other gauges). At the same time we are not over-fitting. This choice is further motivated by the general shape of functions we are attempting to converge to; the presence of additional “wiggles” would necessitate larger *Ansätze*.

3.5 Results

The extremization procedure was carried out for several choices of the gauge parameter ξ , namely 0.0, 0.5, 1.0 and 2.0. The resulting self-energies are shown in

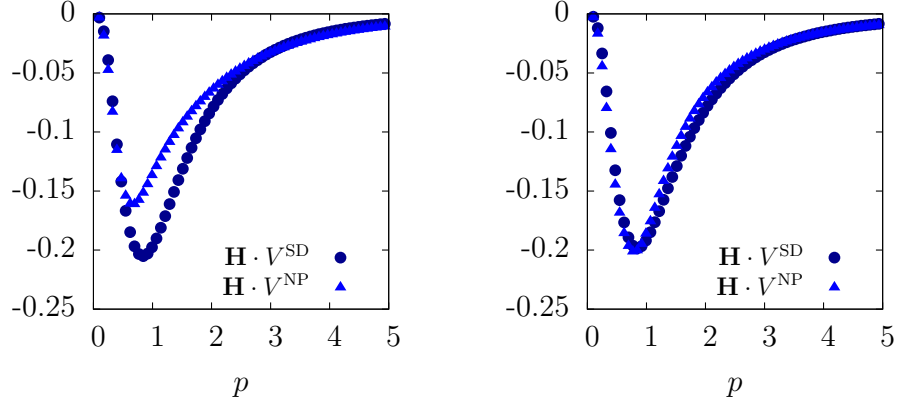


Figure 3–5: Vertex analog of Fig. 3–4 in Landau gauge, illustrating in this case convergence of the H -function (see Eq. (3.62)) and the gluon vertex as a whole. The values reside on the curve $k = p/4$ and $\cos \theta_{pk} = 1/4$. The figure on the left corresponds to $H^{\text{NP}} = 0$, whereas the figure on the right corresponds to H^{NP} which extremizes Γ . Note that the basis, Eq. (3.40), used for the vertex is not orthogonal, so $H^{\text{NP}} = 0$ does not imply that $\mathbf{H} \cdot V^{\text{NP}} \neq 0$, as illustrated here.

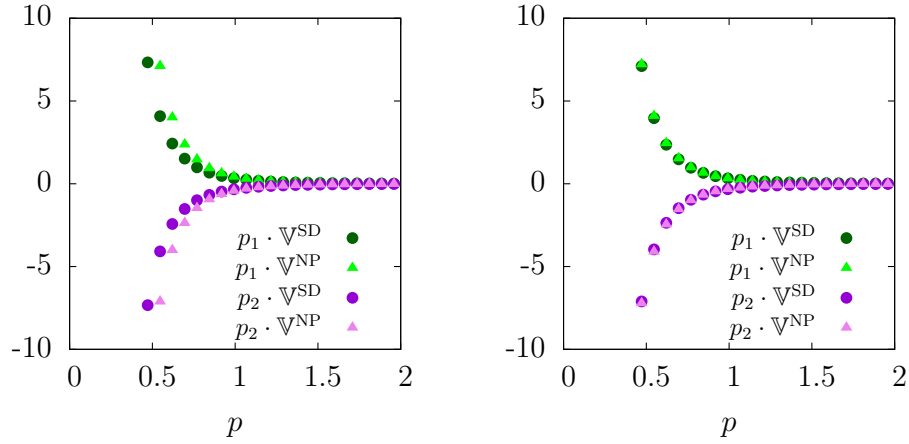


Figure 3–6: Convergence of the ghost-gluon vertex functions in Landau gauge; similar to Fig. 3–5, the figure on the left corresponds to an initial guess of $\mathbb{V}^{\text{NP}} = 0$, whereas that on the right corresponds to the “solution” for \mathbb{V}^{NP} which extremizes Γ .

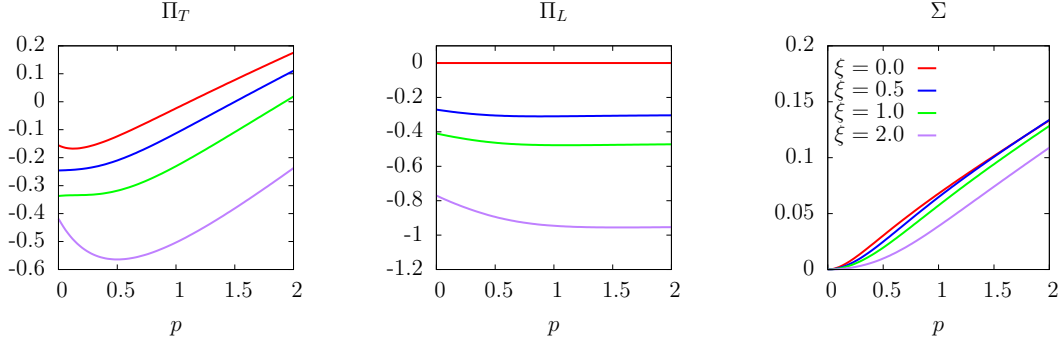


Figure 3-7: Transverse, longitudinal and ghost self-energies.

Fig. 3-7, and the gluon three-vertex functions A through S and the ghost three-point functions \mathbb{A}^{NP} and \mathbb{B}^{NP} are plotted in Fig. 3-9, which shows the Landau gauge results, and Fig. 3-10, which shows the results in Feynman gauge. The Landau gauge variational coefficients are stated in Table 3-2. The results for $\xi = 0.5$ and $\xi = 2.0$ are qualitatively similar.

In Landau gauge, G_L is zero, so it is not included in the variation; hence G_L and Π_L are depicted as zero in the plots. Furthermore, when the tensorial structure $\mathbf{B}_{\mu_1\mu_2\mu_3}$ is contracted against transverse propagators on all three legs, the result is zero; therefore the coefficient B vanishes exactly in Landau gauge, though not in gauges with nonzero ξ . The function S turns out to vanish in all gauges, consistent with the claim in [182] that it should vanish at all loop orders.

The effect of including the vertices and allowing them to vary is shown in Fig. 3-8, where we see a comparison between the 2PI and 3PI solutions. The inclusion of the vertices only has a slight effect the resulting propagators.

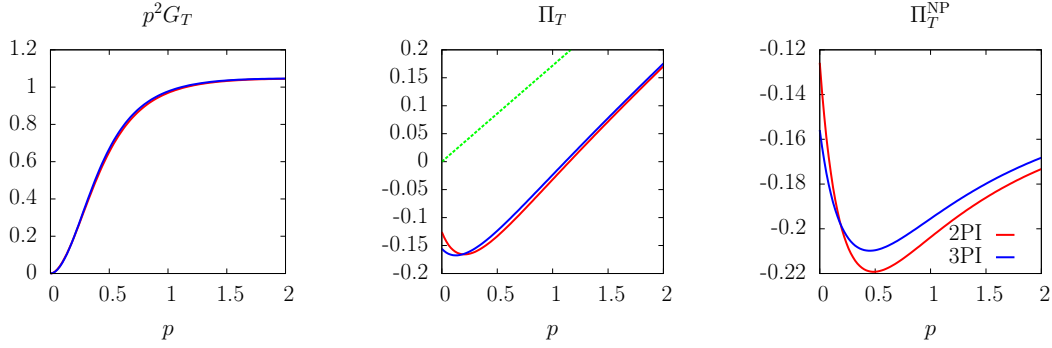


Figure 3–8: Comparison between the 2PI (bare vertices only) and 3PI (vertices included) solutions. The correction to G_T that we obtain when including the vertices is indeed small (in Landau gauge). For reference, the strictly one-loop perturbative result is shown in the middle panel in green.

The dependence of G , V , etc. on the choice of the gauge fixing parameter ξ does not by itself indicate a breakdown or limitation on the 3PI approach. The relevant question is, how dependent are gauge independent quantities on ξ , and how closely do such quantities correspond to the non-perturbative values determined, for instance, using lattice techniques? Any ξ dependence in gauge invariant quantities would be an ambiguity, and any error in their value in comparison to lattice determinations would be a failure, of the 3PI technique. We will further discuss this matter in Chapter 4.

3.6 Discussion

3.6.1 Comparison with other approaches

The majority of the literature on this subject is centred around 4D Yang-Mills theory; however, lattice studies (described shortly) have shown that Green's functions in 3D and 4D exhibit similar qualitative behaviour. Nevertheless, we will try our

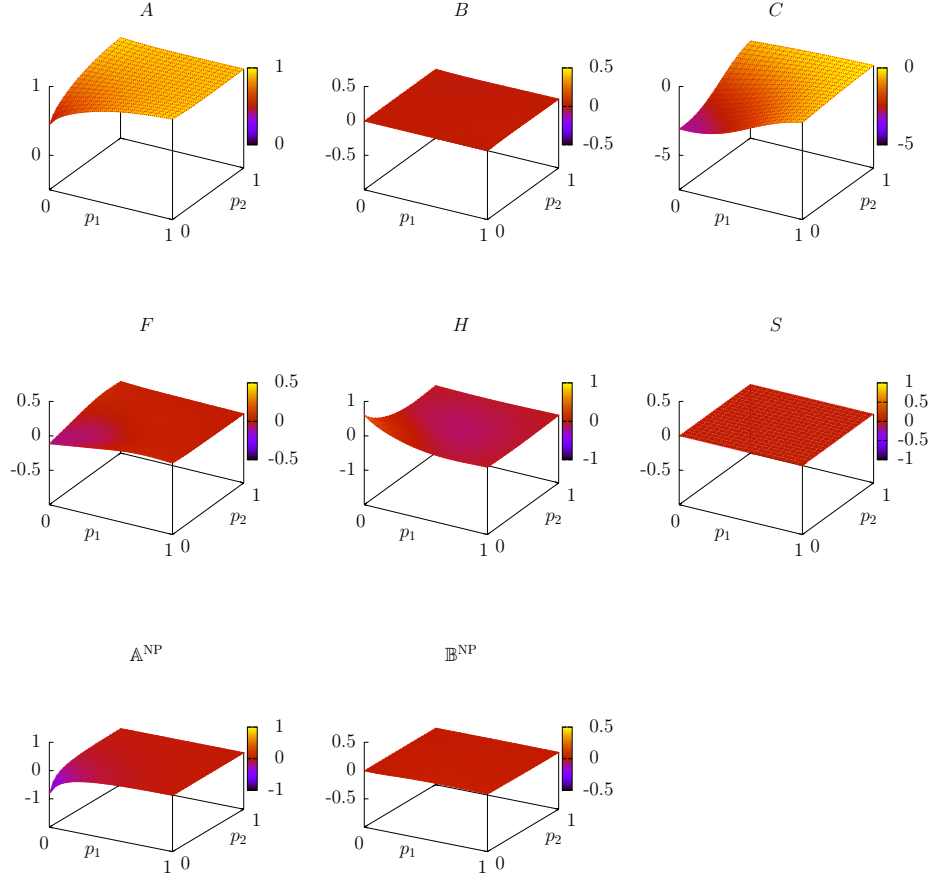


Figure 3-9: Vertex functions with $\xi = 0.0$, $N_{\text{max}}^{\text{P}} = 3$, $N_{\text{max}}^{\text{V}} = 3$, $\cos \theta_{p_1, p_2} = 1/4$.

best to directly compare our results with those obtained in 3D, to the extent that they exist.

The gluon propagator is an interesting quantity, despite not being directly related to any physical observable. G_T as depicted in Fig. 3-8 violates reflection positivity, that is, it does not have a Källén-Lehmann representation in terms of a positive spectral density. Hence, in (3+1) dimensions (or in our case (2+1) dimensions) G_T

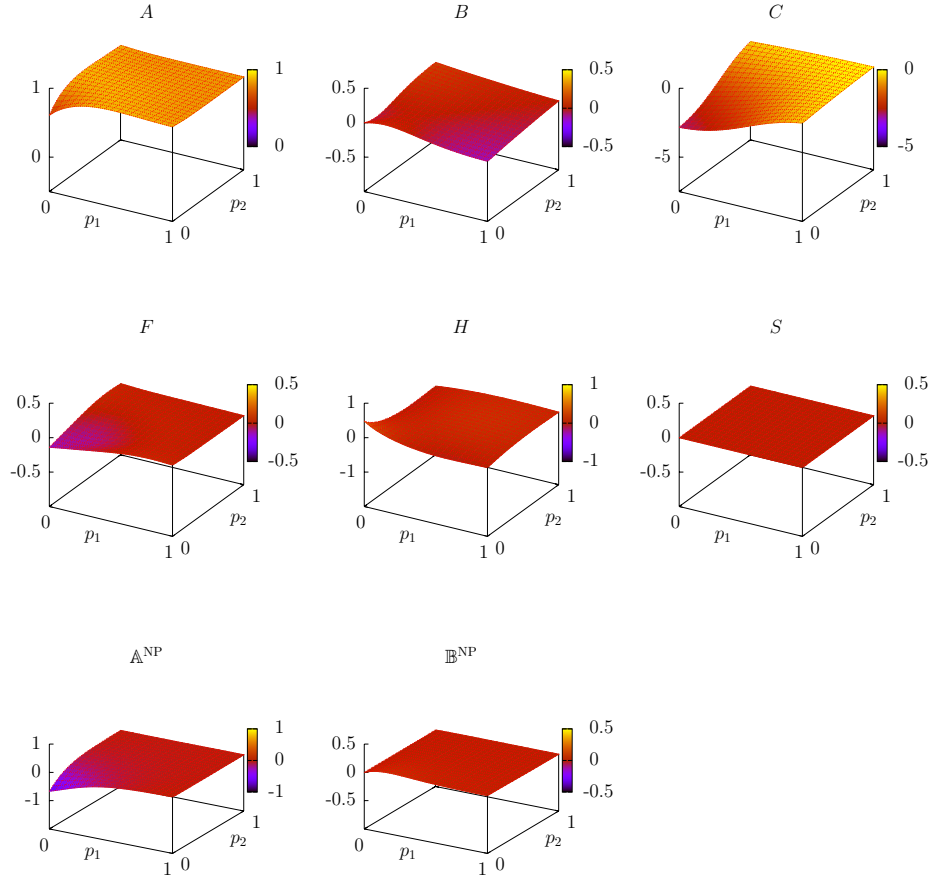


Figure 3-10: Vertex functions with $\xi = 1.0$, $N_{\max}^{\text{P}} = 3$, $N_{\max}^{\text{V}} = 3$, $\cos \theta_{p_1, p_2} = 1/4$.

$a_0^{\{G_T\}}$	-1.56e-01	$a_1^{\{G_T\}}$	-1.03e+00	$a_2^{\{G_T\}}$	-9.14e-01	$a_3^{\{G_T\}}$	-4.47e-01	$b_1^{\{G_T\}}$	4.11e+00	$b_2^{\{G_T\}}$	4.10e+00
$b_3^{\{G_T\}}$	3.82e+00	$a_2^{\{\Delta\}}$	1.79e-01	$a_3^{\{\Delta\}}$	1.13e-01	$b_1^{\{\Delta\}}$	1.73e+00	$b_2^{\{\Delta\}}$	3.49e+00	$b_3^{\{\Delta\}}$	1.75e+00
$a_{000}^{\{H\}}$	1.02e-01	$a_{100}^{\{H\}}$	-4.98e-02	$a_{110}^{\{H\}}$	-2.73e-01	$a_{111}^{\{H\}}$	-5.15e-01	$a_{200}^{\{H\}}$	-8.11e-01	$a_{210}^{\{H\}}$	1.40e-01
$a_{300}^{\{H\}}$	5.49e-01	$b_{100}^{\{H\}}$	1.19e+00	$b_{110}^{\{H\}}$	1.29e-01	$b_{111}^{\{H\}}$	2.38e-01	$b_{200}^{\{H\}}$	1.04e-01	$b_{210}^{\{H\}}$	-1.77e-01
$b_{300}^{\{H\}}$	3.20e-01	$a_{000}^{\{A\}}$	-2.77e-01	$a_{001}^{\{A\}}$	-7.66e-01	$a_{002}^{\{A\}}$	3.70e-01	$a_{003}^{\{A\}}$	8.59e-02	$a_{100}^{\{A\}}$	-9.45e-01
$a_{101}^{\{A\}}$	4.90e-01	$a_{102}^{\{A\}}$	-5.26e-02	$a_{110}^{\{A\}}$	7.11e-01	$a_{111}^{\{A\}}$	-8.68e-01	$a_{200}^{\{A\}}$	7.03e-02	$a_{201}^{\{A\}}$	-3.46e-01
$a_{210}^{\{A\}}$	-2.06e+00	$a_{300}^{\{A\}}$	-7.44e-02	$b_{001}^{\{A\}}$	1.54e+00	$b_{002}^{\{A\}}$	5.90e-01	$b_{003}^{\{A\}}$	6.73e-01	$b_{100}^{\{A\}}$	6.22e+00
$b_{101}^{\{A\}}$	8.78e-01	$b_{102}^{\{A\}}$	7.12e-01	$b_{110}^{\{A\}}$	1.85e+00	$b_{111}^{\{A\}}$	-6.23e-01	$b_{200}^{\{A\}}$	1.93e+00	$b_{201}^{\{A\}}$	-2.77e-01
$b_{210}^{\{A\}}$	-1.69e-01	$b_{300}^{\{A\}}$	3.42e-01	$a_{000}^{\{C\}}$	-1.53e+00	$a_{001}^{\{C\}}$	-1.74e+00	$a_{002}^{\{C\}}$	-6.63e-01	$a_{003}^{\{C\}}$	3.15e-02
$a_{100}^{\{C\}}$	5.94e-02	$a_{101}^{\{C\}}$	-2.47e-01	$a_{102}^{\{C\}}$	-2.09e-02	$a_{110}^{\{C\}}$	3.44e-01	$a_{111}^{\{C\}}$	-4.98e-01	$a_{200}^{\{C\}}$	-2.97e+00
$a_{201}^{\{C\}}$	6.72e-01	$a_{210}^{\{C\}}$	-4.27e-02	$a_{300}^{\{C\}}$	5.05e-01	$b_{001}^{\{C\}}$	4.11e-01	$b_{002}^{\{C\}}$	6.14e-01	$b_{003}^{\{C\}}$	7.04e-01
$b_{100}^{\{C\}}$	2.19e-01	$b_{101}^{\{C\}}$	5.53e-01	$b_{102}^{\{C\}}$	6.94e-01	$b_{110}^{\{C\}}$	4.13e-01	$b_{111}^{\{C\}}$	6.53e-01	$b_{200}^{\{C\}}$	3.68e-01
$b_{201}^{\{C\}}$	6.20e-01	$b_{210}^{\{C\}}$	5.21e-01	$b_{300}^{\{C\}}$	4.46e-01	$a_{000}^{\{F\}}$	-5.67e-02	$a_{001}^{\{F\}}$	-3.53e-03	$a_{002}^{\{F\}}$	9.77e-03
$a_{003}^{\{F\}}$	4.70e-01	$a_{100}^{\{F\}}$	-4.18e-02	$a_{101}^{\{F\}}$	-1.96e-02	$a_{102}^{\{F\}}$	3.20e-01	$a_{110}^{\{F\}}$	-5.84e-02	$a_{111}^{\{F\}}$	2.00e-01
$a_{200}^{\{F\}}$	-5.23e-02	$a_{201}^{\{F\}}$	2.57e-01	$a_{210}^{\{F\}}$	1.37e-01	$a_{300}^{\{F\}}$	2.28e-01	$b_{001}^{\{F\}}$	9.96e-01	$b_{002}^{\{F\}}$	9.96e-01
$b_{003}^{\{F\}}$	9.97e-01	$b_{100}^{\{F\}}$	9.96e-01	$b_{101}^{\{F\}}$	9.97e-01	$b_{102}^{\{F\}}$	9.98e-01	$b_{110}^{\{F\}}$	9.97e-01	$b_{111}^{\{F\}}$	9.98e-01
$b_{200}^{\{F\}}$	9.97e-01	$b_{201}^{\{F\}}$	9.98e-01	$b_{210}^{\{F\}}$	9.99e-01	$b_{300}^{\{F\}}$	9.99e-01	$a_{000}^{\{A\}}$	-8.12e-01	$a_{001}^{\{A\}}$	-1.02e-01
$a_{002}^{\{A\}}$	2.02e-01	$a_{003}^{\{A\}}$	2.12e-01	$a_{010}^{\{A\}}$	3.59e-01	$a_{011}^{\{A\}}$	-6.42e-01	$a_{012}^{\{A\}}$	-3.44e-01	$a_{020}^{\{A\}}$	-3.01e-01
$a_{021}^{\{A\}}$	-1.23e-01	$a_{030}^{\{A\}}$	2.68e-01	$a_{100}^{\{A\}}$	-1.23e-01	$a_{101}^{\{A\}}$	-9.41e-02	$a_{102}^{\{A\}}$	-1.16e-01	$a_{110}^{\{A\}}$	-4.18e-01
$a_{111}^{\{A\}}$	4.75e-01	$a_{120}^{\{A\}}$	2.53e-02	$a_{200}^{\{A\}}$	3.50e-02	$a_{201}^{\{A\}}$	4.01e-01	$a_{210}^{\{A\}}$	-2.83e-01	$a_{300}^{\{A\}}$	-1.65e-01
$b_{001}^{\{A\}}$	6.26e+00	$b_{002}^{\{A\}}$	2.89e+00	$b_{003}^{\{A\}}$	1.82e+00	$b_{010}^{\{A\}}$	6.31e+00	$b_{011}^{\{A\}}$	2.81e+00	$b_{012}^{\{A\}}$	1.71e+00
$b_{020}^{\{A\}}$	2.96e+00	$b_{021}^{\{A\}}$	1.64e+00	$b_{030}^{\{A\}}$	1.57e+00	$b_{100}^{\{A\}}$	5.13e+00	$b_{101}^{\{A\}}$	2.43e+00	$b_{102}^{\{A\}}$	1.55e+00
$b_{110}^{\{A\}}$	2.36e+00	$b_{111}^{\{A\}}$	1.44e+00	$b_{120}^{\{A\}}$	1.36e+00	$b_{200}^{\{A\}}$	2.30e+00	$b_{201}^{\{A\}}$	1.43e+00	$b_{210}^{\{A\}}$	1.31e+00
$b_{300}^{\{A\}}$	1.38e+00	$a_{000}^{\{B\}}$	1.43e-01	$a_{001}^{\{B\}}$	-3.00e-02	$a_{002}^{\{B\}}$	1.92e-01	$a_{010}^{\{B\}}$	1.06e-01	$a_{011}^{\{B\}}$	-1.90e-01
$a_{020}^{\{B\}}$	2.20e-01	$a_{100}^{\{B\}}$	2.53e-01	$a_{101}^{\{B\}}$	3.20e-01	$a_{110}^{\{B\}}$	-3.44e-02	$a_{200}^{\{B\}}$	-4.49e-01	$a_{201}^{\{B\}}$	2.52e-01
$a_{01}^{\{B\}}$	-5.05e-01	$a_{02}^{\{B\}}$	8.21e-02	$a_{10}^{\{B\}}$	-4.71e-02	$a_{11}^{\{B\}}$	2.61e-01	$a_{20}^{\{B\}}$	2.67e-01	$b_{001}^{\{B\}}$	1.00e+00
$b_{002}^{\{B\}}$	1.00e+00	$b_{003}^{\{B\}}$	1.00e+00	$b_{010}^{\{B\}}$	9.99e-01	$b_{011}^{\{B\}}$	1.00e+00	$b_{012}^{\{B\}}$	1.00e+00	$b_{020}^{\{B\}}$	1.00e+00
$b_{021}^{\{B\}}$	1.00e+00	$b_{030}^{\{B\}}$	1.00e+00	$b_{100}^{\{B\}}$	1.00e+00	$b_{101}^{\{B\}}$	1.00e+00	$b_{102}^{\{B\}}$	1.00e+00	$b_{110}^{\{B\}}$	1.00e+00
$b_{111}^{\{B\}}$	1.00e+00	$b_{120}^{\{B\}}$	1.00e+00	$b_{200}^{\{B\}}$	1.00e+00	$b_{201}^{\{B\}}$	1.00e+00	$b_{210}^{\{B\}}$	1.00e+00	$b_{300}^{\{B\}}$	1.01e+00

Table 3-2: $\xi = 0.0$ variational coefficients

can not describe the correlations of physical particles. This violation of reflection positivity is allowed despite its apparent contradiction with the Osterwalder-Schrader axioms; after all, we are dealing with a confining theory, so there is no one-to-one correspondence between fields and physical particles. This is further discussed in greater detail in [183], but the main point is that it is been claimed this behaviour signals confinement [184].

The only propagating degrees of freedom that we can (in principle) observe are colour singlet bound states, *glueballs* for instance. Hence, gluonic two and three-point functions are not “physical,” and, in general the results we have presented are ξ dependent, which is not necessarily a bad thing. Indeed our intention is to use the formalism compute gauge-invariant observables.

However, in the mean time, we are can to an extent analyze $\langle AA \rangle$ and $\langle c\bar{c} \rangle$ as well as the vertices. Though arguably our best insight into IR QCD comes from the lattice, there have been many notable *first-principles* based speculations about the specific IR form of these functions. In general, the main point of contention is the exact value of $G_T(0)$. The most popular schools of thought can be summarized as follows:

The Gribov-Zwanziger confinement hypothesis

In his study on gauge-fixing and gauge copies in Yang-Mills theory [84], Gribov proposed that at one-loop, the IR behaviour of the gluon and ghost propagators is

$$G_T(p) \sim \frac{p^2}{p^4 + m^4}, \quad \Delta(p)|_{p^2 \rightarrow 0} \sim \frac{1}{p^4}. \quad (3.64)$$

This form has the generic feature that G_T vanishes at zero momentum, and moreover, Δ experiences $1/p^4$ IR enhancement, which can possibly be interpreted as signalling linear confinement (in 4D, of course). This form of G_T and Δ was later advocated by Zwanziger, primarily because it vanishes at $p = 0$, which is in accordance with his theorem that $G_T(0)$ (in Landau gauge) must vanish on any finitely spaced lattice in the infinite volume limit [185].

This proposal should be regarded as being fairly dated, and it is not in agreement with any of the more recent lattice data. It also does not accord with the behaviour we determine by solving the 3PI problem.

Schwinger-Dyson equations

These arguments [186] are based on obtaining solutions to a truncated set of Schwinger-Dyson equations for the gluon and ghost propagators, and in a sense, are very reminiscent of what we are doing here. If we assume power behaviour of the gluon and ghost propagators in the infrared,

$$p^2 G_T(p) \sim (p^2)^{\kappa_G}, \quad p^2 \Delta(p) \sim (p^2)^{-\kappa_\Delta}, \quad (3.65)$$

then [187] claims that κ_G, κ_Δ must satisfy

$$\kappa_G = 2\kappa_\Delta + (4 - D)/2, \quad (3.66)$$

and specifically in 3 dimensions $\kappa_G = 0.2952$, implying that the gauge field propagator goes to zero and the ghost propagator diverges more strongly than $1/p^2$. However this result assumes that the loop integral giving rise to a self-energy at momentum p is dominated by momenta of order p , whereas we find for small p that it is instead dominated by momenta of order $g^2 N$. Therefore it is not clear to us that this result of [187] is robust, see also [188]. It is also contradicted by more recent studies [189, 190], which give results (in 4 dimensions) showing $G_T(p)$ going over to a constant, and $\Delta(p) \propto p^{-2}$, in the infrared. These studies are in at least qualitative agreement with lattice investigations. However, since in general Schwinger-Dyson

based approaches are reliant on many simplifying approximations, they have yet to produce any quantitative agreement.

Observations from the lattice

There is a wealth of lattice data related to this subject, and fortunately, different sources are generally in agreement. Simulations have been performed on very large lattices ($V = 96^4$ [191, 192], $V = 80^4$ [193], $V = 128^4$ and $V = 320^3$ [194, 195, 196]), from which one observes qualitative agreement between the results for 3D and 4D (hence we will intermittently compare 3D and 4D data, but *never* 2D). The generic finding is that $p^2\Delta(p)|_{p^2\rightarrow 0}$ and $G_T(0)$ are finite and nonzero.

However, $G_T(0)$ is often seen to scale inversely with volume so it remains an open question as to whether the Zwanziger hypothesis is observable, and it is not known at what volume one should expect to see this effect. The results in Landau gauge currently depict a $1/V^\alpha$ scaling for G_T but it is generally not observed that $G_T(0) \rightarrow 0$ as $V \rightarrow \infty$.

All of the works cited above specifically employ the lattice implementation of Landau gauge. In fact, it is only fairly recently that preliminary 3D and 4D results in Feynman gauge have been made available [197].

In Fig. 3–11 our data is compared directly to the results in [194, 195, 196]. Their calculation was performed for SU(2) on an 320^3 3D lattice with $\beta = 4/ag^2 = 3.0$. To facilitate the comparison we have recast their results so momentum is scaled by g^2N . Their results are qualitatively similar to ours but differ quantitatively at the factor-of-2 level in the deep IR. This might indicate a limitation of the large- N expansion, or it might simply indicate a failure of the 3PI method.

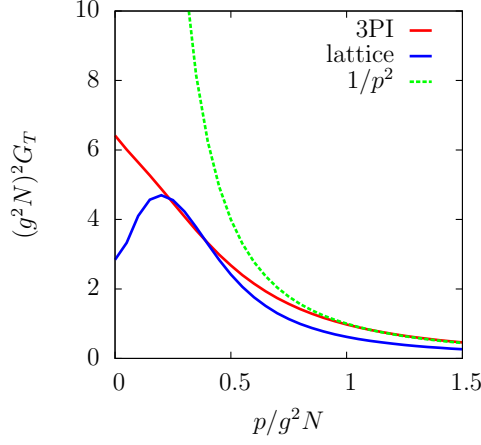


Figure 3–11: A comparison between the results of our calculation ($G_T(p)$ in Landau gauge) and a reproduction of the plot of $aD(p)$ (appropriately rescaled) in [196]. A free $1/p^2$ propagator is shown for reference.

3.6.2 Slavnov-Taylor identities

Planar diagrams on their own form a gauge-invariant subset of the full loop expansion [198]. One may hope that in resumming a “dominant” or “important” set of planar diagrams (which is what we hope to be doing here) gauge-invariance is approximately conserved. This can be measured seeing to what extent our resulting two and three-point functions violate the Ward-Slavnov-Taylor (WST) identities. For the gluon propagator, we have

$$p^\mu p^\nu G_{\mu\nu} = \xi, \quad (3.67)$$

with deviations from this identity shown in Fig. 3–12.

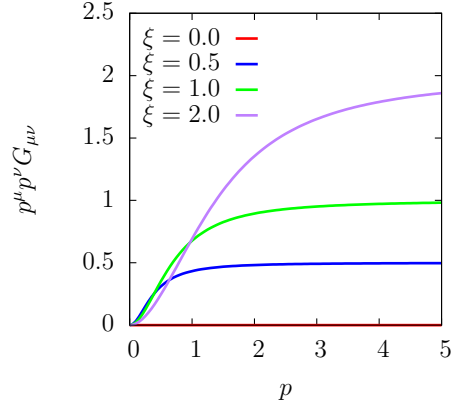


Figure 3–12: Propagator WST identity.

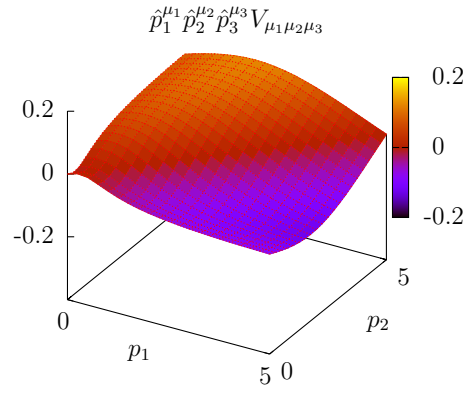


Figure 3–13: Vertex WST identity.

In its most general form, the WST identity for the gluon three-vertex is

$$\begin{aligned} p_1^{\mu_1} V_{\mu_1 \mu_2 \mu_3}(p_1, p_2, p_3) &= \frac{F(p_1)}{J(p_3)} (p_3^2 g_{\alpha \mu_3} - p_{3\alpha} p_{3\mu_3}) \mathbb{V}_{\mu_2}^\alpha(p_3, p_1, p_2) \\ &\quad - \frac{F(p_1)}{J(p_2)} (p_2^2 g_{\alpha \mu_2} - p_{2\alpha} p_{2\mu_2}) \mathbb{V}_{\mu_3}^\alpha(p_2, p_1, p_3), \end{aligned} \quad (3.68)$$

where F and J are defined in this context as $J(p) = p^2 G_T(p)$ and $F(p) = p^2 \Delta(p)$. \mathbb{V} with two Lorentz indices is given by

$$\begin{aligned} \mathbb{V}_{\mu_3}^\alpha(p_1, p_2, p_3) &= g_{\mu_3}^\alpha a(p_3, p_2, p_1) - p_3^\alpha p_{2\mu_3} b(p_3, p_2, p_1) + p_1^\alpha p_{3\mu_3} c(p_3, p_2, p_1) \\ &\quad + p_3^\alpha p_{1\mu_3} d(p_3, p_2, p_1) + p_1^\alpha p_{1\mu_3} e(p_3, p_2, p_1) \end{aligned} \quad (3.69)$$

which is related to the usual ghost-gluon vertex via $\mathbb{V}_{\mu_3}(p_1, p_2, p_3) = p_{1\alpha} \mathbb{V}_{\mu_3}^\alpha(p_1, p_2, p_3)$ (following once again with the decomposition in [178]). From this identity one obtains

$$p_1^{\mu_1} p_2^{\mu_2} p_3^{\mu_3} V_{\mu_1 \mu_2 \mu_3}(p_1, p_2, p_3) = 0. \quad (3.70)$$

With $\hat{p}^\mu \equiv p^\mu/p$, the deviation from the vertex Ward identity is show in Fig. 3–13 for Landau gauge. As previously, the vertex is a function of 3 variables, so to make a 2+1 dimensional plot we have fixed an angular variable to $\cos \theta_{p_1 p_2} = 1/4$.

3.7 Concluding remarks for Chapter 3

In this chapter, the propagators and vertices which extremize the three-loop, three-particle-irreducible action of Yang-Mills theory in 3 dimensions were obtained. This was achieved by writing a nonlinear variational *Ansatz* for three propagators (ghosts and the transverse and longitudinal components of gluons) and for eight vertices (two tensor structures for ghost-gluon vertices and six tensor structures for three-gluon vertices). To avoid divergences it was necessary to add and subtract

terms to one and two-loop self-energies; the added terms are computed in $\overline{\text{MS}}$, the subtraction renders the remaining numerical integrals finite. It was also necessary to compute the first loop corrections to two-point and three-point functions at large momentum explicitly and to incorporate these corrections into our *Ansätze* for those functions.

Now, the next task is to test the resulting resummation against exact non-perturbative results in 3D QCD or Yang-Mills theory in general by comparing the values of gauge invariant questions. As mentioned previously, this matter will be approached by extending the treatment to include a fundamental representation scalar with the goal of exploring the 3D $\text{SU}(2) + \text{Higgs}$ phase diagram, which can also be determined non-perturbatively on the lattice [163]. Based on the observation that the inclusion of vertices results in comparatively small corrections to two-point function (at the expense of significantly increased numerical complexity), we will attempt to resolve the Green's functions in $\text{SU}(N)$ Higgs theory in the three-loop 2PI formalism. This is to be explained in detail throughout the next chapter, but in short, a treatment of a symmetry broken phase using a similar approach to that presented here will bring about a whole new set of numerical challenges; by using the 2PI formalism we can focus on these issues.

It is worth remarking, though, that there are a few possible alternative routes that could be taken involving a study of the pure gauge theory. For instance, one could attempt an evaluation of the $\langle F^2(x)F^2(0) \rangle$ correlator, whose Fourier transform gives the lowest *glueball* mass. It might also be possible to evaluate the correlator of two field strengths connected by a Wilson line, which is of interest in evaluating

the Debye screening mass in full QCD [95, 199]. Unfortunately it is not possible to compute the pressure of 3D Yang-Mills theory at the 3PI level, because the nontrivial contributions to the pressure arise at four-loops. Evaluating the pressure would require a solution to the four-loop 3PI or 4PI problem. Extending this approach to the four-loop 4PI treatment would not raise any new conceptual issues, since all potential UV divergences in the extremization procedure are already encountered at the level of the three-loop 3PI problem. It would be interesting to do so because the non-perturbative contribution to the pressure of 3D Yang-Mills theory is needed to compute the g^6 term in the pressure for full QCD [47, 200]. However the extension to four-loops and 4PI would be prohibitively difficult because the diagram generation and loop integration would become even more cumbersome and the number of possible tensor structures for the four-point function is large.

CHAPTER 4

2PI resummation in $SU(N)$ Higgs theory

4.1 Introduction: the phase diagram of $SU(N)$ Higgs theory

In Chapter 1, Section 1.4.1 we motivated the study of three dimensional non-abelian gauge theories by their relationship to electroweak theory and QCD via dimensional reduction [36, 80, 98, 99, 175]. To quickly summarize: QCD at high temperature $T \gg \Lambda_{\text{QCD}}$ exhibits a natural separation of scales $g^2 T \ll gT \ll T$, so that non-zero bosonic and all fermionic Matsubara modes become heavy compared to the soft scales of the theory. These modes can be integrated out to obtain an effective 3 dimensional description of the soft physics, which is precisely $SU(3)$ Yang Mills coupled to an adjoint real scalar with gauge coupling $g_{3\text{D}}^2 = g_{4\text{D}}^2 T$ and mass $m_A^2 = g^2(N/3 + N_f/6)T^2$ (identified with the 0-mode of the A_0 component of the 4D gauge field). If one is only interested in physics at the supersoft scales, this can be taken one step further by integrating out the A_0 field to yield pure 3D Yang-Mills.

Yang-Mills theory, QCD and electroweak theory are known to undergo a phase transition [33, 39, 72, 201] over certain ranges of the model parameters. Naturally, for physical values of these parameters, one would ask whether we are in a first order, second order or cross-over regime. 3D effective models could potentially shed some light on this matter, except that for QCD, where the effective 3D description is an $SU(3) + \text{adjoint Higgs}$ theory, $T_c \sim \Lambda_{\text{QCD}}$. Thus, in the vicinity of the QCD phase transition (or cross-over) the effective description breaks down, since the underlying

assumption of weak 4D coupling and a separation of scales is not valid. A 3D effective model is still useful for studying the non-perturbative infrared dynamics of hot QCD, just not at temperatures in the vicinity of the scale Λ_{QCD} . However, the situation is different for electroweak theory near its phase transition.

The most general effective 3D description of electroweak theory is an $\text{SU}(2) \times \text{U}(1)$ gauge theory coupled to both fundamental and adjoint scalars. The adjoint scalars arise via the dimensional reduction, while the fundamental scalar is identified with the 4D Higgs field. In practice, an accurate study of the 4D theory does not require such elaborate field content; rather, quantitative predictions can be made by considering the much simpler $\text{SU}(2) + \text{fundamental}$ case [77, 162, 163, 202, 203]. Then, as a further refinement, one may study the effects due to the inclusion of an adjoint field [204, 205], as well as a $\text{U}(1)$ gauge field [75]. Or, in the context of GUTs, the model with an $\text{SU}(5)$ or $\text{SU}(3) \times \text{SU}(2)$ gauge group may be of interest [206, 207]. These models have received a fair amount of attention in the past due to the significance of a phase transition on electroweak baryogenesis [150, 208]. For the models considered, a first order phase transition at physical values of the Higgs mass has been ruled out.

The phase diagram of $\text{SU}(N)$ Higgs theory (as shown in Fig. 4-1) is often parametrized by the dimensionless variables x and y . These are respectively the ratios of the quartic coupling and scalar mass to the gauge coupling. Their values are specified by the physical parameters of the 4D theory, which are essentially m_{H} , m_{W} and T , as well as the 4D gauge coupling. Thus, a region in the 4D parameter space maps directly to a region in 3D. In terms of the 3D vocabulary, for $x \lesssim 1/10$ the

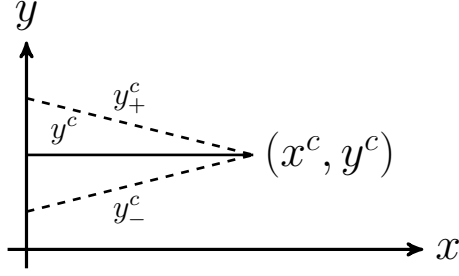


Figure 4–1: Phase diagram for $SU(N)$ Higgs theory, showing a first order line terminating at a critical point. The dashed lines indicate the appearance of metastable configurations in the effective potential.

theory undergoes a first order phase transition, and as x is increased, this becomes a cross-over. Small “ x ” actually corresponds to small m_H relative to the physical value, so the analogous 4D statement is that for small m_H (30 GeV for instance), the electroweak phase transition is first order. For a physical value of m_H , however, we find ourselves in the cross-over region. In 3D we refer to these two phases as a Higgs phase and a symmetric phase; when they are separated by a phase-boundary, they are distinct.

At small x the phase transition can be studied perturbatively by computing the one-loop effective potential for the Higgs VEV. Indeed one finds that in this region, the phase transition is first order. However, the perturbative treatment then goes on to predict a first order phase transition for all values of x ! The limitation of this approach becomes apparent when one considers the fact that the perturbative spectrum for a spontaneously broken gauge theory is fully dependent on the choice of gauge-fixing. Since a critical end point exists at a value of $x \sim 1/10$, we can infer that the perturbative description can only be valid for $x \ll 1/10$.

Therefore, the end point and cross-over must be resolved *non-perturbatively*. Since the lattice has already provided us with a very accurate determination of the phase diagram, we are able to use these results to test the reliability and accuracy of an alternative non-perturbative approach to the lattice, namely that of n PI resummation [113, 118, 147] in a gauge theory setting. In this chapter we will study the application of the n PI (specifically 2PI) formalism to $SU(N)$ Higgs theory.

To quickly review, in the context of a hot gauge theory, the use of an n PI based resummation scheme is primarily motivated by the extremely poor convergence of a weak-coupling expansion [102], since it provides a systematic procedure for reorganizing a perturbation series. In the past, resummations of this sort have been applied to the computation of sub-leading corrections to transport coefficients and thermodynamic quantities in QED [209, 210, 211, 212] and QCD [213]; in QCD other previous applications include HTL resummation [170] and the potential study of aspects of confinement [214]. Furthermore, of particular relevance to this work, the 2PI formalism has been used to study critical phenomena in scalar theory [215]. In Chapters 3 and 4 we are approaching the subject along a different trajectory, in that by applying the n PI formalism to $SU(N)$ Higgs theory our goal is to directly solve the resulting integral equations of motion, and then subsequently derive gauge-invariant quantities from the solutions.

An n PI effective action $\Gamma[\bar{\phi}, G, \dots]$ generates equations of motion for n -point resummed vertices by variation with respect to these n -point functions (reminiscent of and closely related to SD equations). For reasons explained in Chapter 3, Section 3.7, we will specifically consider a three-loop truncation of the case $n = 2$, which

in terms of diagrams can be interpreted as resumming one and two-loop self-energy topologies. By solving the resulting self-consistent equations, we can subsequently compute the gauge-invariant scalar condensate $\langle\phi^\dagger\phi\rangle$ as a function of the parameters x and y on the phase diagram. Then, at a specific value x , from the behaviour of $\langle\phi^\dagger\phi\rangle$ over a range of y we can infer whether or not we are in the cross-over or first order phase transition region. This will allow us to bracket and locate the critical end point.

We will present the technical details of the computation for a single complex scalar field in representation R of $SU(N)$. Results will be given for $N = 2$ (fundamental representation) in Landau and Feynman gauges, however it should be noted that the method straightforwardly generalizes to the inclusion of additional scalar fields.

This chapter is organized as follows: in Section 4.2 we will present the three-loop truncated 2PI effective action for $SU(N)$ Higgs theory, as well as the self-consistent equations that it generates. Additionally, some details pertinent to regularization and renormalization will be reviewed here. In Section 4.3 we will present certain extensions to the algorithm described in Chapter 3 which are needed to solve the 2PI equations of motion numerically. In Section 4.4 we will give an overview of the results, as well as derived quantities such as the scalar condensate and the location of the critical end point. Finally, in Section 4.5, we will discuss the properties of the effective action, and comment on the overall effectiveness of the method.

4.2 SU(N) Yang-Mills + Higgs theory in the n PI formalism

4.2.1 General remarks and notation

It is useful to begin by reviewing a number of the basic conventions that are used throughout this chapter. It should be assumed that T_R^a is a generator of some representation R of SU(N). The fundamental and adjoint representations are denoted by F and A respectively, and d_R is the dimension of R , for instance $d_F = C_A = N$. We have

$$\text{Tr } T_R^a T_R^b = T_R \delta^{ab} \quad (4.1)$$

$$T_{Rim}^s T_{Rmj}^s = C_R \delta_{ij}, \quad (4.2)$$

and additional group theory identities needed in this computation can be found in Appendix A. Following gauge-fixing, the Lagrangian can be divided into a Yang-Mills component and a Higgs component,

$$\mathcal{L}_{\text{YM}} = \frac{1}{2} \text{Tr} F_{\mu\nu} F^{\mu\nu} + \frac{1}{2\xi} (\partial^\mu A_\mu^a)^2 + \partial_\mu \bar{c}^a \partial^\mu c^a - g f_{abc} \partial^\mu \bar{c}^a c^b A_\mu^c \quad (4.3)$$

$$\mathcal{L}_\phi = (D^\mu \phi)^\dagger (D_\mu \phi) + (m^2 + \delta m^2) \phi^\dagger \phi + \frac{\lambda}{2} (\phi^\dagger \phi)^2 \quad (4.4)$$

so that $\mathcal{L} = \mathcal{L}_{\text{YM}} + \mathcal{L}_\phi$ (in general covariant gauge as written). We define the dimensionless ratios

$$x = \frac{\lambda}{2g^2} \quad y = \frac{m^2}{g^4}, \quad (4.5)$$

these quantities are equivalent to those specified in [162] which are commonly used throughout the literature. In Eq. (4.4) an additive counter-term has been explicitly included to cancel the divergent two-loop self-energy graphs (its value is given

in Appendix C). This leads to a scale dependence in m^2 and y accordingly; for a fundamental SU(2) Higgs we have

$$\frac{dy}{d\log\mu} = -\frac{1}{16\pi^2}\left(\frac{51}{16} + 9x - 12x^2\right). \quad (4.6)$$

The renormalization scale is fixed at $\mu = g^2$ throughout. To compare our results to those obtained from the lattice, we should state the relationship between the variables x and y and the parameters of the 4D theory. Once again for SU(2), directly quoting the result in [162],

$$x = -0.00550 + 0.12622\left(\frac{m_H}{80.6\text{GeV}}\right)^2 \quad (4.7)$$

$$y = 0.39818 + 0.15545\left(\frac{m_H}{80.6\text{GeV}}\right)^2 - 0.00190\left(\frac{m_H}{80.6\text{GeV}}\right)^4 - 2.58088\frac{m_H^2}{T^2} \quad (4.8)$$

assuming a value of $g_{4D} = 2/3$ for the 4D gauge coupling.

4.2.2 The three-loop 2PI effective action

The 2PI effective action $\Gamma[G_{ij}]$ is formally defined as the Legendre transform of the generating function of connected diagrams $W[K_{ij}]$ with respect to a two particle source [147]. Using the generic label Φ_i for fields, $W[K_{ij}]$ reads

$$W[K_{ij}] = -\log \int D[\Phi] e^{-S - \frac{1}{2}\Phi_i K_{ij} \Phi_j}. \quad (4.9)$$

Even correlation function can be obtained by differentiation with respect to K_{ij} . For instance,

$$\frac{\delta W[K_{ij}]}{\delta K_{ij}} = \frac{1}{2}G_{ij} \quad (4.10)$$

yields the two-point function G_{ij} . For the two-point functions of SU(N) Higgs theory, we can assume that G_{ij} is proportional to the colour identity of the corresponding

species, and hence so is K_{ij} . Then, for a rotationally symmetric Lagrangian

$$\langle \Phi_i \rangle = \frac{\int D[\Phi] \Phi_i e^{-S - \frac{1}{2} \Phi_i K_{ij} \Phi_j}}{\int D[\Phi] e^{-S - \frac{1}{2} \Phi_i K_{ij} \Phi_j}} = 0. \quad (4.11)$$

I.e., the presence of K_{ij} does not alter the global rotational invariance of the original Lagrangian. So in fact, Eq. (4.10) generates the *connected* two-point function. The consequences of this statement in the context of a spontaneously broken gauge theory will be discussed towards the end of this section, but for now we can proceed with the Legendre transform

$$\Gamma[G_{ij}] = K_{ij} \frac{\delta W[K_{ij}]}{\delta K_{ij}} - W[K_{ij}]. \quad (4.12)$$

In setting $K_{ij} = 0$, equations of motion for G_{ij} are obtained from the stationarity condition

$$\frac{\delta \Gamma[G_{ij}]}{\delta G_{ij}} = 0. \quad (4.13)$$

The solutions we seek correspond to extrema of $\Gamma[G_{ij}]$. Specializing now to the field content of $SU(N)$ Higgs theory, we can write $\Gamma = \Gamma_{\text{YM}} + \Gamma_\phi$ and explicitly state the loop expansion, which we will truncate at three-loops. Γ_{YM} is defined so that it contains those diagrams encountered in the pure Yang-Mills problem while Γ_ϕ contains the additional diagrams which arise when a single arbitrary representation Higgs field is included. Using a diagrammatic notation compatible with the previous

chapter (see Chapter 3, Table 3–1)

$$D_{\mu\nu} = \text{wavy line} \quad (4.14)$$

$$\Delta = \text{dotted line with arrow} \quad (4.15)$$

$$G = \text{double line with arrow} , \quad (4.16)$$

for now we can assume a similar set of *Ansätze* to those used previously

$$G_{\mu\nu}(p) = \frac{1}{p^2 - \Pi_T(p)} \mathbf{T}_{\mu\nu} + \frac{\xi}{p^2 - \xi \Pi_L(p)} \mathbf{L}_{\mu\nu} \quad (4.17)$$

$$\Delta(p) = \frac{1}{p^2 - \Sigma(p)} \quad (4.18)$$

$$D(p) = \frac{1}{p^2 + m^2 - \Pi_\phi(p)}. \quad (4.19)$$

All vertices appearing in the 2PI effective action are at tree-level. These are drawn as

$$\begin{array}{ccc} p_4, a_4, \mu_4 & & p_2, a_2 \\ & \diagdown \quad \diagup & \\ & \text{wavy line} & \\ & \diagup \quad \diagdown & \\ p_3, a_3, \mu_3 & & p_1, a_1 \end{array} = g^2 \mathcal{V}_{\mu_3 \mu_4}^{a_1 a_2 a_3 a_4}(p_1, p_2, p_3, p_4) \quad (4.20)$$

with the corresponding expressions given in Appendix B. Finally, the Higgs mass renormalizes at two-loops; it is necessary to subtract the divergence with an additive counter-term of the form $m^2 = m_\phi^2 + \delta m^2$, with the corresponding vertex

$$\text{double line with arrow and cross} = -\delta m^2. \quad (4.21)$$

Explicitly factoring out minus signs due to ghost loops, we have

$$\begin{aligned}
\Gamma_{\text{YM}} = & \frac{1}{2} \text{Tr} \log D - \frac{1}{2} \text{Tr} [D^{(0)}]^{-1} D - \text{Tr} \log \Delta + \text{Tr} [\Delta^{(0)}]^{-1} \Delta \\
& + \frac{1}{12} \text{ (1-loop wavy bubble) } + \frac{1}{8} \text{ (2-loop wavy bubbles) } - \frac{1}{2} \text{ (1-loop wavy line with ghost loop) } \\
& + \frac{1}{48} \text{ (2-loop wavy bubble) } + \frac{1}{24} \text{ (2-loop wavy bubbles) } + \frac{1}{8} \text{ (2-loop wavy bubbles) } \\
& - \frac{1}{3} \text{ (1-loop wavy line with ghost loop) } - \frac{1}{4} \text{ (1-loop wavy line with ghost loop) } .
\end{aligned} \tag{4.22}$$

For an n -loop pure Yang-Mills planar diagram, the tracing over internal colour indices generically results in an overall colour factor of $(N^2 - 1)N^{n-1}$. Furthermore, since an n -loop vacuum bubble is also proportional to $g^{2(n-1)}$, one finds as earlier that factors of g^2 always appear in the form of 't Hooft coupling $g^2 N$. Hence, for the pure gauge

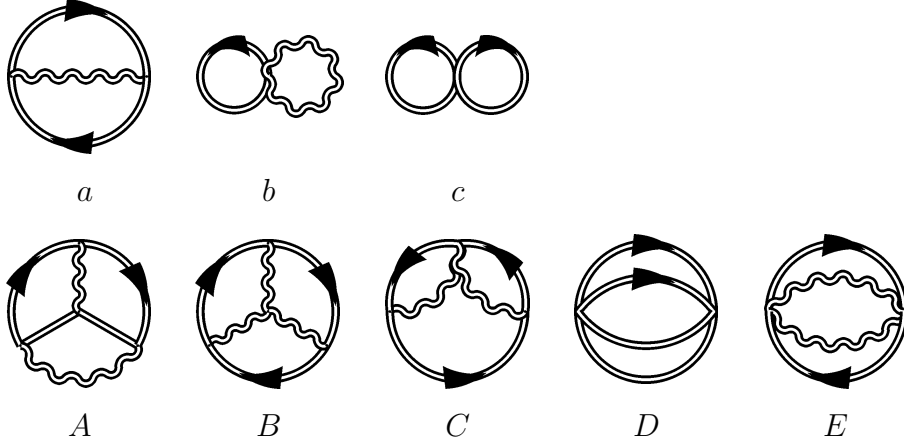
problem, the natural scale is not g^2 , but rather $g^2 N$. The Higgs contribution is

$$\begin{aligned}
\Gamma_\phi = & \text{Tr} \log G - \text{Tr}[G^{(0)}]^{-1} G \\
& + \frac{1}{2} \text{ (circle with wavy line) } + \frac{1}{2} \text{ (two circles connected by a wavy line) } + \frac{1}{2} \text{ (two circles connected by a straight line) } \\
& + \frac{1}{8} \text{ (circle with two internal lines) } + \frac{1}{4} \text{ (circle with wavy line and internal lines) } + \text{ (circle with wavy line and internal lines) } \\
& + \frac{1}{3} \text{ (circle with wavy line and internal lines) } + \frac{1}{4} \text{ (circle with wavy line and internal lines) } + \text{ (circle with a cross) } .
\end{aligned} \tag{4.23}$$

These diagrams have a somewhat more complicated dependence on N (the associated colour factors are stated in Table 4–1). In the previous chapter, as there was only a single mass scale present in the planar pure Yang-Mills problem (namely $g^2 N$), we opted to express all dimensionful quantities in units of $g^2 N$. With scalars present, this is no longer the case, and as a result there is a significance to the specific value of N . For clarity, units of $g^2 N$ will be explicitly stated throughout this chapter.

The power of the 2PI formalism becomes apparent when we perform the variation of Γ with respect to G_T , G_L , Δ and D . For instance, from $\delta\Gamma/\delta D = 0$, we have

$$-D^{-1}(p) + D^{(0)-1}(p) = \Pi_\phi(p) \tag{4.24}$$



(a)	$d_A T_R$
(b)	$2d_A T_R$
(c)	$d_R(1 + d_R)$
(A)	$d_A T_R(C_R - \frac{1}{2}C_A)$
(B)	$\frac{1}{2}d_A T_R C_A$
(C)	$d_A T_R(2C_R - \frac{1}{2}C_A)$
(D)	$2d_R(1 + d_R)$
(E)	$d_A T_R(4C_R - C_A)$

Table 4–1: Colour factors for the two and three-loop Higgs topologies; see also Appendix A.

with (omitting charge arrows)

$$\begin{aligned}
\Pi_\phi(p) = & \text{[Diagram 1]} + \text{[Diagram 2]} + \frac{1}{2} \text{[Diagram 3]} \\
& + \text{[Diagram 4]} + \text{[Diagram 5]} + 2 \text{[Diagram 6]} \\
& + \frac{1}{2} \text{[Diagram 7]} + \frac{1}{2} \text{[Diagram 8]} + \text{[Diagram 9]} + \text{[Diagram 10]} .(4.25)
\end{aligned}$$

Equations of the type Eq. (4.24) / Eq. (4.25) have been generically referred to in this chapter as 2PI equations of motion, and the topologies which appear in Eq. (4.25) correspond to the loop order of the truncation of the effective action. By solving this equation self-consistently in a three-loop truncation, we fully resum one and two-loop self-energy topologies to all orders.

As in Chapter 3, Eq. (4.25) contains terms that are linearly and logarithmically divergent; in dimensional regularization, only the logarithmic divergences appear explicitly as $1/\epsilon$'s, and these are subtracted by the counter-term. This implies that the entire computation must be performed in $\overline{\text{MS}}$, which requires the analytic continuation of these integrals to D dimensions. The regularization procedure which we adopt is described at length in Chapter 3, Section 3.3; to quickly recap the key

points, consider the tadpole graph

$$\mathcal{A} = -\frac{1}{\lambda(d_R + 1)} \text{ (tadpole diagram) } = \frac{1}{\bar{\mu}^{2\epsilon}} \int \frac{d^D q}{(2\pi)^D} D(q) \quad (4.26)$$

with $\bar{\mu}^2 = \mu^2 e^\gamma / 4\pi$, and $D = 3 + 2\epsilon$. Since $D(q)$ is an arbitrary function of q , this integral would need to be performed numerically; in doing so we must set $D \rightarrow 3$. To implement dimensional regularization, we adopt a procedure of “addition and subtraction,” as follows,

$$\mathcal{A} = \frac{1}{\bar{\mu}^{2\epsilon}} \int \frac{d^D q}{(2\pi)^D} \left(D(q) - \frac{1}{q^2} \right) + \frac{1}{\bar{\mu}^{2\epsilon}} \int \frac{d^D q}{(2\pi)^D} \frac{1}{q^2}. \quad (4.27)$$

The rightmost term is simple enough that it can be computed analytically (in $\overline{\text{MS}}$ its value is zero), and the leftmost term is now only logarithmically divergent. Thus, we have removed the linear divergence by subtracting $1/q^2$, and now the next step is to remove the logarithmic one. At large momenta, and near 3 dimensions, $D(q)$ can be expanded as

$$D(q) \sim \frac{1}{q^2} + \frac{g^2 C_R (1 + \epsilon(1 - \xi - \log 4))}{4\mu^{2\epsilon} q^{3-2\epsilon}} + \mathcal{O}\left(\frac{1}{q^4}\right) \quad (4.28)$$

where we have been careful to keep $\mathcal{O}(\epsilon)$ corrections in the $1/q^3$ term. Now, we can add and subtract the subleading term,

$$\begin{aligned} \mathcal{A} = & \frac{1}{\bar{\mu}^{2\epsilon}} \int \frac{d^D q}{(2\pi)^D} \left[D(q) - \frac{1}{q^2} - \frac{g^2 C_R (1 + \epsilon(1 - \xi + \log 4))}{4\mu^{2\epsilon} (q^2 + \omega^2)^{3/2-\epsilon}} \right] \\ & + \frac{1}{\bar{\mu}^{2\epsilon}} \int \frac{d^D q}{(2\pi)^D} \frac{1}{q^2} + \frac{g^2 C_R (1 + \epsilon(1 - \xi - \log 4))}{4\bar{\mu}^{2\epsilon} \mu^{2\epsilon}} \int \frac{d^D q}{(2\pi)^D} \frac{1}{(q^2 + \omega^2)^{3/2-\epsilon}}. \end{aligned} \quad (4.29)$$

The first line of Eq. (4.29) is finite, so we can set $D = 3$ and perform the integral numerically. What we have effectively done is shuffled all of the ϵ dependence into terms which can be integrated analytically. Thus the regularized expression for \mathcal{A} has the form

$$\begin{aligned} \mathcal{A} = & \int \frac{d^3q}{(2\pi)^3} \left[D(q) - \frac{1}{q^2} - \frac{g^2 C_R}{4(q^2 + \omega^2)^{3/2}} \right] \\ & + \frac{g^2 C_R (1 + \epsilon(1 - \xi - \log 4))}{4(4\pi)^{3/2} e^{\epsilon\gamma} \Gamma(3/2 - \epsilon)} \Gamma(-2\epsilon) \left(\frac{\omega}{\mu} \right)^{4\epsilon}. \end{aligned} \quad (4.30)$$

We can then subtract the $1/\epsilon$ divergence with the counter-term, and take the limit $\epsilon \rightarrow 0$. Note here that the subleading term appears with a mass ω . Its value is arbitrary, but it must be included, otherwise one would introduce an IR divergence where originally there was none. For simplicity, we can set $\omega = g^2 N$ noting that the final results of the calculation are ω independent. Though it is certainly permitted, it is not a requirement that ω be set to the scalar mass m (and our reasoning for not doing so is explained in Appendix C).

Other diagrams which appear in Γ are regularized in much the same fashion. In the end we need to compute all of the one and two-loop gluon and Higgs self-energy diagrams which appear in perturbation theory (ensuring that IR divergent diagrams are not introduced inadvertently); the results of this computation are contained in Appendix C. Following regularization, full expressions for the 2PI equations of motion will take on a similar form to e.g. Chapter 3, Eq. (3.30).

4.2.3 Remarks on gauge-fixing

Since the perturbative spectrum of the gauge-fixed action Eq. (4.3) and Eq. (4.4) corresponds to the symmetric phase, the effective action as presented should at least

be suitable to study that phase. One would then ask, *what is the correct way to treat the Higgs phase?* In perturbation theory, this question essentially reads *how should we handle the appearance of one-point functions?* This was addressed in Chapter 1, Section 1.3.2 where we saw that the way to treat spontaneous symmetry breaking perturbatively is to define a shifted scalar field, where the shift breaks a subset of the generators of the gauge symmetry. The disadvantage there is that the resulting perturbative spectrum depends on the gauge-fixing.

So, what we really mean to ask is, *what is the correct way to treat the Higgs phase non-perturbatively, from the perspective of the n PI formalism?* Let us consider the conventional definition of the one-point function; we would need to go back and include a one-particle source in Eq. (4.9),

$$W[J_i, K_{ij}] = -\log \int D[\Phi] e^{-S - J_i \Phi_i - \frac{1}{2} \Phi_i K_{ij} \Phi_j} \quad (4.31)$$

keeping the “symmetric phase” action in W . The value of $W[0, 0]$ is gauge-invariant [146], and in simply stating the path integral, gauge-fixing is not required. However, for non-zero values of J_i , gauge-invariance is explicitly broken. Supposing then that we are in the Higgs phase in Landau gauge, the path integral will be dominated by field configurations with $\Phi_i \neq 0$. Furthermore, by introducing a finite J_i we have also explicitly broken the global rotational invariance (which was maintained in Landau gauge), and hence we have assigned a preferred direction to the scalar field. In this set-up, we can interpret the gauge-fixed one-point function as a directional derivative

$$\langle \Phi_i \rangle = \frac{\delta}{\delta J_i} W[J_i, 0] \Big|_{J_i \rightarrow 0(\vartheta)} \quad (4.32)$$

where $0(\vartheta)$ means “zero is approached along a direction ϑ on the manifold of $SU(N)$ rotations.” In the symmetric phase, W is analytic at $J = K = 0$, so an approach from any direction will yield the same result, consistent with a zero VEV. In the broken phase, W is expected to develop a conical singularity, so the direction has a significance.

The main point here is that a treatment of the broken phase involving VEVs is inherently gauge-dependent, and hence perturbative. Since we are attempting to tackle the problem non-perturbatively, we will opt to avoid introducing a one-particle source altogether (reminiscent of the approach in [216]). As mentioned earlier, covariant gauge-fixing maintains rotational invariance. This is left undisturbed by the non-zero values of K_{ij} assumed in deriving the effective action, since the 2PI equations of motion are diagonal in colour indices. K_{ij} commutes with global $SU(N)$ rotations, and we are taking the limit $K \rightarrow 0$ along that direction. Hence there is no preferred orientation in field space. The path integral Eq. (4.9) may be dominated by field configuration with $\Phi_i \neq 0$, but these are weighted over equally. So now, the statement $\langle \Phi_i \rangle = 0$ in terms of J_i should be interpreted as

$$0 = \int D\vartheta \left[\frac{\delta}{\delta J_i} W[J_i, 0] \Big|_{J_i \rightarrow 0(\vartheta)} \right] \quad (4.33)$$

and we can think of the constraint $D_{ij}(p) \propto \delta_{ij}$ as a gauge choice. Then, the existence of a broken phase would rather be encoded in the *connected* scalar two-point function. Neglecting gauge fields for the moment, the corresponding scalar correlator

(schematically)

$$D(y-x) \sim \int D\vartheta \left\langle (\phi^\dagger(y) + v^*(\vartheta))(\phi(x) + v(\vartheta)) \right\rangle \quad (4.34)$$

approaches a constant at large separation in the broken phase. In momentum space, this would correspond to the formation of a δ -function peak at zero momentum in $D(p)$. However, when gauge fields are present, the scalar propagator is not a gauge-invariant correlator, as Eq. (4.34) does not contain a Wilson link (and therefore, there is no parallel transport between the points x and y). We anticipate that D in Landau gauge would exhibit potentially long (but not infinite) range correlations, and in momentum space, this would correspond to a finite-width peak.

To study $SU(N)$ Higgs theory in the Higgs phase via the 2PI effective action we are essentially seeking solutions of $\Gamma[D]$ which develop a peak-like structure, whose width and height are determined self-consistently. In effect, we are observing the phase transition directly from the scalar condensate, which is proportional to the area under the peak in $D(p)$. This approach is inherently non-perturbative, in spite of the necessity to fix a gauge. Also, by construction the Higgs and symmetric phases are analytically connected, consistent with [72] (assuming fundamental representation matter). The procedure is very analogous to what is done in the 1PI formalism, where one can infer the existence of stable or metastable configurations by seeking out the extrema of the 1PI effective action computed to some loop order.

The main potential drawbacks of the n PI approach here and in general are computational complexity and potential issues related to the gauge-fixing independence of a selective resummation when applied to a gauge theory [115, 116]. Computational

complexity arises from the sheer size of the algebraic expressions for the diagrams involved following tensor contraction and reduction to scalar integrals. Whereas, the issues related to gauge-fixing independence are the reason why we need to include a longitudinal self-energy for the gauge fields. In resumming only a certain class of topologies, we are guaranteed to omit diagrams at higher loop orders; this omission leads to non-zero longitudinal contributions to the gauge field self-energy.

In performing this computation, we wish to mainly determine two things. First, we would like to investigate the overall applicability of the 2PI method as presented in studying Higgs phase. This involves resolving distinct symmetric and Higgs phase solutions over a range of x and y on the phase diagram and determining the range of x over which there is a phase transition or cross-over. Second, due to the gauge-fixing requirement and finite loop order of the truncation, we are attempting to determine the accuracy with which this method can be used to compute gauge-invariant observables (i.e. the location of the critical end point) as well as the degree by which these quantities depend on the gauge parameter.

4.2.4 The use of covariant gauge

Before proceeding onwards to the details of the computations, we should make a few remarks on the choice of working in covariant gauge over specifically R_ξ gauge [88], which is often used in a perturbative treatment of spontaneous symmetry breaking. Recall from Chapter 1, Section 1.3.2 that R_ξ gauge is based upon a redefinition of the scalar field

$$\phi(x) = \chi(x) + v, \tag{4.35}$$

which we can visualize as a field which fluctuates about a constant background. The quantity v is the scalar field VEV.

In a pure scalar theory, a configuration such as Eq. (4.35) with a non-zero VEV is compatible with an ordered phase (analogous to the alignment of spins in a magnetic system). In general, the existence of a broken phase for values of the model parameters where classically the system is in a disordered phase ($v = 0$) can be inferred from the existence of extrema at non-zero v of the effective potential of the scalar theory, $\Gamma[v]$. Therefore, the quantity v *is* an order parameter.

However, in a gauge theory, we are free to perform a local gauge rotation on the fields

$$\phi(x) \rightarrow \Lambda(x)\phi(x) \tag{4.36}$$

which renders the VEV v physically meaningless. That being said, in a fixed gauge we can still perturbatively construct an effective potential $\Gamma[v]$, but it will be gauge-dependent (so that we should really be writing $\Gamma[v, \xi]$) [87, 144]. Certain physical quantities can be extracted from $\Gamma[v, \xi]$, from which we can infer the existence of a phase transition. For example, the value at its extremum is gauge-independent (though necessarily renormalization scale dependent); it is related to the generating function W at vanishing source via Legendre transform. $\Gamma[v, \xi]$ also contains information about the scalar condensate [80]. However, the phases of the system should *not* be inferred from the value of v at the extremum (which would imply that v is a good order parameter), since v is not a physical quantity [217].

Gauge symmetry does not forbid a field redefinition of the form Eq. (4.35) though such a shift results in a complicated perturbation theory, due to the appearance of

crossed scalar / gauge field kinetic terms. The usefulness of R_ξ gauge (perturbatively) stems from the fact that it eliminates these cross-terms, which is achieved by defining a gauge-fixing functional which is explicitly dependent on v .

The use of R_ξ gauge in constructing an effective potential has been criticized on the observation that one is effectively choosing a different gauge-fixing for *each* value of v (see the discussion in Appendix A of Ref. [218]). Furthermore, the value of v at the extremum is determined self-consistently via $\delta\Gamma[v_\xi, \xi]/\delta v_\xi = 0$. Since the gauge parameter explicitly appears in the effective potential, v at the extremum will in general depend on the gauge parameter ξ [87].

In the context of the n PI formalism, the use of R_ξ gauge *non-perturbatively* may present an ambiguity. That is, non-perturbatively, in addition to being dependent on ξ , the VEV is determined via a self-consistency condition on the value of the gauge-fixed one-point function obtained from the gauge-fixed path integral, viz.

$$v = \int D[\Phi] \phi e^{-S(\xi, v)}. \quad (4.37)$$

In principle, this self-consistency condition does not have a unique solution.

Since we are seeking a non-perturbative resolution of the phase diagram, we are motivated to simply sidestep the potential issues concerning the inclusion of a VEV by working in covariant gauge [218, 219] and additionally *not* performing a redefinition of the scalar field. We emphasize that the existence of a broken phase should not be inferred from a non-zero value of v , but rather, should be determined by gauge-invariant quantities.

4.3 Extremization of the effective action

4.3.1 Variational *Ansätze*

In the previous chapter, we extensively described an algorithm which can be used to extremize the effective action when only gauge fields are present. Now we have to address the additional complications which arise due to the presence of a Higgs field. In the symmetric phase, the presence of the Higgs does not really change much at the technical level, and obtaining self-consistent solutions for the gauge field and Higgs propagators proceeds much as earlier.

To begin, we will review the details of the functions which enter into the problem. Since we have assumed a general covariant gauge, we are attempting to solve self-consistently for the following 4 functions: $G_T(p)$, $G_L(p)$, $\Delta(p)$ and $D(p)$, which are respectively the transverse and longitudinal gauge field propagators, the ghost propagator and the Higgs propagator. We can opt for the most part to simplify the problem further by working in Landau gauge, where G_L falls out of the picture; however, computations in Feynman gauge do require a treatment of G_L .

To realize the extremization, we will specify *Ansätze* for these functions in terms of a set $\mathbb{C} = \{c_i\}$ of variational coefficients, such that the variational equations transform into

$$\frac{\delta\Gamma}{\delta\{G_T/G_L/\Delta/D\}} = 0 \rightarrow \frac{\delta\Gamma}{\delta c_i} = 0. \quad (4.38)$$

In principle the set \mathbb{C} needs to be infinitely large; however, in practice it suffices to work with a finite number of coefficients. The size of \mathbb{C} can be increased as needed until convergence is attained. In terms of a finite number of coefficients, there are many ways that we can specify an arbitrary function of $p \in (0, \infty)$. We will choose

Padé approximants; for some $\{a_i\} \cup \{b_j\} \subset \mathbb{C}$, we will define

$$\mathcal{R}_{i_{\max}-j_{\max}}(p, \{a_i\} \cup \{b_j\}) = \frac{a_{i_{\max}} p^{i_{\max}} + \dots + a_0}{b_{j_{\max}} p^{j_{\max}} + g^2 N}. \quad (4.39)$$

Then, for the symmetric phase two-point functions Eq. (4.17), Eq. (4.18) and Eq. (4.19), we can parametrize the self-energies as follows

$$\Pi_T(p) = g^2 \left(\frac{N(\xi^2 + 2\xi + 11)}{64} - \frac{T_R}{16} \right) p + \mathcal{R}_0(p, \{c_i^{\{\Pi_T\}}\}) \quad (4.40)$$

$$\Pi_L(p) = \mathcal{R}_0(p, \{c_i^{\{\Pi_L\}}\}) \quad (4.41)$$

$$\Sigma(p) = \frac{g^2 N}{16} \frac{p^2}{p + \omega_\Sigma} + \mathcal{R}_0(p, \{c_i^{\{\Sigma\}}\}) \quad (4.42)$$

$$\Pi_\phi(p) = \frac{g^2 C_R}{4} \frac{p^2}{p + \omega_{\Pi_\phi}} + \mathcal{R}_0(p, \{c_i^{\{\Pi_\phi\}}\}), \quad (4.43)$$

using third order Padé approximants as in the previous chapter.

The resulting self-consistent equations have the simple form $\Pi_T^{Ansatz}(p) = \Pi_T^{2PI}(p)$ ¹ (where $\Pi_T^{2PI}(p)$ is the gluonic analogue of Eq. (4.25)) and similarly for Π_L , Σ and Π_ϕ . Now, to solve the problem in the Higgs phase, we can leave G_T , G_L and Δ as is, and introduce an additional term to the scalar two-point function as originally defined in Eq. (4.19),

$$D(p) = \frac{\mathcal{R}_0(p, \{c_i^{\{G\}}\})}{p^\gamma(p^{4-\gamma} + \omega_G)} + \frac{1}{p^2 + m^2 - \Pi_\phi(p)}. \quad (4.44)$$

¹ Using the labels “*Ansatz*” and “2PI” to distinguish between the value of the Padé approximant and self-energy functional constructed out of 2PI diagrams. This differs from the previous chapter in that we are not explicitly subtracting the linear-in- p one-loop self-energies.

This *Ansatz* has the advantage that we can smoothly deform a Higgs phase solution into a symmetric one (where the leading term would vanish). This is a necessary feature, as it allows us to demonstrate unambiguously when two distinct solutions coexist, noting that we allow the leading term to vary even when we are in the symmetric phase. In this expressions, γ could also be treated as a variational parameter, but we find that it works best² to simply fix its value at $\gamma = 2$ (additionally, we fix $\omega_G = g^2 N$). The self-consistent equations for G_T , G_L and Δ remain unchanged; however, for D we have $-D^{-1}(p) + D^{(0)-1}(p) = \Pi_\phi^{2\text{PI}}(p)$ since $-D^{-1}(p) + D^{(0)-1}(p) \neq \Pi_\phi^{Ansatz}(p)$ with the additional term.

The full self-energy should be interpreted in the UV as the sum of a one-loop and additional non-perturbative higher loop corrections. Thus, the one-loop terms appearing in Eq. (4.40) to Eq. (4.43) are specified by a perturbative calculation (the exact details of which are given in Appendix C), and remain fixed throughout the variation. This is actually a requirement; to see why this is the case, consider the UV expansion of G_T resulting from Eq. (4.40),

$$G_T(p \gg g^2 N) = \frac{1}{p^2} + \frac{\frac{g^2 N(\xi^2 + 2\xi + 11)}{64} - \frac{g^2 T_R}{16}}{p^3} + \mathcal{O}\left(\frac{1}{p^4}\right), \quad (4.45)$$

as well as the variation of Γ with respect to $c_i^{\{\Pi_T\}}$

$$\frac{\delta \Gamma}{\delta c_i^{\{\Pi_T\}}} = d_A \int \frac{d^3 p}{(2\pi)^3} \frac{\delta G_T(p)}{\delta c_i^{\{\Pi_T\}}} \left(-\Pi_T^{Ansatz}(p) + \Pi_T^{2\text{PI}}(p) \right). \quad (4.46)$$

² That is, upon variation γ is not observed to deviate to any significant degree from $\gamma = 2$.

As explained in Chapter 3, Section 3.3.2, by fixing the tree-level $\mathcal{O}(1/p^2)$ and one-loop $\mathcal{O}(1/p^3)$ behaviour in Eq. (4.45), the term in parentheses in Eq. (4.46) is automatically $\mathcal{O}(1)$ at large momentum, while the derivative of G_T is $\mathcal{O}(1/p^4)$ (or milder, depending on which coefficient we are differentiating with respect to). Hence, Eq. (4.46) is finite. Finally, it is worth noting that at one-loop the inclusion of masses in bare diagrams is subleading in p relative to the massless diagrams; as we are not required to impose any constraints on the two-point functions at $\mathcal{O}(1/p^4)$, it suffices to compute the one-loop corrections in the massless limit.

Since convergence to the perturbative limit is only necessary at large p , looking back at Eq. (4.42) and Eq. (4.43), we opted to include the one-loop contributions with an additional IR suppression factor of $p/(p + \omega_{\Sigma/\Pi_\phi})$. At sufficiently small momenta, a linear term in the denominator of a propagator can lead to formation of a pole. The gauge fields dynamically generate a mass that is sufficiently large to prevent this sort of thing from happening so a suppression factor of this sort is not required. For the Higgs and ghost this is not the case (in fact, the 2PI solution is consistent with $\Delta(p) \sim 1/p^2$ as $p \rightarrow 0$). In solving the problem we will set, $\omega_\Sigma = \omega_{\Pi_\phi} = g^2 N$; again this is arbitrary, and does not affect the final result.

4.3.2 Initial conditions and root finding

To extremize $\Gamma[G_T, G_L, \Delta, D]$, we employ an algorithm based on conjugate gradient descent specialized to the problem at hand. We can visualize the root-finding algorithm as a dynamical system where we choose an initial value for the coefficients c_i and subsequently follow a flow through the gradient field $\partial\Gamma/\partial c_i$ until we reach an attracting fixed point, which corresponds to a solution.

For x below the critical end point, there is a region of metastability where two attractors coexist; we will denote the corresponding solutions as D_+ and D_- (with basins of attraction γ_+ and γ_- respectively). Solutions of the D_+ variety are identified with the symmetric phase, as they are characterized by vanishing \mathcal{R}_0 in Eq. (4.44); i.e. they are essentially massive propagators with a self-energy. On the other hand, the D_- variety tend towards larger values of \mathcal{R}_0 , and hence are characterized by a peak at zero momentum. They are identified with the Higgs phase.

For an initial choice of c_i in the region of (x, y) where two stable solutions coexist, one does not necessarily evolve towards either the Higgs or symmetric phase solutions. Due to the saddle-like behaviour of Γ , there is also a set of initial conditions $c_i \in \gamma_0$ which evolve towards divergent values of D . This is to be discussed in greater detail in Section 4.5 where we give an outline of the phase portrait of the system.

The number of iterations of gradient descent in the extremization procedure (denoted by \mathcal{N}) can be thought of as time evolution, and we are interested in the results at late times. We can observe convergence of the algorithm by plotting the evolution of the LHS and RHS of the self-consistent equations with \mathcal{N} ; this is shown generically in Fig. 4-2. From this figure it is apparent that convergence is attained.

4.4 Analysis and results

We will from this point onwards carry out the analysis in Landau gauge (which eliminates the longitudinal gluon propagator), and set $N = 2$ with the scalar field in the fundamental representation. A comparison with the results in Feynman gauge appears towards the very end, in Section 4.5.6. To summarize thus far, with the

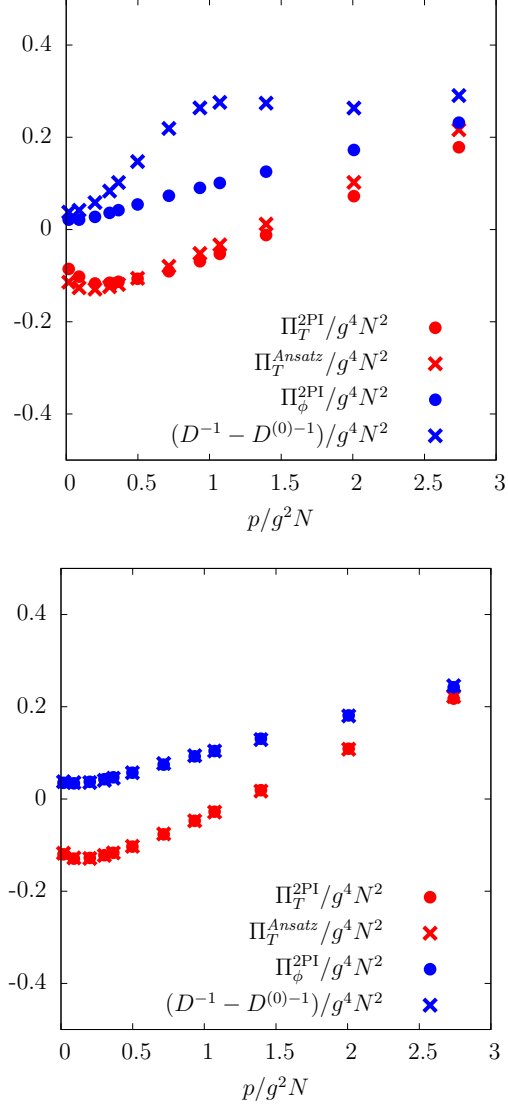


Figure 4–2: Evolution of the 2PI equations of motion under gradient descent, which are solved when the points overlap in the above figures (the ghost equation is not depicted, but it is qualitatively similar). The top panel corresponds to some initial choice of variational coefficients, and at the bottom we see convergence at late times.

Ansätze presented in the previous section parametrized by a set of variational coefficients c_i , the self-consistent solutions of the 2PI equations of motion

$$\Pi_T^{Ansatz}(p) = \Pi_T^{2PI}(p) \quad (4.47)$$

$$\Sigma^{Ansatz}(p) = \Sigma^{2PI}(p) \quad (4.48)$$

$$-D^{-1}(p) + D^{(0)-1}(p) = \Pi_\phi^{2PI}(p) \quad (4.49)$$

coincide with the node

$$\frac{\partial}{\partial c_i} \Gamma[G_T, \Delta, D] = 0. \quad (4.50)$$

This equation in general is divergent, however, we have shown that potential divergences are eliminated with a careful choice of *Ansätze*, and furthermore, those that remain (which lead to renormalization) can be computed in $\overline{\text{MS}}$. At this point, we are ready to present the results and analyze the solutions of Eq. (4.50).

Solutions for the Higgs, gauge and ghost propagator are shown in Fig. 4–3 (Higgs) and Fig. 4–4 (gauge/ghost). These plots are generated for the specific value of $x = 0.125$ (and a range of y); however, at generic values of (x, y) solutions (when they exist) will take on either of these forms. On the bottom panel in Fig. 4–3, we can distinguish between the divergent peak-like and massive behaviour of Higgs (D_-) and symmetric (D_+) phase solutions. Furthermore, at $x = 0.125$, we observe that Γ simultaneously admits two solutions over a range of y , which is evidence of metastability. On the top panel of Fig. 4–3 we see that the symmetric phase D_+ terminates. This occurs approximately at the value of y for which the difference $m^2 - \Pi_\phi(0)$ changes sign. The gauge field propagator in Fig. 4–4 develops a non-perturbative “mass”, and this is mainly due to the presence of the pure-gluon diagrams.

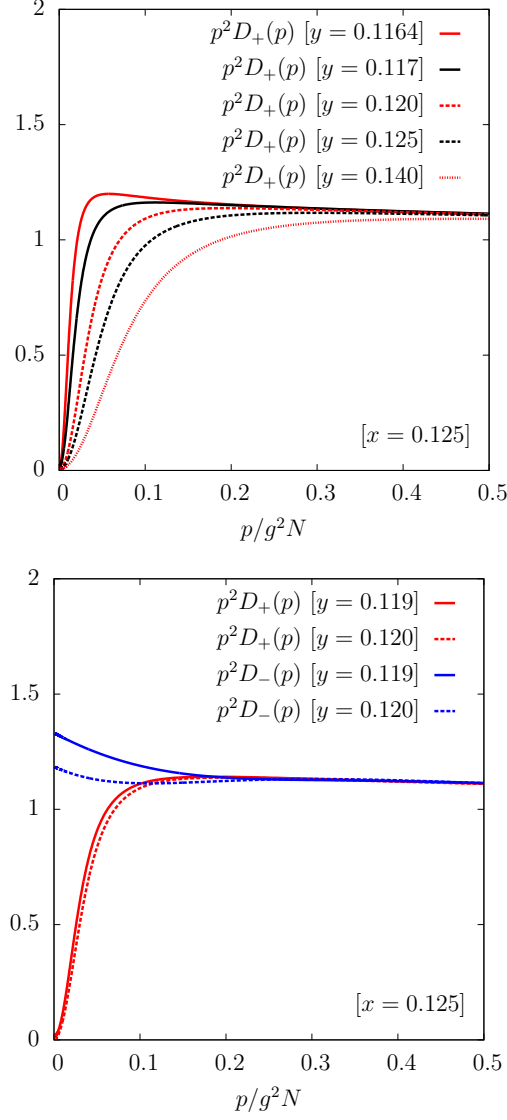


Figure 4–3: Evolution of the symmetric phase solution for Higgs two-point function with increasing y at fixed $x = 0.125$ (top panel), and coexistence of symmetric and Higgs phase solutions (bottom panel).

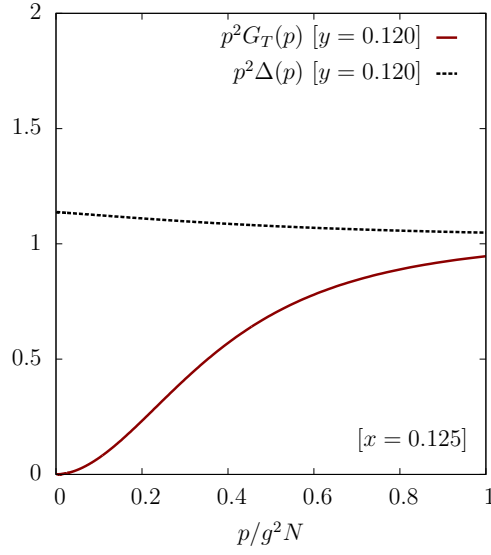


Figure 4-4: Transverse gauge field and ghost two-point functions., showing non-perturbative massive behaviour in G_T .

Though difficult to read from the figure, for reference this mass³ in Landau gauge is approximately $m_T^2 \approx g^4 N^2 / 8$.

Even though the most challenging and numerically intensive task that we face is the direct computation of the propagators G_T , Δ and D from the self-consistent equations (as in Chapter 3), these are no longer the objects that we are interested in. Rather, what we are really interested in is the scalar condensate as a function of x and y , which is an in principle gauge-invariant quantity derived from $D(p)$. The

³ By this we simply mean the non-zero value of $G_T^{-1}(0)$ and *not* the location of a pole. $G_T^{-1}(0)$ is gauge-dependent.

bare scalar condensate is defined as

$$\langle \phi^\dagger \phi \rangle = -\frac{1}{V} \frac{d}{dm^2(\mu)} \log \int D[\Phi] e^{-S}, \quad (4.51)$$

but since this expression is divergent it must be regularized with a counter-term. For a given solution $D(p)$ in either the Higgs or symmetric phase we will define the subtracted condensate as

$$\mathcal{D}_\pm(x, y) = \int \frac{d^3 q}{(2\pi)^3} \left[D_\pm(q) \Big|_{x,y} - \frac{1}{q^2} - \frac{g^2 C_R}{4(q^2 + g^4 N^2)^{3/2}} \right]. \quad (4.52)$$

Due to the divergence in Eq. (4.51), \mathcal{D} is dependent on the renormalization scale μ ,

$$\mathcal{D}(\mu) = \frac{3g^2}{32\pi^2} \log \frac{\mu}{\mu_0} \quad (4.53)$$

noting also the relative factor of 1/2 between Eq. (4.51) and Eq. (4.52). The value of the renormalized condensate is therefore dependent upon the subtraction procedure. However, the relative difference between the values at two points is neither subtraction scheme dependent or scale dependent; i.e. it is *observable*.

Turning now to the phase diagram Fig. 4–1, the location of the critical end point is denoted as (x^c, y^c) . For $x > x^c$ the theory undergoes a cross-over; while for $x < x^c$ there is a curve $y^c(x)$ along which a first order phase transition occurs (when $x > x^c$, $y^c(x)$ is still used to approximately indicate the middle-point of the cross-over). In the vicinity of the first order line, there is a region of metastability $y_-^c(x) < y^c(x) < y_+^c(x)$ (depicted in Fig. 4–1) where we would expect that $\Gamma[D]$ simultaneously admits two solutions. Returning to the dynamical system analogy, y_-^c and y_+^c can be thought

of as bifurcation points, leading the emergence and disappearance of attractors in $\partial\Gamma/\partial c_i$.

So, in terms of the condensate \mathcal{D} , for the majority of the phase diagram \mathcal{D} is a single valued function of y , except in the region of metastability where it splits into Higgs and symmetric phase branches. Plots of $\mathcal{D}(y)$ for $x = 0.125$ and $x = 0.150$ are shown in Fig. 4–5. In both cases we see a branch of symmetric phase solutions which terminates at a critical value of y . Since the symmetric phase is not observed below this value of y , we can identify this point with y_-^c . Additionally, at $x = 0.125$ there is a stable branch of Higgs phase solutions that does not exist above a different critical value of y . For now we will identify this point with y_+^c .

While we observe the appearance of a stable Higgs phase solution at $y_+^c \simeq 0.120$ on the $x = 0.125$ graph, at $x = 0.150$ this stable Higgs phase branch is not seen to exist at all. Therefore, there is a value of x between 0.125 and 0.150 at which Γ makes a change over between these two types of behaviours (said differently, at $x = 0.125$ there is an indication of metastability, whereas at $x = 0.150$ there is none). At a qualitative level, we will associate this value of x with the critical end point. The one peculiarity of Fig. 4–5 is that the stable D_- branch terminates very abruptly at the point y^{end} , and before the point y_-^c is reached. For values of $y < y^{\text{end}}$, the D_- attractor becomes unstable, i.e. there is a second bifurcation. Since this happens smoothly, we can approximately locate the resulting saddle extrema for a small range of y following this bifurcation, which as drawn in Fig. 4–5 is effectively the extension of the D_- branch to smaller values of y . When $y > y^{\text{end}}$ and consequentially, $y > y_+^c$, unstable D_- extrema are not observed. We will come back to this in Section 4.5.

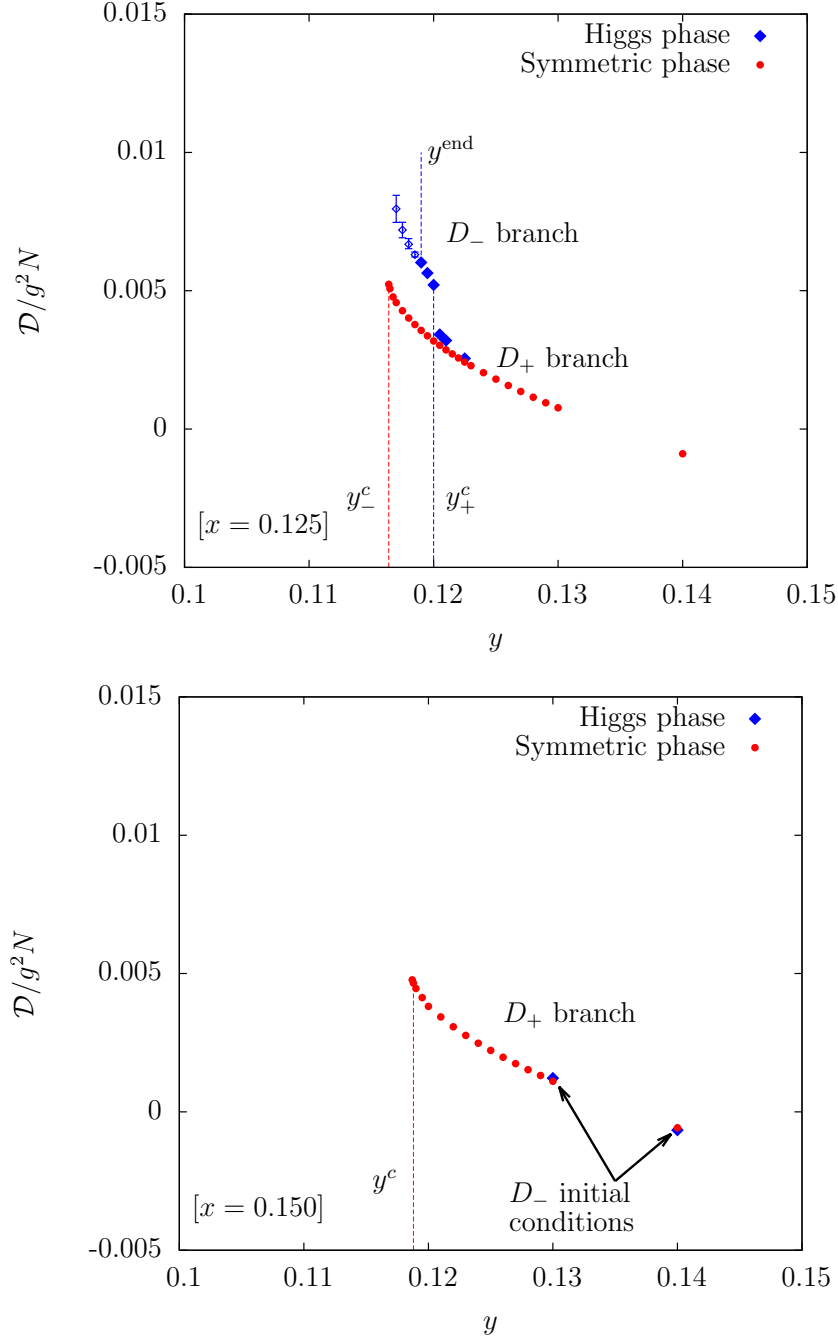


Figure 4-5: Evolution of \mathcal{D} with y at fixed x , showing the appearance of stable branch of Higgs phase solutions at $x = 0.125$. Unstable fixed points are drawn as silhouettes.

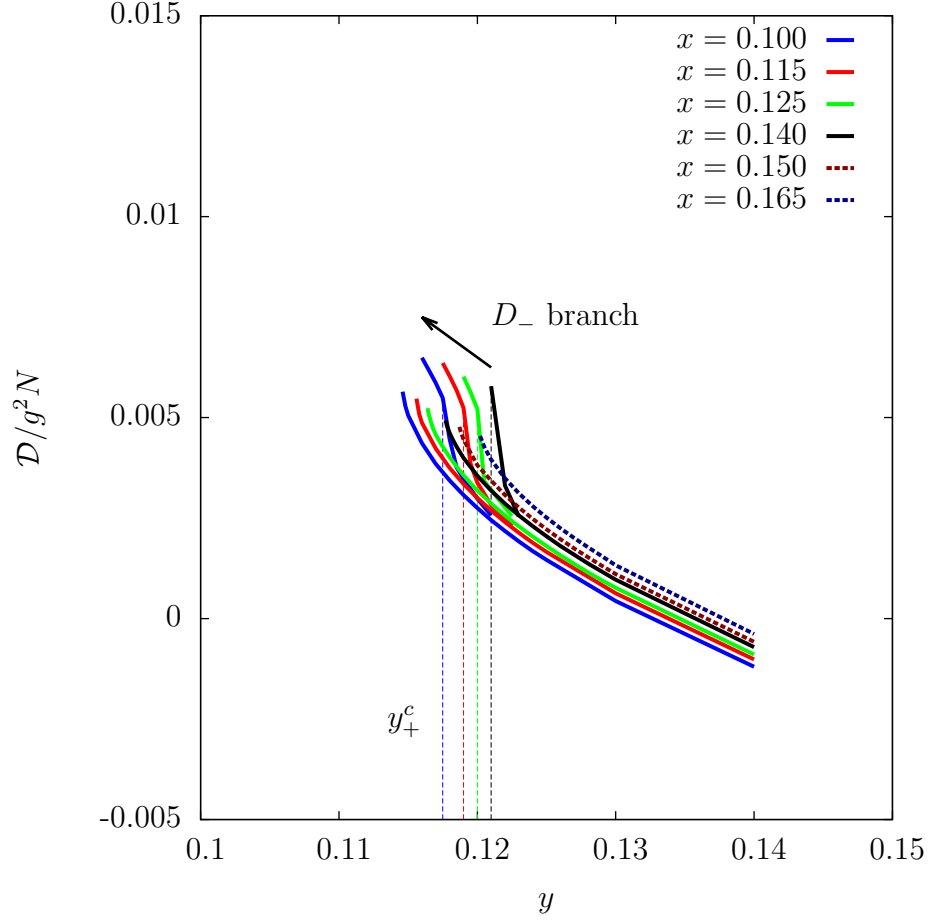


Figure 4-6: Evolution of the stable branches with increasing x . The D_- branch disappears by $x = 0.150$, indicating the absence of a region of metastability. From this we can infer $x^c \simeq 0.150$.

The curve in the top panel of Fig. 4–5 takes on a shape that resembles a hysteresis plot. This hysteretic behaviour is not observed when $x \geq 0.150$, and it is only marginally existent at $x = 0.140$. In Fig. 4–6 we show the evolution of this hysteretic behaviour for $x = 0.100, 0.115, 0.125, 0.140$ and 0.150 (noting that the corresponding 4D parameters are $m_{\text{H}} = 74, 79, 82, 86.5$ and 89.5 GeV). The stable D_- branch exhibits a tendency to increase in size with smaller x .

Returning to Fig. 4–5, there are values of y where the Higgs and symmetric solutions coincide. What we mean is that if we start with initial conditions which resemble the Higgs phase, we will over time evolve towards the symmetric phase solution (noting that some initial conditions will also diverge). At values of y where this occurs, we have evidence for the *non-existence* of a separate Higgs branch. However, to reach this conclusion, we must ensure that the gradient descent algorithm has converged, which in the vicinity of a critical end point, may in principle occur very slowly. The \mathcal{N} dependence of \mathcal{D}_- is shown in Fig. 4–7, with extrapolated values of $\mathcal{D}(\mathcal{N})$ obtained by fitting the curve

$$\mathcal{D}_{\text{fit}}(\mathcal{N}) = A \frac{e^{-\mathcal{N}/\tau_{\mathcal{N}}}}{\mathcal{N}^{\delta}} + c . \quad (4.54)$$

The graphs in Fig. 4–7 distinguish between the case where D_+ and D_- are unique and the case where there is in effect only a symmetric phase D_+ branch. Convergence time depends on the initial conditions and in general the rate is affected by the location (x, y) . In some cases, it occurs very quickly (as in the top panel for instance). However, when this is not the case, plots of $\mathcal{D}(\mathcal{N})$ can be used to obtain an estimate of the number of iterations needed to attain convergence. For instance,

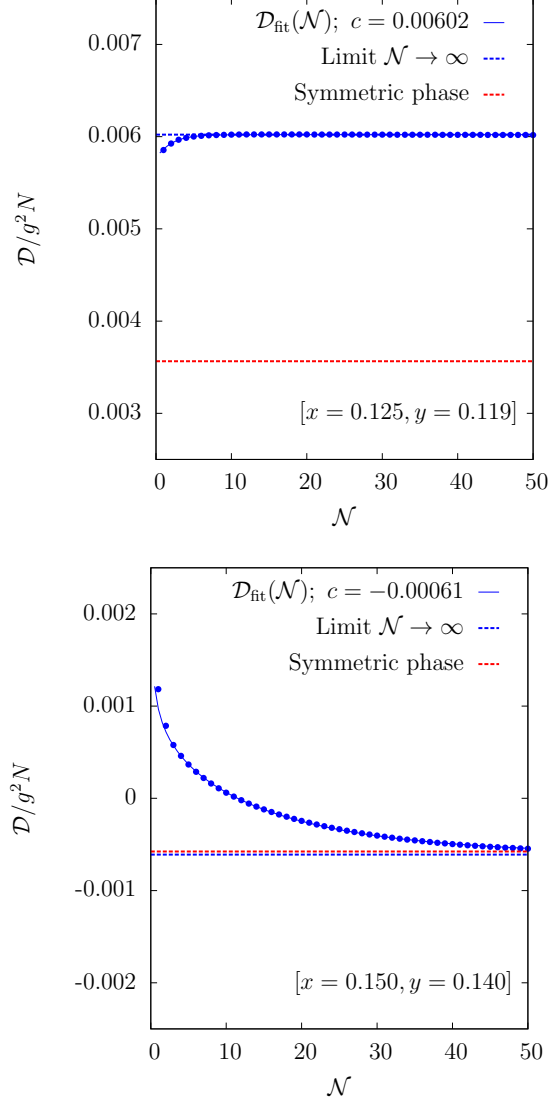


Figure 4–7: Convergence of \mathcal{D} (and hence G) at late times; we show both the cases where D_+ and D_- are distinct (top panel) and equivalent (bottom panel). At generic values of x and y , $\mathcal{D}(\mathcal{N})$ will resemble one of these two graphs (when it converges).

on the bottom panel, had we simply quoted the value at say $\mathcal{N} = 5$ iterations, we would have concluded that the D_+ and D_- solutions are distinct, when clearly this is not the case.

4.5 Discussion

4.5.1 Location of the critical end point

The solutions of the 2PI equations of motion can be used to infer the properties of the phase diagram in much the same manner as stationary points of the effective potential. In both cases, we can identify stable extrema with the ground states of the system. Then our location on the phase diagram can be read directly from the content of plots like Fig. 4–5. For instance, along a fixed x trajectory with $x < x^c$ and starting at $y > y_+^c$ we would be in the symmetric phase region of the phase diagram, Fig. 4–1. In 2PI terms, this region is expressed by the convergence of gradient descent to only a massive symmetric phase solution (or otherwise it may diverge). I.e. for this range of y there is only one phase, as the effective action only has one stable extremum.

Then as we cross y_+^c from above, we enter the region of metastability. In 2PI, a second stable extremum appears. One of these configurations would technically be metastable, which provides evidence that a first order phase transition occurs at this particular value of x .

The distinguishing characteristic that we observe between solutions with $x \lesssim 0.150$ and $x \gtrsim 0.150$ is that for larger values of x , the second branch of a stable Higgs phase solutions never appears. Thus there is a critical value of x^c where the 2PI effective action makes this transition. This is not a rigorous definition of the critical

end point, but it is the primary qualitative evidence that the 2PI solutions provide for the existence of critical end point in the underlying field theory, which appears to be $x^c \simeq 0.150$, (or $m_H^c \simeq 89.5$ GeV).

The results presented nevertheless raise a few questions about what is actually taking place, since what we have observed in the 2PI formalism is not entirely compatible with the layout of the phase diagram. To summarize the similarities and differences between the known phase diagram of $SU(N)$ Higgs theory and the observed properties of the 2PI effective action:

- For $x < x^c$ we anticipate a stable symmetric phase solution which exists for all values of $y > y_-^c$. This is precisely what we have observed.
- For $x < x^c$ we anticipate a Higgs phase solution which exists for all values of $y < y_+^c$. We have observed a stable Higgs phase solution which exists only for values in the range $y \in (y^{\text{end}}, y_+^c)$. The extremal point $\delta\Gamma/\delta D = 0$ corresponding to the Higgs phase appears to continue to lower values $y < y^{\text{end}}$, but it becomes a saddle-node. The point y^{end} does not have an analogue on Fig. 4-1.
- For $x > x^c$ we anticipate a stable symmetric phase branch that exists for all values of $y > y^c$ which smoothly deforms into a stable Higgs branch when $y < y^c$, characteristic of a cross-over. Indeed we observe the first half of this statement, but since Higgs phase solutions do not appear as stable attractors for $y < y^c$, it is difficult or impossible to smoothly resolve the cross-over. Higgs phase solutions (stable or unstable) are not observed when $y > y^c$.
- For $x \lesssim x^c$, we expect to see a very weak first order phase transition and a very small window of metastability, which is consistent with what we observe.

- For $x \rightarrow 0$ approaching the perturbative limit, we anticipate an increasingly larger region of metastability and a strongly first order phase transition. We find that the size of the metastability region and strength of the phase-transition is weakly dependent on x (at least down to about $x \approx 0.075$) and that the 2PI method would not converge to the perturbative limit when $x \ll 1/100$.

So in fact, many of the properties of the 2PI solutions are compatible with the non-perturbative region of the phase diagram in Fig. 4-1. The biggest issue though is that solutions which should in principle be stable actually behave as saddle points. The disagreement concerning convergence to the perturbative limit mentioned in the last point and the saddle-like behaviour can be explained as an artifact of the loop order of the truncation, as we will see.

4.5.2 Properties of the solutions

Throughout this chapter we have adopted the analogy that $\partial\Gamma/\partial c_i$ is a dynamical system with stable attractor(s) corresponding to the solutions. Then, initial conditions generically evolve along the trajectories shown in Fig. 4-8, and the appearance and disappearance of attractors coincide with the points y_-^c , y_+^c etc.

We can simplify this picture further by solely identifying solutions with their corresponding values of \mathcal{D} . Then, a flow through $\partial\Gamma/\partial c_i$ would be projected to a curve $\mathcal{D}(\mathcal{N})$. Looking back at the $x = 0.125$ graph in Fig. 4-5, in this idealized picture $\partial\Gamma/\partial c_i$ behaves qualitatively like the 1D system in Fig. 4-9; some initial conditions follow flows that converge to either of the attractors while others diverge. The appearance and disappearance of the stable D_- branch are shown as two back to back subcritical pitchfork bifurcations, and the D_+ branch ends in a saddle node

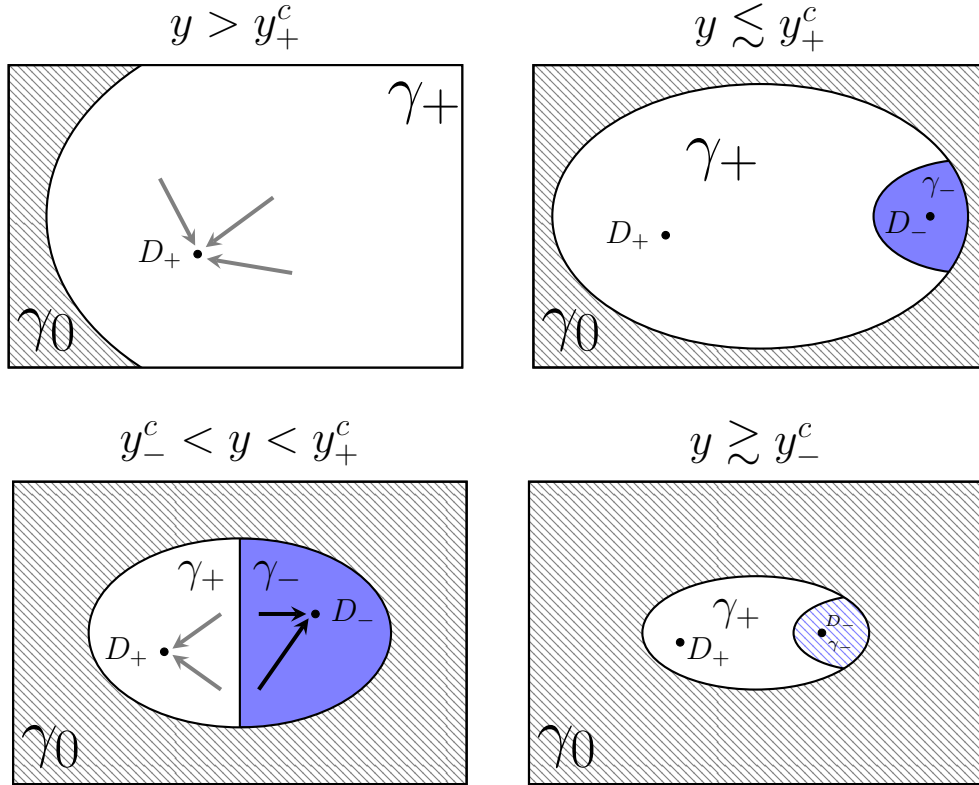


Figure 4–8: Illustration of the basins of attraction for several ranges of y when $x < x^c$. Initial conditions in either the blue or white regions will evolve towards either the symmetric or Higgs phase solution. As y is decreased, convergence is more difficult to attain; eventually, all initial conditions diverge.

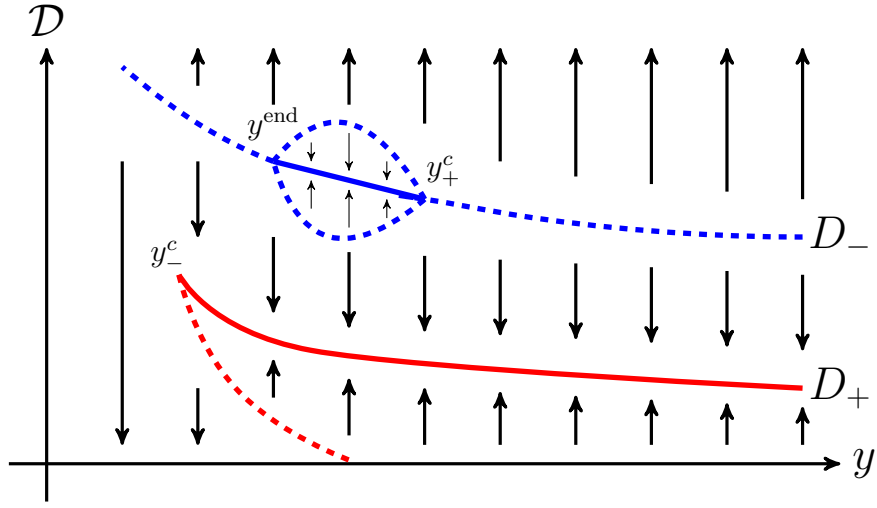


Figure 4–9: Stability of the D_+ and D_- branches in the first order region, mimicking the $x = 0.125$ graph in Fig. 4–5. Saddle nodes are drawn as dashed lines, while stable attractors are solid. The evolution of \mathcal{D} with \mathcal{N} behaves qualitatively like a 1D system, where bifurcations cause the stable D_- branch to appear and disappear. Solutions which evolve downward below the y axis can be interpreted as having formed a pole at finite p .

bifurcation. We should remark as a cautionary note that in the 1D picture all saddle nodes are necessarily stationary, which would imply that Higgs phase extrema exist for $y > y_+^c$, where in fact, Higgs phase saddle points are not observed at large y . In this regard, the visualization in Fig. 4–8 is more accurate.

The question remains, what exactly causes these solutions to appear, vanish or change stability? Looking back at the self-consistent equations, at large momenta the tree-level term is

$$\Gamma^{\text{tree}}[G_T, \Delta, D] = \text{Tr} \log D - DD^{(0)-1} + \frac{1}{2} \text{Tr} \log G_T - \frac{1}{2} G_T G_T^{(0)-1} - \text{Tr} \log \Delta + \Delta \Delta^{(0)-1}, \quad (4.55)$$

which is solved trivially by $D = D^{(0)}$ etc. However, due to the alternating signs of the ghost and gluon propagators, the solution even at tree-level actually corresponds to a saddle point (the gluonic contribution opens downwards, and ghost opens upwards). This situation remains unchanged upon the inclusion of higher loop diagrams.

In practice though, this does not present any additional challenges in solving the problem. By observing that the ghost and gluon propagators are very weakly dependent upon one another, this issue can be bypassed by iteratively adopting a procedure of fixing one propagator and then extremizing with respect to the other, and then vice versa. I.e., we fix G_T , then solve for the corresponding Δ . We update Δ , fix its value, and then solve for G_T , and so forth. This can be repeated until convergence is attained.

However, an actual challenge arises when we consider the contributions from the pure scalar diagrams (omitting group theoretic factors),

$$-\Gamma^{\text{scalar}}[D] = -\text{Tr} \log D + DD^{(0)-1} + \frac{\lambda}{2}DD - \frac{\lambda^2}{8}DDDD \quad (4.56)$$

where we have flipped the overall sign to ensure that the tree-level term opens upwards. With the three-loop term present, Γ is unbounded from above and below. To realize the latter, we simply have to make D arbitrarily large and positive as we approach $p = 0$. But, this is precisely what we expect to eventually happen as we evolve solutions deep into the Higgs phase.

As a remedy, if we assume that D has a relatively wide and small peak, then the negative contribution made by the three-loop diagram is doubly suppressed; it is suppressed by a relative power of x , and additionally, by what is essentially the height-to-width ratio of peak. The two-loop diagram enters with the “correct” overall positive sign and is not affected by the width of the peak, only its area. At small x and \mathcal{D} (which is proportional to the area under the peak) it can dominate. This explains why the observed stability of D_- only exists for a short range; as we move further into the Higgs phase, the action will be extremized by solutions with increasing \mathcal{D} . Eventually this dominance will switch over to the three-loop graph, resulting in saddle-like behaviour. This also accounts for a) why the stable branch becomes slightly longer as x decreases and b) why at larger values of x the three-loop diagram dominates for all y , driving the system to instability. This is essentially the change in behaviour that takes place at x^c .

We will return to this point when we compare the results to the perturbative limit. But for now, we will just comment that the main of consequence of a saddle-shaped Γ is the existence of a region of parameter space (x, y) where there are no stable solutions. For the D_- branch, these were the points $y < y^{\text{end}}$, and for the D_+ branch, $y < y_-^c$. This presents a computational challenge since there is actually a relatively large set of initial conditions in a basin of repulsion γ_0 where solutions will diverge under evolution of gradient descent, corresponding to the trajectory $-\Gamma \rightarrow -\infty$. Additionally, the basin of attraction of the Higgs phase solutions γ_- when it exists tends to be very small, further complicating matters.

4.5.3 Comparison with the lattice

Our original purpose in applying the 2PI formalism to $\text{SU}(N)$ Higgs theory was not specifically to determine the phase diagram (which is already known), but rather, to test the accuracy with which n PI resummation is able to make predictions about the non-perturbative sector of a non-abelian gauge theory. The n PI method relies on approximating the effective action by its truncation at a finite loop order, which results in a selective resummation to all orders of a certain class of topologies. In a gauge theory, this induces gauge-fixing dependence [115, 116], since at least perturbatively, one should include all diagrams at every loop order. This effect could potentially be very mild, but *a priori* it is not clear that accurate results can be obtained from this method anywhere on the phase diagram. The only way to test the reliability of the approximation is to directly compute gauge-invariant observable quantities.

An overview of many of the pertinent results from 3D lattice studies of SU(2) Higgs theory can be found in [78, 220]. In this section we will attempt a direct comparison between lattice and 2PI determined values of x^c , $y_-^c(x)$ and $y_+^c(x)$, citing the results in [77, 162, 163, 202]. In doing so it is favourable to adopt the physically motivated units of temperature T and 4D Higgs mass m_H . To convert our values of x and y to m_H and T , we will make use of the relations Eq. (4.7) and Eq. (4.8) (which we are adopting as a standard to keep the all conversions in this section uniform). We should remark though that not all authors use these exact conventions, and furthermore, the quantities appearing in Eq. (4.7) and Eq. (4.8) are not strictly speaking the physical pole mass of the Higgs field or physical temperature. However, in simply giving an outline of the 4D picture, the associated corrections are unimportant.

Starting with the location of the critical end point, the authors of [163] make the claim that it is bracketed by $70 \text{ GeV} < m_H^c < 95 \text{ GeV}$, and furthermore, they show evidence for $m_H^c \simeq 80 \text{ GeV}$. In terms of x , this would correspond to $0.90 < x^c < 0.17$, with $x^c \simeq 0.119$. Ref. [202] improves this claim to $x^c = 0.102(2)$ with $x^c < 0.107(2)$, corresponding to $m_H^c = 74.38 \text{ GeV}$, $m_H^c < 76.09 \text{ GeV}$. Finally, [77] offers the most precise determination of $x^c = 0.0983(15)$, or $m_H^c = 73.09$, by performing a careful extrapolation to the continuum. The temperature at the critical end point is $T^c \simeq 160 \text{ GeV}$.

The 2PI equations of motion (in Landau gauge) show *qualitative* evidence for a critical point at $0.14 < x^c < 0.15$ with the corresponding range $86.5 \text{ GeV} < m_H^c < 89.5 \text{ GeV}$. Thus, the accuracy of the 2PI determined value of m_H^c is comparable to

x	m_{H}	y_-^c	T_-^c
0.100	73.68 GeV	0.1146	184.38 GeV
0.115	78.75 GeV	0.1156	193.10 GeV
0.125	81.96 GeV	0.1164	198.39 GeV
0.140	86.54 GeV	0.1177	205.62 GeV
0.150	89.46 GeV	0.1187	211.49 GeV

Table 4–2: Temperatures associated with the end points of the curves in Fig. 4–6.

that in [163]. Furthermore, the agreement with [77, 202] is at about the 20% level in terms of the predicted value of m_{H}^c , or, in terms of x , the associated error is 0.05.

Temperatures assigned to the end points of the symmetric phase solutions in Fig. 4–6 are listed in Table. 4–2. Since the associated values of T_+^c are approximately 1 GeV greater than T_-^c (for the tabulated range of x), and furthermore $T_-^c < T^c < T_+^c$, values of T_-^c effectively give a prediction of the phase transition temperature T^c to within 1 GeV. As a comparison, in [162], the authors claim that with $m_{\text{H}} = 60$ GeV, $T^c = 138.38(5)$ GeV and $m_{\text{H}} = 70$ GeV, $T^c = 154.52(10)$ GeV. The corresponding values of y are $y^c = -0.00146$ and $y^c = -0.0153$. For larger values of $m_{\text{H}} = 120$ GeV, the lattice measured temperature rises to $T^c \simeq 213$ GeV, according to [163]. We can roughly extrapolate the trend in our data (Table 4–2) to higher m_{H} , and we can conclude that our results differ from the lattice data by about 20 – 50 GeV over that range in m_{H} . Similar to the 2PI determined values of m_{H}^c , this represents an accuracy of about 20% for predicted values of the phase transition temperature. In terms of y , the associated error is about 0.12.

We can also perform a rough comparison of the observed size of the metastability window. For $x = 0.125$ ($m_H = 81.96$ GeV), we have

$$(y_-^c, y^{\text{end}}, y_+^c) = (0.1164, 0.119, 0.120), \quad (4.57)$$

with corresponding temperatures

$$(T_-^c, T^{\text{end}}, T_+^c) = (198.39 \text{ GeV}, 198.98 \text{ GeV}, 199.21 \text{ GeV}). \quad (4.58)$$

So, from our perspective, at an m_H of about 6 GeV below the critical end point, the metastability window is approximately 0.8 GeV wide. By comparison, at the much smaller $x = 0.064$ ($m_H = 60$ GeV, roughly 12 GeV below the actual critical end point), the authors in [162] find $(T_-^c, T_+^c) = (137.37(12) \text{ GeV}, 138.72(15) \text{ GeV})$. Thus, qualitatively speaking, the sizes of the windows of metastability that we observe are comparable with those on the lattice over the non-perturbative range of x studied.

To summarize, the 2PI approach in Landau gauge shows evidence for critical end point that differs from the true critical point with an error of about $(\Delta x, \Delta y) \approx (0.05, 0.12)$. Correspondingly, the predicted values of x^c and T^c are accurate to within about 20%.

The discrepancy between the 2PI and lattice determined values of y^c is potentially an artifact of the gauge-fixing dependence. Recall that y^c in the 2PI formalism is roughly determined by the value of y where $\Pi_\phi(0) - m^2$ changes sign. Moreover, $\Pi_\phi(p)$ is constructed out of diagrams that contain gauge field lines, which develop a fairly large gauge-dependent mass m_T . On dimensional grounds, for the values of m_T in the range we observe, $\Pi_\phi(0) \sim g^2 m_T$. This mass, as we have shown in the

previous chapter, is dependent on the gauge parameter ξ , and hence the gauge-fixing [221]. Since changing the mass of the transverse gluon propagator effectively shifts the curve $\Pi_\phi(p)$, the 2PI determined values of y^c appear to carry the burden of the gauge-fixing dependence inherent to the selective resummation. The dependence on ξ via m_T is quantitatively a mild effect, but then, any diagram that contains gauge field lines will be in general *explicitly* dependent on the gauge parameter (recall that the one-loop self-energy is proportional to $\xi^2 + 2\xi + 11$). Since diagrams enter with prefactors that are polynomials in the gauge parameter, this in general is not a small effect. We will argue in the next section that the relevant Higgs diagrams which affect x^c do not contain any gauge field lines, and consequentially it appears the corresponding dependence of x^c should be very small, if not negligible altogether.

4.5.4 Comparison with perturbation theory

Going back now to Eq. (4.56), the three-loop diagram enters with a relative minus sign so that it induces saddle-like behaviour in the effective action. However, since it enters with the prefactor λ^2 , at very small x it becomes highly suppressed. It would appear, then, that at small x solutions of the 2PI formalism should approach the perturbative limit.

To see what happens perturbatively in Landau gauge, we can compute the one-loop effective potential. For SU(2), parametrizing the VEV as

$$\phi = \frac{1}{\sqrt{2}} \begin{pmatrix} \phi_1 + i\phi_2 \\ \phi_3 + g\bar{\phi} + i\phi_4 \end{pmatrix}, \quad (4.59)$$

the effective potential reads

$$\begin{aligned} \frac{\Gamma[\bar{\phi}]}{g^6} &= \frac{1}{2}y\bar{\phi}^2 + \frac{1}{4}x\bar{\phi}^4 \\ &- \frac{1}{12\pi} \left[6 \left(\frac{m_T^2}{g^4} + \frac{\bar{\phi}^2}{4} \right)^{3/2} + 3(y + x\bar{\phi}^2)^{3/2} + (y + 3x\bar{\phi}^2)^{3/2} \right]. \end{aligned} \quad (4.60)$$

We have explicitly included a mass term m_T^2 in the gauge field contribution; we will come back to this, but for now in the perturbative treatment we assume that it is zero. As $x \rightarrow 0$, Eq. (4.60) predicts that at small x

$$y_-^c \rightarrow 0 \quad (4.61)$$

$$y_+^c \rightarrow \frac{9}{1024\pi^2 x} \quad (4.62)$$

$$\bar{\phi}_0(y_+^c) \rightarrow \frac{3}{32\pi x}. \quad (4.63)$$

Looking back at Fig. 4–6, the first statement Eq. (4.61) is not quite what we observe. Rather, in 2PI we have that y_-^c approaches an $\mathcal{O}(0.1)$ constant as $x \rightarrow 0$. This disagreement can possibly be attributed to the relatively large non-perturbative mass $m_T^2 \sim g^4 N^2/8$ present in the gauge field propagator. This mass is generated independently of the scalar diagrams; hence the limit $x \rightarrow 0$ in the 2PI formalism does not directly coincide with the limit $x \rightarrow 0$ in Eq. (4.60). Perturbatively speaking, gauge fields are massless at tree-level in the symmetric phase. On dimensional grounds,

the one-loop gluon tadpole diagram makes a contribution of order⁴

$$\text{diagram} \sim + \frac{1}{2} g^2 2C_F (D-1) \frac{\sqrt{m_T^2}}{4\pi} \quad (4.64)$$

which enters with a positive overall sign into the Higgs self-energy and is non-zero even when $x = 0$. Additionally, there are positive contributions coming from other diagrams. Now, recalling that the end of the symmetric phase coincides approximately with the value of y where $\Pi_\phi(0) - m^2$ changes sign, then we would anticipate that the symmetric phase has to come to an end at positive y .

Following the suggestion in [222], we can attempt to quantify the non-perturbative contributions due to the gauge field “mass” by explicitly including m_T^2 in the computation of Eq. (4.60) (we can think of this as including a three-loop term). It should be noted that this procedure does not actually offer a correct description of the non-perturbative physics, as the induced linear term in $\Gamma[\bar{\phi}]$ enters with the wrong sign as determined by the lattice. That being said, with $m_T^2 \sim g^4 N^2 / 8$ and $x \rightarrow 0$, one then finds that y_-^c approaches a constant, specifically,

$$y_-^c \rightarrow \frac{3}{8\pi\sqrt{2}} \quad (4.65)$$

⁴ Corresponding to the “zeroth” order approximation where the gauge field self-energy is treated as a constant, i.e. $G_{\mu\nu} \approx \frac{1}{p^2 + m_T^2} \mathbf{T}_{\mu\nu}$. Of course the full calculation would involve a momentum dependent self-energy (which is linear-in- p); however, it is easy to verify that this approximation at least serves to correctly estimate the order of magnitude of the diagram, given the values of m_T considered.

which is exactly equal to the diagram Eq. (4.64) (computed in perturbation theory), and comparable in magnitude to what we observe. In doing this, what we have shown is that perturbation theory can be “modified” to match the 2PI result, and that we can easily account for the discrepancy with Eq. (4.61). Similar to what we found in the previous section, this is a place where the gauge-dependence of m_T as well as the diagrams themselves will affect the final results.

As for Eq. (4.62), even at the relatively small $x = 1/100$, the window of metastability is still not that large numerically as it extends from zero to about $y_+^c \simeq 0.1$. But eventually for $x \ll 1/100$, we expect the window of metastability to become divergently large. The question now is, *can we approach this limit using the 2PI formalism, where solutions will be characterized by relatively large values of \mathcal{D} ?* The answer is no, and in this case the disagreement is not due to the dynamically generated gauge field mass, but rather, this limitation is due to the 2PI formalism’s inability to treat the broken phase in the small x limit.

4.5.5 Effectiveness of the 2PI formalism in the Higgs phase

Consider, for a moment, that the effective action had been truncated at two-loops, and that we are at small enough values of x where Eq. (4.62) and Eq. (4.63) should hold. Then, we expect that $\bar{\phi}_0 \sim 1/x$, which means that \mathcal{D} would need to become quite large. In this case, the peak in $D(p)$ would also become quite narrow (a condition that is enforced diagrammatically by the one-loop gluon self-energy diagram with a Higgs in the loop). So we can approximately write

$$D(p) \approx g^2 \nu (2\pi)^3 \delta^3(p) + \frac{1}{p^2 + m^2 - \Pi_\phi(p)} \quad (4.66)$$

where $\nu \sim 1/x^2$. At the one-loop level, we see that this would actually be necessary to satisfy the self-consistent equation at zero momentum,

$$\frac{1}{g^4} \left(\frac{1}{2} \text{[gluon tadpole]} + \text{[bubble]} \right) \sim \sqrt{\nu} - x\nu \simeq -y \quad (4.67)$$

since the contribution from the gluon tadpole $\sqrt{g^4\nu + m_T^2} \approx g^2\sqrt{\nu}$ (roughly) now also becomes large in this limit. These diagrams enter with equal and opposite sign, and their approximate cancellation is only achieved with $\nu \sim 1/x^2$. But now we have revealed a problem with the n PI hierarchy in the broken phase; with a very large and narrow peak in $G(p)$, the three-loop diagram cannot be considered suppressed,

$$\frac{1}{g^4} \text{[three-loop]} \sim x^2\nu^3 g^6 (2\pi)^3 \delta^3(p) \quad (4.68)$$

as it yields a divergent contribution at zero momentum! But then if this is case, we should also consider the next loop order

$$\frac{1}{g^4} \text{[four-loop]} \sim -x^3\nu^5 \left(g^6 (2\pi)^3 \delta^3(p) \right)^2 \quad (4.69)$$

which is even *more* divergent. So, at zero momentum, we obtain an alternating series of the form

$$\Pi_\phi(p) \approx -g^4 x\nu \left(c_1 - c_2 x\nu^2 g^6 (2\pi)^3 \delta^3(p) + c_3 \left(x\nu^2 g^6 (2\pi)^3 \delta^3(p) \right)^2 - \dots \right) \quad (4.70)$$

indicating that we should actually be resumming the whole series of 2PI diagrams (as well as considering the higher loop corrections to the four-vertex and so forth). The situation is very analogous to what takes place with the 1PI formalism in the broken phase. Recall that the 1PI effective action is a generating function for *one-particle-irreducible* vertices V_n , so that

$$\Gamma[\bar{\phi}] = V_0 + \frac{1}{2}\bar{\phi}^2 V_2 + \frac{1}{3!}\bar{\phi}^3 V_3 + \frac{1}{4!}\bar{\phi}^4 V_4 + \dots \quad (4.71)$$

The vertex functions are then obtained by differentiation

$$\left. \frac{\delta^n \Gamma[\bar{\phi}]}{\delta \bar{\phi}^n} \right|_{\bar{\phi}=\bar{\phi}_0} = V_n^{\bar{\phi}_0}(p_1^2, p_2^2, \dots, p_n^2). \quad (4.72)$$

When $\bar{\phi}_0 \neq 0$ even the one-loop correction to $V_n^{\bar{\phi}_0}$ in effect receives one-loop contributions from all orders of the sequence V_n ! Due to the additional vertices, these higher order terms are naturally suppressed by additional powers of coupling. Except, in a 3D theory the coupling constants carry dimension so in actuality we would need to have suppression by a dimensionless ratio like x . But then higher order terms are in turn enhanced by additional powers of $\bar{\phi}_0$, which can be large (which is precisely what happens in the $x \rightarrow 0$ limit). I.e., *perturbative* corrections to the n -point functions in the broken phase can be *non-perturbative* in terms of the n -point functions of the symmetric phase.

These arguments actually suggest that the 2PI formalism as presented is not very suitable for studying the broken phase. However, we should recall what we originally set out to do. We wanted to study a method that could reveal non-perturbative features of the phase diagram (for instance, the critical end point), and

it just so happens to be that this comes at the cost of being able to describe the region of parameter-space where perturbation theory is valid. The problems with the n PI hierarchy in the broken phase came about with the assumption that the scalar two-point functions would take on the form Eq. (4.66). The fact that this creates a problem should really be interpreted that the 2PI equations of motion favour solutions with a wide peak; where the width is determined self-consistently. Then, the 2PI formalism is limited to range of x and y where this is indeed the case in the underlying field theory.

4.5.6 Comparison between Landau and Feynman gauges

Up to now, we have argued diagrammatically that critical values of y are expected to exhibit dependence on the gauge parameter ξ . However, since it is difficult to quantify this effect without an explicit computation, we will now briefly present a comparison between Landau and Feynman gauges. The results in Feynman gauge are best summarized by a $\xi = 1$ analogue of Fig. 4–6, shown in Fig. 4–10.

In setting $\xi = 1$ and resolving the equations of motion (following the usual procedure), we observe that qualitatively very little has changed. Feynman gauge solutions exhibit similar features to those in Landau gauge, and once again we observe a disappearance of a stable Higgs branch somewhere between $x = 0.125$ and $x = 0.150$. This is consistent with the observation that dependence on x enters primarily through diagrams without gauge field lines. The biggest change though is the observed shift in the critical range of y , which as we have previously argued, is determined by diagrams *with* gauge field lines. In Landau gauge, critical values of y were observed in the vicinity of $y^c \sim 0.120$ over the range of x considered. Now,

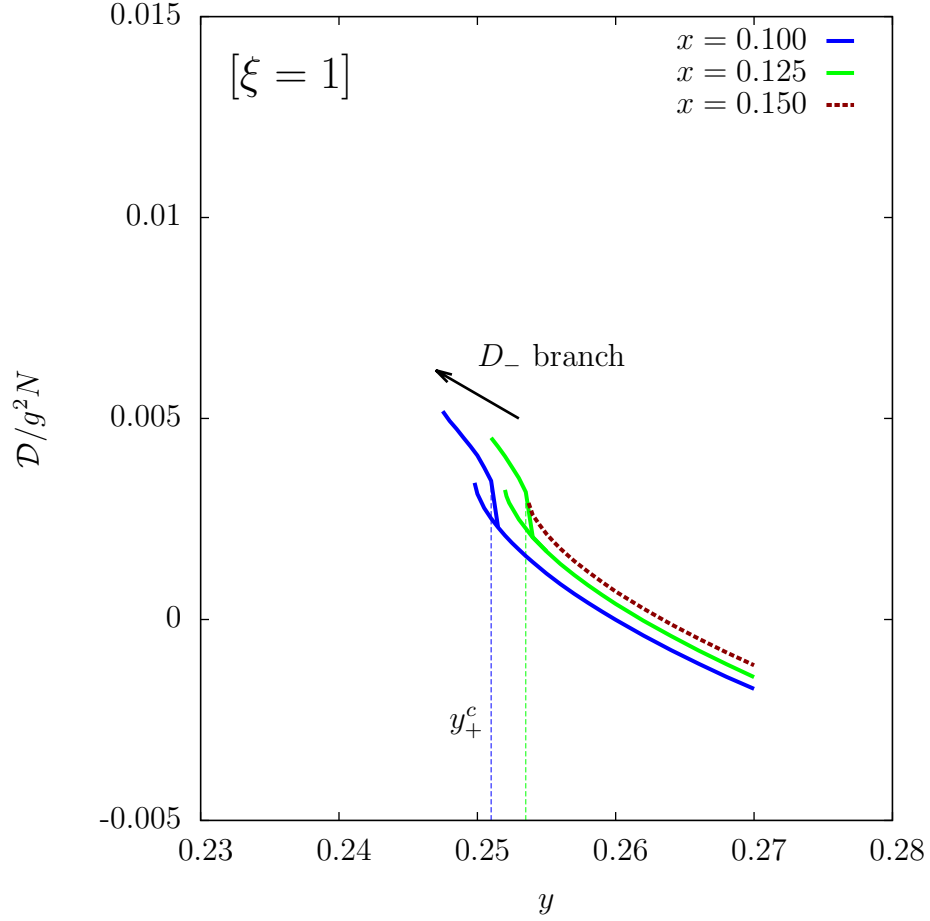


Figure 4–10: Feynman gauge analogue of Fig 4–6, showing the evolution of the D_+ and D_- branches with x . As in Landau gauge, the D_- branch disappears by $x = 0.150$, but the critical range of y has shifted.

this range occurs in the vicinity of $y^c \sim 0.250$! To understand the origin of this shift, let us reconsider the one-loop gluon tadpole, except now in Feynman gauge. Schematically,

$$\text{tadpole diagram} \sim +\frac{1}{2}g^2 2C_F \left[(D-1) \frac{\sqrt{m_T^2}}{4\pi} + \xi \frac{\sqrt{m_L^2}}{4\pi} \right] \quad (4.73)$$

treating the longitudinal self-energy approximately as a mass m_L . Given the form of $\Pi_L(p)$ as determined in Chapter 3, the presence of a massive longitudinal propagator clearly increases the already positive contribution made by this particular diagram.

4.6 Concluding remarks for Chapter 4

In this chapter we have directly solved the three-loop 2PI effective action and obtained resummed correlators which correspond to both the symmetric and Higgs phases of the theory. We found that these solutions coexist over a region of the phase diagram, indicative of metastability and a first order phase transition. Subsequently, we have also observed that there is a point x where the metastability ceases to be observed, which we identified with the critical end point of the theory, x^c . Based on the solutions in both Landau and Feynman gauges and general diagrammatic arguments, we were able to demonstrate that observed critical values of y are dependent on the gauge-fixing.

Concerning the numerical accuracy of the predictions made in Landau gauge, the location of the critical end point we inferred agrees with the lattice reported value to an accuracy of about $(\Delta x, \Delta y) \simeq (0.05, 0.12)$. In terms of the physical parameters

of the 4D theory the accuracy is at about the 20% level. The resolution of x_c does not change in Feynman gauge.

Since the resulting 2PI equations of motion involve an infinite resummation, the results are inherently non-perturbative. Even though in writing the effective action we had to fix a gauge, we were not restricted by construction to the perturbative spectrum of R_ξ gauge, and furthermore, we were able to sidestep ambiguities concerning the non-perturbative definition of a VEV. What we observed is that the results from the 2PI formalism become increasingly reasonable as we approach non-perturbative values of x . However, the whole set-up comes at a cost to our ability to perform perturbation theory, which requires an expansion of the scalar field about its tree-level minimum. Related to this limitation, and due to the saddle-like extrema which we have observed in the effective action, it proves to be impossible to study the broken phase whenever the scalar condensate is large.

CHAPTER 5

Conclusions

Following the application of the 3PI formalism to Yang-Mills theory and a subsequent comparison of the results to gauge-fixed lattice studies, we applied the 2PI formalism to $SU(2)$ Higgs theory in three spacetime dimensions. The goal throughout was to learn about the usefulness and applicability of the n PI formalism to the study of non-abelian gauge theories in 3 and potentially 4 dimensions. In this matter, $SU(2)$ fundamental Higgs theory provides an excellent testing ground since its properties have been studied extensively on the lattice. Furthermore, as a 3D theory it is super-renormalizable so its structure in the UV is relatively easy to describe using perturbation theory. In effect we could direct the focus towards non-perturbative IR physics.

Since the n PI formalism provides a self-consistent resummation scheme it could be particularly relevant to the study of hot 4D gauge theories. But its practical application requires a truncation at a finite loop order and thus its results can only ever be approximate. Consequentially, a truncated n PI effective action also suffers from ambiguities related to gauge-fixing, introduced directly by this truncation (as one effectively removes certain diagrams from the perturbative expansion). The associated limitations, and whether or not this renders the method unreliable in practice are

difficult to predict theoretically. The best way to shed light on this matter is therefore to use the formalism to directly compute gauge-invariant observables, which we have attempted.

Concerning the applicability of the n PI formalism to a gauge theory, the most promising finding is the apparent qualitative evidence for a critical end point (x^c, y^c) on the phase diagram of $SU(N)$ Higgs theory, located within a close vicinity of its measured value. This is a particularly interesting finding because the critical end point *cannot* be resolved using perturbation theory. Therefore, this would indicate that the 2PI and in general n PI approaches, which are based on Feynman diagrams and require working in a fixed gauge, are able to identify *some* non-perturbative phenomena. Unfortunately, based on the properties of the solutions, it is not clear how the prediction of x^c can be made mathematically robust through a study of the two-point functions alone. This presents one ambiguity.

Furthermore, critical values of y^c which are associated with the critical temperature in the 4D theory are inherently dependent on the gauge parameter (in covariant gauge) through the gauge field propagator and self-energy. The gluon self-energy and other diagrams involving gauge field lines are known from Chapter 3 to be (strongly) gauge-fixing dependent. Due to the $\mathcal{O}(0.1g^4N^2)$ *non-perturbative* ξ dependent correction to the transverse and longitudinal self-energies obtained via the resummation, observed values of y^c are *positive* and consistently larger than their lattice measured values in a three-loop truncation of the effective action. Varying the gauge parameter has a direct effect on y^c which presents another ambiguity concerning a measured observable.

The study of $SU(N)$ Higgs theory has therefore revealed several limitations to the n PI method in the context of a non-abelian gauge theory. In addition to the described ambiguities in physical observables, the application of the formalism is *difficult* numerically, especially if one wishes to consider higher-loop truncations or higher n -particle-irreducibility. If qualitative predictions can be made at best, then it may be hard to justify the numerical expense. However, this work does not preclude the possibility that further refinements may be possible with the goal of obtaining quantitatively accurate answers to non-perturbative and gauge-invariant questions. This matter is left open for a future investigation.

Finally, having worked with the 3D theory, it appears that the extension to 4 or 3+1 dimensions would be extremely challenging. The problem in 4D is that one is simultaneously solving non-perturbative infrared physics and (perturbative) ultraviolet physics. The effective action is extremely sensitive to the ultraviolet form of the propagators and vertices; a procedure along the lines of what has been done here encounters quadratic UV divergences at every loop order when evaluating self-energies, and quartic divergences when varying the propagators in a way which changes their UV behaviour – at every loop order. It would be much harder to “cover up” gauge non-invariance in 4D because divergently large gauge boson masses would arise at every loop order, whereas in 3D we only encounter them at one-loop (where they vanish in dimensional regularization); at two-loops there are $1/\epsilon$ ’s but they all cancel. Thus it is not clear what additional techniques would have to be developed to successfully extend the procedure that has been described here to 4 dimensions. This is also left open for future investigation.

Appendix A

Group theory for $SU(N)$

This appendix gives an overview of the group theoretic relations required for a three-loop computation of vacuum diagrams in a non-abelian gauge theory coupled to scalars (many additional identities and formulas for group invariants can be found in [223]). To start, an irreducible and in general complex representation R of $SU(N)$ consists of $N^2 - 1$ traceless $d_R \times d_R$ Hermitian generators T_R^a . These generators form a Lie algebra

$$[T_R^a, T_R^b] = if^{abc}T_R^c \quad (1)$$

$$[[T_R^a, T_R^b], T_R^c] + [[T_R^b, T_R^c], T_R^a] + [[T_R^c, T_R^a], T_R^b] = 0. \quad (2)$$

The structure constants f_{abc} are chosen to be completely anti-symmetric; they define the $d_A \times d_A$ generators of the adjoint representation $F^a = T_A^a$ via

$$F_{bc}^a = -if^{abc}. \quad (3)$$

Since $(F^a)^* = -F^a$, the adjoint representation is real. The Dynkin index of a representation is denoted by T_R ,¹ and it specifies a normalization of the generators

$$\text{Tr } T_R^a T_R^b = T_R \delta^{ab}. \quad (4)$$

¹ The notation T_R for the Dynkin index and T_R^a for the generators may lead to confusion; generator matrices are specifically indexed by a superscript.

As a convention, the fundamental representation is chosen so that $T_F = 1/2$. Furthermore the quadratic Casimir is defined as

$$T_R^s T_R^s = C_R \mathbf{1}_{d_R}. \quad (5)$$

From these two expressions, we obtain the well-known relationship

$$T_R d_A = C_R d_R. \quad (6)$$

The totally symmetric anomaly coefficients d^{abc} of the fundamental representation are defined as

$$d^{abc} = \frac{1}{T_F} \text{Tr } T_F^a \{T_F^b, T_F^c\} \quad (7)$$

so that in general

$$A_R d^{abc} = \frac{1}{T_R} \text{Tr } T_R^a \{T_R^b, T_R^c\}. \quad (8)$$

The anomaly coefficients of representation R can be related to those of the fundamental representation with

$$A_R = \text{Tr} \{ (T_R^a)^3 \} / \text{Tr} \{ (T_F^a)^3 \} \quad (9)$$

for any a where the trace is non-zero; $A_F = 1$ by definition. By specifying the anomaly coefficients we can write down a general formula for the product of two generators

$$T_R^a T_R^b = \frac{T_R}{d_R} \delta^{ab} \mathbf{1}_{d_R} + \frac{1}{2} (i f^{abc} + A_R d^{abc}) T_R^c + \frac{1}{2} M_R^{ab}. \quad (10)$$

In the fundamental representation, $M_F^{ab} = 0$, and in general M_R^{ab} is traceless, Hermitian, symmetric in a and b and satisfies $\text{Tr} \{ T^a M_R^{bc} \} = 0$ [224]. Finally, a very

usefully identity for the product of three generators with index s summed over is

$$T^s T^a T^s = \left(C_R - \frac{1}{2} C_A \right) T^a. \quad (11)$$

Appendix B

Euclidean space Feynman rules for Yang-Mills and $SU(N)$ Higgs theory

The Feynman rules for covariant gauge perturbative calculations in $SU(N)$ Higgs theory are derived from the Lagrangian

$$\mathcal{L} = \frac{1}{2} \text{Tr} F_{\mu\nu} F^{\mu\nu} + \frac{1}{2\xi} (\partial^\mu A_\mu^a)^2 + \partial_\mu \bar{c}^a \partial^\mu c^a - g f_{abc} \partial^\mu \bar{c}^a c^b A_\mu^c \quad (12)$$

$$+ (D^\mu \phi)^\dagger (D_\mu \phi) + (m^2 + \delta m^2) \phi^\dagger \phi + \frac{\lambda}{2} (\phi^\dagger \phi)^2 \quad (13)$$

Gauge field, scalar and ghost propagators are denoted by the symbols G , D and Δ throughout Chapters 3 and 4. In Euclidean space at tree-level these are

$$G_{\mu\nu}^{(0)}(p) = \frac{1}{p^2} \left(\mathbf{T}_{\mu\nu}(p) + \xi \mathbf{L}_{\mu\nu}(p) \right) \quad (14)$$

$$D^{(0)}(p) = \frac{1}{p^2 + m^2} \quad (15)$$

$$\Delta^{(0)}(p) = \frac{1}{p^2} \quad (16)$$

where the gauge field propagator is specified by the transverse and longitudinal projectors

$$\mathbf{T}_{\mu\nu}(p) = g_{\mu\nu} - \frac{p_\mu p_\nu}{p^2} \quad (17)$$

$$\mathbf{L}_{\mu\nu}(p) = \frac{p_\mu p_\nu}{p^2}. \quad (18)$$

With all momenta assumed to be flowing outwards, the bare Yang-Mills vertices are

$$gV_{\mu_1\mu_2\mu_3}^{(0)a_1a_2a_3} = \frac{g}{3!}F^{a_1a_2a_3}((p_2 - p_3)_{\mu_1}g_{\mu_2\mu_3} + (p_3 - p_1)_{\mu_2}g_{\mu_1\mu_3} + (p_1 - p_2)_{\mu_3}g_{\mu_1\mu_2}) \quad (19)$$

$$g\mathbb{V}_{\mu_3}^{(0)a_1a_2a_3} = gF^{a_1a_2a_3}p_{1\mu_3} \quad (20)$$

$$\begin{aligned} g^2V_{\mu_1\mu_2\mu_3\mu_4}^{(0)a_1a_2a_3a_4} &= \frac{g^2}{4!}(F^{a_1a_2s}F^{a_3a_4s}(g_{\mu_1\mu_3}g_{\mu_2\mu_4} - g_{\mu_1\mu_4}g_{\mu_2\mu_3}) \\ &\quad + F^{a_1a_3s}F^{a_4a_2s}(g_{\mu_1\mu_4}g_{\mu_2\mu_3} - g_{\mu_1\mu_2}g_{\mu_3\mu_4}) \\ &\quad + F^{a_1a_4s}F^{a_2a_3s}(g_{\mu_1\mu_2}g_{\mu_3\mu_4} - g_{\mu_1\mu_3}g_{\mu_2\mu_4})). \end{aligned} \quad (21)$$

where (a_1, p_1) are the colour indices and momentum of the outgoing ghost in \mathbb{V} . The presence of a complex scalar results in the following additional vertices,

$$g\mathcal{V}_{\mu_3}^{(0)a_1a_2a_3} = gT_{a_1a_2}^{a_3}(p_1 - p_2)_{\mu_3} \quad (22)$$

$$g^2\mathcal{V}_{\mu_3\mu_4}^{(0)a_1a_2a_3a_4} = -\frac{g^2}{2!}T_{a_1s}^{\{a_3}T_{sa_2}^{a_4\}}g_{\mu_3\mu_4} \quad (23)$$

$$\lambda\mathcal{V}^{(0)a_1a_2a_3a_4} = -\frac{\lambda}{2!2!}(\delta_{a_1a_2}\delta_{a_3a_4} + \delta_{a_1a_4}\delta_{a_2a_3}). \quad (24)$$

where the outgoing scalar(s) are indexed by (a_1, p_1) (Eq. (22) and Eq. (23)) and a_1, a_3 (Eq. (24)).

Appendix C

Self-energies computed in dimensional regularization

In regularizing the 2PI effective action, one makes use of one and two-loop self-energy corrections computed in perturbation theory. In pure Yang-Mills, all one and two-loop integrals are massless from the onset. However, the inclusion of a Higgs field now in principle adds massive propagators to many of the diagrams. But, since we really only need to know the UV limit of these diagrams, it actually suffices to compute them with a massless scalar field.

In the following section, though some results are valid for arbitrary D , ϵ should be treated as a small parameter; i.e. it is assumed that we are working at or near 3 dimensions, $D = D_0 + 2\epsilon$, with $D_0 = 3$. Finally, since the Higgs mass renormalizes at the two-loop level in three dimensions, it is useful to define the $\overline{\text{MS}}$ scale $\bar{\mu}^2 = \mu^2 e^\gamma / 4\pi$. The master one-loop topology is

$$\text{Diagram: A circle with an incoming line on the left labeled } p \text{ and an outgoing line on the right. The top arc is labeled } p_1 \text{ and the bottom arc is labeled } p_2. \text{ } = J_1^{(\text{D})}(n_1, m_1; n_2, m_2) \quad \left\{ \begin{array}{l} p_1 = q \\ p_2 = q - p \end{array} \right. \quad (25)$$

with

$$J_1^{(\text{D})}(n_1, m_1; n_2, m_2) = \left(\frac{1}{\bar{\mu}^2}\right)^{\frac{\text{D}-\text{D}_0}{2}} \int \frac{d^{\text{D}}q}{(2\pi)^{\text{D}}} \frac{1}{(q^2 + m_1^2)^{n_1} ((q-p)^2 + m_2^2)^{n_2}}. \quad (26)$$

One-loop gluon self-energy

The presence of a scalar field adds two additional diagrams to the one-loop gluon self-energy relative to the the pure Yang-Mills expression,

$$\begin{aligned}
 \Pi_{m^2;\mu\nu}^{(1,\epsilon)} = & \frac{1}{2} \text{ (gluon loop) } + \frac{1}{2} \text{ (ghost loop) } - \text{ (Higgs loop) } \\
 & + \text{ (scalar loop) } + \text{ (fermion loop) } .
 \end{aligned} \tag{27}$$

The result is strictly transverse; we will separate the Yang-Mills and Higgs contributions as follows,

$$\Pi_{m^2;\mu\nu}^{(1,0)} = g^2 p \left(\pi_{\text{YM}}^{(1,0)} + \pi_{m^2}^{(1,0)} \right) \mathbf{T}_{\mu\nu} \tag{28}$$

$$\Pi_{0;\mu\nu}^{(1,\epsilon)} = g^2 \left(\frac{p^{1+2\epsilon}}{\mu^{2\epsilon}} \right) \left(\pi_{\text{YM}}^{(1,\epsilon)} + \pi_0^{(1,\epsilon)} \right) \mathbf{T}_{\mu\nu}. \tag{29}$$

For Chapter 3, we also define the pure Yang-Mills contribution

$$\Pi_{\mu\nu}^{\text{B}(1,\epsilon)} = g^2 \left(\frac{p^{1+2\epsilon}}{\mu^{2\epsilon}} \right) \pi_{\text{YM}}^{(1,\epsilon)} \mathbf{T}_{\mu\nu}. \tag{30}$$

The terms which appear in the limit $D \rightarrow 3$ are

$$\pi_{\text{YM}}^{(1,0)} = \frac{C_A}{64} (\xi^2 + 2\xi + 11) \tag{31}$$

$$\pi_{m^2}^{(1,0)} = -\frac{T_R}{16\pi} \left(-\frac{4m}{p} + \frac{4m^2 + p^2}{p^2} \left(\pi - 2 \arctan \frac{2m}{p} \right) \right) \tag{32}$$

and it is also useful to take the $m \rightarrow 0$ limit and keep terms $\mathcal{O}(\epsilon)$,

$$\pi_{\text{YM}}^{(1,\epsilon)} = \frac{C_A}{64} ((\xi^2 + 2\xi + 11)(1 - 2\epsilon \log 2) + \epsilon(12 - 12\xi - 2\xi^2)) \quad (33)$$

$$\pi_0^{(1,\epsilon)} = -\frac{T_R}{16} (1 - 2\epsilon \log 2 - \epsilon). \quad (34)$$

One-loop Higgs self-energy

The calculation of the one-loop correction of the Higgs self-energy proceeds forward in much the same manner,

$$\Pi_{\phi;m^2}^{(1,\epsilon)} = \text{diagram 1} + \text{diagram 2} + \frac{1}{2} \text{diagram 3} \quad (35)$$

with

$$\Pi_{\phi;m^2}^{(1,0)} = g^2 p \pi_{\phi;m^2}^{(1,0)} \quad (36)$$

$$\Pi_{\phi;0}^{(1,\epsilon)} = g^2 \left(\frac{p^{1+2\epsilon}}{\mu^{2\epsilon}} \right) \pi_{\phi;0}^{(1,\epsilon)}. \quad (37)$$

For the $D \rightarrow 3$ and massless limits we have

$$\pi_{\phi;m^2}^{(1,0)} = \frac{\tilde{\lambda}(d_R + 1)}{4\pi} \frac{m}{p} + \frac{C_R}{4\pi} \left((2 - \xi) \frac{m}{p} + \frac{2(p^2 - m^2)}{p^2} \arctan \frac{p}{m} \right) \quad (38)$$

$$\pi_{\phi;0}^{(1,\epsilon)} = \frac{C_R}{4} (1 - 2\epsilon \log 2 + \epsilon(1 - \xi)). \quad (39)$$

where we have defined the dimensionless quartic coupling $\tilde{\lambda} = \lambda/g^2$, so that $\tilde{\lambda} = 2x$.

One-loop ghost self-energy

The one-loop ghost self-energy is constructed out of a single diagram,

$$\Sigma^{(1,\epsilon)} = \dots \text{ (diagram) } \dots \quad (40)$$

for which in $D = 3 + 2\epsilon$, ξ dependence only appears at $\mathcal{O}(\epsilon)$,

$$\Sigma^{(1,\epsilon)} = g^2 \left(\frac{p^{1+2\epsilon}}{\mu^{2\epsilon}} \right) \sigma^{(1,\epsilon)} = g^2 \left(\frac{p^{1+2\epsilon}}{\mu^{2\epsilon}} \right) \frac{C_A}{16} (1 - 2\epsilon \log 2 + \epsilon(1 - \xi)). \quad (41)$$

Two-loop topologies

The massless two-loop master topology is

$$\text{ (diagram) } = J_2^{(D)}(n_1, n_2, n_3, n_4, n_5) \quad \left\{ \begin{array}{l} p_1 = q_1 \\ p_2 = q_2 \\ p_3 = q_1 - p \\ p_4 = q_2 - p \\ p_5 = q_1 - q_2 \end{array} \right. \quad (42)$$

$$J_2^{(D)}(n_1, n_2, n_3, n_4, n_5) = \left(\frac{1}{\bar{\mu}^2} \right)^{D-D_0} \int \frac{d^D q_1}{(2\pi)^D} \frac{d^D q_2}{(2\pi)^D} \frac{1}{(q_1^2)^{n_1} (q_2^2)^{n_2} ((q_1 - p)^2)^{n_3} ((q_2 - p)^2)^{n_4} ((q_1 - q_2)^2)^{n_5}}. \quad (43)$$

The remaining two topologies are related to $J_2^{(D)}$ by shrinking one or more of the propagators to a point, for instance

$$J_2^{(D)}(n_1, n_2, n_3, n_4, 0) = J_1^{(D)}(n_1, 0; n_3, 0) J_1^{(D)}(n_2, 0; n_4, 0) \quad (44)$$

$$J_2^{(D)}(n_1, 0, 0, n_2, n_3) = J_2^{(D)}(n_1, n_2, n_3) \quad (45)$$

$$J_2^{(D)}(n_1, n_2, n_3, 0, n_4) = J_2^{(D)}(n_1, n_2, n_3, n_4) \quad (46)$$

where the number of propagators should be inferred from the arguments. In computing the two-loop self-energies we encounter UV divergences arising from the integrals

$$J_1^{(D)}(n_1, 0; n_2, m) = (m^2)^{D/2-\alpha-\beta} \frac{\Gamma(D/2 - n_1) \Gamma(n_1 + n_2 - D/2)}{(\bar{\mu}^2)^{\frac{D-D_0}{2}} (4\pi)^{D/2} \Gamma(D/2) \Gamma(n_2)} \times {}_2F_1\left(n_1, n_1 + n_2 - \frac{D}{2}; \frac{D}{2} \middle| -\frac{p^2}{m^2}\right) \quad (47)$$

$$J_2^{(D)}(n_1, n_2, n_3) = \frac{\Gamma(D/2 - n_1) \Gamma(D/2 - n_2) \Gamma(D/2 - n_3)}{(\bar{\mu}^2)^{D-D_0} (4\pi)^D \Gamma(n_1) \Gamma(n_2) \Gamma(n_3)} \times \frac{\Gamma(n_1 + n_2 + n_3 - D)}{\Gamma(3D/2 - n_1 - n_2 - n_3)} (p^2)^{D-n_1-n_2-n_3}. \quad (48)$$

The massive one-loop scalar integral is needed since recursively one-loop diagrams (i.e. the one-loop diagrams with a self-energy insertion in one of the propagators) are IR divergent when they are massless.

Two-loop gluon self-energy

At two-loops, a number of additional diagrams are present,

$$\pi_{\text{YM};\mu\nu}^{(\text{UV}2,\epsilon)} \propto \frac{1}{6} \text{diagram}_1 + \frac{1}{2} \text{diagram}_2 + \text{diagram}_3 + \frac{1}{4} \text{diagram}_4 - \text{diagram}_5 - 2 \text{diagram}_6 - 2 \text{diagram}_7 \quad (49)$$

$$\pi_{\text{YM};0;\mu\nu}^{(\text{IR}2,\epsilon)} \propto \text{diagram}_8 + \frac{1}{2} \text{diagram}_9 \quad (50)$$

$$\pi_{0;\mu\nu}^{(\text{UV}2,\epsilon)} \propto \text{diagram}_{10} + \text{diagram}_{11} + 2 \text{diagram}_{12} + 4 \text{diagram}_{13} + \text{diagram}_{14} \quad (51)$$

$$\pi_{0;\mu\nu}^{(\text{IR}2,\epsilon)} \propto \text{diagram}_{15} + \text{diagram}_{16} \quad (52)$$

using a notation where the subscript zero refers to the mass of the scalars in the loops being set to $m^2 = 0$. As mentioned at the start of this section, for the purpose of regularizing this calculation genuinely two-loop topologies can be computed in the massless limit. However, recursively one-loop diagrams (labelled with the superscript IR2) will exhibit IR divergences without the inclusion of a regulator mass ω . We have (retaining the superscript IR to indicate that the full expression involves the

specifically IR regulated diagrams)

$$\Pi_{0;\mu\nu}^{B(2,\epsilon)} = g^4 \left(\frac{p^{4\epsilon}}{\mu^{4\epsilon}} \right) \left(\pi_{YM;\mu\nu}^{(UV2,\epsilon)} + \pi_{YM;0;\mu\nu}^{(IR2,\epsilon)} + \pi_{0;\mu\nu}^{(UV2,\epsilon)} + \pi_{0;\mu\nu}^{(IR2,\epsilon)} \right). \quad (53)$$

For Chapter 3, we also define the pure Yang-Mills contribution

$$\Pi_{YM;\mu\nu}^{B(2,\epsilon)} = g^4 \left(\frac{p^{4\epsilon}}{\mu^{4\epsilon}} \right) \left(\pi_{YM;\mu\nu}^{(UV2,\epsilon)} + \pi_{YM;0;\mu\nu}^{(IR2,\epsilon)} \Big|_{T_R=0} \right), \quad (54)$$

noting that it should not be interpreted that these expressions are transverse. The IR regulated gluon and scalar propagators are defined as

$$G_{\mu\nu}^{B(IR1,\epsilon)}(q) = g^2 \frac{\pi_{YM}^{(1,\epsilon)} + \pi_0^{(1,\epsilon)}}{\mu^{2\epsilon}(q^2 + \omega^2)^{\frac{3}{2}-\epsilon}} \left(g^{\mu\nu} - \frac{q_\mu q_\nu}{q^2 + \omega^2} \right) \quad (55)$$

$$D^{B(IR1,\epsilon)}(q) = g^2 \frac{\pi_{\phi;0}^{(1,\epsilon)}}{\mu^{2\epsilon}(q^2 + \omega^2)^{\frac{3}{2}-\epsilon}}. \quad (56)$$

Now, regarding the notation: at this point there are two quantities which can be regarded as masses, m^2 and ω^2 . m^2 refers to the Higgs mass which enters the problem via the scalar propagator, which we have already set to zero. Whereas, ω^2 is an unphysical regulator mass introduced to regulate IR divergences in some two-loop diagrams. So, for instance, the diagrams which comprise $\pi_{YM;0;\mu\nu}^{(IR2,\epsilon)}$ are calculated using finite ω^2 , but setting $m^2 = 0$. One may ask why we do not simply regulate the IR divergences by keeping the scalar field massive from the onset? The reason for this is that a) a number of divergences arise from a $1/p^3$ gauge field propagator, so this would not solve the problem entirely, and b) in general these diagrams are introduced to regularize the UV divergences in the problem. To compute the leading order UV behaviour, it is sufficient to set $m^2 = 0$, which drastically simplifies the majority of the diagrams which must be calculated. Then, the IR divergences which would arise in the bare perturbation theory are handled with ω^2 , of which the final results will be independent regardless.

Defining $\chi = p/m$, the individual components are

$$\begin{aligned} \pi_{\text{YM};\mu\nu}^{(\text{UV}2,\epsilon)} = & \frac{C_A^2}{16\pi^2} \left[\frac{(\xi+2)(\xi^2+2\xi+11)}{48\epsilon} g_{\mu\nu} \right. \\ & - \frac{8(7\xi^3+75\xi^2+221\xi+233)+18\zeta(2)(\xi^2+3)(\xi^2+2\xi^2+17)}{768} \mathbf{T}_{\mu\nu} \\ & \left. - \frac{7\xi^3+32\xi^2+79\xi+42}{48} \mathbf{L}_{\mu\nu} \right] \end{aligned} \quad (57)$$

$$\begin{aligned} \pi_{\text{YM};0;\mu\nu}^{(\text{IR}2,\epsilon)} = & \frac{C_A}{16\pi^2} \left[-\frac{4(\xi+2)(\pi_{\text{YM}}^{(1,0)}+\pi_{\phi;0}^{(1,0)})}{3\epsilon} g_{\mu\nu} + \left[\frac{4(\pi_{\text{YM}}^{(1,0)}+\pi_0^{(1,0)})}{3} \left(2(\xi+2)\log 4\chi^2 \right. \right. \right. \\ & - \frac{8(\xi+2)\chi^6+(20\xi+42)\chi^4+3(5\xi+11)\chi^2+4(\xi+2)}{\chi^3(\chi^2+1)^{\frac{3}{2}}} \text{arcsinh}(\chi) \\ & + \left. \frac{(5\xi+16)\chi^4+5(2\xi+5)\chi^2+4(\xi+2)}{\chi^2(1+\chi^2)} \right) + \frac{(\xi+2)(C_A(\xi^2+6\xi-6)-2T_R)}{24} \left. \right] \mathbf{T}_{\mu\nu} \\ & + \left[\frac{4(\pi_{\text{YM}}^{(1,0)}+\pi_0^{(1,0)})}{3} \left(2(\xi+2)\log 4\chi^2 - \frac{4(\xi+2)\chi^4+2(\xi-1)\chi^2-8(\xi+2)}{\chi^3(\chi^2+1)^{\frac{1}{2}}} \text{arcsinh}(\chi) \right. \right. \\ & + \left. \left. \frac{(5\xi+6)\chi^2-8(\xi+2)}{\chi^2} \right) + \frac{(\xi+2)(C_A(\xi^2+6\xi-6)-2T_R)}{24} \right] \mathbf{L}_{\mu\nu} \end{aligned} \quad (58)$$

$$\begin{aligned} \pi_{0;\mu\nu}^{(\text{UV}2,\epsilon)} = & \frac{T_R}{16\pi^2} \left[\frac{4C_R-(\xi+2)C_A}{12\epsilon} g_{\mu\nu} \right. \\ & + \frac{16(18\zeta(2)-8(\xi-3))C_R+(18\zeta(2)(\xi^2-5)+80\xi+272)C_A}{96} \mathbf{T}_{\mu\nu} \\ & \left. - \frac{2(\xi+5)C_R-(3\xi+4)C_A}{6} \mathbf{L}_{\mu\nu} \right] \end{aligned} \quad (59)$$

$$\begin{aligned} \pi_{0;\mu\nu}^{(\text{IR}2,\epsilon)} = & \frac{T_R}{16\pi^2} \left[-\frac{4\pi_{\phi;0}^{(1,0)}}{3\epsilon} g_{\mu\nu} + \left[\frac{4\pi_{\phi;0}^{(1,0)}}{3} \left(2\log 4\chi^2 - \frac{16(\chi^2+1)^{\frac{3}{2}}}{\chi^3} \text{arcsinh}(\chi) \right. \right. \right. \\ & + \left. \frac{22\chi^2+16}{\chi^2} \right) + \frac{(\xi-1)C_R}{2} \left. \right] \mathbf{T}_{\mu\nu} + \left[\frac{4\pi_{\phi;0}^{(1,0)}}{3} \left(2\log 4\chi^2 - \frac{4(\chi^4-4\chi^2-8)}{\chi^3(\chi^2+1)^{\frac{1}{2}}} \text{arcsinh}(\chi) \right. \right. \\ & + \left. \left. \frac{6\chi^2-32}{\chi^2} \right) + \frac{(\xi-1)C_R}{2} \right] \mathbf{L}_{\mu\nu}. \end{aligned} \quad (60)$$

Two-loop Higgs self-energy

The two-loop Higgs self-energy is specified by the diagrams

$$\pi_{\phi;0}^{(\text{UV2},\epsilon)} \propto \text{---} \text{---} \text{---} + \text{---} \text{---} \text{---} + 2 \text{---} \text{---} \text{---} + \frac{1}{2} \text{---} \text{---} \text{---} + \frac{1}{2} \text{---} \text{---} \text{---} + \text{---} \text{---} \text{---} \quad (61)$$

$$\pi_{\phi;0}^{(\text{IR2},\epsilon)} \propto \text{---} \text{---} \text{---} + \text{---} \text{---} \text{---} + \frac{1}{2} \text{---} \text{---} \text{---} + \text{---} \text{---} \text{---} \quad (62)$$

where once again IR divergences are handled with a regulator mass ω . Including a counter-term, we have

$$\Pi_{\phi;0}^{(2,\epsilon)} = g^4 \left(\frac{p^{4\epsilon}}{\mu^{4\epsilon}} \right) \left(\pi_{\phi;0}^{(\text{UV2},\epsilon)} + \pi_{\phi;0}^{(\text{IR2},\epsilon)} \right) - \delta m^2 \quad (63)$$

with

$$\begin{aligned} \pi_{\phi;0}^{(\text{UV}2,\epsilon)} = & \frac{1}{16\pi^2} \left[\frac{C_R(C_A(\xi-1)(\xi+3) + 4C_R(2\xi-3)) - 4(1+d_R)\tilde{\lambda}^2}{16\epsilon} \right. \\ & + \frac{C_R[C_A(12\zeta(2) + 3\xi^2 + 22\xi + 27) - 4C_R(18\zeta(2) + \xi^2 + 6\xi - 1)]}{16} \\ & \left. + \frac{3(1+d_R)\tilde{\lambda}^2}{2} \right] \end{aligned} \quad (64)$$

$$\begin{aligned} \pi_{\phi;0}^{(\text{IR}2,\epsilon)} = & \frac{\tilde{\lambda}(1+d_R)}{16\pi^2} \left[\frac{2\pi_{\phi;0}^{(1,0)}}{\epsilon} - 4\pi_{\phi;0}^{(1,0)}(\log 4\chi^2 - 1) + \frac{(1-\xi)C_R}{2} \right] \\ & + \frac{C_R}{16\pi^2} \left[\frac{4(\pi_{\text{YM}}^{(1,0)} + \pi_0^{(1,0)}) - 2\xi\pi_{\phi;0}^{(1,0)}}{\epsilon} - \left[8(\pi_{\text{YM}}^{(1,0)} + \pi_0^{(1,0)}) - 4\xi\pi_{\phi;0}^{(1,0)} \right] \log 4\chi^2 \right. \\ & + \frac{8 \left[(\pi_{\text{YM}}^{(1,0)} + \pi_0^{(1,0)}) (8\chi^4 + 15\chi^2 + 6) + 3\pi_{\phi;0}^{(1,0)}(\chi^2 + 1)(3\xi(\chi^2 + 1) - 1) \right]}{3\chi(\chi^2 + 1)^{\frac{3}{2}}} \text{arcsinh}(\chi) \\ & \left. - \frac{1}{24} \left[32(\pi_{\text{YM}}^{(1,0)} + \pi_0^{(1,0)}) \frac{\chi^2 + 3}{\chi^2 + 1} + 96\pi_{\phi;0}^{(1,0)}(7\xi - 2) \right. \right. \\ & \left. \left. + 3C_A(\xi^2 + 6\xi - 6) - 6T_R - 12C_R\xi(\xi - 1) \right] \right] \end{aligned} \quad (65)$$

$$\delta m^2 = \frac{1}{16\pi^2\epsilon} \left[\frac{C_R(7C_A - 6C_R - 2T_R)}{8} g^4 + \frac{C_R(d_R + 1)}{2} g^2 \lambda - \frac{d_R + 1}{4} \lambda^2 \right] \quad (66)$$

Due to the counter-term, the scale dependence of m^2 is given by the RG equation

$$\frac{dm^2}{d\log \mu} = \beta_{m^2}(g^2, \lambda) \quad (67)$$

with

$$\beta_{m^2}(g^2, \lambda) = -\frac{\partial \delta m^2}{\partial g^2} \frac{dg^2}{d\log \mu} - \frac{\partial \delta m^2}{\partial \lambda} \frac{d\lambda}{d\log \mu} = -2\epsilon g^2 \frac{\partial \delta m^2}{\partial g^2} - 2\epsilon \lambda \frac{\partial \delta m^2}{\partial \lambda}. \quad (68)$$

For instance, with an SU(2) fundamental Higgs in Landau gauge,

$$\beta_{m^2}(g^2, \lambda) = -\frac{1}{16\pi^2} \left[\frac{51}{16} g^4 + \frac{9}{2} g^2 \lambda - 3\lambda^2 \right]. \quad (69)$$

Appendix D

Three-gluon and ghost-gluon vertices

In this appendix we will present our results for the one-loop corrections to the three-gluon and ghost-gluon vertices valid for covariant gauge in 3D. The generalization to arbitrary D is available in the literature [179].

When working in covariant gauge, one encounters scalar integrals of the form

$$C_{\alpha\beta\gamma}^0 = \int \frac{d^D q}{(2\pi)^D} \frac{1}{[(q-p_2)^2]^\alpha [(q+p_1)^2]^\beta [q^2]^\gamma} \quad (70)$$

where α , β and γ can take on values between -3 and 2 over the course of the calculation. In three dimensions, all of the triangle integrals with integer α , β and γ are finite in DR. Moreover, they can all be expressed in terms of

$$C_{111}^0 = \frac{1}{8p_1 p_2 p_3} \quad (71)$$

$$C_{011}^0 = \frac{1}{8p_1} \quad (72)$$

$$C_{101}^0 = \frac{1}{8p_2} \quad (73)$$

$$C_{110}^0 = \frac{1}{8p_3} \quad (74)$$

with $p_3^2 = (p_1 + p_2)^2$ and $p_i = \sqrt{p_i^2}$. The relations between triangle integrals with different α , β and γ can be obtained from the generic expression for $C_{\alpha\beta\gamma}^0$ which is known in terms of Appel's hypergeometric function [225]

$$F_4(a, b; c, d|x, y) = \sum_{i=0}^{\infty} \sum_{j=0}^{\infty} \frac{(a)_{i+j} (b)_{i+j}}{(c)_i (d)_j} \frac{x^i y^j}{i! j!} \quad (75)$$

making use of the Pockhammer symbol $(a)_i = \Gamma(a+i)/\Gamma(a)$. In any (Euclidean) dimension, omitting the $\overline{\text{MS}}$ scale, the expression reads

$$\begin{aligned}
C_{\alpha\beta\gamma}^0 = & \frac{1}{(4\pi)^{D/2}\Gamma(\gamma)\Gamma(\beta)\Gamma(\alpha)\Gamma(D-\gamma-\beta-\alpha)} \left[\right. \\
& (p_3^2)^{D/2-\gamma-\beta-\alpha}\Gamma(\gamma)\Gamma(\gamma+\beta+\alpha-D/2)\Gamma(D/2-\gamma-\beta)\Gamma(D/2-\gamma-\alpha) \\
& \times F_4\left(\gamma, \gamma+\beta+\alpha-D/2; \gamma+\beta-D/2+1, \gamma+\alpha-D/2+1 \middle| \frac{p_1^2}{p_3^2}, \frac{p_2^2}{p_3^2}\right) \\
& + (p_2^2)^{D/2-\gamma-\alpha}(p_3^2)^{-\beta}\Gamma(\beta)\Gamma(D/2-\alpha)\Gamma(D/2-\gamma-\beta)\Gamma(\gamma+\alpha-D/2) \\
& \times F_4\left(\beta, D/2-\alpha; \gamma+\beta-D/2+1, D/2-\gamma-\alpha+1 \middle| \frac{p_1^2}{p_3^2}, \frac{p_2^2}{p_3^2}\right) \\
& + (p_1^2)^{D/2-\gamma-\beta}(p_3^2)^{-\alpha}\Gamma(\alpha)\Gamma(D/2-\beta)\Gamma(D/2-\gamma-\alpha)\Gamma(\gamma+\beta-D/2) \\
& \times F_4\left(\alpha, D/2-\beta; D/2-\gamma-\beta+1, \gamma+\alpha-D/2+1 \middle| \frac{p_1^2}{p_3^2}, \frac{p_2^2}{p_3^2}\right) \\
& + \Gamma(D-\gamma-\beta-\alpha)(p_1^2)^{D/2-\gamma-\beta}(p_2^2)^{D/2-\gamma-\alpha}(p_3^2)^{\gamma-D/2} \\
& \times \Gamma(D/2-\gamma)\Gamma(\gamma+\beta-D/2)\Gamma(\gamma+\alpha-D/2) \\
& \left. \times F_4\left(D-\gamma-\beta-\alpha, D/2-\gamma; D/2-\gamma-\beta+1, D/2-\gamma-\alpha+1 \middle| \frac{p_1^2}{p_3^2}, \frac{p_2^2}{p_3^2}\right) \right]. \quad (76)
\end{aligned}$$

At the one-loop level, the three-gluon and ghost-gluon vertices have the following form

$$\begin{aligned}
gV_{\mu_1\mu_2\mu_3}^{\text{B}(1)a_1a_2a_3}(p_1, p_2, p_3) = & gF^{a_1a_2a_3} \left[A^{\text{B}(1)}(p_1, p_2; p_3) \mathbf{A}_{\mu_1\mu_2\mu_3} \right. \\
& + B^{\text{B}(1)}(p_1, p_2; p_3) \mathbf{B}_{\mu_1\mu_2\mu_3} + C^{\text{B}(1)}(p_1, p_2; p_3) \mathbf{C}_{\mu_1\mu_2\mu_3} + F^{\text{B}(1)}(p_1, p_2; p_3) \mathbf{F}_{\mu_1\mu_2\mu_3} \\
& \left. + H^{\text{B}(1)}(p_1, p_2, p_3) \mathbf{H}_{\mu_1\mu_2\mu_3} + S^{\text{B}(1)}(p_1, p_2, p_3) \mathbf{S}_{\mu_1\mu_2\mu_3} + \text{cyclic perms.} \right] \quad (77)
\end{aligned}$$

$$gV_{\mu_3}^{\text{B}(1)a_1a_2a_3}(p_1, p_2, p_3) = gF^{a_1a_2a_3} \left[\mathbb{A}^{\text{B}(1)}(p_1, p_2, p_3) p_{1\mu_3} + \mathbb{B}^{\text{B}(1)}(p_1, p_2, p_3) p_{2\mu_3} \right] \quad (78)$$

with the tensors **A** through **S** as defined in Chapter 3, Section 3.4. The vertex functions are as follows:

$$\begin{aligned}
A^{B(1)}(p_1, p_2; p_3) = & -\frac{g^2 N}{1024 p_1^3 p_2^3 p_3 (p_1 + p_2 + p_3)^2} \left[16 p_1^2 p_2^2 (p_1 + p_2 + p_3) [4(p_1 - p_2)^2 (p_1 + p_2) \right. \\
& + (5p_1^2 + 6p_1 p_2 + 5p_2^2) p_3 + 3(p_1 + p_2) p_3^2 + 6p_3^3] - 4[(p_1^2 - p_2^2)^2 (p_1^4 + 2p_1^3 p_2 \\
& + 4p_1^2 p_2^2 + 2p_1 p_2^3 + p_2^4) - 2p_1 p_2 (p_1 + p_2) (p_1^4 - 4p_1^3 p_2 - 2p_1^2 p_2^2 - 4p_1 p_2^3 + p_2^4) p_3 \\
& - (p_1^6 - 11p_1^4 p_2^2 - 16p_1^3 p_2^3 - 11p_1^2 p_2^4 + p_2^6) p_3^2 + 8p_1^2 p_2^2 (p_1 + p_2) p_3^3 \\
& - (p_1 - p_2)^2 (p_1^2 + 4p_1 p_2 + p_2^2) p_3^4 + 2p_1 p_2 (p_1 + p_2) p_3^5 + (p_1^2 + p_2^2) p_3^6] (1 - \xi) \\
& + (p_1 + p_2 + p_3)^2 [(p_1 - p_2)^2 (p_1^4 + 2p_1^3 p_2 + 2p_1 p_2^3 + p_2^4) - 2(p_1 + p_2)^3 (p_1^2 - 3p_1 p_2 + p_2^2) p_3 \\
& \left. + 2(p_1^4 - p_1^2 p_2^2 + p_2^4) p_3^2 - 2(p_1^3 + p_2^3) p_3^3 + (p_1^2 + p_2^2) p_3^4] (1 - \xi)^2 \right] \quad (79)
\end{aligned}$$

$$\begin{aligned}
B^{B(1)}(p_1, p_2; p_3) = & -\frac{g^2 N (p_1 - p_2)}{1024 p_1^3 p_2^3 p_3 (p_1 + p_2 + p_3)^2} \left[16 p_1^2 p_2^2 p_3^2 [2(p_1 + p_2)^3 \right. \\
& - 9(p_1 + p_2)^2 p_3 - 20(p_1 + p_2) p_3^2 - 9p_3^3] - 4[2p_1^2 (p_1 - p_2)^2 p_2^2 (p_1 + p_2)^3 \\
& + 4p_1^2 p_2^2 (p_1^2 - p_2^2)^2 p_3 - (p_1 + p_2) (p_1^6 + 2p_1^5 p_2 - 3p_1^4 p_2^2 - 4p_1^3 p_2^3 - 3p_1^2 p_2^4 + 2p_1 p_2^5 + p_2^6) p_3^2 \\
& + 2p_1 p_2 (p_1 + p_2)^2 (p_1^2 - 6p_1 p_2 + p_2^2) p_3^3 + (p_1 + p_2) (p_1^4 - 26p_1^2 p_2^2 + p_2^4) p_3^4 - 12p_1^2 p_2^2 p_3^5 \\
& + (p_1 + p_2)^3 p_3^6 - 2p_1 p_2 p_3^7 - (p_1 + p_2) p_3^8] (\xi - 1) \\
& + (p_1 + p_2 + p_3)^2 [2p_1^2 (p_1 - p_2)^2 p_2^2 (p_1 + p_2) - (p_1 + p_2) (p_1^4 + p_2^4) p_3^2 \\
& + 2(p_1 - p_2)^2 (p_1^2 + 3p_1 p_2 + p_2^2) p_3^3 - 2(p_1 + p_2) (p_1^2 + p_2^2) p_3^4 \\
& \left. + 2(p_1^2 + p_1 p_2 + p_2^2) p_3^5 - (p_1 + p_2) p_3^6] (1 - \xi)^2 \right] \quad (80)
\end{aligned}$$

$$\begin{aligned}
C^{B(1)}(p_1, p_2; p_3) = & \frac{g^2 N}{512 p_1^3 p_2^3 (p_1 + p_2) p_3 (p_1 + p_2 + p_3)^2} \left[48 p_1^2 p_2^2 (p_1 + p_2)^2 p_3 \right. \\
& + [(p_1 - p_2)^2 (p_1 + p_2)^5 - 2p_1^3 p_2 (p_1 + p_2)^2 p_3 - 2p_1 p_2^3 (p_1 + p_2)^2 p_3 - p_1^4 (p_1 + p_2) p_3^2 \\
& - (p_1 + p_2) p_2^4 p_3^2 - (p_1 + p_2)^3 p_3^4 + 2p_1 p_2 p_3^5 + (p_1 + p_2) p_3^6] (\xi - 1) (3 + \xi) \\
& \left. + 2p_1^2 (p_1 + p_2) p_2^2 p_3^2 (81 + 5[2 + \xi] \xi) + 4p_1^2 p_2^2 p_3^3 (29 + [6 + \xi] \xi) \right] \quad (81)
\end{aligned}$$

$$\begin{aligned}
F^{\text{B}(1)}(p_1, p_2; p_3) = & -\frac{g^2 N}{512 p_1^3 p_2^3 (p_1 + p_2) p_3^3 (p_1 + p_2 + p_3)^3} \left[\begin{aligned}
& - (p_1 - p_2)^2 (p_1 + p_2)^6 \\
& - 3(p_1 - p_2)^2 (p_1 + p_2)^5 p_3 \Big] (\xi - 1)^2 (3 + \xi) + \Big[(p_1 + p_2) p_3^7 (-3 + \xi) (3 + \xi) \\
& + (3 + \xi) (-20 p_1^3 p_2 (p_1 + p_2)^2 p_3^2 - 20 p_1 p_2^3 (p_1 + p_2)^2 p_3^2 - p_1^4 (p_1 + p_2) p_3^3 (9 + \xi) \\
& - p_2^4 (p_1 + p_2) p_3^3 (9 + \xi) + p_1^4 p_3^4 (11 + \xi) + 4 p_1^3 p_2 p_3^4 (11 + \xi) + 4 p_1 p_2^3 p_3^4 (11 + \xi) \\
& + p_2^4 p_3^4 (11 + \xi) - p_1^4 (p_1 + p_2)^2 p_3^2 (7 + 3\xi) - p_2^4 (p_1 + p_2)^2 p_3^2 (7 + 3\xi) \Big] (\xi - 1) \\
& + 2 p_1^2 p_2^2 (p_1 + p_2)^2 p_3^2 (-113 + 3\xi(-1 + [-5 + \xi]\xi)) \\
& + 2 p_1^2 p_2^2 (p_1 + p_2) p_3^3 (-303 + \xi(-25 + [23 + \xi]\xi)) \\
& + 2 p_1^2 p_2^2 p_3^4 (-215 + \xi(33 + [35 + 3\xi]\xi)) + \Big[3(p_1 + p_2)^3 p_3^5 (\xi - 1) \\
& + 12(p_1 + p_2)(p_1^2 + p_2^2) p_3^5 - p_3^6 [5 p_1^2 + 14 p_1 p_2 + 5 p_2^2 \\
& - 3(p_1 + p_2)^2 \xi] \Big] (1 - \xi)(-3 - \xi) \Big]
\end{aligned} \right. \tag{82}
\end{aligned}$$

$$\begin{aligned}
H^{\text{B}(1)}(p_1, p_2, p_3) = & \frac{g^2 N}{1024 p_1^3 p_2^3 p_3^3 (p_1 + p_2 + p_3)^3} \left[\left[p_1^9 + 6[p_1^7 p_2 p_3 - p_1^5 p_2^3 p_3 - p_1^3 p_2^5 p_3 - p_1^5 p_2 p_3^3 \right. \right. \\
& - p_1^3 p_2 p_3^5] + 3p_1^8 (p_2 + p_3) + 3p_1 p_2^4 (p_2 - p_3)^2 (p_2 + p_3)^2 + 6p_1 p_2^3 (p_2 - p_3)^2 p_3 (p_2 + p_3)^2 \\
& + 6p_1 p_2 (p_2 - p_3)^2 p_3^3 (p_2 + p_3)^2 + 3p_1 (p_2 - p_3)^2 p_3^4 (p_2 + p_3)^2 + p_2^4 (p_2 - p_3)^2 (p_2 + p_3)^3 \\
& + 2p_2^3 (p_2 - p_3)^2 p_3 (p_2 + p_3)^3 + 2p_2 (p_2 - p_3)^2 p_3^3 (p_2 + p_3)^3 \\
& + (p_2 - p_3)^2 p_3^4 (p_2 + p_3)^3 \Big] (\xi - 1)^2 (3 + \xi) + \left[2p_1^2 p_2^5 p_3 (p_2 + p_3) \right. \\
& + 2p_1^2 p_2 p_3^5 (p_2 + p_3) \Big] (13 - \xi) + 2[p_1^3 p_2^6 + p_1^3 p_3^6 + p_1^6 p_2^2 (p_2 + p_3) + p_1^6 p_3^2 (p_2 + p_3)] (7 - \xi) \\
& + [2p_1^7 p_2^2 - 4p_1^5 p_2^4 + 2p_1^7 p_3^2 - 4p_1^5 p_3^4 - 4p_1^4 p_2^4 (p_2 + p_3) + 2p_1^2 p_2^6 (p_2 + p_3) \\
& - 4p_1^4 p_3^4 (p_2 + p_3) + 2p_1^2 p_3^6 (p_2 + p_3) + 6p_1 p_2^2 (p_2 - p_3)^2 p_3^2 (p_2 + p_3)^2 \\
& + 2p_2^2 (p_2 - p_3)^2 p_3^2 (p_2 + p_3)^3] (5 + \xi) + 2p_1^6 p_2 p_3 (p_2 + p_3) (11 + \xi) \\
& - [2p_1^4 p_2^3 p_3 (p_2 + p_3) + 2p_1^4 p_2 p_3^3 (p_2 + p_3)] (23 + \xi) \Big] (\xi - 1) (3 + \xi) \\
& + 4p_1^4 p_2^2 p_3^2 (p_2 + p_3) (78 - 5\xi + 7\xi^3) - 2[p_1^3 p_2^4 p_3^2 + p_1^3 p_2^2 p_3^4] (-225 + \xi(53 + [25 - 13\xi]\xi)) \\
& - 4p_1^3 p_2^3 p_3^3 (-217 + 3\xi(17 + [7 - 5\xi]\xi)) + 4p_1^5 p_2^2 p_3^2 (-18 + \xi(13 + [20 + \xi]\xi)) \\
& + [2p_1^2 p_2^4 p_3^2 (p_2 + p_3) + 2p_1^2 p_2^2 p_3^4 (p_2 + p_3)] (3 + \xi(-3 + [29 + 3\xi]\xi)) \\
& + 4p_1^2 p_2^3 p_3^3 (p_2 + p_3) (111 + \xi(-25 + [-27 + 5\xi]\xi)) \Big] \tag{83}
\end{aligned}$$

$$S^{\text{B}(1)}(p_1, p_2, p_3) = 0. \tag{84}$$

The regulator ω_V mentioned in Chapter 3, Section 3.4 is included in the A function by making the transformation

$$\begin{aligned}
& \frac{1}{p_1^3 p_2^3 p_3 (p_1 + p_2 + p_3)^2} \longrightarrow \\
& \frac{1}{(p_1 + \omega_V)^3 (p_2 + \omega_V)^3 (p_3 + \omega_V) (p_1 + p_2 + p_3 + \omega_V)^2} \tag{85}
\end{aligned}$$

and likewise for B through H . The one-loop ghost vertices are

$$\begin{aligned}
\mathbb{A}^{\text{B}(1)}(p_1, p_2, p_3) = & \frac{g^2 N}{512 p_1 p_2 p_3^3 (p_1 + p_2 + p_3)} \left[16 p_3^2 [-p_1^3 + p_1^2 (-p_2 + p_3) \right. \\
& - (p_2 - p_3)^2 (p_2 + p_3) + p_1 (3p_2^2 + 2p_2 p_3 + p_3^2)] + 4(p_1 - p_2 - p_3) [(p_1^2 - p_2^2)^2 \\
& + 2p_1 (p_1 - p_2)(p_1 + p_2)p_3 + (5p_1 - p_2)(p_1 + p_2)p_3^2 + 2(p_1 + p_2)p_3^3 - 2p_3^4] (1 - \xi) \\
& - (p_1^2 - p_2^2 - p_3^2) [(p_1 - p_2)^2 (p_1 + p_2) + (p_1 - p_2)^2 p_3 \\
& \left. + (p_1 + p_2)p_3^2 - 3p_3^3] (1 - \xi)^2 \right], \tag{86}
\end{aligned}$$

$$\begin{aligned}
\mathbb{B}^{\text{B}(1)}(p_1, p_2, p_3) = & -\frac{g^2 N}{512 p_1 p_2 p_3^3 (p_1 + p_2 + p_3)} \left[32 p_1 p_3^2 [(p_1 - p_2)p_2 + p_3^2] \right. \\
& - 4(p_1^2 - p_2^2 + p_3^2) [p_1^3 + (p_2 - p_3) [(p_2 + p_3)^2 - p_1(p_2 + 3p_3) - p_1^2]] (1 - \xi) \\
& + (p_1^2 - p_2^2 + p_3^2) [(p_1 - p_2)^2 (p_1 + p_2) + (p_1 - p_2)^2 p_3 \\
& \left. + (p_1 + p_2)p_3^2 - 3p_3^3] (1 - \xi)^2 \right]. \tag{87}
\end{aligned}$$

Appendix E

Phase space integrations

In performing numerical integrals over the vacuum diagrams encountered in Chapters 3 and 4 we need efficient parametrizations of the phase space integrals. At two-loops the most interesting diagram is the sunset, at three-loops it is the *Mercedes-Benz* diagram. All other diagrams can be solved by being reduced to these two (as we will describe), so we will concentrate on them.

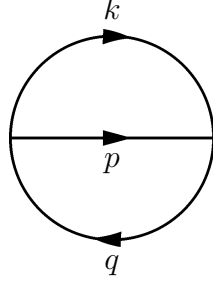
In D dimensions an n -loop diagram involves nD real integrations. However the symmetry group $O(D)$ helps reduce this because certain angular integrations are trivial. Namely, there are $D(D-1)/2$ global angular integrations. Selecting n D -vectors reduces $O(D)$ to $O(D-n)$ (for $n \leq D-2$) or reduces it completely (for $n \geq D-1$). Therefore, for $n \leq D-2$, $D(D-1)/2 - (D-n)(D-n-1)/2 = nD - n(n+1)/2$ of the integrals are global angular integrals which can be performed immediately since none of the invariants depend on them. This leaves $n(n-1)/2$ nontrivial integrations, for $n \leq D-2$. For $n \geq D-1$ there are $nD - D(D-1)/2$ nontrivial integrations.

In an n -loop connected vacuum diagram built entirely with three-point vertices there are $3n-3$ propagators. For $D=3$ and $n \geq 2$ this happens to equal the number of integration variables. Therefore, in $D=3$ dimensions, in diagrams composed using three-point vertices and where each propagator has a distinct momentum (which is the case for 2PI or 3PI diagrams), it should be possible to arrange for the integration variables to be precisely the magnitudes of the momenta on all propagators. This

is a very convenient choice, provided that all dot products of propagator momenta have simple enough expressions.

Two-loops: sunset

We apply these ideas first to the sunset diagram, that is, two vertices connected by three lines:



The “natural” integration variables are

$$\int \frac{d^3 p d^3 k}{(2\pi)^6} = \frac{8\pi^2}{(2\pi)^6} \int_0^\infty p^2 dp \int_0^\infty k^2 dk \int_{-1}^1 d \cos \theta_{pk} \quad (88)$$

where we have performed the trivial integral over the Eulerian angles, in the form of the direction of the \vec{p} integral and the azimuthal angle of \vec{k} if \vec{p} is taken as the \vec{z} axis.

The dot product $\vec{p} \cdot \vec{k} = pk \cos \theta_{pk}$ and

$$q^2 = (\vec{p} + \vec{k})^2 = p^2 + k^2 + 2pk \cos \theta_{pk} \quad \Rightarrow \quad \cos \theta_{pk} = \frac{q^2 - p^2 - k^2}{2pk}. \quad (89)$$

If we change variables from $p, k, \cos \theta_{pk}$ to p, k, q we should differentiate the above holding p, k fixed, giving

$$d \cos \theta_{pk} = \frac{q}{pk} dq. \quad (90)$$

Therefore we can rewrite the integration as

$$\int \frac{d^3 p d^3 k}{(2\pi)^6} = \frac{1}{2^3 \pi^4} \int_0^\infty p dp \int_0^\infty k dk \int_{|p-k|}^{p+k} q dq = \frac{1}{2^6 \pi^4} \int_0^\infty dp^2 \int_0^\infty dk^2 \int_{(p-k)^2}^{(p+k)^2} dq^2 \quad (91)$$

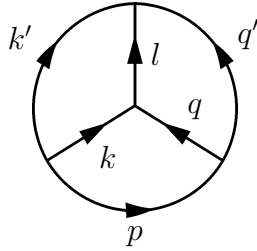
which are a convenient set of integration variables. In particular, all dot products we will encounter can be written directly in terms of the integration variables using

$$-\vec{p} \cdot \vec{q} = \frac{k^2 - p^2 - q^2}{2}, \quad -\vec{k} \cdot \vec{q} = \frac{p^2 - k^2 - q^2}{2}, \quad \vec{p} \cdot \vec{k} = \frac{q^2 - p^2 - k^2}{2}. \quad (92)$$

The remaining two-loop diagram, the figure-eight, can be performed using the same integration variables; the two lines have momentum \vec{p} and \vec{k} , so the q integral can be done directly, $\int q dq = 2pk$. This sort of reduction always works, because we can always consider a four-point vertex to be two three-point vertices connected by a propagator, with the propagator collapsed to a point. So diagrams containing four-point vertices can be written with the same variables as the diagram containing this “collapsed” propagator.

Three-loops: *Mercedes-Benz*

Now we seek a similar set of integration variables for the *Mercedes-Benz* diagram,



Note that $\vec{l} = \vec{k} + \vec{q}$ and similarly $\vec{k}' = -\vec{p} - \vec{k}$ and $\vec{q}' = \vec{p} - \vec{q}$. The phase space

is determined by the triple integral

$$\int \frac{d^3p d^3k d^3q}{(2\pi)^9} = \int_0^\infty p^2 dp k^2 dk q^2 dq \frac{16\pi^2}{(2\pi)^9} \int_{-1}^1 d \cos \theta_{pk} \int_{-1}^1 d \cos \theta_{pq} \int_0^\pi d\phi_{pk;pq} \quad (93)$$

where ϕ is the azimuthal angle between the pk plane and the pq plane, we have used the symmetry of the ϕ integration to reduce it from $[0, 2\pi]$ to $[0, \pi]$, and Eulerian angles have again been performed.

Using the same trick as before, we can rewrite this integral as

$$\frac{1}{2^5 \pi^7} \int_0^\infty dp \int_0^\infty k dk \int_0^\infty q dq \int_{|p-k|}^{p+k} k' dk' \int_{|p-q|}^{p+q} q' dq' \int_0^\pi d\phi_{pq;pk} . \quad (94)$$

and we would like to rewrite the ϕ integral as an l integral. To do so, write out an expression for l^2 :

$$l^2 = (\vec{k} + \vec{q})^2 = k^2 + q^2 + 2\vec{k} \cdot \vec{q}, \quad (95)$$

$$\vec{k} \cdot \vec{q} = kq (\cos \theta_{pq} \cos \theta_{pk} + \sin \theta_{pq} \sin \theta_{pk} \cos \phi) = \frac{l^2 - k^2 - q^2}{2} \quad (96)$$

$$kq \cos \theta_{pq} \cos \theta_{pk} = \frac{(p^2 + q^2 - q'^2)(k'^2 - p^2 - k^2)}{4p^2} \quad (97)$$

$$kq \sin \theta_{pq} \sin \theta_{pk} = \sqrt{(k^2 - k^2 \cos^2 \theta_{pk})(q^2 - q^2 \cos^2 \theta_{pq})} \quad (98)$$

and hence

$$\cos \phi = \frac{p^4 + 2p^2 l^2 + k^2 q^2 + k'^2 q'^2 - (q^2 k'^2 + q'^2 k^2) - p^2 (k^2 + q^2 + k'^2 + q'^2)}{\sqrt{(2p^2 q^2 + 2p^2 q'^2 + 2q^2 q'^2 - p^4 - q^4 - q'^4)(2p^2 k^2 + 2p^2 k'^2 + 2k^2 k'^2 - p^4 - k^4 - k'^4)}} . \quad (99)$$

Since the range of $\cos \phi$ is from -1 to $+1$, we find that the range of l^2 at fixed p, k, q, k', q' is between

$$\frac{1}{2p^2} \left[\left(p^2(k^2+q^2+k'^2+q'^2) + q^2k'^2 + k^2q'^2 - p^4 - k^2q^2 - k'^2q'^2 \right) \right. \\ \left. \pm \sqrt{(2p^2q^2+2p^2q'^2+2q^2q'^2-p^4-q^4-q'^4)(2p^2k^2+2p^2k'^2+2k^2k'^2-p^4-k^4-k'^4)} \right], \quad (100)$$

where the $+$ ($-$) sign represents the maximum (minimum) allowed value of l^2 .

Differentiating the expression for $\cos \phi$ holding p, k, q, k', q' fixed, we find

$$\sin \phi d\phi = \frac{4p^2 l dl}{\sqrt{(\dots)(\dots)}} \quad (101)$$

where $\sqrt{(\dots)(\dots)}$ is the same long square root in the above expressions. Therefore

$$d\phi = \frac{4p^2 l dl}{\sin \phi \sqrt{(\dots)(\dots)}}. \quad (102)$$

Writing $\sin \phi = \sqrt{1 - \cos^2 \phi}$ and after significant algebra we find

$$d\phi = \frac{2p l dl}{\sqrt{X}}, \quad (103)$$

$$X = p^2 l^2 (k^2 + k'^2 + q^2 + q'^2 - p^2 - l^2) + q^2 k'^2 (k^2 + q'^2 + p^2 + l^2 - q^2 - k'^2) \\ + k^2 q'^2 (q^2 + k'^2 + p^2 + l^2 - k^2 - q'^2) - k^2 k'^2 p^2 - q^2 q'^2 p^2 - k^2 q^2 l^2 - k'^2 q'^2 l^2 \quad (104)$$

Note that the expression for X has a symmetry, if hard to see. The momenta are in three pairs; (p, l) , (q, k') , and (q', k) which are “opposite” momenta in the diagram (momenta which do not touch at a vertex). The first terms involve pairs of “opposite” momenta, the last terms involve triples of momenta meeting at a vertex.

The total integration becomes

$$\frac{1}{2^4\pi^7} \int \frac{p dp \, k dk \, q dq \, k' dk' \, q' dq' \, l dl}{\sqrt{X}} \quad (105)$$

with integration limits listed previously. We have not written the integration limits in a symmetric way, but they are symmetric.

The dot product of a pair of momenta which share a vertex are of form

$$\vec{p} \cdot \vec{k} = \frac{k'^2 - p^2 - k^2}{2}, \quad \vec{p} \cdot \vec{q} = \frac{p^2 + q^2 - q'^2}{2} \quad (106)$$

where the sign difference is because in the first case the momenta are both directed out of the vertex while in the latter case one momentum enters and one exits the common vertex. For momenta which do not share a vertex, the dot product is

$$\vec{p} \cdot \vec{l} = \vec{p} \cdot (\vec{k} + \vec{q}) = \frac{q^2 + k'^2 - k^2 - q'^2}{2} \quad (107)$$

and similarly for $\vec{k} \cdot \vec{q}'$ and $\vec{q} \cdot \vec{k}'$. (For a mnemonic, note that q, k' are going from the beginning of one line to the end of the other; k, q' connect the beginnings of each line or the ends of each line). We see that all dot products, including those for momenta on lines which do not meet at a vertex, have simple expressions in terms of momenta on lines.

As mentioned before, we can use the same integration variables for three-loop diagrams with one or more four-point vertices. For instance, when the l propagator is collapsed into a four-point vertex, one can immediately do the l integral;

$$\int \frac{l dl}{\sqrt{X}} = \frac{\pi}{2p}. \quad (108)$$

However, if the integrand involves dot products which depend on l then we cannot do the l integral immediately; we should instead interpret it as an angular integration which does not change the magnitudes of any momenta on the remaining lines, but which does affect some of their dot products.

Appendix F

Remarks on the regularization of $\Gamma[D_+] - \Gamma[D_-]$

This appendix is included to address the divergences that one would encounter when computing $\Gamma[D_+] - \Gamma[D_-]$, where D_+ and D_- are the two-point functions of the broken and symmetric phases, when they coexist. Even though $\Gamma[D]$ is divergent, when D is a solution such that $\delta\Gamma/\delta D = 0$, these divergences can be subtracted with counter-terms that are computable perturbatively (in three dimensions). In other words, the counter-terms are independent on the non-perturbative $\mathcal{O}(g^4)$ correction to the self-energies. As a result, the difference $\Gamma[D_+] - \Gamma[D_-]$ is necessarily finite; a computation of this sort could potentially be of interest as it would for example determine the exact point at which a phase transition occurs.

To demonstrate the necessary cancellations, we will consider a symbolic 2PI effective action $\Gamma[D]$ with a single two-loop and single three-loop diagram. Integration of momentum p will be denoted by the shorthand

$$\int_p = \frac{1}{\bar{\mu}^{2\epsilon}} \int \frac{d^D p}{(2\pi)^D} \quad (109)$$

with $D = 3 + 2\epsilon$ as always. The effective action is

$$\Gamma[D] = \int_p \left[\log D(p) - D(p)(p^2 + m^2) + D(p) \left(\frac{\Pi^{(1)}(p)}{s_1} + \frac{\Pi^{(2)}(p)}{s_2} \right) \right] \quad (110)$$

$$- D(p)(Z_1 + Z_2) \Big] - Z_\Gamma. \quad (111)$$

The symmetry factors s_i count the number of propagators in the corresponding vacuum diagram (for instance, the *Mercedes-Benz* has $s = 6$). The counter-terms Z_1 and Z_2 render the one and two-loop self-energy diagrams finite in $D = 3$, since the values of s_1 and s_2 are such that

$$\frac{\delta\Gamma}{\delta D(p)} = D^{-1}(p) + p^2 + m^2 + \Pi^{(1)}(p) + \Pi^{(2)}(p) - Z_1 - Z_2. \quad (112)$$

Z_1 and Z_2 can be computed perturbatively from the leading order behaviour of $\Pi^{(1)}$ and $\Pi^{(2)}$,

$$\Pi^{(1)}(p) = c_{3/2}p + Z_1 \frac{p^{4\epsilon}}{\mu^{4\epsilon}} + \text{non-perturbative } \mathcal{O}(1) \quad (113)$$

$$\Pi^{(2)}(p) = Z_2 \frac{p^{4\epsilon}}{\mu^{4\epsilon}} + \text{non-perturbative } \mathcal{O}(1). \quad (114)$$

To isolate the UV divergences in Γ , it is useful to work with the following large p expansion of $D(p)$

$$D(p) = \frac{1}{p^2 + m^2} + \frac{c_{3/2}}{(p^2 + m^2)^{3/2}} + \frac{c_2 + d_2 \log p}{(p^2 + m^2)^2} + \frac{c_{5/2} + d_{5/2} \log p}{(p^2 + m^2)^{5/2}} + \mathcal{O}\left(\frac{1}{p^6}\right). \quad (115)$$

Let us start by considering the cancellations which occur between the $\log D$ and $D(p)(p^2 + m^2)$ terms.

$$\int_p \log D(p) - D(p)(p^2 + m^2) \sim \Lambda^3 + \Lambda^2 + \Lambda + \log \Lambda + \text{finite} \quad (116)$$

diverges cubically, so to capture the subleading terms we must expand the integrand to $\mathcal{O}(1/p^3)$. The logarithm gives us

$$\log D(p) \sim \log \frac{1}{p^2 + m^2} + \log \left(1 + \frac{c_{3/2}}{(p^2 + m^2)^{1/2}} + \frac{c_2 + d_2 \log p}{p^2 + m^2} + \frac{c_{5/2} + d_{5/2} \log p}{(p^2 + m^2)^{3/2}} \right) \quad (117)$$

Integrating over the leading term, we have

$$\int_p \log \frac{1}{p^2 + m^2} = -\frac{2\Gamma(1 - D/2)m^D}{(4\pi)^{D/2}D}. \quad (118)$$

For large p , the rightmost term in Eq. (117) has the form $\log(1 + z) \sim (-1)^{n-1}z^n/n$ since z is small. The divergent terms that arise at each n in this expansion are

$$n = 1 \quad \int_p \frac{c_{3/2}}{(p^2 + m^2)^{1/2}} + \frac{c_2 + d_2 \log p}{p^2 + m^2} + \frac{c_{5/2} + d_{5/2} \log p}{(p^2 + m^2)^{3/2}} \quad (119)$$

$$n = 2 \quad -\frac{1}{2} \int_p \frac{c_{3/2}^2}{p^2 + m^2} + \frac{2c_{3/2}(c_2 + d_2 \log p)}{(p^2 + m^2)^{3/2}} \quad (120)$$

$$n = 3 \quad \frac{1}{3} \int_p \frac{c_{3/2}^3}{(p^2 + m^2)^{3/2}}. \quad (121)$$

At this point, one should note that the $\log p$ terms in the numerator arise when we take the limit $D \rightarrow 3$; they should really be interpreted in this context as $\frac{1}{4\epsilon}(p^{4\epsilon} - 1)$. For a *finite* integral (in dimensional regularization), the resulting correction is $\mathcal{O}(\epsilon)$. Continuing on,

$$\int_p D(p)(p^2 + m^2) = \int 1 + \frac{c_{3/2}}{(p^2 + m^2)^{1/2}} + \frac{c_2 + d_2 \log p}{p^2 + m^2} + \frac{c_{5/2} + d_{5/2} \log p}{(p^2 + m^2)^{3/2}} + \text{finite} \quad (122)$$

which cancel all of the $n = 1$ divergences in Eq. (119) from the logarithm. At this point we are only left with the divergent integrals from Eq. (120) and Eq. (121), and

of that lot, the only term which cannot be computed perturbatively is

$$- \int \frac{c_{3/2} c_2}{(p^2 + m^2)^{3/2}} \quad (123)$$

since c_2 is determined by the self-consistent solution. Let us now consider the contribution from the one-loop diagram, by assuming that $s_1 = 3$ (as would be the case in a gauge theory). Using generic labels for momentum, on dimensional grounds

$$\frac{1}{s_1} \int_p D(p) \Pi^{(1)}(p) = \frac{\pi_1}{s_1} \int_p \int_k \mathcal{Q}^2 D(p) D(k) D(q) \quad (124)$$

where π_1 is a constant with mass dimension 1, and \mathcal{Q} indicates momenta associated with the vertices. Referring back to the UV expansion of G ,

$$D(p) = \sum_{i=0} D_i(p); \quad D_i(p) = \left. \frac{c_{i/2+1} + d_{i/2+1} \log p}{(p^2 + m^2)^{i/2+1}} \right|_{i \leq 3} \quad (125)$$

and for $i > 3$ higher powers of $\log p$ will appear in the numerator. However, we do not need to worry about the exact form of D_i in that case. We have

$$\frac{1}{s_1} \int_p D(p) \Pi^{(1)}(p) = \sum_{i,j,k \geq 0} \frac{\pi_1}{s_1} \int_p \int_k \mathcal{Q}^2 D_i(p) D_j(k) D_k(q) = \sum_{i,j,k=0} I_{ijk}. \quad (126)$$

Divergent contributions only arise for specific choices of i , j and k . The relevant cases are

$$I_{000} = \frac{1}{s_1} \int_p \frac{1}{p^2 + m^2} \left(c_{3/2} p + \mathcal{O}(1) + \mathcal{O}(1/p) \right) \quad (127)$$

$$I_{100} = \frac{1}{s_1} \int_p \frac{c_{3/2}}{(p^2 + m^2)^{3/2}} \left(c_{3/2} p + \mathcal{O}(1) \right) \quad (128)$$

$$I_{110} = \frac{1}{s_1} \int_p \frac{c_{3/2}}{(p^2 + m^2)^{3/2}} \frac{1}{2} \left(Z_1 \frac{p^{4\epsilon}}{\mu^{4\epsilon}} + \mathcal{O}(1) \right) \quad (129)$$

$$I_{200} = \frac{1}{s_1} \int_p \frac{(c_2 + d_2 \log p) c_{3/2} p}{(p^2 + m^2)^2} \quad (130)$$

$$I_{n10} = \frac{1}{s_1} \int_p D_n(p) \frac{1}{2} \left(Z_1 \frac{p^{4\epsilon}}{\mu^{4\epsilon}} \right) \Big|_{n \geq 2}, \quad (131)$$

I_{000} , I_{100} and I_{110} can be computed perturbatively (where it should be noted that it would be necessary to account for $\mathcal{O}(\epsilon)$ contributions to $c_{3/2}$). For $n \geq 2$ in the last line, the constant can be dropped since the integral over p is finite. The non-perturbative I_{200} cancels with one of the terms in Eq. (120),

$$-\frac{1}{2} \int_p \frac{2c_{3/2}(c_2 + d_2 \log p)}{(p^2 + m^2)^{3/2}} + I_{200} + I_{020} + I_{002} = \text{finite}. \quad (132)$$

For I_{n01} , we can permute the indices to obtain an overall factor of $2s_1$

$$I_n = I_{n01} + 5 \text{ perms.} = \int_p D_n(p) \left(Z_1 \frac{p^{4\epsilon}}{\mu^{4\epsilon}} \right) \Big|_{n \geq 2}. \quad (133)$$

Looking back at $\Gamma[D]$, this series is cancelled by the term proportional to $Z_1 D(p)$,

$$-Z_1 \int_p D(p) + \sum_{i \geq 2} I_n = -Z_1 \int_p \frac{1}{p^2 + m^2} + \frac{c_{3/2}}{(p^2 + m^2)^{3/2}} + \text{finite}. \quad (134)$$

At this point, all of the divergent integrals that we are left with are proportional to coefficients which can be computed perturbatively, since the two-loop graph eliminated the problematic divergence proportional to c_2 that we had encountered earlier. We should now see what arises from the three-loop graph (for simplicity we can suppose that $s_2 = 4$)

$$\frac{1}{s_2} \int_p D(p) \Pi^{(2)}(p) = \sum_{i,j,k,l \geq 0} \frac{\pi_2}{s_2} \int_p \int_k \int_q D_i(p) D_j(k) D_k(q) D_l(z) = \sum_{i,j,k,l \geq 0} J_{ijkl} \quad (135)$$

where π_2 is a coefficient with mass dimension 2. The interesting cases are

$$J_{0000} = \frac{1}{s_2} \int_p \frac{1}{p^2 + m^2} \left(Z_2 \frac{p^{4\epsilon}}{\mu^{4\epsilon}} + \mathcal{O}(1) + \mathcal{O}(1/p) \right) \quad (136)$$

$$J_{1000} = \frac{1}{s_2} \int_p \frac{c_{3/2}}{(p^2 + m^2)^{3/2}} \left(Z_2 \frac{p^{4\epsilon}}{\mu^{4\epsilon}} + \mathcal{O}(1) \right) \quad (137)$$

$$J_{n000} = \frac{1}{s_2} \int_p G_n(p) \left(Z_2 \frac{p^{4\epsilon}}{\mu^{4\epsilon}} \right). \quad (138)$$

J_{0000} and J_{1000} are perturbative, and for $n \geq 2$, J_{n000} cancels with Z_2 mass counter-term as earlier. Defining

$$J_n = J_{n000} + 3 \text{ perms.} \quad (139)$$

we have

$$-Z_2 \int_p D(p) + \sum_{i \geq 2} J_n = -Z_2 \int_p \frac{1}{p^2 + m^2} + \frac{c_{3/2}}{(p^2 + m^2)^{3/2}} + \text{finite.} \quad (140)$$

After putting everything together, the residual divergent terms are

$$a) \quad \int_p -\frac{1}{2} \frac{c_{3/2}^2}{(p^2 + m^2)} + \frac{1}{3} \frac{c_{3/2}^3}{(p^2 + m^2)^{3/2}} \quad (141)$$

$$b) \quad -(Z_1 + Z_2) \int_p \frac{1}{p^2 + m^2} + \frac{c_{3/2}}{(p^2 + m^2)^{3/2}} \quad (142)$$

$$c) \quad I_{000} + s_1 I_{100} + s_1 I_{110} + J_{0000} + s_2 J_{1000}. \quad (143)$$

References

- [1] **STAR Collaboration** Collaboration, J. Adams et al., *Experimental and theoretical challenges in the search for the quark gluon plasma: The STAR Collaboration’s critical assessment of the evidence from RHIC collisions*, *Nucl.Phys.* **A757** (2005) 102–183, [[nucl-ex/0501009](#)].
- [2] **PHENIX Collaboration** Collaboration, K. Adcox et al., *Formation of dense partonic matter in relativistic nucleus-nucleus collisions at RHIC: Experimental evaluation by the PHENIX collaboration*, *Nucl.Phys.* **A757** (2005) 184–283, [[nucl-ex/0410003](#)].
- [3] **BRAHMS Collaboration** Collaboration, I. Arsene et al., *Quark gluon plasma and color glass condensate at RHIC? The Perspective from the BRAHMS experiment*, *Nucl.Phys.* **A757** (2005) 1–27, [[nucl-ex/0410020](#)].
- [4] **PHENIX Collaboration** Collaboration, A. Adare et al., *J/ψ suppression at forward rapidity in Au+Au collisions at $\sqrt{s_{NN}} = 200$ GeV*, *Phys.Rev.* **C84** (2011) 054912, [[arXiv:1103.6269](#)].
- [5] B. Muller, J. Schukraft, and B. Wyslouch, *First Results from Pb+Pb collisions at the LHC*, *Ann.Rev.Nucl.Part.Sci.* **62** (2012) 361–386, [[arXiv:1202.3233](#)].
- [6] **CMS Collaboration** Collaboration, S. Chatrchyan et al., *Observation of sequential Upsilon suppression in PbPb collisions*, *Phys.Rev.Lett.* **109** (2012) 222301, [[arXiv:1208.2826](#)].
- [7] Y. Aoki, G. Endrodi, Z. Fodor, S. Katz, and K. Szabo, *The Order of the quantum chromodynamics transition predicted by the standard model of particle physics*, *Nature* **443** (2006) 675–678, [[hep-lat/0611014](#)].
- [8] Y. Aoki, Z. Fodor, S. Katz, and K. Szabo, *The QCD transition temperature: Results with physical masses in the continuum limit*, *Phys.Lett.* **B643** (2006) 46–54, [[hep-lat/0609068](#)].

- [9] Y. Aoki, S. Borsanyi, S. Durr, Z. Fodor, S. D. Katz, et al., *The QCD transition temperature: results with physical masses in the continuum limit II.*, *JHEP* **0906** (2009) 088, [[arXiv:0903.4155](#)].
- [10] S. Borsanyi, G. Endrodi, Z. Fodor, A. Jakovac, S. D. Katz, et al., *The QCD equation of state with dynamical quarks*, *JHEP* **1011** (2010) 077, [[arXiv:1007.2580](#)].
- [11] **Wuppertal-Budapest Collaboration** Collaboration, S. Borsanyi et al., *Is there still any T_c mystery in lattice QCD? Results with physical masses in the continuum limit III*, *JHEP* **1009** (2010) 073, [[arXiv:1005.3508](#)].
- [12] A. Bazavov, T. Bhattacharya, M. Cheng, C. DeTar, H. Ding, et al., *The chiral and deconfinement aspects of the QCD transition*, *Phys.Rev.* **D85** (2012) 054503, [[arXiv:1111.1710](#)].
- [13] D. H. Rischke, *The Quark gluon plasma in equilibrium*, *Prog.Part.Nucl.Phys.* **52** (2004) 197–296, [[nucl-th/0305030](#)].
- [14] A. D. Linde, *Infrared Problem in Thermodynamics of the Yang-Mills Gas*, *Phys.Lett.* **B96** (1980) 289.
- [15] M. A. Stephanov, *QCD phase diagram and the critical point*, *Prog.Theor.Phys.Suppl.* **153** (2004) 139–156, [[hep-ph/0402115](#)].
- [16] K. Fukushima and T. Hatsuda, *The phase diagram of dense QCD*, *Rept.Prog.Phys.* **74** (2011) 014001, [[arXiv:1005.4814](#)].
- [17] M. Troyer and U.-J. Wiese, *Computational complexity and fundamental limitations to fermionic quantum Monte Carlo simulations*, *Phys.Rev.Lett.* **94** (2005) 170201, [[cond-mat/0408370](#)].
- [18] P. Petreczky, *Lattice QCD at non-zero temperature*, *J.Phys.* **G39** (2012) 093002, [[arXiv:1203.5320](#)].
- [19] **STAR Collaboration** Collaboration, M. Aggarwal et al., *An Experimental Exploration of the QCD Phase Diagram: The Search for the Critical Point and the Onset of De-confinement*, [arXiv:1007.2613](#).
- [20] **STAR Collaboration** Collaboration, B. Mohanty, *STAR experiment results from the beam energy scan program at RHIC*, *J.Phys.* **G38** (2011) 124023, [[arXiv:1106.5902](#)].

- [21] **STAR Collaboration** Collaboration, M. Aggarwal et al., *Higher Moments of Net-proton Multiplicity Distributions at RHIC*, *Phys.Rev.Lett.* **105** (2010) 022302, [[arXiv:1004.4959](#)].
- [22] M. Stephanov, *Non-Gaussian fluctuations near the QCD critical point*, *Phys.Rev.Lett.* **102** (2009) 032301, [[arXiv:0809.3450](#)].
- [23] C. Athanasiou, K. Rajagopal, and M. Stephanov, *Using Higher Moments of Fluctuations and their Ratios in the Search for the QCD Critical Point*, *Phys.Rev.* **D82** (2010) 074008, [[arXiv:1006.4636](#)].
- [24] S. Datta, R. V. Gavai, and S. Gupta, *The QCD Critical Point : marching towards continuum*, *Nucl.Phys.A904-905* **2013** (2013) 883c–886c, [[arXiv:1210.6784](#)].
- [25] O. Scavenius, A. Mocsy, I. Mishustin, and D. Rischke, *Chiral phase transition within effective models with constituent quarks*, *Phys.Rev.* **C64** (2001) 045202, [[nucl-th/0007030](#)].
- [26] S. Klimt, M. F. Lutz, and W. Weise, *Chiral phase transition in the $SU(3)$ Nambu and Jona-Lasinio model*, *Phys.Lett.* **B249** (1990) 386–390.
- [27] K. Rajagopal and F. Wilczek, *The Condensed matter physics of QCD*, [hep-ph/0011333](#).
- [28] D. J. Gross and F. Wilczek, *Ultraviolet Behavior of Nonabelian Gauge Theories*, *Phys.Rev.Lett.* **30** (1973) 1343–1346.
- [29] M. Czakon, *The Four-loop QCD beta-function and anomalous dimensions*, *Nucl.Phys.* **B710** (2005) 485–498, [[hep-ph/0411261](#)].
- [30] **Particle Data Group** Collaboration, J. Beringer et al., *Review of Particle Physics (RPP)*, *Phys.Rev.* **D86** (2012) 010001.
- [31] S. Bethke, *The 2009 World Average of $\alpha(s)$* , *Eur.Phys.J.* **C64** (2009) 689–703, [[arXiv:0908.1135](#)].
- [32] A. De Rujula, H. Georgi, and S. Glashow, *Hadron Masses in a Gauge Theory*, *Phys.Rev.* **D12** (1975) 147–162.
- [33] R. D. Pisarski and F. Wilczek, *Remarks on the Chiral Phase Transition in Chromodynamics*, *Phys.Rev.* **D29** (1984) 338–341.

- [34] D. de Florian and M. Grazzini, *Higgs production through gluon fusion: Updated cross sections at the Tevatron and the LHC*, *Phys.Lett.* **B674** (2009) 291–294, [[arXiv:0901.2427](#)].
- [35] J. Kiskis, R. Narayanan, and H. Neuberger, *Does the crossover from perturbative to nonperturbative physics in QCD become a phase transition at infinite N ?*, *Phys.Lett.* **B574** (2003) 65–74, [[hep-lat/0308033](#)].
- [36] T. Appelquist and R. D. Pisarski, *High-Temperature Yang-Mills Theories and Three-Dimensional Quantum Chromodynamics*, *Phys.Rev.* **D23** (1981) 2305.
- [37] S. Nadkarni, *Dimensional Reduction in Hot QCD*, *Phys.Rev.* **D27** (1983) 917.
- [38] C.-N. Yang and R. L. Mills, *Conservation of Isotopic Spin and Isotopic Gauge Invariance*, *Phys.Rev.* **96** (1954) 191–195.
- [39] B. Svetitsky and L. G. Yaffe, *Critical Behavior at Finite Temperature Confinement Transitions*, *Nucl.Phys.* **B210** (1982) 423.
- [40] K. Holland, P. Minkowski, M. Pepe, and U. Wiese, *Exceptional confinement in $G(2)$ gauge theory*, *Nucl.Phys.* **B668** (2003) 207–236, [[hep-lat/0302023](#)].
- [41] K. G. Wilson, *Confinement of Quarks*, *Phys.Rev.* **D10** (1974) 2445–2459.
- [42] P. Deligne, P. Etingof, D. Freed, L. Jeffrey, D. Kazhdan, et al., *Quantum fields and strings: A course for mathematicians. Vol. 1, 2*. American Mathematical Soc., 1999.
- [43] J. Carlson, A. Jaffe, A. Wiles, C. M. Institute, and A. M. Society, *The Millennium Prize Problems*. American Mathematical Society, 2006.
- [44] A. Casher, H. Neuberger, and S. Nussinov, *Chromoelectric Flux Tube Model of Particle Production*, *Phys.Rev.* **D20** (1979) 179–188.
- [45] J. Engels, F. Karsch, H. Satz, and I. Montvay, *Gauge Field Thermodynamics for the $SU(2)$ Yang-Mills System*, *Nucl.Phys.* **B205** (1982) 545.
- [46] J. M. Cornwall, *Dynamical Mass Generation in Continuum QCD*, *Phys.Rev.* **D26** (1982) 1453.
- [47] K. Kajantie, M. Laine, K. Rummukainen, and Y. Schroder, *The Pressure of hot QCD up to $g^6 \ln(1/g)$* , *Phys.Rev.* **D67** (2003) 105008, [[hep-ph/0211321](#)].

- [48] **APE Collaboration** Collaboration, M. Albanese et al., *Glueball Masses and String Tension in Lattice QCD*, *Phys.Lett.* **B192** (1987) 163–169.
- [49] F. Karsch, E. Laermann, and M. Lutgemeier, *Three-dimensional $SU(3)$ gauge theory and the spatial string tension of the $(3+1)$ -dimensional finite temperature $SU(3)$ gauge theory*, *Phys.Lett.* **B346** (1995) 94–98, [[hep-lat/9411020](#)].
- [50] L. S. Brown and W. I. Weisberger, *Remarks on the Static Potential in Quantum Chromodynamics*, *Phys.Rev.* **D20** (1979) 3239.
- [51] S. Nadkarni, *Nonabelian Debye Screening. 1. The Color Averaged Potential*, *Phys.Rev.* **D33** (1986) 3738.
- [52] A. V. Smilga, *Are $Z(N)$ bubbles really there?*, *Annals Phys.* **234** (1994) 1–59.
- [53] B. Svetitsky, *Symmetry Aspects of Finite Temperature Confinement Transitions*, *Phys.Rept.* **132** (1986) 1–53.
- [54] G. Boyd, J. Engels, F. Karsch, E. Laermann, C. Legeland, et al., *Thermodynamics of $SU(3)$ lattice gauge theory*, *Nucl.Phys.* **B469** (1996) 419–444, [[hep-lat/9602007](#)].
- [55] J. Engels, J. Fingberg, and M. Weber, *Finite Size Scaling Analysis of $SU(2)$ Lattice Gauge Theory in $(3+1)$ -dimensions*, *Nucl.Phys.* **B332** (1990) 737.
- [56] J. Fingberg, U. M. Heller, and F. Karsch, *Scaling and asymptotic scaling in the $SU(2)$ gauge theory*, *Nucl.Phys.* **B392** (1993) 493–517, [[hep-lat/9208012](#)].
- [57] R. D. Pisarski and M. Tytgat, *Why the $SU(\text{infinity})$ phase transition might be of second order*, [hep-ph/9702340](#).
- [58] R. V. Gavai, *On the deconfinement transition in $SU(4)$ lattice gauge theory*, *Nucl.Phys.* **B633** (2002) 127–138, [[hep-lat/0203015](#)].
- [59] B. Lucini, M. Teper, and U. Wenger, *The High temperature phase transition in $SU(N)$ gauge theories*, *JHEP* **0401** (2004) 061, [[hep-lat/0307017](#)].
- [60] B. Lucini, M. Teper, and U. Wenger, *Properties of the deconfining phase transition in $SU(N)$ gauge theories*, *JHEP* **0502** (2005) 033, [[hep-lat/0502003](#)].

- [61] P. Hasenfratz, F. Karsch, and I. Stamatescu, *The $SU(3)$ Deconfinement Phase Transition in the Presence of Quarks*, *Phys.Lett.* **B133** (1983) 221.
- [62] M. Guidry, *Gauge Field Theories: An Introduction with Applications*. Wiley, 2008.
- [63] C. Alexandrou, A. Borici, A. Feo, P. de Forcrand, A. Galli, et al., *The Deconfinement phase transition in one flavor QCD*, *Phys.Rev.* **D60** (1999) 034504, [[hep-lat/9811028](#)].
- [64] **WHOT-QCD Collaboration** Collaboration, H. Saito et al., *Phase structure of finite temperature QCD in the heavy quark region*, *Phys.Rev.* **D84** (2011) 054502, [[arXiv:1106.0974](#)].
- [65] F. R. Brown, F. P. Butler, H. Chen, N. H. Christ, Z.-h. Dong, et al., *On the existence of a phase transition for QCD with three light quarks*, *Phys.Rev.Lett.* **65** (1990) 2491–2494.
- [66] J. Bernstein, *Spontaneous symmetry breaking, gauge theories, the higgs mechanism and all that*, *Rev.Mod.Phys.* **46** (1974) 7–48.
- [67] F. Englert and R. Brout, *Broken Symmetry and the Mass of Gauge Vector Mesons*, *Phys.Rev.Lett.* **13** (1964) 321–323.
- [68] P. W. Higgs, *Broken symmetries, massless particles and gauge fields*, *Phys.Lett.* **12** (1964) 132–133.
- [69] P. W. Higgs, *Broken Symmetries and the Masses of Gauge Bosons*, *Phys.Rev.Lett.* **13** (1964) 508–509.
- [70] C. Burgess and G. Moore, *The Standard Model: A Primer*. Cambridge University Press, 2012.
- [71] S. Elitzur, *Impossibility of Spontaneously Breaking Local Symmetries*, *Phys.Rev.* **D12** (1975) 3978–3982.
- [72] E. H. Fradkin and S. H. Shenker, *Phase Diagrams of Lattice Gauge Theories with Higgs Fields*, *Phys.Rev.* **D19** (1979) 3682–3697.
- [73] D. Kirzhnits and A. D. Linde, *Macroscopic Consequences of the Weinberg Model*, *Phys.Lett.* **B42** (1972) 471–474.

- [74] F. Karsch, T. Neuhaus, A. Patkos, and J. Rank, *Gauge boson masses in the 3-D, $SU(2)$ gauge Higgs model*, *Nucl.Phys.* **B474** (1996) 217–234, [[hep-lat/9603004](#)].
- [75] K. Kajantie, M. Laine, K. Rummukainen, and M. E. Shaposhnikov, *A Nonperturbative analysis of the finite T phase transition in $SU(2) \times U(1)$ electroweak theory*, *Nucl.Phys.* **B493** (1997) 413–438, [[hep-lat/9612006](#)].
- [76] M. C. Ogilvie, *Phases of Gauge Theories*, *J.Phys.* **A45** (2012) 483001, [[arXiv:1211.2843](#)].
- [77] K. Rummukainen, K. Kajantie, M. Laine, M. E. Shaposhnikov, and M. Tsypin, *The Ising model universality of the electroweak theory*, *Nucl.Phys.Proc.Suppl.* **73** (1999) 653–655, [[hep-lat/9809121](#)].
- [78] M. Laine and K. Rummukainen, *What’s new with the electroweak phase transition?*, *Nucl.Phys.Proc.Suppl.* **73** (1999) 180–185, [[hep-lat/9809045](#)].
- [79] M. Claudson, E. Farhi, and R. Jaffe, *The Strongly Coupled Standard Model*, *Phys.Rev.* **D34** (1986) 873.
- [80] K. Farakos, K. Kajantie, K. Rummukainen, and M. E. Shaposhnikov, *3-d physics and the electroweak phase transition: A Framework for lattice Monte Carlo analysis*, *Nucl.Phys.* **B442** (1995) 317–363, [[hep-lat/9412091](#)].
- [81] M. E. Peskin and D. V. Schroeder, *An Introduction to quantum field theory*. Westview Press, 1995.
- [82] M. Srednicki, *Quantum field theory*. Cambridge University Press, 2007.
- [83] A. Di Giacomo, H. G. Dosch, V. Shevchenko, and Y. Simonov, *Field correlators in QCD: Theory and applications*, *Phys.Rept.* **372** (2002) 319–368, [[hep-ph/0007223](#)].
- [84] V. Gribov, *Quantization of Nonabelian Gauge Theories*, *Nucl.Phys.* **B139** (1978) 1.
- [85] G. F. Sterman, *An Introduction to quantum field theory*. Cambridge University Press, 1994.
- [86] L. Faddeev and V. Popov, *Feynman Diagrams for the Yang-Mills Field*, *Phys.Lett.* **B25** (1967) 29–30.

- [87] N. Nielsen, *On the Gauge Dependence of Spontaneous Symmetry Breaking in Gauge Theories*, *Nucl.Phys.* **B101** (1975) 173.
- [88] K. Fujikawa, B. Lee, and A. Sanda, *Generalized Renormalizable Gauge Formulation of Spontaneously Broken Gauge Theories*, *Phys.Rev.* **D6** (1972) 2923–2943.
- [89] M. Bellac, *Thermal Field Theory*. Cambridge Monographs on Mathematical Physics. Cambridge University Press, 2000.
- [90] H. A. Weldon, *Covariant Calculations at Finite Temperature: The Relativistic Plasma*, *Phys.Rev.* **D26** (1982) 1394.
- [91] V. Klimov, *Collective Excitations in a Hot Quark Gluon Plasma*, *Sov.Phys.JETP* **55** (1982) 199–204.
- [92] A. Rebhan, *The NonAbelian Debye mass at next-to-leading order*, *Phys.Rev.* **D48** (1993) 3967–3970, [[hep-ph/9308232](#)].
- [93] E. Braaten and A. Nieto, *Next-to-leading order Debye mass for the quark - gluon plasma*, *Phys.Rev.Lett.* **73** (1994) 2402–2404, [[hep-ph/9408273](#)].
- [94] J.-P. Blaizot, E. Iancu, and R. R. Parwani, *On the screening of static electromagnetic fields in hot QED plasmas*, *Phys.Rev.* **D52** (1995) 2543–2562, [[hep-ph/9504408](#)].
- [95] P. B. Arnold and L. G. Yaffe, *The NonAbelian Debye screening length beyond leading order*, *Phys.Rev.* **D52** (1995) 7208–7219, [[hep-ph/9508280](#)].
- [96] P. H. Ginsparg, *First Order and Second Order Phase Transitions in Gauge Theories at Finite Temperature*, *Nucl.Phys.* **B170** (1980) 388.
- [97] A. Jakovac, *Reduction of the n component scalar model at two loop level*, *Phys.Rev.* **D53** (1996) 4538–4551, [[hep-ph/9502313](#)].
- [98] K. Kajantie, M. Laine, K. Rummukainen, and M. E. Shaposhnikov, *Generic rules for high temperature dimensional reduction and their application to the standard model*, *Nucl.Phys.* **B458** (1996) 90–136, [[hep-ph/9508379](#)].
- [99] E. Braaten and A. Nieto, *Effective field theory approach to high temperature thermodynamics*, *Phys.Rev.* **D51** (1995) 6990–7006, [[hep-ph/9501375](#)].

- [100] K. Farakos, K. Kajantie, K. Rummukainen, and M. E. Shaposhnikov, *3-D physics and the electroweak phase transition: Perturbation theory*, *Nucl.Phys.* **B425** (1994) 67–109, [[hep-ph/9404201](#)].
- [101] G. D. Moore, *$O(a)$ errors in 3-D $SU(N)$ Higgs theories*, *Nucl.Phys.* **B523** (1998) 569–593, [[hep-lat/9709053](#)].
- [102] J. O. Andersen and M. Strickland, *Resummation in hot field theories*, *Annals Phys.* **317** (2005) 281–353, [[hep-ph/0404164](#)].
- [103] U. Kraemmer and A. Rebhan, *Advances in perturbative thermal field theory*, *Rept.Prog.Phys.* **67** (2004) 351, [[hep-ph/0310337](#)].
- [104] J.-P. Blaizot, E. Iancu, and A. Rebhan, *Thermodynamics of the high temperature quark gluon plasma*, [hep-ph/0303185](#).
- [105] B. M. Kastening, *Renormalization group improvement of the effective potential in massive ϕ^{**4} theory*, *Phys.Lett.* **B283** (1992) 287–292.
- [106] A. Gynther, M. Laine, Y. Schroder, C. Torrero, and A. Vuorinen, *Four-loop pressure of massless $O(N)$ scalar field theory*, *JHEP* **0704** (2007) 094, [[hep-ph/0703307](#)].
- [107] L. Dolan and R. Jackiw, *Symmetry Behavior at Finite Temperature*, *Phys.Rev.* **D9** (1974) 3320–3341.
- [108] K. Takahashi, *Perturbative Calculations at Finite Temperatures*, *Z.Phys.* **C26** (1985) 601–613.
- [109] P. B. Arnold and O. Espinosa, *The Effective potential and first order phase transitions: Beyond leading-order*, *Phys.Rev.* **D47** (1993) 3546, [[hep-ph/9212235](#)].
- [110] J. Kapusta and C. Gale, *Finite-Temperature Field Theory: Principles and Applications*. Cambridge monographs on mathematical physics. Cambridge University Press, 2006.
- [111] R. Norton and J. Cornwall, *On the Formalism of Relativistic Many Body Theory*, *Annals Phys.* **91** (1975) 106.
- [112] A. Vasiliev, *Functional Methods in Quantum Field Theory and Statistical Physics*. Taylor & Francis, 1998.

- [113] J. Berges, *N-particle irreducible effective action techniques for gauge theories*, *Phys.Rev.* **D70** (2004) 105010, [[hep-ph/0401172](#)].
- [114] M. Carrington and Y. Guo, *Techniques for n-Particle Irreducible Effective Theories*, *Phys.Rev.* **D83** (2011) 016006, [[arXiv:1010.2978](#)].
- [115] A. Arrizabalaga and J. Smit, *Gauge fixing dependence of Phi derivable approximations*, *Phys.Rev.* **D66** (2002) 065014, [[hep-ph/0207044](#)].
- [116] M. Carrington, G. Kunstatter, and H. Zaraket, *2PI effective action and gauge invariance problems*, *Eur.Phys.J.* **C42** (2005) 253–259, [[hep-ph/0309084](#)].
- [117] S. Borsanyi and U. Reinosa, *The Pressure of QED from the two-loop 2PI effective action*, *Phys.Lett.* **B661** (2008) 88–94, [[arXiv:0709.2316](#)].
- [118] G. Baym, *Selfconsistent approximation in many body systems*, *Phys.Rev.* **127** (1962) 1391–1401.
- [119] C. de Dominicis and P. C. Martin, *Stationary Entropy Principle and Renormalization in Normal and Superfluid Systems. I. Algebraic Formulation*, *J.Math.Phys.* **5** (1964) 14–30.
- [120] Y. Ivanov, J. Knoll, and D. Voskresensky, *Selfconsistent approximations to nonequilibrium many body theory*, *Nucl.Phys.* **A657** (1999) 413–445, [[hep-ph/9807351](#)].
- [121] Y. Ivanov, J. Knoll, and D. Voskresensky, *Resonance transport and kinetic entropy*, *Nucl.Phys.* **A672** (2000) 313–356, [[nucl-th/9905028](#)].
- [122] D. Roder, J. Ruppert, and D. H. Rischke, *Selfconsistent calculations of spectral densities in the $O(N)$ model: Improving the Hartree-Fock approximation by including nonzero decay widths*, *Nucl.Phys.* **A775** (2006) 127–151, [[hep-ph/0503042](#)].
- [123] U. Reinosa and Z. Szep, *Broken phase scalar effective potential and Phi-derivable approximations*, *Phys.Rev.* **D83** (2011) 125026, [[arXiv:1103.2689](#)].
- [124] K. Kajantie, M. Laine, and Y. Schroder, *A Simple way to generate high order vacuum graphs*, *Phys.Rev.* **D65** (2002) 045008, [[hep-ph/0109100](#)].

- [125] J. S. Schwinger, *On the Green's functions of quantized fields. 1.*, *Proc.Nat.Acad.Sci.* **37** (1951) 452–455.
- [126] J. S. Schwinger, *On the Green's functions of quantized fields. 2.*, *Proc.Nat.Acad.Sci.* **37** (1951) 455–459.
- [127] F. Dyson, *The S matrix in quantum electrodynamics*, *Phys.Rev.* **75** (1949) 1736–1755.
- [128] J. Rammer, *Quantum Field Theory of Non-equilibrium States*. Cambridge University Press, 2007.
- [129] E. Braaten and E. Petitgirard, *Solution to the three loop Phi derivable approximation for scalar thermodynamics*, *Phys.Rev.* **D65** (2002) 041701, [[hep-ph/0106045](#)].
- [130] E. Braaten and E. Petitgirard, *Solution to the three loop Phi derivable approximation for massless scalar thermodynamics*, *Phys.Rev.* **D65** (2002) 085039, [[hep-ph/0107118](#)].
- [131] J. O. Andersen and M. Strickland, *Three-loop Phi-derivable approximation in QED*, *Phys.Rev.* **D71** (2005) 025011, [[hep-ph/0406163](#)].
- [132] J. Berges, *Controlled nonperturbative dynamics of quantum fields out-of-equilibrium*, *Nucl.Phys.* **A699** (2002) 847–886, [[hep-ph/0105311](#)].
- [133] G. Aarts, D. Ahrensmeier, R. Baier, J. Berges, and J. Serreau, *Far from equilibrium dynamics with broken symmetries from the 2PI - 1/N expansion*, *Phys.Rev.* **D66** (2002) 045008, [[hep-ph/0201308](#)].
- [134] V. Smirnov, *Feynman Integral Calculus*. Springer, 2006.
- [135] A. Grozin, *Lectures on QED and QCD: Practical calculation and renormalization of one- and multi-loop Feynman diagrams*. World Scientific Publishing, 2007.
- [136] H. A. Weldon, *Analytic properties of finite temperature selfenergies*, *Phys.Rev.* **D65** (2002) 076010, [[hep-ph/0203057](#)].
- [137] J. Espinosa, M. Quiros, and F. Zwirner, *On the phase transition in the scalar theory*, *Phys.Lett.* **B291** (1992) 115–124, [[hep-ph/9206227](#)].

- [138] S. Groote, J. Korner, and A. Pivovarov, *On the evaluation of sunset - type Feynman diagrams*, *Nucl.Phys.* **B542** (1999) 515–547, [[hep-ph/9806402](#)].
- [139] B. A. Freedman and L. D. McLerran, *Fermions and Gauge Vector Mesons at Finite Temperature and Density. 1. Formal Techniques*, *Phys.Rev.* **D16** (1977) 1130.
- [140] P. Cvitanović, *Field theory*. Notes prepared by E. Gyldenkerne (Nordita, Copenhagen), 1983.
- [141] P. Fendley, *The Effective Potential and the Coupling Constant at High Temperature*, *Phys.Lett.* **B196** (1987) 175.
- [142] M. Carrington, *The Effective potential at finite temperature in the Standard Model*, *Phys.Rev.* **D45** (1992) 2933–2944.
- [143] H. Kleinert and V. Schulte-Frohlinde, *Critical Properties of ϕ^4 -Theories*. World Scientific, 2001.
- [144] R. Jackiw, *Functional evaluation of the effective potential*, *Phys.Rev.* **D9** (1974) 1686.
- [145] M. Chaichian and A. Demichev, *Path Integrals in Physics: Volume II Quantum Field Theory, Statistical Physics and other Modern Applications*. Taylor & Francisackiw, 2001.
- [146] R. Fukuda and T. Kugo, *Gauge Invariance in the Effective Action and Potential*, *Phys.Rev.* **D13** (1976) 3469.
- [147] J. M. Cornwall, R. Jackiw, and E. Tomboulis, *Effective Action for Composite Operators*, *Phys.Rev.* **D10** (1974) 2428–2445.
- [148] J. Luttinger and J. C. Ward, *Ground state energy of a many fermion system. 2.*, *Phys.Rev.* **118** (1960) 1417–1427.
- [149] J. Berges, *Introduction to nonequilibrium quantum field theory*, *AIP Conf.Proc.* **739** (2005) 3–62, [[hep-ph/0409233](#)].
- [150] A. G. Cohen, D. Kaplan, and A. Nelson, *Progress in electroweak baryogenesis*, *Ann.Rev.Nucl.Part.Sci.* **43** (1993) 27–70, [[hep-ph/9302210](#)].
- [151] J. M. Cline, *Baryogenesis*, [hep-ph/0609145](#).

- [152] M. Prakash, M. Prakash, R. Venugopalan, and G. Welke, *Nonequilibrium properties of hadronic mixtures*, *Phys.Rept.* **227** (1993) 321–366.
- [153] A. Muronga and D. H. Rischke, *Evolution of hot, dissipative quark matter in relativistic nuclear collisions*, *nucl-th/0407114*.
- [154] A. Nakamura and S. Sakai, *Transport coefficients of gluon plasma*, *Phys.Rev.Lett.* **94** (2005) 072305, [*hep-lat/0406009*].
- [155] H. Song and U. W. Heinz, *Extracting the QGP viscosity from RHIC data - A Status report from viscous hydrodynamics*, *J.Phys.* **G36** (2009) 064033, [*arXiv:0812.4274*].
- [156] R. Rapp and H. van Hees, *Heavy-Quark Diffusion, Flow and Recombination at RHIC*, *J.Phys.* **G32** (2006) S351–S358, [*hep-ph/0606117*].
- [157] R. Rapp and H. van Hees, *Heavy Quark Diffusion as a Probe of the Quark-Gluon Plasma*, *arXiv:0803.0901*.
- [158] B. Svetitsky, *Diffusion of charmed quarks in the quark-gluon plasma*, *Phys.Rev.* **D37** (1988) 2484–2491.
- [159] F. D. Steffen and M. H. Thoma, *Hard thermal photon production in relativistic heavy ion collisions*, *Phys.Lett.* **B510** (2001) 98–106, [*hep-ph/0103044*].
- [160] S. Turbide, R. Rapp, and C. Gale, *Hadronic production of thermal photons*, *Phys.Rev.* **C69** (2004) 014903, [*hep-ph/0308085*].
- [161] **PHENIX Collaboration** Collaboration, G. David, *Direct Photons at RHIC*, *arXiv:0810.0872*.
- [162] K. Kajantie, M. Laine, K. Rummukainen, and M. E. Shaposhnikov, *The Electroweak phase transition: A Nonperturbative analysis*, *Nucl.Phys.* **B466** (1996) 189–258, [*hep-lat/9510020*].
- [163] K. Kajantie, M. Laine, K. Rummukainen, and M. E. Shaposhnikov, *Is there a hot electroweak phase transition at $m(H)$ larger or equal to $m(W)$?*, *Phys.Rev.Lett.* **77** (1996) 2887–2890, [*hep-ph/9605288*].

- [164] F. Karsch, E. Laermann, and A. Peikert, *Quark mass and flavor dependence of the QCD phase transition*, *Nucl.Phys.* **B605** (2001) 579–599, [[hep-lat/0012023](#)].
- [165] P. de Forcrand and O. Philipsen, *The QCD phase diagram for small densities from imaginary chemical potential*, *Nucl.Phys.* **B642** (2002) 290–306, [[hep-lat/0205016](#)].
- [166] J. Berges, S. Borsanyi, D. Sexty, and I.-O. Stamatescu, *Lattice simulations of real-time quantum fields*, *Phys.Rev.* **D75** (2007) 045007, [[hep-lat/0609058](#)].
- [167] G. Aarts, E. Seiler, and I.-O. Stamatescu, *The Complex Langevin method: When can it be trusted?*, *Phys.Rev.* **D81** (2010) 054508, [[arXiv:0912.3360](#)].
- [168] S. Gupta, *QCD at finite density*, *PoS LATTICE2010* (2010) 007, [[arXiv:1101.0109](#)].
- [169] E. Braaten and R. D. Pisarski, *Soft Amplitudes in Hot Gauge Theories: A General Analysis*, *Nucl.Phys.* **B337** (1990) 569.
- [170] J. Blaizot, E. Iancu, and A. Rebhan, *Approximately selfconsistent resummations for the thermodynamics of the quark gluon plasma. 1. Entropy and density*, *Phys.Rev.* **D63** (2001) 065003, [[hep-ph/0005003](#)].
- [171] P. B. Arnold, G. D. Moore, and L. G. Yaffe, *Effective kinetic theory for high temperature gauge theories*, *JHEP* **0301** (2003) 030, [[hep-ph/0209353](#)].
- [172] P. B. Arnold, G. D. Moore, and L. G. Yaffe, *Transport coefficients in high temperature gauge theories. 2. Beyond leading log*, *JHEP* **0305** (2003) 051, [[hep-ph/0302165](#)].
- [173] S. Caron-Huot and G. D. Moore, *Heavy quark diffusion in QCD and $N=4$ SYM at next-to-leading order*, *JHEP* **0802** (2008) 081, [[arXiv:0801.2173](#)].
- [174] S. Caron-Huot, *$O(g)$ plasma effects in jet quenching*, *Phys.Rev.* **D79** (2009) 065039, [[arXiv:0811.1603](#)].
- [175] K. Kajantie, M. Laine, K. Rummukainen, and M. E. Shaposhnikov, *3-D $SU(N)$ + adjoint Higgs theory and finite temperature QCD*, *Nucl.Phys.* **B503** (1997) 357–384, [[hep-ph/9704416](#)].

- [176] E. S. Swanson, *A Primer on Functional Methods and the Schwinger-Dyson Equations*, *AIP Conf.Proc.* **1296** (2010) 75–121, [[arXiv:1008.4337](#)].
- [177] M. Carrington and Y. Guo, *A New Method to Calculate the n-Particle Irreducible Effective Action*, *Phys.Rev.* **D85** (2012) 076008, [[arXiv:1109.5169](#)].
- [178] J. S. Ball and T.-W. Chiu, *Analytic Properties of the Vertex Function in Gauge Theories. 1.*, *Phys.Rev.* **D22** (1980) 2542.
- [179] A. I. Davydychev, P. Osland, and O. Tarasov, *Three gluon vertex in arbitrary gauge and dimension*, *Phys.Rev.* **D54** (1996) 4087–4113, [[hep-ph/9605348](#)].
- [180] E. Braaten and G. Weller, *An improved low-discrepancy sequence for multidimensional quasi-monte carlo integration.*, *Journal of Computational Physics* **33** (1979) 249–258.
- [181] A. K. Rajantie, *Feynman diagrams to three loops in three-dimensional field theory*, *Nucl.Phys.* **B480** (1996) 729–752, [[hep-ph/9606216](#)].
- [182] N. Ahmadinia and C. Schubert, *A covariant representation of the Ball-Chiu vertex*, *Nucl.Phys.* **B869** (2013) 417–439, [[arXiv:1210.2331](#)].
- [183] R. Alkofer and L. von Smekal, *The Infrared behavior of QCD Green’s functions: Confinement dynamical symmetry breaking, and hadrons as relativistic bound states*, *Phys.Rept.* **353** (2001) 281, [[hep-ph/0007355](#)].
- [184] A. Cucchieri, T. Mendes, and A. R. Taurines, *Positivity violation for the lattice Landau gluon propagator*, *Phys.Rev.* **D71** (2005) 051902, [[hep-lat/0406020](#)].
- [185] D. Zwanziger, *Vanishing of zero momentum lattice gluon propagator and color confinement*, *Nucl.Phys.* **B364** (1991) 127–161.
- [186] L. von Smekal, A. Hauck, and R. Alkofer, *A solution to coupled Dyson-Schwinger equations for gluons and ghosts in Landau gauge*, *Annals Phys.* **267** (1998) 1, [[hep-ph/9707327](#)].
- [187] D. Zwanziger, *Nonperturbative Landau gauge and infrared critical exponents in QCD*, *Phys.Rev.* **D65** (2002) 094039, [[hep-th/0109224](#)].

- [188] P. Boucaud, J. Leroy, A. Le Yaouanc, A. Lokhov, J. Micheli, et al., *The Infrared behaviour of the pure Yang-Mills green functions*, hep-ph/0507104.
- [189] A. Aguilar, D. Binosi, and J. Papavassiliou, *Gluon and ghost propagators in the Landau gauge: Deriving lattice results from Schwinger-Dyson equations*, *Phys.Rev.* **D78** (2008) 025010, [arXiv:0802.1870].
- [190] C. S. Fischer, A. Maas, and J. M. Pawłowski, *On the infrared behavior of Landau gauge Yang-Mills theory*, *Annals Phys.* **324** (2009) 2408–2437, [arXiv:0810.1987].
- [191] I. Bogolubsky, E. Ilgenfritz, M. Müller-Preussker, and A. Sternbeck, *The Landau gauge gluon and ghost propagators in 4D $SU(3)$ gluodynamics in large lattice volumes*, *PoS LAT2007* (2007) 290, [arXiv:0710.1968].
- [192] I. Bogolubsky, E. Ilgenfritz, M. Müller-Preussker, and A. Sternbeck, *Lattice gluodynamics computation of Landau gauge Green’s functions in the deep infrared*, *Phys.Lett.* **B676** (2009) 69–73, [arXiv:0901.0736].
- [193] O. Oliveira and P. Silva, *The lattice infrared Landau gauge gluon propagator: from finite volume to the infinite volume*, *PoS QCD-TNT09* (2009) 033, [arXiv:0911.1643].
- [194] A. Cucchieri and T. Mendes, *What’s up with IR gluon and ghost propagators in Landau gauge? A puzzling answer from huge lattices*, *PoS LAT2007* (2007) 297, [arXiv:0710.0412].
- [195] A. Cucchieri and T. Mendes, *Constraints on the IR behavior of the ghost propagator in Yang-Mills theories*, *Phys.Rev.* **D78** (2008) 094503, [arXiv:0804.2371].
- [196] A. Cucchieri, D. Dudal, T. Mendes, and N. Vandersickel, *Modeling the Gluon Propagator in Landau Gauge: Lattice Estimates of Pole Masses and Dimension-Two Condensates*, *Phys.Rev.* **D85** (2012) 094513, [arXiv:1111.2327].
- [197] A. Cucchieri, T. Mendes, and E. M. S. Santos, *Simulating linear covariant gauges on the lattice: A New approach*, *PoS QCD-TNT09* (2009) 009, [arXiv:1001.2002].
- [198] P. Cvitanovic, P. Lauwers, and P. Scharbach, *Gauge Invariance Structure of Quantum Chromodynamics*, *Nucl.Phys.* **B186** (1981) 165.

- [199] M. Laine and O. Philipsen, *The Nonperturbative QCD Debye mass from a Wilson line operator*, *Phys.Lett.* **B459** (1999) 259–264, [[hep-lat/9905004](#)].
- [200] A. Hietanen, K. Kajantie, M. Laine, K. Rummukainen, and Y. Schroder, *Plaquette expectation value and gluon condensate in three dimensions*, *JHEP* **0501** (2005) 013, [[hep-lat/0412008](#)].
- [201] D. Kirzhnits and A. D. Linde, *Symmetry Behavior in Gauge Theories*, *Annals Phys.* **101** (1976) 195–238.
- [202] M. Gurtler, E.-M. Ilgenfritz, and A. Schiller, *Where the electroweak phase transition ends*, *Phys.Rev.* **D56** (1997) 3888–3895, [[hep-lat/9704013](#)].
- [203] T. Evans, H. Jones, and A. Ritz, *On the phase structure of the 3-D $SU(2)$ Higgs model and the electroweak phase transition*, *Nucl.Phys.* **B517** (1998) 599–621, [[hep-ph/9710271](#)].
- [204] K. Farakos, K. Kajantie, K. Rummukainen, and M. E. Shaposhnikov, *The Electroweak phase transition at $m(H)$ approximately $= m(W)$* , *Phys.Lett.* **B336** (1994) 494–501, [[hep-ph/9405234](#)].
- [205] K. Kajantie, M. Laine, A. Rajantie, K. Rummukainen, and M. Tsypin, *The Phase diagram of three-dimensional $SU(3)$ + adjoint Higgs theory*, *JHEP* **9811** (1998) 011, [[hep-lat/9811004](#)].
- [206] A. Rajantie, *$SU(5)$ + adjoint Higgs model at finite temperature*, *Nucl.Phys.* **B501** (1997) 521–544, [[hep-ph/9702255](#)].
- [207] M. Laine and A. Rajantie, *Lattice continuum relations for 3-D $SU(N)$ + Higgs theories*, *Nucl.Phys.* **B513** (1998) 471–489, [[hep-lat/9705003](#)].
- [208] V. Rubakov and M. Shaposhnikov, *Electroweak baryon number nonconservation in the early universe and in high-energy collisions*, *Usp.Fiz.Nauk* **166** (1996) 493–537, [[hep-ph/9603208](#)].
- [209] G. Aarts and J. M. Martinez Resco, *Transport coefficients from the 2PI effective action*, *Phys.Rev.* **D68** (2003) 085009, [[hep-ph/0303216](#)].
- [210] U. Reinosa and J. Serreau, *2PI functional techniques for gauge theories: QED*, *Annals Phys.* **325** (2010) 969–1017, [[arXiv:0906.2881](#)].

- [211] M. Carrington and E. Kovalchuk, *QED electrical conductivity using the 2PI effective action*, *Phys.Rev.* **D76** (2007) 045019, [[arXiv:0705.0162](#)].
- [212] J. O. Andersen and M. Strickland, *Three-loop Phi-derivable approximation in QED*, *Phys.Rev.* **D71** (2005) 025011, [[hep-ph/0406163](#)].
- [213] M. Carrington and E. Kovalchuk, *Leading order QCD shear viscosity from the three-particle irreducible effective action*, *Phys.Rev.* **D80** (2009) 085013, [[arXiv:0906.1140](#)].
- [214] L. Fister and J. M. Pawłowski, *Confinement from Correlation Functions*, *Phys.Rev.* **D88** (2013) 045010, [[arXiv:1301.4163](#)].
- [215] M. Alford, J. Berges, and J. M. Cheyne, *Critical phenomena from the two particle irreducible $1/N$ expansion*, *Phys.Rev.* **D70** (2004) 125002, [[hep-ph/0404059](#)].
- [216] W. Buchmüller, Z. Fodor, and A. Hebecker, *Gauge invariant treatment of the electroweak phase transition*, *Phys.Lett.* **B331** (1994) 131–136, [[hep-ph/9403391](#)].
- [217] H. H. Patel and M. J. Ramsey-Musolf, *Baryon Washout, Electroweak Phase Transition, and Perturbation Theory*, *JHEP* **1107** (2011) 029, [[arXiv:1101.4665](#)].
- [218] P. B. Arnold, *Phase transition temperatures at next-to-leading order*, *Phys.Rev.* **D46** (1992) 2628–2635, [[hep-ph/9204228](#)].
- [219] M. Laine, *The Two loop effective potential of the 3-d $SU(2)$ Higgs model in a general covariant gauge*, *Phys.Lett.* **B335** (1994) 173–178, [[hep-ph/9406268](#)].
- [220] K. Rummukainen, *Finite T electroweak phase transition on the lattice*, *Nucl.Phys.Proc.Suppl.* **53** (1997) 30–42, [[hep-lat/9608079](#)].
- [221] M. C. A. York, G. D. Moore, and M. Tassler, *3-loop 3PI effective action for 3D $SU(3)$ QCD*, *JHEP* **1206** (2012) 077, [[arXiv:1202.4756](#)].
- [222] J. Espinosa, M. Quiros, and F. Zwirner, *On the nature of the electroweak phase transition*, *Phys.Lett.* **B314** (1993) 206–216, [[hep-ph/9212248](#)].
- [223] T. van Ritbergen, A. Schellekens, and J. Vermaseren, *Group theory factors for Feynman diagrams*, *Int.J.Mod.Phys.* **A14** (1999) 41–96, [[hep-ph/9802376](#)].

- [224] J.-P. Derendinger, *Lecture Notes on the Standard Model of Elementary Particle Physics*. 2010.
- [225] E. Boos and A. I. Davydychev, *A Method of evaluating massive Feynman integrals*, *Theor.Math.Phys.* **89** (1991) 1052–1063.